



Oliver Mayer

Controlled formation  
of Cobalt-Particles in  
nanoscaled  
self-assembled  
structures









# Controlled formation of Cobalt- Particles in nanoscaled self-assembled structures

Dissertation  
zur Erlangung des Doktorgrades  
*Dr. rer. nat.*  
der Fakultät für Naturwissenschaften  
der Universität Ulm

vorgelegt von

Oliver Mayer  
aus Prag / Tschechische Republik

2006

*Cover illustration –*

*Front: Block copolymer micelles of  
PS(710)-b-P2VP(210) loaded with  
CoCl<sub>2</sub> L=0.2*

*Back: Block copolymer micelles of  
PS(710)-b-P2VP(210) with Q=10%  
loaded with Co<sub>2</sub>(CO)<sub>8</sub> L=5,  
decomposed at 170 °C*

Amtierender Dekan: Prof. Dr. K.-D. Spindler

1. Gutachter: Prof. Dr. M. Möller
2. Gutachter: Prof. Dr. K. Landfester

Tag der Promotion: 19.6.2006

*“Are you really Italian?” – “Assolutamente. Sì. My name is Otto, it means eight”*

*“But you think you're an intellectual, don't you, ape?” “Apes don't read philosophy.”*

*“Yes, they do, Otto. They just don't understand it.”*

*(A Fish called Wanda)*

## TABLE OF CONTENTS

<b>CHAPTER 1 .....</b>	<b>1</b>
Introduction.....	1
1.1 Magnetic nanoparticles.....	1
1.2 Contents of this thesis.....	3
1.3 References.....	4
 <b>CHAPTER 2 .....</b>	 <b>7</b>
Literature Overview.....	7
2.1 General Introduction .....	7
2.2 Phase behaviour of amphiphilic block copolymers .....	11
2.3 Synthesis and properties of nanoparticles .....	18
2.4 Block copolymers as nanoreactors.....	27
2.5 Magnetic nanoparticles.....	33
2.6 References.....	42
 <b>CHAPTER 3 .....</b>	 <b>53</b>
Generation of cobalt nanoparticles in surfactant stabilised systems.....	53
3.1 Introduction.....	53
3.2 Experimental.....	55
3.3 Results and discussion .....	56
3.4 Conclusions .....	65
3.5 References.....	65
 <b>CHAPTER 4 .....</b>	 <b>69</b>
Monodisperse cobalt-nanoparticles from sulfosuccinate systems.....	69
4.1 Introduction.....	69
4.2 Experimental.....	70
4.3 Results and discussion .....	73

4.4	Conclusions .....	99
4.5	References .....	100
<b>CHAPTER 5.....</b>		<b>103</b>
	Complexation of cobalt-precursors in PS- <i>b</i> -P2VP block copolymer micelles ....	103
5.1	Introduction .....	103
5.2	Experimental .....	104
5.3	Results and discussion .....	107
5.4	Conclusion .....	125
5.5	References .....	127
<b>APPENDIX CHAPTER 5 .....</b>		<b>129</b>
	Synthesis of polymers and complexes .....	129
A5.1	Diblock copolymers by living anionic polymerisation	129
A5.2	Synthesis of glyoximato-complexes of Co(II)	136
A5.3	Synthesis of Co(II)-hydrazino complexes	137
A5.4	References	138
<b>CHAPTER 6.....</b>		<b>141</b>
	Co-nanoparticle formation in polymeric nanoreactors .....	141
6.1	Introduction .....	141
6.2	Experimental .....	142
6.3	Results and discussion .....	144
6.4	Conclusion .....	162
6.5	References .....	163
<b>CHAPTER 7.....</b>		<b>167</b>
	Surface modification of Co-nanoparticles .....	167
7.1	Introduction .....	167
7.2	Experimental .....	168
7.3	Results and discussion .....	170

7.4	Conclusion.....	179
7.5	References.....	180
	<b>APPENDIX CHAPTER 7.....</b>	<b>183</b>
	Stoichiometric calculations on core-shell-type particles .....	183
	A7.1 Oxide shell around particles      183	
	A7.2 Calculation for the amount of the shell compound      188	
	<b>CHAPTER 8 .....</b>	<b>191</b>
	Summary .....	191
	Zusammenfassung .....	194
	Appendix.....	197





## List of abbreviations

Å	Angström
A <sub>s</sub>	Specific Surface
ATRP	Atom Transfer Radical Polymerisation
AOT	Sodium-bis(2-ethylhexyl-)sulfosuccinate
B	Magnetic Field
BHT	2,6-Di(tert-)butyl-4-methylphenol
cmc	Critical micelle concentration
COD	Cyclooctadienyl
CPU	Central Processing Unit
DMF	Dimethylformamide
DMG	Dimethylgloximato
DMSO	Dimethyl Sulfoxide
DP	Degree of Polymerisation
dpi	Dots per Inch
EA	Elemental analysis
EDAX	Energy Dispersive Analysis by X-Ray
FC	Field Cooling
FT-IR	Fourier-Transform Infrared Spectrometry
G	Gauss
GB	Gigabyte
$\Delta G_m$	Gibbs-free Enthalpy of Mixing
GMR	Giant Magneto Resist
H	External Magnetic Field
HR-TEM	High-Resolution Transmission Electron Microscopy
HR-TG	High-Resolution Thermogravimetry
IR	Infrared
JCDPS	Joint Committee for Powder Diffraction Studies
M	Magnetisation
MALDI-TOF	Matrix-Assisted Laser Desorption/Ionization – Time of Flight
Me	Methyl
N	Degree of Polymerisation
nm	Nanometre
NMR	Nuclear Magnetic Resonance
OBDD	Ordered Bicontinuous Double Diamond
ODT	Order-Disorder Transition
P2VP	Poly(2-vinylpyridine)

## List of abbreviations

---

P4VP	Poly(4-vinylpyridine)
PBd	Poly(butadiene)
PBd- <i>b</i> -PMAA	Poly(butadiene)-Poly(methacrylic acid) block copolymer
PDMS- <i>b</i> -PFS	Poly(dimethylsiloxane)-poly(ferrocenyl-dimethylsilane) block copolymer
PS	Poly(styrene)
PS- <i>b</i> -P2VP	Poly(styrene)-Poly(2-vinylpyridine) block copolymer
PS- <i>b</i> -P4VP	Poly(styrene)-Poly(4-vinylpyridine) block copolymer
PS- <i>b</i> -PB	Poly(styrene)-Poly(butadiene) block copolymer
PS- <i>b</i> -PI	Poly(styrene)-Poly(isoprene) block copolymer
PTFE	Poly(trifluoroethylene)
PVA	Poly(vinyl acetate)
py	Pyridino
Q	Degree of Quaternisation
RI	Refractive Index
rpm	Rotations per Minute
SEC	Size Exclusion Chromatography
SAXS	Small-Angle X-Ray Spectroscopy
SFM	Scanning Force Microscopy
SQUID	Semiconducting Quantum Interference Device
SSL	Strong Segregation Limit
STM	Scanning Tunneling Microscopy
T	Tesla
T <sub>B</sub>	Blocking Temperature
T <sub>C</sub>	Curie-Temperature
TDS	Tridecyl-sulfosuccinate
TEM	Transmission Electron microscopy
T <sub>G</sub>	Glass Transition Temperature
THF	Tetrahydrofuran
TOPO	Trioctyl Phosphineoxide
UHV	Ultrahigh Vacuum
UV-VIS	Ultraviolet-Visible Spectrometry
VSM	Vibrating Sample Magnetometry
WSL	Weak Segregation Limit
$\chi$	Flory-Huggins Interaction Parameter
XPS	X-Ray Photoelectron Spectroscopy
Z <sub>A</sub>	Aggregation Number
ZFC	Zero Field Cooling

# ***Chapter 1***

---

## ***Introduction***

### **1.1 Magnetic nanoparticles**

Within the time this thesis was written on a personal computer, millions of magnetisation and demagnetisation processes took place. These processes are located in the inside life of a personal computer mainly on mass storage media. In fact, the rapidly growing importance of electronic data processing was accompanied by a growing demand for bigger throughput mass storage media.

Due to the rapidly growing sizes of electronic data basing on new fields of multimedia, one focus, which is directed to science, is the building of bigger storage density. Moore's law concerning the increase of CPU frequencies can be directly transferred to mass storage media, where an increase of storage density follows a similar empirical law. Hard disks with a capacity of more than 100 GB got standard at the time this thesis was written and will still grow in the future. In order to be able to fabricate such high density, colloidal and nano-sized magnetic particles are necessary. The current hard disks consist of small particle films of Pt-Co alloys in the size regime of 20 nm [1-3]. Magnetism on the nanoscale is very interesting towards this development by several reasons. First, the media density like described above can only increase, if the smallest addressable units become smaller and smaller. Moreover, new effects like the giant magneto resist effect (GMR) [4, 5] allow access of new dimensions in mass storage media, which is manifested in a new generation of magnetic reading heads. Finally, new knowledge about nanoscale magnetism and magnetic particle film formation opens the door for future technologies, which will allow mankind to enter new media, which so far are not possible to realise, though already being planned [6].

Recently, much effort has been devoted to the controlled synthesis of nanometre size metallic particles. Indeed, the study of their novel properties resulting from surface or quantum size effects is of both fundamental and increasing technical interest [7]. In particular, nanoparticles of magnetic materials have attracted considerable and increasing attention due to their potential applications in very demanding fields. Except for magnetic storage technology [8] usage of magnetic nanoparticles is possible also in drug targeting [9], refrigeration [10], printing [11] and spin-valve technology [12].

The preparation of magnetic particles in the nanoscale offers a broad variety of approaches. Among them, the solution-phase metal salt reduction has the advantage to produce high amounts of colloids which can be further handled for different purposes. However, the reductant, as well as the counter-ion, is often an additional contamination source of the final metal [13, 14]. The decomposition of metal carbonyl complexes is thus a nice alternative, which has been used since many years to produce various metals (mainly Fe, Ni, Co) [15]. In these methods, the main by-product is gaseous and disappears from the reaction location. The decomposition can be induced either by pyrolysis or by ultrasound. Pyrolysis allows the formation of crystalline solids [16], while the ultrasonic procedure often produces amorphous materials [17-19]. The synthesis of Co nanoparticles starting from the cobalt carbonyl complex is thus quite attractive.

The combination of polymer and nanoparticle properties offers materials with an attractive spectrum of properties [20]. Either, an useful combination of properties in one material is resulting or new material's aspects arise from a synergetic effect [21]. The usage of designed block copolymers offers an effective tool for nanoscaled surfaces and bulk-phase tailoring. The formation of self-organised structures gives a geometrical control in the nanoscale. When nanoparticles are confined in such a structure, a very defined structuring of these nanoparticles is possible. Thus, the usage of the micellar core as nanoscaled reactor for the intrinsic formation of metallic nanoparticles is a first step towards an intelligent material [22, 23]. Using magnetic nanoparticles in a defined polymeric environment represents a precursor for a magnetically switchable material. Switching can be achieved by applying an external magnetic field. Introducing the idea, that on the surface of a magnetic particle a small layer of gold could be deposited, a switchable dichroic layer could be designed. Due to the nanoscaled optical properties of some noble metals like gold, silver or copper [24], which are size-dependent, the coated layer could become a colour switch. Either by generating anisotropically shaped particles or by spontaneous chain formation due to magnetisation of the particles, the switching by an external field could induce a colour change then by irradiation of the sample by polarised light.

## 1.2 Contents of this thesis

The thesis is organised in the following way:

**Chapter 2** gives an introduction to the different facets of the topics objected by this thesis. Some phenomenons, which were already mentioned in the introduction above will be discussed in further details.

The experimental part of this thesis is divided into three parts. The first part consists of the chapters 3 and 4 and deals with the formation of Co-nanoparticles in surfactant-stabilised systems. **Chapter 3** is a description of experiments, which were done in order to be able to synthesise magnetic nanoparticles in the presence of surfactants. **Chapter 4** picks the most successful approaches described in Chapter 3 and shows how a modification of the synthetic procedure is increasing the quality of the achieved particles. Also kinetic experiments are shown in order to be able to understand how these modifications influence the synthesis. Finally, the properties of the resulting nanoparticle solutions including ordered arrangement are described. The main focus is directed to the behaviour in magnetic fields and the behaviour against air, which is one of the key properties for those non-noble nanoparticles.

The second part of this thesis comprises the chapters 5 and 6. Here, the generation of cobalt particles in block copolymer micelles is described. **Chapter 5** shows, how cobalt-precursors are incorporated into block copolymer micelles of mainly PS-*b*-P2VP in non-polar solvents, i.e. in reverse polymeric micelles. Also the synthesis of these block copolymers is discussed. An outlook is given to other polymeric "nano-vessels" different from PS-*b*-P2VP. **Chapter 6** summarises experiments, where the conversion of these precursors to metallic cobalt is the subject. Modifications of the micellar reactors are discussed in order to get metallic cobalt particles.

The last part of the thesis is **Chapter 7**, where approaches are shown how to incorporate a second metal to the cobalt particles. Alloying and core-shell structures of Cobalt particles with another metal are also described.

Finally, **Chapter 8** summarises the main results obtained in this thesis and gives connecting points for further work on this topic.

## 1.3 References

- [1] G. Bate, *J. Mag. Mag. Mater.* **1991**, *100*, 413.
- [2] H. Laidler, K. O'Grady, *Datatech Magazine Vol.1*, 93; available online at <http://www.semiconductorsfabtech.com>.
- [3] B. Heinz, B. L. Gehman, *Datatech Magazine Vol. 2*, 79 available online at <http://www.semiconductorsfabtech.com>.
- [4] A.K. Menon, B. K. Gupta, *Datatech Magazine, Vol.2*, 13 available online at <http://www.semiconductorsfabtech.com>.
- [5] M.A. Howson, *Contemp. Phys.* **1994**, *35*, 347.
- [6] A.K. Menon, B. K. Gupta, *Datatech Magazine Vol.4*, 17 available online at <http://www.semiconductorsfabtech.com>.
- [7] K.J. Klabunde (Ed.), *Nanoscale Materials in Chemistry*, Wiley Interscience, John Wiley & Sons Inc., New York, 1st ed., **2001**.
- [8] S. Sun, C. B. Murray, *J. Appl. Phys.* **1999**, *85*, 4325.
- [9] J. Kreuter, *J. Controlled Release* **1991**, *16*, 169.
- [10] V.K. Pecharsky, K.A. Gschneidner Jr., *J. Mag. Mag. Mater.* **1999**, *200*, 44.
- [11] C. Kormann, E. Schwab, F.W. Raulfs, K.H. Beck, *U.S.Patent 5,500,141*, **1996**.
- [12] J.C. Lodder, D.J. Monsma, R. Vlutters, T. Shimatsu, *J. Mag. Mag. Mater.* **1999**, *198-199*, 119.

- [13] C. Petit, A. Taleb, M.P. Pileni, *J. Phys. Chem. B* **1999**, *103*, 1805.
- [14] C. Petit, A. Taleb, M. P. Pileni, *Adv. Mater.* **1998**, *10*, 259.
- [15] D. P. Dinega, M. G. Bawendi, *Angew. Chem. Int. Ed. Engl.* **1999**, *38*, 1788.
- [16] V. F. Puentes, K.M. Krishnan, P. Alivisatos, *Appl. Phys. Lett.* **2001**, *78*, 2187.
- [17] K.S. Suslick, S-B. Choe, A.A. Cichowlas, M. W. Grinstaff, *Nature* **1991**, *353*, 414.
- [18] Yu. Koltypin, G. Kataby, X. Cao, R. Prozorov, A. Gedanken, *J. Non-cryst. Solids* **1996**, *201*, 159.
- [19] G. Kataby, A. Ulman, R. Prozorov, A. Gedanken, *Langmuir* **1998**, *14*, 1512.
- [20] A.D. Pomogailo, *Russ. Chem. Rev.* **1997**, *66*, 679.
- [21] D.Yu. Godovski, *Adv. Polym. Sci.* **1995**, *119*, 79.
- [22] R. Savic, L. Luo, A. Eisenberg, D. Maysinger, *Science*, **2003**, *300*, 615.
- [23] B.L. Frankamp, O. Uzun, F. Ilhan, A.K. Boal, V.M. Rotello, *J. Am. Chem. Soc.* **2002**, *124*, 892.
- [24] J.A. Creighton, D.G. Eadon, *J. Chem. Soc. Faraday Trans.* **1991**, *87*, 3881.





## Chapter 2

---

### *Literature Overview*

#### 2.1 General Introduction

##### *Definition and classification of colloidal systems*

Roughly speaking, the term 'colloids' is used for chemical systems containing particles or thin films in the size range between 1 nm and 1  $\mu\text{m}$ . Colloidal systems represent the borderline between macroscopical matter and discrete molecules. A colloidal dispersed system consists of a dispersion agent and a dispersed component. Both terms are used analogous to the terms 'solvent' and 'dissolved component' in macroscopical fluids. The general difference between these both termini is the fact, that the dispersion does not contain necessarily two phases. A closer look into this class of matter shows, that the area of colloids can be separated further into different classes of colloids [1]:

*Phase colloids* are multi-phase systems, where the components are not compatible with each other. The dispersed part of these colloids consists of particles, which are stabilised inside of the dispersion agent. Sols and aerosols represent this class of colloids. The kind of stabilisation splits the phase colloids into two groups, the lyophilic and the lyophobic colloids. The first are stabilised by sterical or electrostatic interactions of the dispersion agent with the dispersed medium, while the latter are kept stable by electrostatic charges on the particles' surfaces due to repulsive forces. In the special case of aqueous solutions, the terms hydrophilic and hydrophobic colloids are used instead of lyophobic and lyophilic. But also homogeneous solutions can be colloids. In *molecular colloids* the size of the homogeneously dis-

solved molecules is responsible for the colloidal properties; polymer solutions are of that kind. The dispersed medium is of molecular origin and the stabilisation is realised by solvation. The final class of colloids is called *associative* or *micellar colloids*. These systems are neither solvated nor multi-phased. Such colloids contain dispersed matter, which is bound reversibly to bigger associates. These associates, also called micelles, behave like a homogeneous phase. They form a homogeneous two-phase system. Micellar systems are usually formed, if the dispersed phase is an amphiphilic compound. From a molecular point of view this means, that one part of the dispersed molecule is soluble in the chosen dispersion agent, while the other part is insoluble. The association behaviour can thus be explained by the collapse of the insoluble part of the molecules protected by a shell of the soluble part.

Colloids do not behave as Newton-like liquids, the viscosity is not constant concerning stress and shear forces. One other characteristic property of colloids is the polydispersity of the dispersed component. This means, the component is usually not uniform by means of the size or the molecular composition, but has a certain size distribution. In the case of a polymer solution, the chain length of the dissolved polymer is not uniform. For phase colloidal particles, except for the polydispersity in size, there is additionally a dispersity in shape, which is important especially for systems containing crystalline particles. An important parameter for colloidal systems is the specific surface  $A_s$  of a dispersed particle defined by its surface to volume ratio. This parameter is of special interest in the growing field of nanoscience, because the surface to volume ratio conducts many physical and chemical properties of small particles. If the specific surface of a colloidal particle is big, i.e. in the case of very small particles, the surface contribution for a certain property is responsible for the behaviour of the colloid. This is a big difference compared to bulk materials and solutions, where the surface contribution of materials properties is almost negligible and mainly directed by the volume effects.

A special case of a colloidal system are the so-called microemulsions [2]. An emulsion is usually formed in a liquid-liquid system by vigorous stirring, because the formation of additional surface can only be reached by additional energy supply. To avoid phase separation due to ripening processes, the small droplets in an emulsion are stabilised by an emulgator. This is an additive, which compatibilises the both phases because it has to have an affinity to both present phases. A microemulsion follows the same principle like a conventional emulsion, however, the size of the emulsified droplets is very small within the size range of colloidal systems. Unlike the macroscopical emulsions, microemulsions are transparent and thermodynamically stable. A microemulsion is formed spontaneously and the formation of

a microemulsion needs either a special emulgator or a mixture of an surfactant with a co-surfactant.

### *Micelle formation in low-molecular surfactant solutions*

The class of associative colloids is formed by micellar solutions. Surfactants are amphiphilic compounds, which form micellar associates in a solvent. One part of these molecules is chemically miscible with the solvent and is called the lyophilic or, in the special case of aqueous solutions, the hydrophilic part. In contrast with this, the other part is incompatible with the solvent and is called the lyophobic part, for aqueous systems the hydrophobic part. If the difference of the incompatibility of both parts of the molecule is high enough, micelles can be formed in solution. Micelles are called inverse in the case of non-polar solvents. A schematical view of a globular micellar associate is given in Figure 2-1.

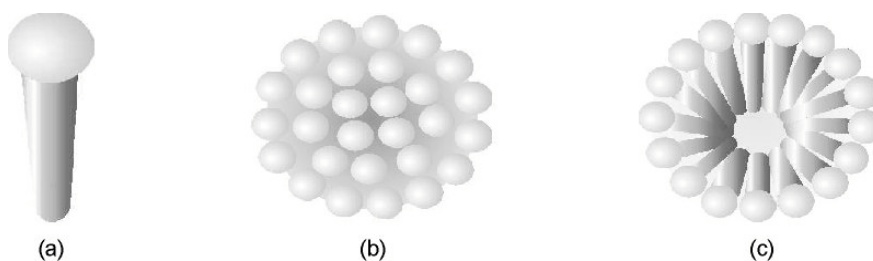


*Figure 2-1: Association behaviour of surfactants (schematic view): (a) Single surfactant molecule with spherical lyophilic part and a lyophobic tail; (b) Top view on a spherical associate, (c) Cross cut through one layer*

The responsible mechanism for the association is the tendency, that the contact surface between the solvent and the incompatible part is minimised. This can be reached either by transfer to the solution's surface to form a new interface layer or by forming an association, where the incompatible part is shielded against the solvent. Because of the first mechanism, surfactants gained their name: they form a new surface and are thus surface-active, i.e. they influence the surface tension of the solution. The second mechanism occurs beyond a certain concentration, the critical micelle concentration (cmc). Below the cmc, there are simply not enough surfactant molecules present in the solution, to form stable associates. If the cmc is reached, associates form, which is accompanied by a discontinuous change of the solution's properties like viscosity or electrical conductivity [1]. This micellisation process is dynamical, which means, that there is a steady flow and exchange of surfactant between the associates, micelles also split and recombine. However, sterical hindering can stabilise micelles by inhibiting splitting processes. If a solution contains additional substances, which

are incompatible with the solvent, but compatible with the lyophobic part of the surfactant, the associates are able to uptake these substances. This is called solubilisation and is the basic of the washing process.

A characteristic size is the aggregation number  $Z_A$ , the mean number of amphiphilic molecules per micelle. By knowledge of the aggregation number and the molecular architecture of the surfactant, one can calculate the micelle's dimensions. Due to the concentration and the structure of the surfactant, the micellar shape is not restricted to a globular form. It was found, that micelles can form a very detailed and complicated spectrum of shapes and phases. This spectrum is usually presented as a micellar phase diagram [3, 4]. An example can be seen in Figure 2-2.

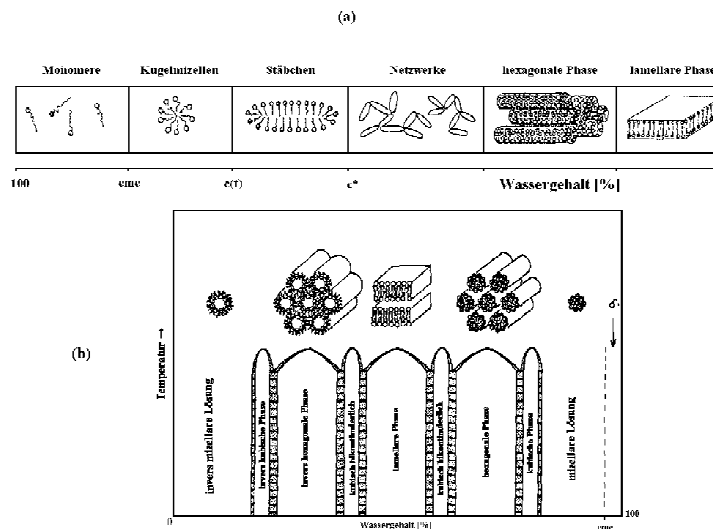


Figure 2-2: Schematic structure of (a) association behaviour with increasing surfactant concentration (b) the surfactant's phase diagram, which shows the formation of mesophases [3].

As shown in Figure 2-2a, the micelles at low surfactant concentration form first loose spheres. Still, solvent can penetrate the shield of the micellar surface and lead to non-favourable interaction with the lyophobic part of the surfactant. Thus, at higher surfactant concentrations, the spheres get packed more densely. Increasing the concentration further, the space needed for a head group of the micelle cannot be afforded anymore by a more dense packed sphere. Then, elongated structures start to be formed. The aspect ratio of the micelle grows now with increasing concentration. This leads finally to networks and ordered structures, to the so-called mesophase surfactant structures. These offer a variety in shape and ordering, which is show in Figure 2-2b. Such phases are formed at ca. 30 Vol. % surfactant in the solution. These lyotropic mesophases show liquid crystalline behaviour.

## 2.2 Phase behaviour of amphiphilic block copolymers

Block copolymers are macromolecular compound consisting of two or more connected homopolymer blocks. Differing from graft copolymers, the connection between the building blocks is located at the respective ends of the homopolymer chain. Block copolymers are synthesised by living radical[5], cationic[6] or anionic polymerisation [7] but also by linking preformed stocks. The chemical nature of the polymeric blocks can be either varied by the choice of monomers or by polymer analogous transformation e.g. of polydienes [8]. The blocks of a block copolymer can be miscible or incompatible towards each other. In the latter case, the block copolymers are called amphiphilic.

### *Bulk phase behaviour*

Microphase separation takes place in amphiphilic block copolymers, because the blocks are immiscible. The extent of this phase separation is mainly conducted by the polymerisation degree ( $N$ ) and the compatibility of the respective monomer units represented by the Flory-Huggins interaction parameter  $\chi$  [9, 10]. In the equilibrium state, phase separation occurs, if this lowers the Gibbs-free enthalpy of mixing to a minimal value. The Gibbs-free enthalpy of mixing per segment  $\Delta G_m$  for a system containing two homopolymers with segments A and B, can be written as [11]:

$$\Delta G_m = \Delta H_m - T \cdot \Delta S_m = k_1 \cdot \chi_{A-B} + \left[ \frac{k_2}{N_A} + \frac{k_3}{N_B} \right] \quad (\text{Eq. 2-1}),$$

where  $k_{1-3}$  are constants containing temperature and the respective volume fractions,  $N_{A,B}$  are the polymerisation degrees of A and B. The interaction parameter  $\chi_{A-B}$  contains both, the interaction energies between different segments and the same segments. The model of a homopolymer mixture can be transferred to the case of block copolymers, taking into account an additional entropic factor for the connection points between the blocks [9]. One can conclude from equation 2-1, that the bigger  $\chi_{A-B}$  and the smaller  $\frac{1}{N}$  are, the stronger the phase separation will occur. Thus, the product  $N\chi_{A-B}$  gives an estimation about the

strength of the segregation between the blocks of a block copolymer. A classification of block copolymers can be made using approximate values of  $N\chi_{A-B}$ [12]:

- $N\chi_{A-B} < 10$ : The entropic term dominates the phase behaviour, which means a higher disordered state of the whole polymer. A higher disordered state represents the formation of more or less perturbed polymer coils. For this case, microphase separation does not occur.
- $N\chi_{A-B} \geq 10$ : A transition to a higher ordered state occurs (ODT – order-disorder-transition). The blocks start to form an individual phase within the bulk polymer. However, still both blocks are present inside of a certain volume, but no more in equal volume fractions. The regime beyond the value 10 is called the weak segregation limit (WSL).
- $N\chi_{A-B} >> 10$ : This case is called the strong segregation limit (SSL). Here, a complete separation of microphases has taken place. Inside of a bulk piece of block copolymer, a certain volume doesn't have to contain both blocks anymore.

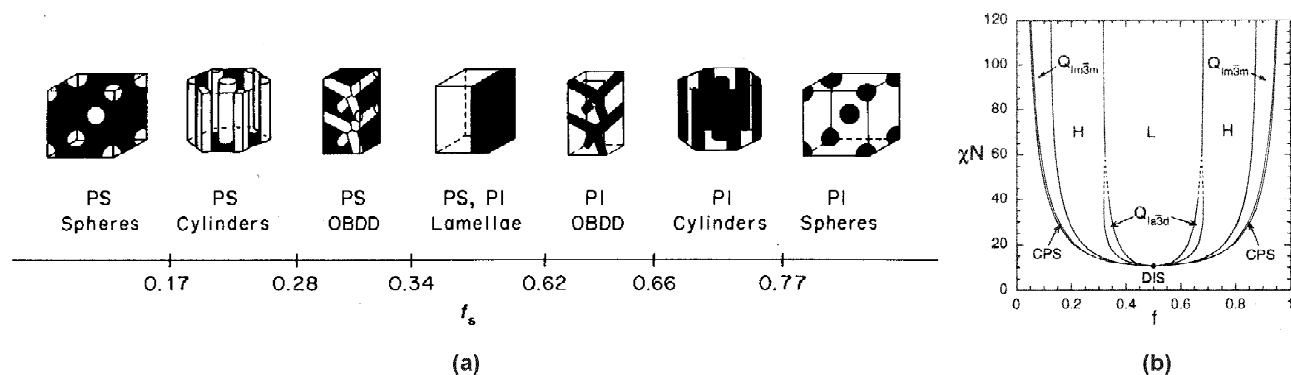


Figure 2-3: Ordered phases of PS-b-PI: (a): Schematic overview of different ordered phases depending on the volume fraction of Polystyrene  $f_s$  at given  $N\chi_{A-B}$  (from [11]); (b) The plot of  $N\chi_{A-B}$  versus volume fraction  $f$  gives a phase diagram with stability zones of numerous structures for the system PS-b-PI (from [13]).

All considerations so far were valid for symmetrical block copolymers, where the formation of lamellar phases is preferred. If the block length ratio is varied for a specific block copolymer, it is possible to sketch a phase diagram in dependence of the volume fraction of one of the blocks. A typical phase diagram is sketched in Figure 2-3. At a volume fraction of 0.5, lamellae are observed. The more the block length ratio differs from the symmetrical case, the less there occurs a lamellar spreading of both blocks, but the smaller block forms cylindrical or spherical shaped phases inside of a matrix of the bigger block. Also bicontinu-

ous gyroid phases can occur [13, 14]. Concerning the product  $N\chi_{A-B}$  the phase behaviour is changing due to a net decrease of contacts between incompatible blocks with increasing block lengths.

The described phase behaviour is, however, limited to system with non-crystallisable blocks. Moreover, the situation changes also, if shear forces are applied [15] or if the system consists of more than two blocks or components like in polymer blends [16].

### *Block copolymers in solution*

Introducing a block copolymer into a solvent increases the system by one additional component. This component is again interacting with the blocks of the block copolymer and thus influencing the mixing properties. Referring to one particular block, the interactions can be attractive or repulsive. In the case of a  $\theta$ -solvent the interactions are balanced and the coil is found to be undisturbed. In the case, that the quality of the solvent is either good or bad for both of the blocks, the polymer dissolves (swells) or precipitates, respectively. If a block copolymer is brought into a selective solvent, the blocks are stretched within the micelles due to the repulsion between the blocks [17].

The case, in which a solvent is good for the first block, but bad for the other is called to be selective for the first block. Already in very diluted solution, the formation of associates of block copolymer molecules starts and so-called block copolymer micelles are formed. The name is derived from the low molecular analogons, the surfactant micelles, because the main principle is the same. The well-soluble block swells and is soluble, whereas the other insoluble block collapses in the core of these associates. However, there are also basic differences between both sorts of micelles[18]:

- Because of the polymers' polydispersity, the transitional changes at the cmc are not abrupt, but more smooth.
- In principle, already single block copolymer molecules, the unimers, are able to form an internal associate, the so-called monomolecular micelle.
- For higher molecular weights, the cmc can be reached extremely slow.
- Exchange kinetics of the block copolymer can be extremely slow, e.g. reaction to dilution is retarded.

A sketch of an unimeric micelle in comparison to a block copolymer micelle is shown in Figure 2-4:

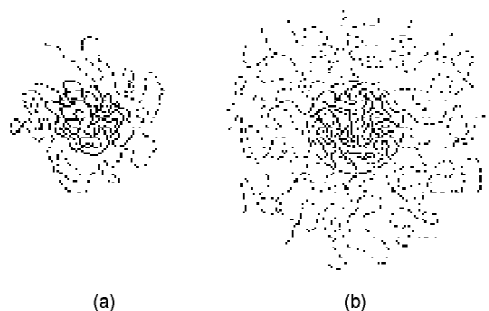


*Figure 2-4: View on a diblock copolymer dissolved in a selective solvent: (a) Single macromolecule; the soluble part surrounds the collapsed insoluble block; (b) Association of several macromolecules leads to micellisation (from [17]).*

In Figure 2-5, the concentration behaviour of block copolymer micelles is depicted. Starting at a low concentration, after adding a polymer into a solvent, the formation of unimeric micelles begins. Approaching the cmc of the polymer, the formation of loose associates takes place, where still lots of solvent can be captured. The associates have bigger dimensions as the micelles, which are formed at concentrations beyond the cmc. Depending on the concentration and the block length ratio, non-spherical aggregates can be formed [19-21].

Spherical block copolymer micelles consist of a corona formed from the soluble block and

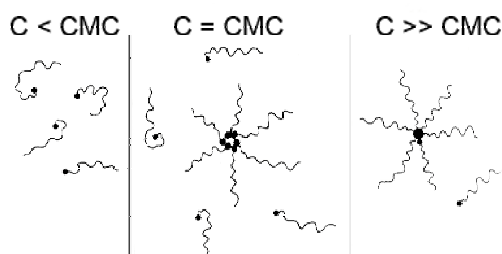


*Figure 2-5: Concentration behaviour of block copolymer macromolecules and micelles (from [18]).*

of a core of the insoluble block. The shape of such micelles leads to a classification of micelles into two types, the hairy micelles and the crew-cut micelles (see Figure 2-6). Crew-cut micelles have a short soluble chain, but a big insoluble chain, whereas for hairy micelles, it is vice versa. The classification is important for the behaviour of the micelles concerning aggregation numbers and diameter and also the solubility. Also, the phase diagrams of those



two types are different and for crew-cut micelles the formation of non-spherical micelles is more pronounced than for hairy micelles [22].

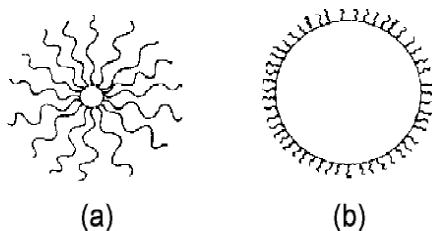


Figure 2-6: Scheme for (a) hairy or star micelles and (b) crew-cut micelles (from [23]).

The association behaviour of block copolymer micelles follows the principle of closed associates [24, 25]. Open association occurs, when the kinetics of association consist of several steps with similar equilibrium constants. This results in a relatively broad distribution of differently evolved associates. Compared to an open association, a closed association is a multi-step process dominated by a small number of crucial association steps. Assuming a low polydispersity block copolymer, the kinetics of block copolymer micelle formation can be described approximately by an equilibrium between unimers and the final micelles.

From a thermodynamical point of view, the formation of block copolymer micelles is determined by two versatile forces. On the one hand, attractive interactions between the macromolecules and the solvent are forcing the formation of associates, on the other hand, the association is limited by sterical interactions, which avoid the generation of a second macroscopic phase and thus, the precipitation of the polymer. The value of the cmc is in general very low, compared to the values for surfactant micelles. This is mainly caused by the small entropic contribution to the free micelle formation enthalpy  $\Delta G_{mic}^0$ . Therefore, the cmc is reached quickly due to the big enthalpic contribution [26].

The analysis of micelles is possible by several methods. For critical data, i.e. the measurement of the cmc, dynamical and static light scattering can be used [18, 27, 28]. With these methods, it is also possible to determine size, weight and the aggregation number of the micelles. Visualisation of block copolymers is often achieved by transmission electron microscopy (TEM), the size can then be measured directly from the micrographs. Electronically similar blocks cannot easily be distinguished by TEM. Therefore, in order to increase the contrast between core and corona of a micelle, one of the blocks is stained by a heavy metal compound like  $\text{OsO}_4$  or uranyl acetate. Other methods used for determination of

block copolymer micelle parameters are viscometry, SEC, SAXS and fluorescence spectrometry [29, 30].

In this context, Monte-Carlo simulations have been made for block copolymer micelles in the weak segregation limit (WSL) [31]. In these calculations, the composition of a micellar solution has been visualised in dependence of the distance from the central point of a mi-

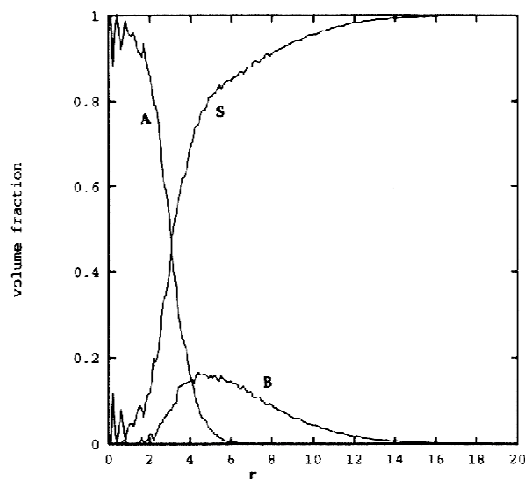


*Figure 2-7: Composition of a block copolymer micelle in the WSL. The graph shows the radial distribution of the concerned components with increasing distance from the micellar core ( $A$  = insoluble block,  $B$  = soluble block,  $S$  = solvent); taken from [31].*

celle. The results are shown in Figure 2-7. In these calculations it could be shown, that inside of the micellar cores there is still a finite amount of solvent present. Other results of this model were, that an exchange of the polymer between micelles is very slow and that the increase of the polymer concentration leads to an increase of the aggregation number of the micelles.

#### *Thin film deposition of block copolymers*

The amphiphilic behaviour of block copolymers leads to interesting interface properties, which play an interesting role for their deposition in thin films on a suitable substrate. Such films gain a growing interest in modern high-tech applications like the fabrication of decorated substrate surfaces and lithographic etching masks in the sub-micron range [32-34]. Casting from micellar solutions of a block copolymer can be done in a selective or a non-selective solvent. An alternating arrangement of blocks can be observed, if the polymer

is casted from a non-selective solvent. Then the driving forces of the deposition process are the interactions of the components with the substrate and the air. In the simplest case of symmetrical block copolymers, lamellar phases are built, which are arranged as double layers [35]. The last layer is built from the block with the smallest surface energy.

If the amount of polymer is not high enough to cover the complete surface of the substrate, lateral phase separation occurs [36, 37]. This situation is depicted in Figure 2-8 and can happen for example in a diluted solution of PS-*b*-P2VP, which is wetting the surface of mica. The unfavourable interaction between both blocks and the attractive interaction of the P2VP block towards the mica surface lead to a loss of its coil structure. The PS-block on the other hand forms islands in order to reduce the contact area to the substrate, which is non-favourable.

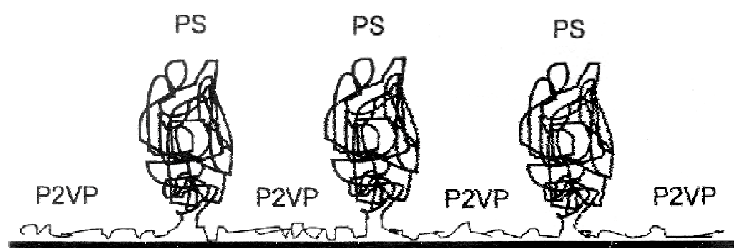


Figure 2-8: Lateral phase separation of PS-*b*-P2VP on mica. The scheme shows a deposition from a diluted solution (from [36]).

If a solution in a selective solvent, i.e. a micellar solution, is deposited on a substrate, a monomicellar film can be formed. Such a deposition can be used to illustrate the structure of the solution, if the solvent evaporates quickly. Then, the system's state in solution is frozen on the substrate. However, if the evaporation process is slow, the interactions of the blocks with the substrate start to play an increased role and a thermodynamical equilibrated state is approached. This relaxation of the polymer structure is not observed, if the dissolved state is very stable like in ionomers or in the case, that the adsorbing block enters the glassy state [38, 39]. In the case, that the most attractive interactions to the substrate are with the core block, the micelles are not bound directly to the substrate, but unimers, which are present inside the solution form brush-like connectors between micelles and the substrate [40].

Above a certain concentration, the micelles are deposited in a closely packed arrangement. Compared to three-dimensional arrangements of spheres, the most stable packing on a two-dimensional film is not a cubic packed, but a hexagonal packed structure [41]. This structure is preferred due to geometrical reasons. For the hexagonal packing, the overlap area

between the micellar shells is the smallest and leads to a balance between a freedom in conformations and a necessary overlap for a complete coverage of the substrate [42, 43].

The morphology of deposited micellar solutions can vary with the micelle concentration. For certain PS-*b*-P2VP micelles, it could be shown, that beyond concentrations containing hexagonal arrays, also worm-like and lamellar micelle arrangements could be realised [44]. This transfer is just possible for not too stable micelles. In the case of protonated PS-*b*-P2VP micelles containing tetrachloroauric acid no worm-like micelles could be observed, whereas micelles containing the lithium-salt did undergo this transfer.

## 2.3 Synthesis and properties of nanoparticles

If the dimensions of matter in the solid state lie between 3 and 100 nm, the resulting particles are called nanoparticles, particles below 3 nm are called nanoclusters [45]. Two kinds of approaches have been made in order to be able to manufacture these particles: 1. The top-down approach, which means a decrease of particle size, is realised mainly by physical methods. 2. The bottom-up approach includes the building of a nanoparticle from the atom or the molecule up to a defined array of matter. The latter is done mainly by chemical methods.

### *Top-down approach by physical methods*

Physical methods in order to gain nanoparticles lead often to naked or ligand-free clusters [46], in which the surface of the particles is not modified, but is built from the cluster material. The particular preparation methods contribute some difficulties, which are namely a big instrumental effort, the use of ultrahigh-vacuum techniques, poor size distributions of resulting particles and the access only to negligible amounts of the desired materials [47]. Nevertheless, this approach delivered the first important results about nanoparticles and their properties and due to the ligand-free environment the obtained results were free from outer contributions to the achieved results. Some of the most important techniques involving the top-down approach are listed below:

- The matrix-method uses evaporation of a metal in the ultra-high vacuum (UHV). Condensing this vapour in presence of a matrix like a noble gas leads to metal clusters, which can be isolated within this matrix [46].
- A molecular beam, which can be formed by pulsed laser evaporation of bulk material, can contain naked particles, which can be analysed by spectroscopy or even be separated by methods like MALDI-TOF.
- Controlled deposition of matter can be achieved by placement of atoms on surfaces by the help of an STM-tip [48, 49].
- Other methods for obtaining a fine distribution of matter use colloidal milling, ultrasounds or light-bows.

#### *Bottom-up approach by chemical methods*

From the synthetical point of view, chemical methods by the bottom-up method are more favourable due to their more uniform products, the bigger product scale and better stability by chemical protection of the resulting nanoparticles. Chemical protection can be achieved either by surface interaction to a present protecting agent, by ligating, covalently bonded chemical groups or by kinetical confinement of the particles. Unfortunately, many of the methods, which use the mentioned stabilisation techniques, result in particles, whose properties are influenced by the protective chemicals, so not the particles themselves are examined, but the composite of particle and protective shell [47]. In this point, still most of the reported chemical methods are not delivering clear facts, and physical methods give the more precise results for the particles themselves.

The focussed materials, which are synthesised in the nanoscale, are metals, semiconductors, supraconductive compounds, dyes and magnets. Also compounds of interest in biological processes gain growing interest [50]. The following review on synthetical methods gives a brief overview on published nanoparticle syntheses. The selection is small compared to the activities made in nanomaterials research in the past two decades, which emphasises the importance of this research field, maybe even the most active, in the recent years.

If one considers a metallic cluster compound with no bridging ligands present in their molecular structure, the metal-metal bonds are finite in number and geometry. Only above a minimum size one finds a core with metallic properties, surrounded by a shell of surface atoms bound to the ligands in the outer sphere. This is the molecular approach to synthesise

nanoparticles, where the resulting particle is still a part of a discrete compound with a fixed chemical formula. Big efforts in this field were made in the chemistry of oxomolybdates [51]. Pt and Pd-particles can be synthesised via hydrogen reduction of the respective phenanthroline derivatives, Rh, Ru and Au-particles are accessible via diborane reduction of the phosphanes and arsanes in organic solvents [52]. Stable Au-particles were prepared, which contain a core of gold, where the central gold atom is surrounded by full shells corresponding to the metal lattice. full-shell clusters contain a discrete number of metal atoms; the numbers of atoms forming a full-shell cluster are called the "magic numbers" [47].

Electrolytic methods are used to generate metallic nanoparticles, stabilised by charged species in the electrolyte solution. Quarternary ammonia salts are of widespread use in this technique [53, 54]. Even naked particles can be generated on the electrodes' surfaces, using pulsed electrolysis. Here, the nucleation of the particle is generated by the electrical pulse and the growth takes place in the zero-flow period, by which the size of the particles can be regulated [55, 56].

A method often used is the ultrasonification of thermally unstable transition metal complexes like carbonyl complexes [57, 58]. These sonochemical methods often lead to amorphous particles, which can be stabilised e.g. by surfactants. Also, radiolysis of metal salts can be used for reductive metal nanoparticle synthesis [59, 60]. Except for stabilisers, also radiolytic scavengers like PVA have to be added to the reaction mixtures.

For the colloid chemical approach, the sterical stabilisation is rather important, because colloidal stabilisation by surface charges only leads to broad particle size distributions, non-ordered structuring and the particles tend to form aggregates [61]. If the particle surface is protected by an interaction with another compound, particles get stable against aggregation. One of the best-known methods using this principle is the citrate method for the synthesis of protected gold particles. Here, the citrate acts as reducing and protecting agent during the reduction of  $\text{HAuCl}_4$  [62, 63]. Three classes of protecting agents got used frequently in the past: organic thiol compounds, amphiphilic surfactants and polymers.

Polymers, both homopolymers and copolymers, are frequently used as auxiliary components during controlled nanoparticle synthesis. This control is manifesting e.g. in the shape [64], the colour and size [65] or the catalytic activity [66] of the so produced nanoparticles. Methods, incorporated into polymeric synthesis are widespread [67]:

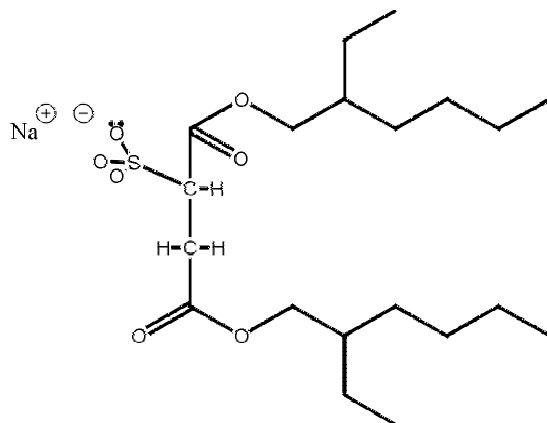
- **Simultaneous polymerisation:** The metal precursor is introduced, while a polymerisation takes place simultaneously. The metallic or organometallic precursors even can play

the role of the polymerisation's initiator or catalyst. This results in small particles embedded in a thin polymer film.

- **Thermal decomposition:** A volatile metal compound is decomposed in the presence of a polymer in solution or in melt. Localisation of the precursor is usually realised by chemisorption or complex formation to the functional groups of the polymer. After decomposition, the solution is kept stable by metal bonding to the polymer, by the viscosity of the polymer or by kinetical confinement of the particles. Control over size and polydispersity of the nanoparticles is brought off by variation of solvent, the polymer's block length or the insertion ratio of the copolymer.
- **Reduction:** Metal salts or other metal compounds are reduced in polymer containing solutions. Due to the ionic character of intermediately occurring species, many seeds are generated in the initial state, which are subsequently bond to the functional groups of the polymers. Therefore, just a small portion of the material is available for seed growth and the resulting particles are very small.

An outstanding method is the usage of amphiphilic compounds as templates for nanoparticle synthesis. Both can be used, low molecular surfactants and amphiphilic polymers. Here, the lyophobic phase, can form micelles, which control the maximum size of the nanoparticles and shift the reaction into a small compartment inside of the system. The nature of this environment is responsible for the characteristics of the resulting nanoparticles. In general, polymeric micelles are bigger in size and form micelles under closed association kinetics. The conclusion is, that bigger micelles with smaller particle size distributions can be expected.

Amongst the great number of existing low molecular weight surfactants, AOT has gained a big interest in nanoparticle synthesis. This surfactant can be used to form inverse micelles, which contain a non-polar solvent and functional groups inside the micellar core. AOT is an abbreviation for Sodium-bis-(2-ethylhexyl)-sulfosuccinate:



Many different noble-metal nanoparticles (e.g. Cu, Ag, Au) could be synthesised by using AOT as key component [68-71]. The most successful syntheses use water droplets in the micellar core as reaction solvent. In most cases, the heavy metal salt of the surfactant is reduced by either hydrazine hydrate ( $\text{N}_2\text{H}_4 \cdot \text{H}_2\text{O}$ ) or sodium borohydride ( $\text{NaBH}_4$ ). Many investigations have been made in the past concerning the reaction mechanism of the particle formation. Important parameters, which influence the particles are the type of solvent used, the used content of water and AOT, the nature of the reducing agent and the reduction mechanism. The latter also is responsible for either metal or metal oxide particle formation. Variation of the water content also influence the aspect ratio of the particles, higher water content can end up with anisotropic particles [72].

### *Nanoparticles in ordered structures*

In the past years, the challenge in synthetic nanochemistry consists in arranging particles in generic structures. Such structuring can be of great interest, when the properties of nanoparticles are needed in arrays of defined environment like in lithographic processes, when the particles need to be addressed or when exact knowledge of particle amount is needed. Films can be cast in the most dense packing of particles in a two-dimensional array. Furthermore, the distance between the particles can be chosen so small, that there is a finite possibility for the electrons to tunnel from one particle to the next one. Thus, if the mean free path of the electron is longer than the interparticle distance, a coupling between neighboured particles takes place. Depending on the number of directions, in which such a coupling can take place, one can distinguish different kind of systems [73-76]:

- **0D-systems**, called quantum dots. These kind of systems consist of completely isolated particles. Non-ordered particle arrays can be seen approximately as 0D-systems,



- **1D-systems**, called quantum wires or quantum wells. Those are ordered in a line without any other lateral interaction to other quantum wires,
- **2D-systems** consist of a monomolecular layer of ordered nanoparticles. Such systems can be generated by casting of a particle containing solution on a substrate,
- **3D systems** are ordered nanoparticles in a crystal-like three-dimensional object, where the arrangement spreads all over this crystal.

Ordered systems can be either formed by coupling quantum dots or intrinsically by the material. The latter case is true, if the system is not built of particles, but if the metal is e.g. a rod with two dimensions in the nanometre scale. The arrangement of quantum dots in a regular pattern can be realised by templates. Amphiphilic compounds like surfactants and block copolymers can act as templates due to their phase behaviour. Combination of these structures, either in bulk or in solution, and the metallic precursors entrapped inside of the lyophobic part of the associates leads to ordered nanostructures. This approach is called the self-assembly of nanoparticles, which is a mixture between chemical nanoparticle synthesis and supramolecular superstructures [77, 78].

Synthetic routes towards ordered systems have been reported increasingly in the past years. Quantum wires are accessible by the usage of rod-like micelles or by seed control [79-82], 2D-systems were made by usage of low molecular surfactants [83, 84] or phase transfer agents [85, 86]. Another way to get areas of ordered nanoparticles is the modification of substrates [87, 88]. Here, thiols are often used, due to their high affinity to gold and other noble metals [89-91]. Thiol modification of particle surfaces was used to form superstructures as well. Gold and silver particles could be incorporated into three-dimensional networks or superstructures [92-95].

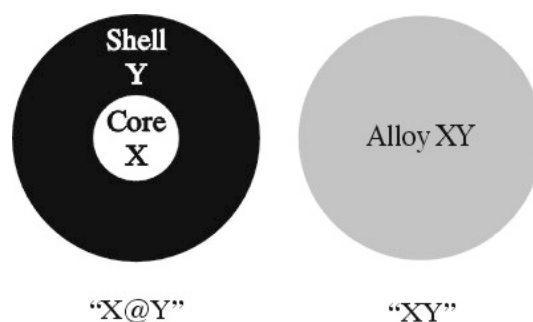


Figure 2-9: Schematic cross section through a core-shell particle (left). *X* is the core building particle, *Y* is the other material, building the shell. On the right, the same particle as one homogeneous *XY*-alloy nanoparticle.

### *Core-Shell nanoparticles*

Core-Shell particles consist of a core particle from a homogeneous material covered with an inorganic shell, which covers the whole surface of the inner particle. By definition, the outer material is not an organic layer and the type of bond is not a covalent one. The nomenclature of core-shell-particles uses the "@"-character. An Au@Sn-nanoparticle is a particle of gold, which is covered by a shell of tin. Figure 2-9 shows a schematic sketch of bimetallic particles. Except for bimetallic particles, also the coverage with a non-metallic inorganic compound like SiO<sub>2</sub> is possible.

Synthetic approaches always have to take into account, that both components should neither be completely miscible nor completely incompatible. In the first case, instead of a core-shell particle, an alloyed particle will be generated. On the other hand, if both components are not compatible with each other, the surface of the core particle will not be covered completely and gaps will occur on the interface. The most successful strategies to gain core-shell particles start with a stable nanoparticle solution. These particles are used then as seed for a secondary material deposition. Just a few successful syntheses of core-shell particles were reported so far. The main problems are a complete coverage of the inner material, secondary particle seeding, aggregation, electrochemical oxidation of the inner particle and alloy formation. Gold was used as core material to form a stable bimetallic core-shell nanoparticles with tin, lead and palladium, respectively [96-98]. Also, SiO<sub>2</sub> could be successfully deposited on gold nanoparticles [99].

### *General properties of nanoparticles*

The reason for the great interest in nanoparticle synthesis is the change of materials' properties, when matter gets a size between the bulk and the atomic state [100]. Roughly speaking, this critical size is, depending on the focussed property, below 25 nm of particle diameter. Reason for this change in physical and chemical behaviour is the change in electronic structure, the surface to volume ratio and the absence of long-range interactions within the particle because they exceed the particles' dimensions.

Metals, for example, lose their metallic properties, when the particle size gets small enough [101, 102]. Metallic nanoparticles are small excerpts from a metal lattice, with a central atom surrounded by coordination spheres with icosahedral or anti-icosahedral symmetry. This corresponds to a closest packed structure. It was proved, that this model reflects in the increased stability of clusters with a certain number of atoms, the so called

magic numbers. Gold clusters with 13, 55, 147 etc. atoms were found to be particularly stable [101, 103].

For nanoparticles, the electronic structure is not the same as in the bulk state. This is an

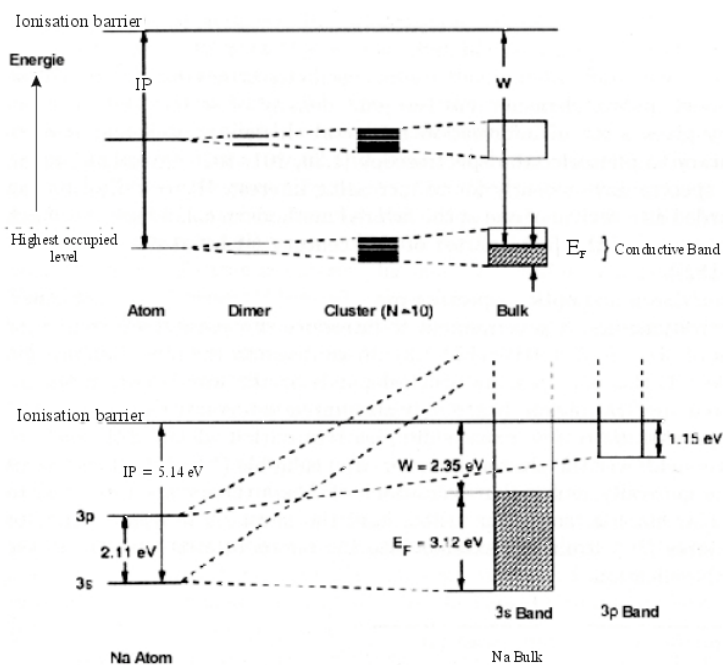
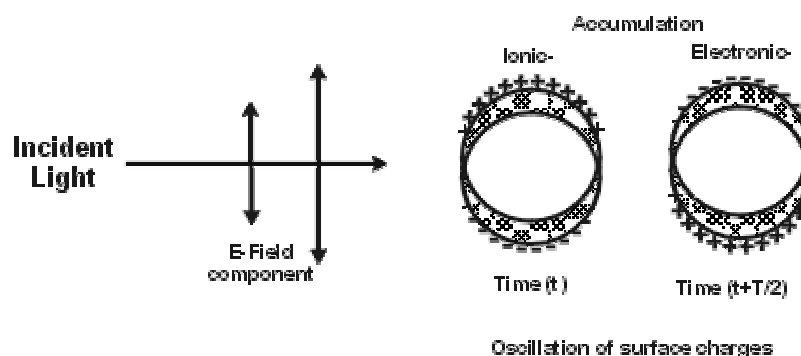


Figure 2-10: Top: Energy level scheme of metals displayed for increasing particle sizes; bottom: Valency electron scheme of sodium displayed for the transition from an atom to the metallic state. In the cluster state, discrete energy levels are still present. IP denotes the ionisation potential,  $E_F$  the Fermi-energy and  $W$  the work function of the electron state. (from [45])

effect called the "size quantisation" [59, 104]. The main point for this behaviour is the difference in splitting of orbitals, when the particle's lattice is built. Because of the limited number of involved atoms, this splitting is ended up before a complete band structure can form. The size quantisation effect is sketched in Figure 2-10. In metals and semiconductors, an electron is more and more entrapped in energy levels, when the particle diameter decreases. This leads to possible new transitions in the lower energy states of the nanoparticles. Practically, one can have a look on the different colour of some semiconductor compounds as a function of the particle diameter. One example is  $\text{Cd}_3\text{P}_2$ , which can be synthesised in almost every colour [45]. Due to the increase of discrete energy levels, the Fermi-energy is shifted towards smaller values. This means especially for metals, that the nobility of metals decrease. A metal nanoparticle gets more non-noble the smaller it is [105, 106]. It has to be denoted, that stabilising ligands around nanoparticles can influence the latter results.

In bulk matter, the free-energy contribution of the surface fraction is negligible because of its small amount. This approach is no more valid for nanoparticles, where the surface to volume ratio can even be bigger than 1. Hence, thermodynamical properties of a certain compound can vary significantly from the bulk state [104]. A systematical research about the melting temperature of gold was done with gold particles down to 2 nm of size [107]. From a value of 1063°C in bulk, the melting point decreases down to less than 350°C with significant decrease for particles with less than 10 nm. Other properties like coordination numbers, electric and magnetic susceptibilities and bond lengths also change compared to the bulk state [101, 104, 108, 109]. An interesting application for the high surface to volume ratio is the use of nanoparticle as active catalytic sites. Although, the regenerativity of the employed particles is still a critical process, first successful catalyses have been made and further development of the particle systems is in progress [66, 110].

The optical properties of metallic nanoparticles are not the same as for the bulk state. It is well known, that e.g. gold in colloidal solution gets colours depending on the particle size, in many cases it has purple colour. This is a fact, which is known already since thousands of years and which was first described by the Mie-theory in 1908 [111]. The reason for the colours is the occurrence of surface plasmon oscillations, whose frequencies are in the visible region of the electromagnetic spectrum. Coloured metal solutions could be observed amongst others with Au, Ag, Cu, while Fe, Co, Ni and Pt do not show colours, because the oscillations are damped away through the particle lattice. A detailed collections of surface plasmon spectra are shown in [112]. The principle of plasmon oscillations is depicted in Figure 2-11.



*Figure 2-11: Excitation of surface plasmons in small particles: Electromagnetic irradiation causes a collective translational excitation of electrons. This leads to an oscillating accumulation of charges on the surface [45].*

The wave length of a plasmon resonance varies with the particle size and the electrons are scattered, if the wave length is bigger than the mean free path of the electrons. Scattering broadens the plasmon band in the UV-VIS-spectrum and lowers its intensity. Because of the dependence of the bands position on the dielectric constant, the medium and the chemical environment of the oscillating particle influences the colour.

For particles, which are not spherical, but anisotropic in one or all dimensions, the Eigenfrequency is split into the components of direction. This leads to two or three different absorption maxima in the plasmon spectrum. With polarised light, the colour of the solution can be changed, depending on the excitation plane used. For control of this property, it is important to have aligned particles in order to keep the orientation in plane. Except for self-assembly of particles, also uni- or biaxial stretching of polymer embedded particles (Ag, Au) could be successfully used to produce foils with polarisation-depending colour[113, 114].

## **2.4 Block copolymers as nanoreactors**

If block copolymer micelles are used for nanoparticle syntheses, the micellar core can be considered as a nanoreactor. The size of a inverse micellar core is in the nanometre scale, typically around 10 to 40 nm. If the reaction takes place inside of the micelle, the micelle can be interpreted as a reactor, with the core-building block represents the wall of the reactor. The reaction runs then in a locally fixed environment. This leads to an excellent control over stability, structuring, conductivity, shape and size of the resulting particles. In the following section, the concept will be focussed on PS-*b*-P2VP and PS-*b*-PEO. Generally, the concept can be expanded for all micelle containing reaction schemes running the same way. For surfactant micelles, the open association principle makes the reactors unstable, so the model is just in approximate agreement.

### *The Concept*

The nanoreactor strategy [115] is a three step process.

- In the first step, the polymeric micelles are formed. Therefore, a selective solvent has to be found, which dissolves the micellar corona and collapses the core. In many applications, reverse micelles are formed in a non-polar solvent, in order to get functional groups into the micellar core.
- Those are needed for the second step, when a precursor component is solubilised into the micellar core. The precursor component mustn't be soluble in the solvent, but has to have a high affinity to the inner block. The procedure of precursor incorporation is called "Loading", the loading factor describes the ratio between bonded precursor and active functional sites in the micellar core. Loading of the micelles usually increases the polarity of the micellar core. Thus, the micelles get stabilised by the precursor incorporation.
- The last step is the transformation of the precursor into the desired nanoparticle material. Here, thermal decomposition and reduction steps are often made, if a metal nanoparticle is desired.

A scheme for the nanoreactor concept is given in Figure 2-12:

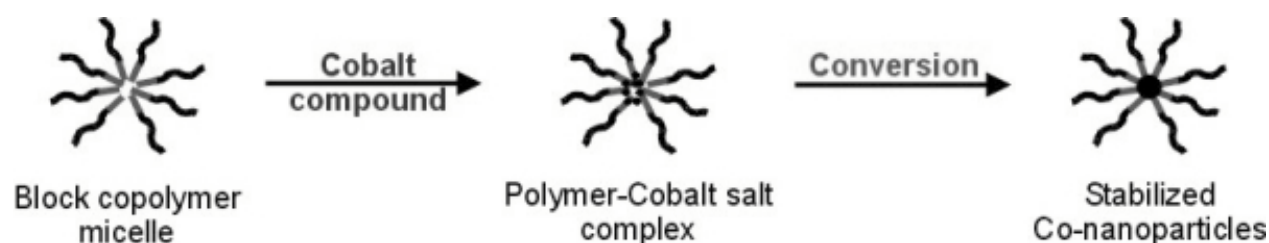


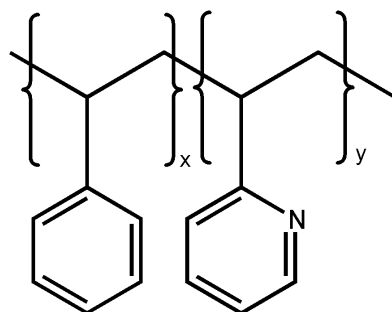
*Figure 2-12: Schematic picture of the nanoreactor concept. The three steps described in the text are presented for the example Cobalt.*

For the right choice of precursor material, the solubility in the solvent is a key step. If the solubility is too high, localisation inside of the micellar core is not possible. Therefore, the conversion step will take place also outside of the micelles and will lead to aggregation. Polar components like salts or complex salts are preferentially used for this purpose. Covalent

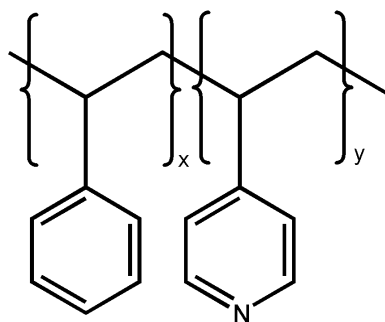
or very stable compounds, like metals, their oxides or polymeric inorganic substances are not used.

### *Poly-vinylpyridines used as micellar reactors*

Poly-(vinylpyridine) is used in two isomeric forms, where the N-atom of the pyridine base is either in 2- or in 4-position to the polymeric backbone. The structure formulas of both polymers are:

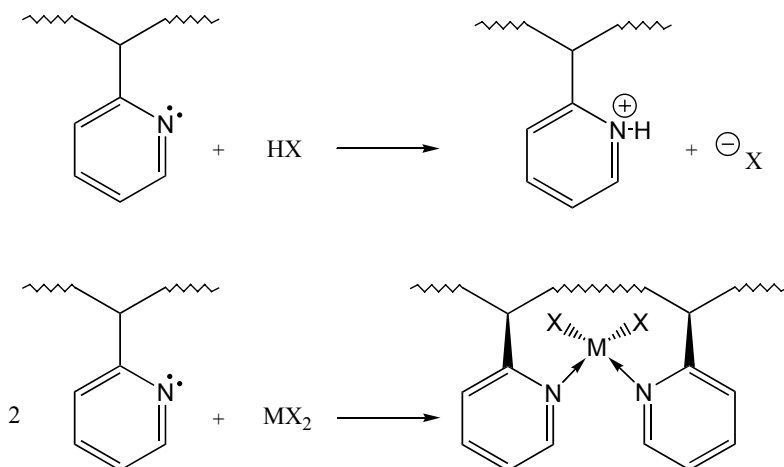


Polystyrene-*block*-Poly(2-vinylpyridine) {P2VP}



Polystyrene-*block*-Poly(4-vinylpyridine) {P4VP}

Using PS-*b*-P2VP as nanoreactor, two types of acid-base reactions can take place with the 2-vinylpyridine units building the micellar core. Either the reaction between precursor and pyridine unit is a protonating acid-base reaction or there is a Lewis-acid-base reaction occurring:



Taking the Pearson acid-base concept as a point of view, the hardness or softness of the corresponding acid-base pairs should be similar, to be able to form a stable micelle-precursor complex. On the other hand it should be not too similar, so that the conversion of the precursor is still possible.

If the loading is a quantitative process, there is a continuous flow of the precursor into the micellar cores. This leads to a homogeneous distribution over all micelles, which is a requirement for the formation of uniform nanoparticles. The loading of the micelles is driven by the added amount of precursor. Varying the loading of the micelle below the maximum capacity of the micellar core, the size of resulting nanoparticles can be influenced by the available amount of matter. Carrying out the conversion reaction, the type of interaction between the formed product and the functional groups of the micellar core is different from that of the loaded micelles. This last step is critical towards micelle stability. In the best case, there is still an attractive interaction between product and micelles. However, also just a kinetic confinement of the product in the micellar cores is possible. Here, a subsequent stabilisation is needed to keep a stable nanoparticle solution. If stabilisation is not effective, the particles will start to ripen or to aggregate after a certain time period. The relaxation time of kinetically confined nanoparticles increases, when the block length (i.e. the degree of polymerisation) of both blocks is increased.

As a model system, tetrachloroauric-(III)-acid ( $\text{HAuCl}_4 \cdot \text{H}_2\text{O}$ ) is used as precursor for gold nanoparticles, which are formed by reduction of the precursor. It was found, that the gold compound is preferentially distributed into the P2VP-phase, when a substrate is covered one half with PS and the other half with P2VP [116]. Heating over the  $T_g$  of P2VP does not take an effect on the particles bound to the P2VP phase.

The auric acid is transferred to gold by reduction. For using the nanoreactor concept, the reducing agent has to be very well soluble in the micellar core with a high selectivity. If an excess of reducing agent is taken, however, the micellar cores are swollen and the micelles are destabilised. The interphase between the incompatible blocks is increased, which is why the system starts to react via coagulation of the micelles to lower this interface. Some of the micellar cores become a reservoir for precursor salt. With this undefined supply of metal salt, the particle sizes gets broader in distribution and the control over the nanoscale reaction is lost. Thus, there is a need to keep stoichiometry or to inactivate the reducing agent after the reaction, when an excess is needed [115]. Another possibility is to take a reducing agent, which is soluble in the outer phase. Anyway, the seed formation starts on the interface between both blocks and the reaction takes place slowly. Under these conditions, intermicellar exchange of precursor is favoured and the particle distribution broadens as well [117].

The usage of either PS-*b*-P2VP or PS-*b*-P4VP makes a difference in reactivity. In P2VP, the hetero-atom is more sterically hindered, compared with P4VP. Thus, protonation or com-



plexing of the precursor is quicker in a PS-*b*-P4VP micellar solution. However, the reduction is not so easy to control, especially concerning the localisation of the particle seeds. Also, often the reaction delivers many small particles inside of the core, which means a quick and quantitative nucleation and almost no seed growth. Overcoming these problems, different metal particles could be synthesised using the PS-*b*-P4VP nanoreactors [117-119].

In PS-*b*-P2VP, semiconductors and silver could be synthesised successfully [120, 121]. The most striking results and the most successful optimisation by means of the nanoreactor concept could be made for the synthesis of gold nanoparticles [122, 123]. Here, the reduction of the  $\text{HAuCl}_4$  is incorporated Ana toluene solution of the block copolymer. Anhydrous hydrazine is taken as reducing agent in a big excess. This is important for a simultaneous nucleation of gold particles and to ensure the formation of one nucleus per micelle. Two things were done to prevent the coagulation of the micelles:

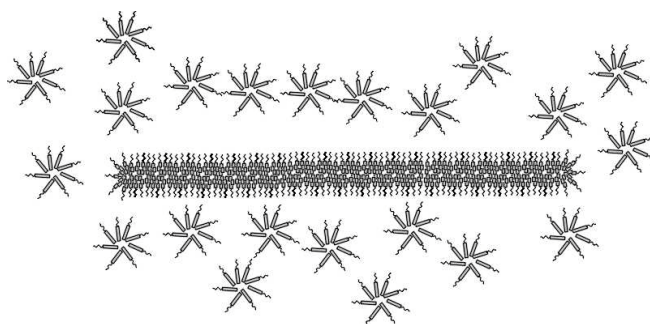


*Figure 2-13: Schematic picture of the formation of metastable micellar wires from spherical micelles during evaporation. The spherical micelles connect just at the thin ends, which leads to axial growth of the cylinders. Some of the presented nanowires had lengths of some hundreds of nanometres. The lateral diameter of this micelles decreases from sterical reasons.*

- Casting a film on a substrate out of the solution. This freezes the coagulation process, because liquid components evaporate quicker than the coagulation takes place. The micellar pattern with the gold particles stays stable, the liquid state is frozen by the film formation.
- Hydrazine is precipitated by addition of a stoichiometric amount of hydrochloric acid (HCl). The so produced precipitate of  $\text{N}_2\text{H}_5\text{Cl}$  is not kept in the micellar core, but precipitates from the solution. It can be removed by a centrifuge. Small amount of excess hydrochloric acid does not destabilise the micelles, because it is protonating the pyridine's N-atom.

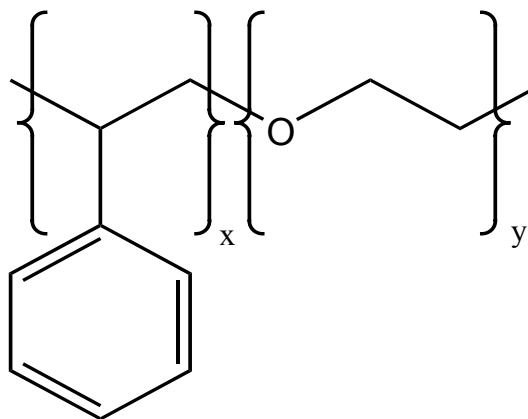
The template function of the block copolymer offers the possibility of variations in the particle's size and shape and the interparticle distance within a casted film. Like shown in Figure 2-13, under certain conditions, cylindrical or worm-like micelles can form out of a block copolymer solution. When crew-cut micelle were used within the nanoreactor concept, spherical micelles were formed first. During the evaporation process, metastable worm-like micelles were observed, which could be frozen by a complete evaporation of the solvent [114, 124]. When the micelles are loaded decently with  $\text{HAuCl}_4$ , these micelles were formed by association of many spherical micelles.

The film formation o micellar solutions containing either precursor or reduced metal nanoparticles was investigated thoroughly [36, 37]. Intermicellar interactions, which were already observed in non-loaded micellar solutions [125], can be frozen by casting a monomicellar film on a substrate. Complete and homogeneous wetting on the substrate results in a hexagonal packing of the micelles, which is the closest packing of spheres in a 2D-system. The loading of a micelle with different amounts of metal salt can change the size of the micellar core. This is because the polarity of the micellar core increases with higher loading, which leads to stretching of the corona-core interface, and thus to an increase of the core diameter

If a  $\text{HAuCl}_4$ -loaded micellar film is put into the electron beam of an electron microscope, the electron beam is able to reduce the precursor to metallic gold [36]. This can be seen by the generation of small dots of increased contrast on electron micrographs. Monomicellar films of structured gold nanoparticles can be used as precursors for lithographic processes [126, 127].

*Other polymeric nanoreactors*

Polystyrene-polybutadiene diblock copolymers were so far not used to incorporate precursors selectively. But a systematical examination was made with polymers, which were modified from a PS-*b*-PB [128]. Here, the double bond of the butadiene units was used for an analogous reaction. Thereby, micelles with different functional groups in the side chain could be synthesised. Micelles could be formed with hydroxy, ester, ether and halogen functionality. A conversion of incorporated metal salts, however, didn't yield the desired results.



PS(x)-b-PEO(y)

A successful variation was done with the use of PS-*b*-PEO block copolymers. This polymer can form stable reverse micelles in unpolar solvents. In micellar solutions, the active binding site is the oxygen atom in the polymer backbone. Protonic acids like  $\text{HAuCl}_4$  can not be used as precursors, because of hydrolytic chain degradation. When instead, a salt like  $\text{LiAuCl}_4$  is used, loading of the micelle takes place. With this polymer, gold and palladium nanoparticles could be synthesised [129]. By reduction of the precursors in the electron beam and subsequent annealing, the great number of nuclei in the micellar core could be joint to a single particle per micelle.

## 2.5 Magnetic nanoparticles

*Magnetism of materials*

An excellent introduction for magnetism and magnetic effects is given in [130].

An electron moving in an orbital causes a magnetic moment. When an orbital is occupied by two electrons, both spin moments cancel each other out. In the case of singly occupied

orbitals, a magnetic moment results from the moving electron. Compounds without unpaired electrons are diamagnetic, compounds with one or more unpaired electrons are paramagnetic. Best examples for paramagnetic compounds are high spin complexes, where the spin moments base on unpaired electrons in orbitals resulting from ligand field splitting. Diamagnetic compounds have a magnetic susceptibility with negative value and do not respond to an external magnetic field. Paramagnetic compounds have positive magnetic susceptibilities and the spins orient into the direction of an external field. Saturation magnetisation, which means complete orientation of the spins, can only be reached by a very strong external field.

The latter magnetic properties can be ascribed directly to the electron structure of the regarded compound. However, there are kinds of magnetism, which occur in the solid state and are originated in a cooperative coupling of neighboured unpaired spins[131, 132]. The coupling of the neighboured spins leads to an effect, called super-exchange and expresses itself in different kinds of macroscopic magnetism. Those are shown in Figure 2-14.

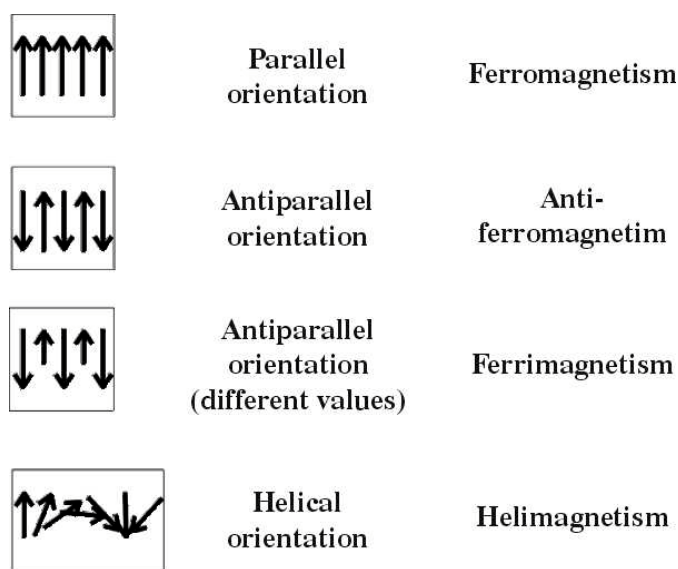


*Figure 2-14: Coupling scheme of neighboured spins in compounds with cooperative magnetism. Orientation and amount patterns of neighbouring spin moments lead to different macroscopic magnetic materials.*

Helimagnetic materials exist among rare earth metals and their compounds. Antiferromagnetism (e.g. FeO, CoO) does not show many differences to diamagnetism. Here, the crystalline lattice is built up by two anti-sense sublattices. Antiferromagnetism can be observed in the transition to paramagnetism at the Néel-temperature[131].

Ferro- and ferrimagnetism is a well-known phenomenon and is used for example in permanent magnets. The main difference between these both sorts of cooperative magnetism is the magnitude of the effect. Ferrimagnets can be compared to antiferromagnets, only the magnitude of the moments in one sublattice is smaller than in the other. This leads to weakening of the parallel coupling. Ferrimagnets often have a spinel-type structure. In ferromagnets, there is a complete coupling in one orientation. This leads to an easy axis inside of a ferromagnetic crystal. The occurring super-exchange leads to an anomalous amplification of the sum of magnetic moments. The magnetisation, which is the sum of magnetic moments per volume unit, is orders of magnitude higher, than it would be expected by addition of electron spin moments.

At room temperature, 4 metals are ferromagnetic (Fe, Co, Ni, Gd), other ferromagnetic compounds are  $\text{CrO}_2$ ,  $\text{CrBr}_3$ , EuO and the alloys  $\text{SmCo}_5$ , Alnico V and Permalloy. Ferromagnetic behaviour is more pronounced at low temperature, because of the low influence of the thermal energy. Above the Curie-temperature,  $T_C$ , the ferromagnetism disappears and the ferromagnets become paramagnetic. At this temperature, the thermal energy perturbs the spin-super-exchange and the coupling disappears.

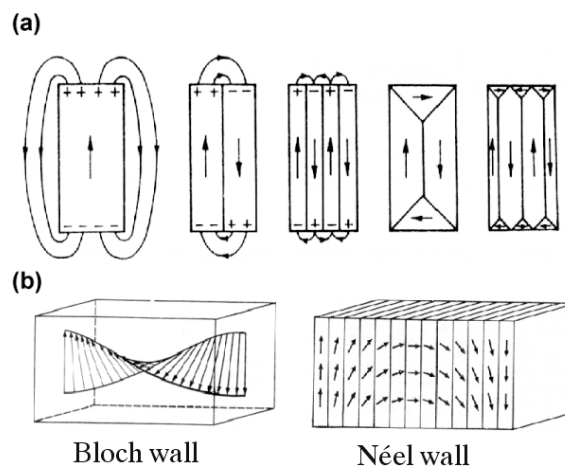


*Figure 2-15: (a) Formation of Weiss-domains in ferromagnetic materials. The external field is lowered by insertion of  $180^\circ$ -domain walls and disappears by additional insertion of perpendicular domain walls. (b) Continuous directional shift of coupled spins forms the structure of domain walls. (from [133])*

Quenching of a magnet from above  $T_C$  will not lead to a permanent magnet. That means, that not all of the spins are arranging in the same direction to get spin coupling. Complete arrangement of spins would cause a high energetic scatter-field. Instead of that, magnetic domains, the so-called Weiss-domains, are formed inside of the crystal. These domains are

arranged anti-parallel or perpendicular to each other (Figure 2-15a) and are separated by so called domain walls (Figure 2-15b). Domain walls mean an energy loss, because spin coupling is revoked throughout the domain walls. However, the internal neutralisation of magnetisations is an overall energetic advantage. Figure 2-16 shows a schematic cross-section of a ferromagnetic bulk material. It can be seen, that the microcrystallites inside of the bulk material also represent "natural" domain walls.

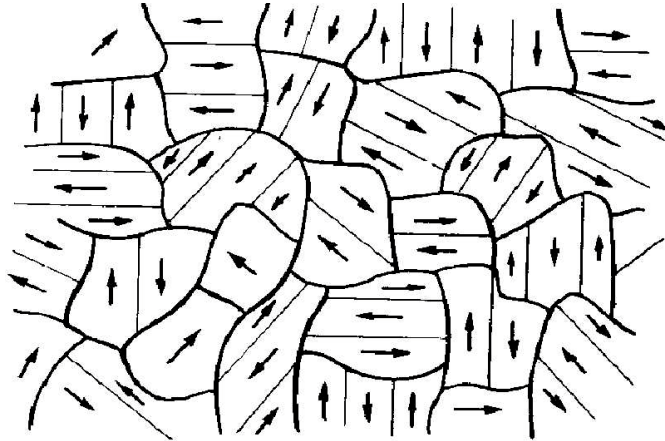


*Figure 2-16: Schematic cross-section through a cross-section of a ferromagnetic material. Grain boundaries act as borders of Weiss-domains [from 130].*

If an external magnetic field  $\mathbf{H}$  is applied to a non-magnetised ferromagnetic materials, the plot of  $\mathbf{H}$  against the magnetisation  $\mathbf{M}$  of the material or the overall field  $\mathbf{B}$ , a hysteresis loop is forming, when the field is varied from  $+H$  to  $-H$  and vice versa. Figure 2-17 shows the onset of a hysteresis loop.

In the onset of Figure 2-17(a) between A and B, domain walls are shifted in order to eliminate unfavourable spin directions. In point B, all the domains are oriented to the easy axis of the crystal. Grain boundaries are shifted under irreversible energy loss by friction, sound and deformation (magnetostriction). Between B and C, the remained domains rotate in field direction until saturation is reached. When the polarity of the external field  $\mathbf{H}$  is reversed, the magnetisation curve follows the course until the applied field goes to zero (D). This point is called the remanence of the material, describing which field remains, when no more field is applied. A remanent field occurs, because of the irreversible character of the magnetisation process. Following the curve, the intersection with the field axis (E) is reached. This point is called the coercivity and denotes the field, which has to be applied to demagnetise the ferromagnet.

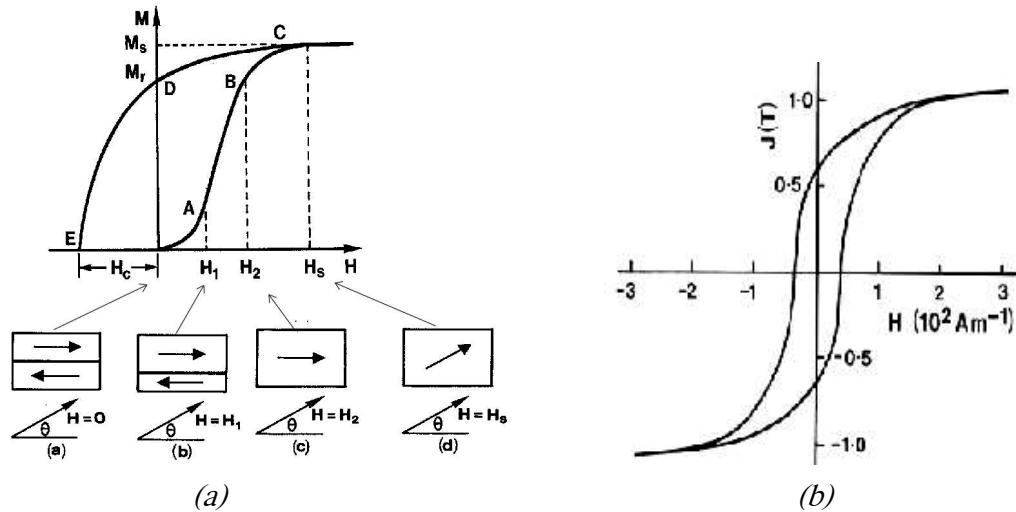


Figure 2-17: (a) Zero-field-cooling (ZFC) of a ferromagnet. Starting from a zero-field, an external field  $H$  is applied and plotted against the magnetisation. The field is first continuously increased until saturation is reached and thereupon reversed.. More see text; (b) Hysteresis loop of a soft magnetic material (68 Permalloy Ni-Fe) (from [134])

Coercivity and remanence are two important values for ferro- or ferrimagnetic materials. Soft magnetic materials, which are often used in microelectronic applications have high remanence but small coercivities, thus thin and high hysteresis loops. On the other hand, permanent magnets have high coercivity and a desired remanence, which defines the strength of the magnet. The remanence is an expression for a kinetically defined non-equilibrium state. Therefore, there is a relaxation time, in which the system can demagnetise. For the most ferromagnetic bulk materials this, however, is in the range of years and more.

### Small particle ferromagnetism

With decreasing particle size, the magnetic properties of ferromagnetic materials start to differ from their bulk properties [135-139]. When the size of a ferromagnetic particle falls below a certain value, the formation of domain walls is no longer favourable. As a consequence, the particle stays one single domain and the considerations for bulk materials cannot be applied to the particle. Spontaneous magnetisation occurs as consequence of the missing Weiss-domains. A critical particle diameter  $d_c$  can be calculated by

$$d_c = \frac{6\sqrt{2}}{D \cdot M_s^2} \cdot \sqrt{\frac{J \cdot S^2 \cdot K_1}{a}} \quad (\text{Eq. 2-2}),$$

where  $D$  is the demagnetisation factor,  $M_s$  the saturation magnetisation,  $J$  the exchange Integral,  $S^2$  the product of the spin vectors,  $K_1$  the first anisotropy constant and  $a$  the lattice constant. Following equation 2-2, for iron a mean critical diameter of 47 nm was calculated [139]. An array of magnetic nanoparticles forms associates of dipoles described by the chain of spheres-model [140, 141]. Its magnetisation can be described as:

$$\frac{M}{M_{\text{Sat}}} = \coth\left(\frac{\mu \cdot H}{k \cdot T}\right) - \frac{k \cdot T}{\mu \cdot H} \quad (\text{Eq. 2-3}),$$

where  $M$  and  $M_{\text{Sat}}$  are magnetisation and saturation magnetisation, respectively,  $kT$  is the thermal energy,  $H$  the external field and  $\mu$  the magnetic moment of the particles. In single-domain particles, super-exchange coupling is still present. This leads to a high magnetic moment of the particles. Due to the missing arrays of magnetic domains, however, magnetic nanoparticles do not show hysteresis in general. Just, when the thermal energy is low or the particle size is big enough, the fluctuation of the easy axes of the particles is blocked. In this case, the particles behave like usual ferromagnets.

In the other case, i.e. higher temperatures and small particle sizes, the particles are in the superparamagnetic state. No hysteresis loop occurs in the magnetisation curve, because the particles are mobile enough for relaxational response. Still, the magnetic moments are very high, and the magnetisation curve resembles those of paramagnets. The main difference is, that saturation is reached with lower external magnetic fields and hysteresis can be reached by lowering the temperature.

The Curie-temperature exists for single-domain particles and a transition can be observed, when the coupling between neighbouring spins disappears. Compared with the bulk-values, the Curie-temperature is around 10% lower [139].

The temperature, at which a particle changes from the ferromagnetic to the superparamagnetic state is called the blocking temperature  $T_B$ . The blocking temperature is also influenced by the systems' kinetics and the time, which is needed to get the particles into equilibrium [142]. The relaxation time  $\tau$  for this process is depending on the type of measurement, which is used to determine a magnetisation curve. If  $\tau$  is smaller than the duration of the experiment, the particles will relax during the measurement and not show hysteresis. For example in SQUID-magnetometry, a measurement lasts at least minutes, while in Möss-



bauer-spectroscopy the measurement duration is in the range of femtoseconds. This means, that in the latter, superparamagnetism appears at lower temperature and smaller particles. The relaxation time  $\tau$  can be calculated by:

$$\frac{1}{\tau} = f_0 \cdot \exp\left(\frac{-E_B}{k \cdot T}\right) \quad (\text{Eq. 2-4}),$$

where  $f_0$  is the Larmor-frequency and  $E_B$  the energy barrier to be crossed for shifting the easy axis. The ferromagnetic character disappears in particles smaller than 3 nm due to missing spin coupling.

### *Synthesis of magnetic particles in micelles and polymers*

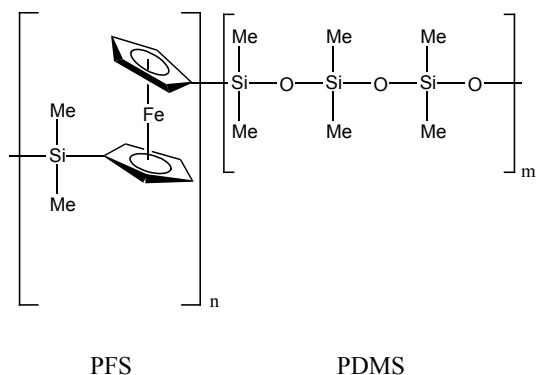
Ferro- and ferrimagnetic nanoparticles were a focus for synthetic approaches in the past decade. Due to the better availability, synthesis of ferrimagnetic oxides was preferred. Synthesis of metallic or alloy nanoparticles always involve the risk of subsequent oxidation. Especially when small particles are the desired product, quantitative oxidation can take place and thwarts the intention of magnetic nanoparticle synthesis.

Low molecular surfactants were often used to synthesise  $\gamma\text{-Fe}_2\text{O}_3$  nanoparticles, which are superparamagnetic [143-145]. As micellar compound, AOT and methyl-hydroxylamine were used, respectively. Particles of 3-10 nm in size were obtained. Spinel-type ferrites could be synthesised using AOT as surfactant [146]. The size of the cobalt ferrite particles was 2-6 nm, they showed superparamagnetic behaviour. By variation of the reaction path, partially anisotropic particles were obtained [147]. AOT was also used as nanoreactor to reduce Co-(II)-compounds to metallic cobalt nanoparticles [148-150]. An extraordinary route for localisation was used recently in a salt occlusion method [151]. Nanoimprint lithography was used to pattern nickel by electroplating [152].

Polymers were used frequently as protecting agents for magnetic nanoparticle synthesis [67, 153-155]. However, the polymeric matrix can influence the magnetic properties [156, 157]. A route for magnetic nanoparticles is the use of metal-ion containing monomers and subsequent thermolysis of the products. Ferromagnetic cobalt ferrite of 8 nm size was formed by statistical copolymerisation of cobalt- and ferrous acrylates [158].

By use of living anionic ring opening polymerisation, anisotropic iron nano-worms could be formed [159-161]. Ferrocenyl-dimethylsilane was copolymerised with dimethylsiloxane to form PDMS-*b*-PFS block copolymers. This block copolymer forms worm-like micelles in

unpolar solvents. In TEM, the iron atoms are responsible for an amplified contrast of the polymers and the ferrocenyl-containing blocks are visualised. The polymer cylinders are organising in lamellae, where each cylinder has around 70 nm in diameter and 400 nm in length. Iron nanoparticles are formed, when the organic components are pyrolysed. The particles show superparamagnetic behaviour.



The first systematic research in narrowly distributed magnetic nanoparticles was done with cobalt particles synthesised in the presence of functionalised statistic copolymers [162, 163]. Spherical cobalt nanoparticles with sizes between 5 and 70 nm were obtained, which formed chains due to magnetic dipolar interactions. As starting material,  $\text{Co}_2(\text{CO})_8$  was used, to be thermally decomposed within the solutions. The solutions varied in added polymer, solvent and the amount of  $\text{Co}_2(\text{CO})_8$  used. Best results were obtained with long-chain polymers with unpolar backbone and altering polar side chains, like poly(methylmethacrylate-*co*-ethylacrylate-*co*-vinylpyrrolidone). The vinylpyrrolidone groups are the nucleating size and their concentration within the polymer rule the resulting size of the nanoparticles. The polymer has to be the only binding site for the cobalt nuclei, which excludes the use of polar solvents and good solubility of  $\text{Co}_2(\text{CO})_8$  in the solvent. Using poly(acrylnitrile)-*co*-poly(methylenesuccinic acid), similar results could be reached in DMF at elevated temperatures [164].

An analogous approach to iron particles was made using polystyrene-*co*-poly(2-vinylpyridine) in unpolar solvents [165, 166]. Due to the higher stability of  $\text{Fe}(\text{CO})_5$  towards thermal decomposition, a high-boiling solvent has to be used. The work had to be carried out under strict exclusion of air and water, because the iron particles are extremely sensitive towards oxidation. By exposure to oxygen, controlled oxidation was carried out under formation of iron oxides. The initial experiment yielded stable systems of monodisperse Fe-nanoparticles of 5 to 20 nm in size. Smaller particles showed superparamagnetic behaviour, while the bigger formed chains of particles shown in Figure 2-18.

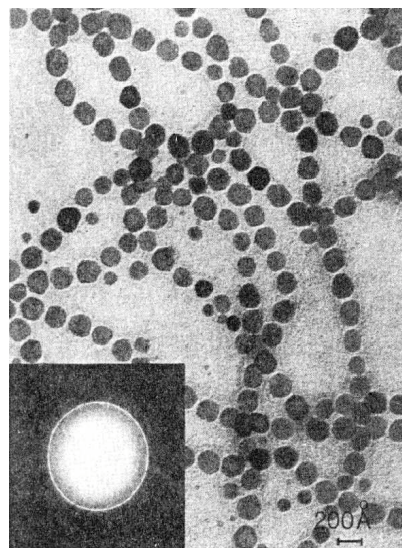


*Figure 2-18: Chains of spherical Fe-nanoparticles from [165]. Particles were made from  $\text{Fe}(\text{CO})_5$  in *o*-dichlorobenzene. In the left corner, an electron diffraction pattern is shown.*

Using the nanoreactor concept with PS-*b*-P4VP-micelles, experiments using  $\text{Co}_2(\text{CO})_8$  and  $\text{CoCl}_2$  were carried out in order to obtain Co-nanoparticles [117, 167].  $\text{Co}_2(\text{CO})_8$  was thermally decomposed, while  $\text{CoCl}_2$  was reduced by lithium-triethylborohydride (i.e. super hydride). Toluene and THF were used as solvents, where the polymer forms micelles and the precursors are bound to the micellar core.  $\text{Co}_2(\text{CO})_8$  was partially dissolved in the solvents and didn't yield uniform particles. Anhydrous  $\text{CoCl}_2$  led to very small particles with a size below 1 nm. When a film was casted from the solution and annealed, particles of 3-5 nm in diameter could be obtained. At loadings of  $L=1$ , the approach with  $\text{Co}_2(\text{CO})_8$  led to 10 nm spherical particles inside of the micellar cores, whereas outside of the micelles cubic particles were formed.

## 2.6 References

- [1] H.D. Dörfler, *Grenzflächen- und Kolloidchemie*, VCH Verlag, Weinheim, 1994.
- [2] S. Friberg, P. Bothorel (eds.), *Microemulsions: Structure and dynamics*, CRC Press, Boca Raton, 1986.
- [3] H. Hoffmann, W. Ulbricht, *Chem. unserer Zeit*, 1995, 29, 76.
- [4] J.N. Israelachvili, D.J. Mitchell, B.W. Ninham, *J. Chem. Soc. Faraday Trans. 2*, 1976, 72, 1525.
- [5] D.A. Shipp, J.L. Wang, K. Matyaszewski, *Macromolecules*, 1998, 31, 8005.
- [6] M. Sawamoto, J.P. Kennedy, *J. Macromol. Sci. Chem.* 1982, 18, 1293.
- [7] N. Hadjichristidis, H. Iatrou, S. Pispas, M. Pitsikalis, *J. Polym. Sci. A*, 2000, 38, 3211.
- [8] S. Förster, M. Antonietti, *Adv. Mater.* 1998, 10, 195.
- [9] R.A. Brown, A.J. Masters, C. Price, X.F. Yuan, *Chain segregation in block copolymers*, in: Allen, Bevington, Booth, Price (eds.), *Comprehensive Polymer Science Vol.2: Polymer properties*, Pergamon Press, Oxford, 1989, 155.
- [10] L. Leibler, *Macromolecules*, 1980, 13, 1602.
- [11] F.S. Bates, *Science*, 1991, 251, 898.
- [12] F.S. Bates, G.H. Fredrickson, *Annu. Rev. Phys. Chem.* 1990, 41, 525.
- [13] M.W. Matsen, F.S. Bates, *Macromolecules*, 1996, 29, 1091.
- [14] S. Förster, A.K. Khandpur, J. Zhao, F.S. Bates, I.W. Hamley, A.J. Ryan, W. Bras, *Macromolecules*, 1994, 27, 6922.

- 
- [15] K.A. Koppi, M. Tirell, F.S. Bates, K. Almdal R.H. Colby, *J. Phys. II (Paris)*, **1992**, *2*, 1941.
- [16] M.W. Matsen, F.S. Bates, *Curr. Opinion Colloid Interface Sci.* **1996**, *1*, 329.
- [17] G. Riess, G. Hurtrez, P. Bahadur, *Block copolymers* in: Mark, Bikales, Overberger, Menges (eds.), *Encyclopedia of Polymer Science and Engineering Vol.2*, John Wiley & Sons, New York, 2<sup>nd</sup> edition, **1985**, 324.
- [18] Z. Gao, A. Eisenberg, *Macromolecules*, **1993**, *26*, 7353.
- [19] S. Mößmer, *PhD Thesis*, University of Ulm, **2000**.
- [20] T. Odijk, *Curr. Opinion Colloid Interface Sci.* **1996**, *1*, 337.
- [21] F. Lequeux, *Curr. Opinion Colloid Interface Sci.* **1996**, *1*, 341.
- [22] S. Förster, M. Zisenis, E. Wenz, M. Antonietti, *J. Chem. Phys.* **1996**, *104*, 9956.
- [23] M. Moffit, K. Khougaz, A. Eisenberg, *Acc. Chem. Res.* **1996**, *29*, 95.
- [24] Z. Tuzar, P. Kratochvil, *Adv. Colloid Interface Sci.* **1976**, *6*, 201.
- [25] H.G. Elias, *Makromoleküle Vol.1*, Ed. Hüthig & Wepf, Basles, 5<sup>th</sup> ed. **1990**.
- [26] I. Astafieva, X.F. Zhong, A. Eisenberg, *Macromolecules*, **1993**, *26*, 7339.
- [27] K. Khougaz, Z. Gao, A. Eisenberg, *Macromolecules*, **1994**, *27*, 6341.
- [28] J.R. Quintana, M. Villacampa, I.A. Katime, *Macromolecules*, **1993**, *26*, 606.
- [29] D. Nguyen, C.E. Williams, A. Eisenberg, *Macromolecules*, **1994**, *27*, 5090.
- [30] A. Watanabe, M. Matsuda, *Macromolecules*, **1985**, *18*, 273.
- [31] Y. Wang, W.L. Mattice, D.H. Napper, *Langmuir*, **1993**, *9*, 66.
- [32] Y. Xia, J.J. McClelland, R. Gupta, D. Qin, X.M. Zhao, L.L. Sohn, R.J. Celotta, G.M. Whitesides, *Adv. Mater.* **1997**, *9*, 147.

- [33] M. Park, C. Harrison, P.M. Chaikin, R.A. Register, D.H. Adamson, *Science*, **1997**, *276*, 1401.
- [34] P. Mansky, C. Harrison, P.M. Chaikin, R.A. Register, N. Yao, *Appl. Phys. Lett.* **1996**, *68*, 2586.
- [35] T.P. Russell, *Curr. Opin. Colloid Interface Sci.* **1996**, *1*, 107.
- [36] J.P. Spatz, S. Sheiko, M. Möller, *Adv. Mater.* **1996**, *8*, 513.
- [37] J.P. Spatz, M. Möller, M. Noeske, R.J. Behm, M. Pietralla, *Macromolecules*, **1997**, *30*, 3874.
- [38] L. Zhang, A. Eisenberg, *Science*, **1995**, *268*, 1728.
- [39] H.E. Johnson, S. Granick, *Science*, **1992**, *255*, 966.
- [40] J.P. Spatz, A. Roescher, S. Sheiko, G. Krausch, M. Möller, *Adv. Mater.* **1995**, *7*, 731.
- [41] E.L. Thomas, D.J. Kinning, D.B. Alward, C.S. Henkee, *Macromolecules*, **1987**, *20*, 2934.
- [42] H. Yokoyama, T.E. Mates, E.J. Kramer, *Macromolecules*, **2000**, *33*, 1888.
- [43] H. Yokoyama, E.J. Kramer, M.H. Rafailovich, J. Sokolov, S.A. Schwarz, *Macromolecules*, **1998**, *31*, 8826.
- [44] J.P. Spatz, S. Sheiko, M. Möller, *Macromolecules*, **1996**, *29*, 3220.
- [45] U. Kreibig, M. Vollmer, *Optical properties of metal clusters*, Springer Series in Materials Science Vol.25, Ed. Springer, Berlin, **1995**.
- [46] G. Ozin, S.A. Mitchell, *Angew. Chem.* **1983**, *95*, 706.
- [47] G. Schmid, *Chem. unserer Zeit*, **1988**, *22*, 85.
- [48] J.A. Strosio, D.M. Eigler, *Science*, **1991**, *254*, 1319.
- [49] D.M. Kolb, R. Ullmann, T. Will, *Science*, **1997**, *275*, 1097.

- [50] J.H. Fendler, *Chem. Rev.* **1987**, *87*, 877.
- [51] *Oxomolybdates: From Structures to Functions in a new era of Nanochemistry*, in: *The Chemistry of Nanomaterials: Synthesis, Properties and Applications*, Vol. II, C.N. Rao, A. Müller, A.K. Cheetham (eds.), Wiley-VCH, Weinheim, **2004**, 45.
- [52] G. Schmid, *Chem. Rev.* **1992**, *92*, 1709.
- [53] M.T. Reetz, W. Helbig, *J. Am. Chem. Soc.* **1994**, *116*, 7401.
- [54] M.T. Reetz, S.A. Quaiser, *Angew. Chem.* **1995**, *107*, 2461.
- [55] H. Natter, M. Schmelzer, S. Janßen, R. Hempelmann, *Ber. Bunsenges. Phys. Chem.* **1997**, *101*, 1706.
- [56] J.V. Zoval, R.M. Stiger, P.R. Biernacki, R.M. Penner, *J. Phys. Chem.* **1996**, *100*, 837.
- [57] K.S. Suslick, S.B. Choe, A.A. Cichowlas, M.W. Grinstaff, *Nature*, **1991**, *353*, 414.
- [58] Yu. Koltipin, G. Katabi, X. Cao, R. Prozorov, A. Gedanken, *J. Non-cryst. solids* **1996**, *201*, 159.
- [59] A. Henglein, *Chem. Rev.* **1989**, *89*, 1861.
- [60] J.L. Marginier, J. Belloni, M.O. Delcourt, J.P. Chevalier, *Nature*, **1985**, *317*, 344.
- [61] A.L. Jackelen, M. Jungbauer, G.N. Glavee, *Langmuir*, **1999**, *15*, 2322.
- [62] M.K. Chow, C.F. Zukoski, *J. Colloid Interface Sci.* **1994**, *165*, 97.
- [63] J. Turkevich, P.C. Stevenson, J. Hillier, *Discuss. Faraday Soc.* **1951**, *11*, 55.
- [64] T.S. Ahmadi, Z.L. Wang, T.C. Green, A. Henglein, M.A. El-Sayed, *Science*, **1996**, *272*, 1924.
- [65] W. Mahl, *Inorg. Chem.* **1988**, *27*, 435.
- [66] A.B.R. Mayer, J.E. Mark in: *Nanotechnology*, ACS Symposium Series 622, G.M. Chow, K.E. Gonsalvez (eds.), Washington **1996**.

- [67] A.D. Pomogailo, *Russ. Chem. Rev.* **1997**, *66*, 679.
- [68] M.P. Pileni (ed.), *Structure and reactivity in reverse micelles*, Studies in physical and theoretical chemistry Vol.65, Elsevier, Amsterdam, **1989**.
- [69] I. Lisiecki, M.P. Pileni, *J. Am. Chem. Soc.* **1993**, *115*, 3887.
- [70] C. Petit, P. Lixon, M.P. Pileni, *J. Phys. Chem.* **1993**, *97*, 12974.
- [71] J.P. Wilcoxon, R.L. Williamson, R. Baughman, *J. Chem. Phys.* **1993**, *98*, 9933.
- [72] J. Tanori, M.P. Pileni, *Adv. Mater.* **1995**, *7*, 862.
- [73] G. Schmid, G.L. Hornyak, *Curr. Opin. Solid State Mater. Sci.* **1997**, *2*, 204.
- [74] G. Schmid, *J. Chem. Soc. Faraday Trans.* **1998**, 1077.
- [75] Z.L. Wang, *Adv. Mater.* **1998**, *10*, 13.
- [76] C.P. Collier, T. Vossmeier, J.R. Heath, *Annu. Rev. Phys. Chem.* **1998**, *49*, 371.
- [77] M. Antonietti, C. Göltner, *Angew. Chem.* **1997**, *109*, 944.
- [78] G.M. Whitesides, J.P. Mathias, C.T. Seto, *Science*, **1991**, *254*, 1312.
- [79] K. Esumi, K. Matsuhisa, K. Torigoe, *Langmuir*, **1995**, *11*, 3285.
- [80] J. Tanori, M.P. Pileni, *Langmuir*, **1997**, *13*, 639.
- [81] H. Matsui, S. Pan, G.E. Douberly Jr. *J. Phys. Chem. B*, **2001**, *105*, 1683.
- [82] N.R. Jana, L. Gaerheart, C.J. Murphy, *Chem. Commun.* **2001**, 617.
- [83] M.T. Reetz, M. Winter, B. Tesche, *Chem. Commun.* **1997**, 147.
- [84] M.P. Pileni, *Ber. Bunsenges. Phys. Chem.* **1997**, *101*, 1578.
- [85] G. Schmid, N. Beyer, *Eur. J. Inorg. Chem.*, **2000**, 835.
- [86] G. Schmid, M. Bäuml, N. Beyer, *Angew. Chem.* **2000**, *112*, 187.



- 
- [87] P. Eibeck, J.P. Spatz, S. Mößmer, M. Möller, T. Herzog, P. Ziemann, *Nanostruct. Mater.* **1999**, *12*, 383.
- [88] M. Gleiche, L.F. Chi, H. Fuchs, *Nature*, **2000**, *403*, 173.
- [89] A. Ulman, *Chem. Rev.* **1996**, *96*, 1533.
- [90] A.R. Bishop, R.G. Nuzzo, *Curr. Opin. Colloid Interface Sci.* **1996**, *1*, 127.
- [91] K.V. Sarathy, G.U. Kulkarni, C.N.R. Rao, *Chem. Commun.* **1997**, 537.
- [92] W.D. Luedtke, U. Landman, *J. Phys. Chem.* **1996**, *100*, 13323.
- [93] A. Courty, O. Araspin, C. Fermon, M.P. Pileni, *Langmuir*, **2001**, *17*, 1372.
- [94] A. Badia, W. Gao, S. Singh, L. Demers, L. Cuccia, L. Reven, *Langmuir*, **1996**, *12*, 1262.
- [95] M. Brust, D. Bethell, D.J. Schiffrin, C. Kiely, *Adv. Mater.* **1995**, *7*, 795.
- [96] A. Henglein, M. Giersig, *J. Phys. Chem.* **1994**, *98*, 6931.
- [97] F. Henglein, A. Henglein, P. Mulvaney, *Ber. Bunsenges. Phys. Chem.* **1994**, *98*, 180.
- [98] G. Schmid, H. West, J.O. Malm, J.O. Bovin, C. Grenthe, *Chem. Eur. J.*, **1996**, *2*, 1099.
- [99] M. Giersig, M. Liz-Marzán, T. Ung, D. Su, P. Mulvaney, *Ber. Bunsenges. Phys. Chem.* **1997**, *101*, 1617.
- [100] P. Moriarty, *Rep. Prog. Phys.* **2001**, *64*, 297.
- [101] G. Schmid, *Chem. Rev.* **1992**, *92*, 1709.
- [102] H.G. Boyen, G. Kästle, F. Weigl, B. Koslowski, C. Dietrich, P. Ziemann, J.P. Spatz, S. Riethmüller, C. Hartmann, M. Möller, G. Schmid, M.G. Garnier, P. Oelhafen, *Science*, **2002**, *297*, 1533.
- [103] B.K. Teo, N.J.A. Sloan, *Inorg. Chem.* **1985**, *24*, 4545.
- [104] A.P. Alivisatos, *J. Phys. Chem.* **1996**, *100*, 13226.

- [105] W.J. Plieth, *J. Phys. Chem.* **1982**, *86*, 3166.
- [106] W.J. Plieth, *Surf. Sci.* **1985**, *156*, 530.
- [107] P. Buffat, J.P. Borel, *Phys. Rev. A*, **1976**, *13*, 2287.
- [108] G. Schmid, L.F. Chi, *Adv. Mater.* **1998**, *10*, 515.
- [109] S. Krüger, S. Vent, N. Rösch, *Ber. Bunsenges. Phys. Chem.* **1997**, *101*, 1640.
- [110] C. Hartmann, *Thesis*, University of Ulm, **2002**.
- [111] G. Mie, *Ann. Phys.* **1908**, *25*, 377.
- [112] J.A. Creighton, D.G. Eadon, *J. Chem. Soc. Faraday Trans.* **1991**, *87*, 3881.
- [113] Y. Dirix, C. Bastiaansen, W. Cesari, P. Smith, *Adv. Mater.* **1999**, *11*, 223.
- [114] S. Mößmer, *Thesis*, University of Ulm, **1999**.
- [115] M. Möller, J.P. Spatz, *Curr. Opin. Colloid Interface Sci.*, **1997**, *2*, 177.
- [116] M.S. Kunz, K.R. Shull, A.J. Kellock, *J. Colloid Interface Sci.* **1993**, *156*, 240.
- [117] L. Bronstein, M. Antonietti, P. Valetsky in: *Nanoparticles and nanostructured films*, J.H. Fendler (ed.), Wiley-VCH, Weinheim, **1998**, Chapter 7.
- [118] S. Klingelhöfer, W. Heitz, A. Greiner, S. Oestreich, S. Förster, M. Antonietti, *J. Am. Chem. Soc.* **1997**, *119*, 10116.
- [119] M.V. Seregina, L.M. Bronstein, O.A. Platonova, D.M. Chernysov, P.M. Valetsky, J. Hartmann, E. Wenz, M. Antonietti, *Chem. Mater.* **1997**, *9*, 923.
- [120] M. Möller, H. Künstle, M. Kunz, *Synth. Metals*, **1991**, *41-43*, 1159.
- [121] R. Saito, S. Okamura, K. Ishizu, *Polymer*, **1992**, *33*, 1099.
- [122] J.P. Spatz, S. Mößmer, M. Möller, *Chem. Eur. J.* **1996**, *2*, 1552.
- [123] S. Riethmüller, *Thesis*, University of Ulm, **2003**.

- 
- [124] J. P. Spatz, S. Mößmer, M. Möller. *Angew. Chem.* **1996**, *108*, 1673.
- [125] C. Schnee, M. Mirke, M. Schmidt, *Polymer Prepr.* **1994**, *35*, 52.
- [126] J.P. Spatz, S. Mößmer, M. Möller, T. Herzog, H.G. Boyen, P. Ziemann, B. Kabius, *Langmuir*, **2000**, *16*, 407.
- [127] J.P. Spatz, T. Herzog, S. Mößmer, P. Ziemann, M. Möller in: *Micro- and Nanopatterning Polymers*, ACS Symp. Ser. *706*, **1998**.
- [128] M. Antonietti, S. Förster, J. Hartmann, S. Oestreich, *Macromolecules*, **1996**, *29*, 3800.
- [129] J.P. Spatz, A. Roescher, M. Möller, *Adv. Mater.* **1996**, *8*, 337.
- [130] R.P. Feynman, R.B. Leighton, M. Sands, *Feynman Lectures on Physics (bilingual)*, Vol.II, Electromagnetism and Structure of Matter, Oldenbourg, München, 2<sup>nd</sup> edition, **1991**, 137.
- [131] J. Crangle, *The magnetic properties of solids*, Edward Arnold Ltd., London, **1977**.
- [132] S. Jäger, E. Perthel, *Magnetische Eigenschaften von Festkörpern*, Akademie Verlag Berlin, 2<sup>nd</sup> ed. **1996**.
- [133] C. Weissmantel, C. Hamann, *Grundlagen der Festkörperphysik*, Springer, Berlin, 2<sup>nd</sup> ed., **1981**.
- [134] R.A: McCurrie, *Ferromagnetic materials- Structure and properties*, Academic press, London, **1994**.
- [135] C.P. Bean, J.D. Livingston, *J. Appl. Phys.* **1959**, *30*, 120S.
- [136] D.D. Awschalom, D.P. DiVincenzo, *Phys. Today*, **1995**, *(4)*, 43.
- [137] E.P. Wohlfarth in: *Magnetism*, Vol.III, G.T. Rado, H. Suhl (ed.), Academic Press, New York, **1963**, Chapter 7.
- [138] M.A. Howson, *Contemp. Phys.* **1994**, *35*, 347.
- [139] D.L. Beke, *Cryst. Res. Technol.* **1998**, *33*, 1039.

- [140] D. Beischer, A. Winkel, *Naturwiss.* **1937**, *25*, 420.
- [141] R. Pastor-Satorras, J.M. Rubí, *J. Mag. Mag. Mater.* **2000**, *221*, 124.
- [142] S. Mørup, *Europhys. Lett.* **1994**, *28*, 671.
- [143] C.J. O'Connor, Y.S.L. Buisson, S. Li, S. Banerjee, R. Premchandran, T. Baumgartner, V.T. John, G.L. McPherson, J.A. Akkara, D.L. Kaplan, *J. Appl. Phys.* **1997**, *81*, 4741.
- [144] N. Feltin, M.P. Pileni, *J. Phys. IV (Paris)*, **1997**, *7*, C1-609.
- [145] Y. Ahn, E.J. Choi, S. Kim, H.N. Ok, *Mater. Lett.* **2001**, *50*, 47.
- [146] N. Moumen, M.P. Pileni, *Chem. Mater.* **1996**, *8*, 1128.
- [147] N. Duxin, N. Brun, C. Colliex, M.P. Pileni, *Langmuir*, **1998**, *14*, 1984.
- [148] X.M. Lin, C.M. Sorensen, K.J. Klabunde, G.C. Hadjipanayis, *Langmuir*, **1998**, *14*, 7140.
- [149] C. Petit, M.P. Pileni, *J. Mag. Mag. Mater.* **1997**, *166*, 82.
- [150] J.S. Yin, Z.L. Wang, *Phys. Rev. Lett.* **1997**, *79*, 2570.
- [151] I. Hussain, I. Gameson, P.A. Anderson, M. Slaski, P.P. Edwards, A. Dyer, *J. Chem. Soc., Dalton Trans.* **1996**, 775.
- [152] W. Wu, B. Cui, X. Sun, W. Zhang, L. Zhuang, L. Kong, S.Y. Chou, *J. Vac. Sci. Technol. B*, **1998**, *16*, 3825.
- [153] J. Ramos, A. Millán, F. Palacio, *Polymer*, **2000**, *41*, 8461.
- [154] J.P. Stevenson, M. Rutnakornpituk, M. Vadala, A.R. Esker, S.W. Charles, S. Wells, J.P. Dailey, J.S. Riffle, *J. Mag. Mag. Mater.*, **2001**, *225*, 47.
- [155] M. Rutnakornpituk, .S. Thompson, L.A. Harris, K.E. Farmer, A.R. Esker, J.S. Riffle, J. Connolly, T.G. St. Pierre, *Polymer*, **2002**, *43*, 2337.
- [156] D. Yu. Godovski, *Adv. Polym. Sci.* **1995**, *119*, 79.

- [157] F.E. Spada, A.E. Berkowitz, N.T. Prokey, *J. Appl. Phys.* **1991**, *69*, 4475.
- [158] A.S. Rozenberg, E.I. Aleksandrova, G.I. Dzhardimalieva, N.V. Kir'yakov, P.E. Chizhov, V.I. Petrinov, A.D. Pomogailo, *Russ. Chem. Bull.* **1995**, *44*, 858.
- [159] P. Nguyen, P. Gómez-Elipe, I. Manners, *Chem. Rev.* **1999**, *99*, 1515.
- [160] J.A. Massey, K.N. Power, M.A. Winnik, I. Manners, *Adv. Mater.* **1998**, *10*, 1559.
- [161] J.A. Massey, K.N. Power, I. Manners, M.A. Winnik, *J. Am. Chem. Soc.* **1998**, *120*, 9533.
- [162] J.R. Thomas, *J. Appl. Phys.* **1966**, *37*, 2914.
- [163] P.H. Hess, P.H. Parker Jr. *J. Appl. Polym. Sci.* **1966**, *10*, 1915.
- [164] L.M. Bronstein, P.M. Valetsky, S.P. Solodovnikov, R.A. Register, *Macromol. Symp.* **1996**, *106*, 73.
- [165] C.H. Griffiths, M.P. O'Horo, T.W. Smith, *J. Appl. Phys.* **1979**, *50*, 7108.
- [166] T.W. Smith, D. Wychick, *J. Phys. Chem.* **1980**, *84*, 1621.
- [167] O.A. Platonova, L.M. Bronstein, S.P. Solodovnikov, I.M. Yanovskaya, E.S. Oblonkova, P.M. Valetsky, E. Wenz, M. Antonietti, *Colloid Polym. Sci.* **1997**, *275*, 426.



# *Generation of cobalt nanoparticles in surfactant stabilised systems*

## 3.1 Introduction

Recently, much effort has been devoted to the controlled synthesis of nanometre-size metallic particles. Indeed, the study of their novel properties resulting from surface or quantum size effects is of both fundamental and pressing technical interest [1]. In particular, nanoparticles of magnetic materials have attracted considerable and increasing attention due to their potential applications in very demanding fields such as magnetic storage technology [2].

Among the various methods to prepare metallic particles, the solution-phase metal salt reduction has the advantage to produce high amount of colloids which can be further handled for different purposes. However, the reducing agent is often an additional contamination source of the final metal [3, 4]. The decomposition of metal carbonyl complexes is thus an interesting alternative which has been used since many years to produce various metals (mainly Fe, Ni, Co) [5]. The decomposition can be induced either by ultrasounds or by pyrolysis. Pyrolysis allows the formation of crystalline solids [6, 7], while the ultrasonic procedure produces amorphous materials [8-10]. The synthesis of Co nanoparticles starting from the cobalt carbonyl complex is thus quite attractive.

Moreover, the control of the particles size and size-distribution is of main importance because of the size dependence of the particles properties. Monodisperse solutions are required for that reason. In addition, the colloidal solution has to be stable enough towards

aggregation in a system where the forces between the particles can be quite large (strong magnetic interactions). Different methods appear in the literature, which allow the preparation of nanometre-sized particles of controlled diameter, i.e. in inverse microemulsions [11], with block-copolymers micellar solutions as microreactors [12, 13], or in presence of surfactants [14-17]. The organic component of these systems (surfactant or block copolymer) plays a major role in the control of the size, the size distribution and the stability of the nanoparticles dispersion. Depending on the system, suspension in water or hydrophobic organic solvent can be achieved. Particularly, the use of block copolymers has the unique ability to generate quasi-regular arrays of the nanoparticles included in the micellar core by simple self-assembly of the diblock copolymer and deposition of micellar monofilms onto surfaces.

This chapter aims in reporting on the use of commercially available surfactants in small amounts to prepare monodisperse colloidal solutions of Co nanoparticles of controlled size. Various surfactants or mixtures of them have been tested in order to control the particles growth and the suspension stability. The synthetical route of pyrolysis of  $\text{Co}_2(\text{CO})_8$  was chosen in order to have a suitable precursor for Co particle formation. A special stress is given towards a broad range of interacting functional groups towards the particles surface. It is well known, that particle size and shape is driven by this specific interaction [18-20]. For this work, spherical particles in a size range between 4 and 15 nm were the main goal. In this size range, magnetic effects in the nanoscale are very sensitive to small changes of the particle diameter. To get the greatest benefit of colloidal cobalt solutions both, the ferromagnetic and the superparamagnetic regime, are of interest. Ferromagnetic fluids should combine permanent magnetic moments in the nanometre-range and the liquid state depending on the thermal state, whereas superparamagnetic fluids are showing their strong magnetic moments just when being influenced by an external field.

To achieve the best results for both, particles of tuneable size and a reproducible experimental environment, this chapter represents mainly the monitoring of many different surfactant systems as first step towards further modification of the synthetic procedure and examination of the main properties of the systems, which is shown in Chapter 4.



## 3.2 Experimental

### *Chemicals*

Cobalt carbonyl ( $\text{Co}_2(\text{CO})_8$ ), an orange solid (Fluka, 95% stabilised with n-hexane), was stored at  $-20^\circ\text{C}$  and has been used as received. Oleic acid (OA) (Acros, 97%) was dried by toluene azeotropic distillation and bis-(2-ethylhexyl)sulfosuccinate sodium salt (AOT) (Fluka) by overnight heating at  $80^\circ\text{C}$  in a vacuum. Both products were stored in a nitrogen filled glove-box, where the water and oxygen contents were kept below 1 ppm. TOPO (Aldrich, 99%), TDS (ChemService >95%) and Decanol (Aldrich, 99%) were used as received. Mesitylene and toluene have been dried three days over  $\text{LiAlH}_4$  and distilled twice at  $60^\circ\text{C}$  under dynamic vacuum, further condensed below room temperature in a high vacuum line under dynamic conditions using an oil diffusion pump. The latter process was carried out using Trioctyl-aluminium as drying agent.

### *Synthesis procedure*

In order to avoid any traces of oxygen, all syntheses were performed in a 10 mL glass tube, where the solution has been degassed via three freezing-evacuation-melting cycles by means of a high vacuum line. The tube was filled with the surfactants, the cobalt carbonyl complex and the solvent inside of the glove-box and then connected to the high vacuum line. All glassware used for the high-vacuum procedure, including this tube, was heated in an oven at  $230^\circ\text{C}$  for some days. The whole high-vacuum apparatus was dried with a hot gun prior to use under dynamic vacuum in order to remove water traces on the glass surfaces. The solution was frozen in liquid nitrogen and the tube was evacuated. The connection towards the pump is closed and the solution is allowed to warm up to ambient temperature. This operation was repeated until no gas evolution could be observed anymore (this state was reached usually after three cycles). The tube was finally closed under vacuum, immersed in a silicone bath heated at  $170^\circ\text{C}$  and kept at this temperature for 20 minutes. After cooling to room-temperature, the tube was again transferred into the glove-box for sample preparation.

### *Electron microscopy*

**Transmission electron microscopy (TEM)** images were recorded with a Philips EM 400 T microscope operating at 80 kV. Copper grids (mesh size:  $200 \times 200 \mu\text{m}^2$ ) were coated with a Formvar film (around 20 nm thickness) and a layer of carbon (approximately 5 nm thickness) and used as substrates for TEM analysis. The samples were prepared by evaporating a droplet of the solutions on the grid, which was in contact with a soaking tissue in order to avoid multilayer formation.

**High-resolution TEM (HRTEM)** images were recorded with a CM 200 FEG (CS corrector) on a holey-copper grid, where a drop of the colloidal solution was evaporated in the way described above. Sample preparation was carried out inside of the glove-box. EDAX analyser coupled with HRTEM gives the semi-quantitative composition of the samples. Upon transfer of the samples inside the microscope, contact with the air cannot be avoided completely. Negatives were scanned on an Umex Astra scanner operating at 600 dots per inch (dpi) using constant picture sizes. Adobe Photoshop 5.5 was used for evaluation particle sizes and distances.

## **3.3 Results and discussion**

In order to get a well-defined colloidal solution of Co nanoparticles, the surfactant has to play mainly two functions. First, it has to control the formation and the growth of the nuclei formed during the first stages of the heating in order to get a monodisperse system. On the other hand, it has to stabilise the particles against aggregation to avoid precipitation of not dispersible aggregates. The surfactant has to regulate the kinetics of the metal growth so that the nucleation is faster than the growth of the nuclei, in these conditions monodispersity can be achieved. Rapid heating of the solution is thus required to induce the pyrolysis of the complex and fast formation of the nuclei. The subsequent adsorption of the surfactant to the nuclei surface allows one to regulate the growth rate of the nanocrystals.

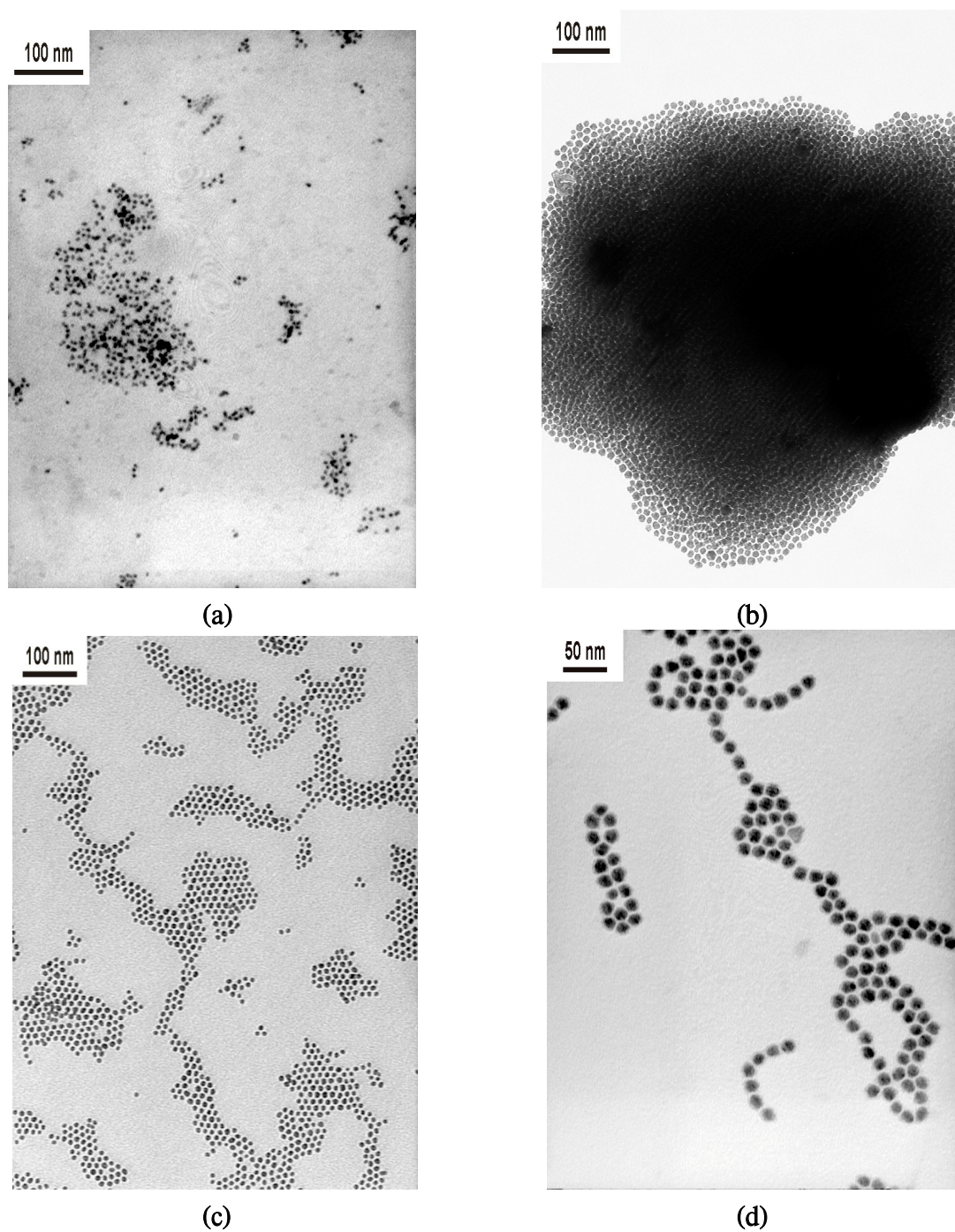


*Figure 3-1: TEM images of Co particles formed in presence of :*

- a) AOT (16 mg: entry 1, Table 3-1)*
- b) AOT (9 mg: entry 2, Table 3-1) directly after synthesis*
- c) after addition of oleic acid (6  $\mu$ l) to b)*
- d) same as in c) with other magnification*

When the cobalt carbonyl complex (160 mg) is thermally decomposed (20 min, 170 °C) in a mesitylene solution (2 mL) containing AOT (16 mg) as unique surfactant, a suspension of 6 nm diameter particles is obtained (Figure 3-1a). However, when the cobalt to surfactant ratio is increased in order to get bigger particles, the previously orange solution becomes colourless upon heating and a magnetic black precipitate is formed. Figure 3-1b shows the TEM analysis of this black solid. Clearly, the solid is built by the aggregation of 10 nm diameter particles. The AOT surfactant is thus able to control the growth of the nuclei and allows the formation of nanoparticles.

However, this surfactant is not efficient enough to compensate the interactions between the particles when these become bigger, so that aggregation occurs at the end of the process.

In order to avoid this aggregation, oleic acid which has a longer alkyl chain than AOT and is well-known to interact strongly with Co, is then added to the black solid in presence of mesitylene. The flask is firstly immersed in an ultrasound bath for 15 min, then heated at 150 °C for another 15 min in order to redisperse the nanoparticles. Indeed, a black suspension is obtained, from which one drop has been evaporated on a TEM grid (Figure 3-1c and 3-1d). Oleic acid is very efficient for particles stabilisation since aggregates are no more observed on the TEM grid. A monolayer of hexagonal packing of particles is rather formed. In addition, at the locations where the particles are less densely packed, strings and rings organisation of the nanoparticles are observed, typical arrangements for magnetic interacting particles. It is also interesting to note that since directly after synthesis, the particles aggregates precipitate in the bottom of the flask, the mesitylene can be easily separated from the solid and Co nanoparticles suspensions can be prepared in various solvents. For example, toluene solutions can be available, even if this solvent is not suitable for the particles synthesis due to its low boiling temperature. A summary of key experiments made is given in table 3-1.

Since oleic acid appears to prevent the aggregation of the particles, it has been substituted to AOT for the Co synthesis. However, in this case, well-defined particles are not obtained, the interaction between the Co nuclei and the surfactant are too strong, which precludes the particles growth.

A successful synthesis of nanoparticles has been reached by using a mixture of both surfactants. The effect of various parameters on the particle formation and size has then been studied by using mixtures of oleic acid and AOT surfactants. The results are summarised in Table 3-1 (entry 4-11). In each experiment, after 20 min of heating, the initially orange solution turned black. Keeping the cobalt carbonyl concentration constant, the ratio of both

*Table 3-1: Experimental conditions for the synthesis of Co nanoparticles*

No.	Co <sub>2</sub> (CO) <sub>8</sub> [mg]	AOT [mg]	OA [ $\mu$ l]	Solvent [mL]	T [°C]	Particles size [nm]
<b>1</b>	160	16	-	Mesitylene, 4	170	6
<b>2</b>	125	9	-	Mesitylene, 2	170	10 Aggregation
<b>3</b>	125	-	6	Mesitylene, 2	170	No particles
<b>4</b>	125	6	2	Mesitylene, 2	170	10
<b>5</b>	125	3	4	Mesitylene, 2	170	11
<b>6</b>	200	6	2	Mesitylene, 2	170	12
<b>7</b>	500	6	2	Mesitylene, 4	170	No particles
<b>8</b>	25	6	2	Mesitylene, 4	170	7
<b>9</b>	125	6	2	Mesitylene, 2	110	No particles
<b>10</b>	86	15	26	Mesitylene, 2	170	No particles
<b>11</b>	125	6	2	Mesitylene, 4	170	10

surfactants can be varied with only low influence on the particles size (see Table 3-1, entry 4 and 5 - Figure 3-2a and b. The particles size is more dependent on the cobalt carbonyl to surfactant molar ratio (see Table 3-1 entry 4, 6 and 8 – Figure 3-2b and c. When this ratio is decreased from 20 to 4, the particle size decreases significantly from 12 to 6 nm. If a too large amount of surfactants is used (see Table 3-1, entry 10), no particles are obtained. Achieving bigger diameters for Co particles is impeded, because of the solubility limit of the cobalt complex in the medium (Table 3-1 entry 7). When 500 mg of cobalt complex are used, parts of the complex remain insoluble and after heating only big irregular structures are formed.



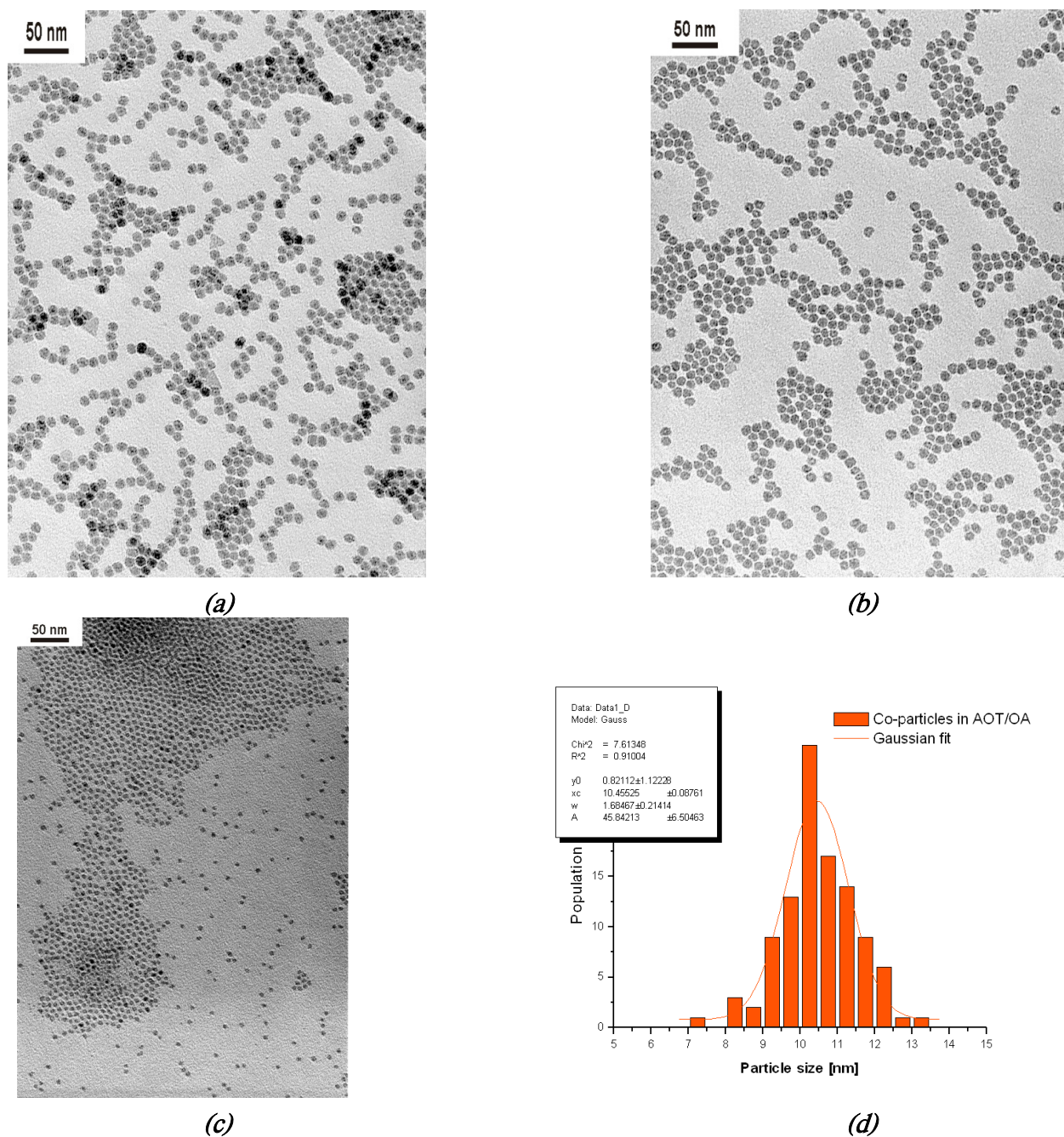


Figure 3-2: TEM images of Co-particles formed in a mixture of AOT and oleic acid. The molar ratios of each experiment is denoted.

a) AOT/OA = 0.5 and Co/surfactants  $\sim 20$ ; table 3-1 entry 4.

b) AOT/OA = 2 and Co/surfactants  $\sim 20$ ; table 3-1 entry 5.

c) AOT/OA = 2 and Co/surfactants  $\sim 4$ ; table 3-1 entry 8.

d) Particle size distribution for Figure 3-2b)

The measurement of the size and the size distribution (see Figure 3-2d) gives a mean particle size of 10.5 nm for the sample corresponding to Table 3-1, entry 4, with a standard deviation of 0.8 nm, which corresponds to a percentual value of 8.0 %. This value lies in the regime between 5 and 10% of standard deviation. This range is often given as the narrow size distribution regime [21, 22]. More narrow size distributions only can be achieved by further size selection by special techniques developed for nanoparticles like size selective precipitation or digestive ripening [23, 24]. Thus, the achieved distribution is narrow, but can be optimised using a fine tuning of syntheses parameters. This subject will be resumed in the following chapter of this thesis.

The conditions described so far (i.e. low concentrations of AOT and OA), which have allowed us to prepare Co nanoparticles with sizes between 5 and 12 nm, have been compared to conditions recently published by Puentes et al. [19], where particles of 16 nm diameter have been obtained. In that work, TOPO (Trioctyl-phosphine oxide) is used as surfactant in rather high concentrations (0.1 g of TOPO combined with 0.2 mL oleic acid for 0.5 g of  $\text{Co}_2(\text{CO})_8$ ). The experiments are carried out at higher temperature with *o*-dichlorobenzene as a solvent (182°C boiling temperature). These conditions when transposed to our experimental procedure (Table 1 entry 10), prevent the formation of particles. Stronger interactions between Co and TOPO as compared to AOT, slower surfactant exchange dynamics in the less polar solvent and the lower temperature might be an explanation for the observed different behaviour.

When the solution was diluted, keeping the Co to surfactant ratio constant, the particle size was not affected. A twice diluted solution, compared to the concentration used in the most experiments, still allows control over particle formation (Table 1 entry 4 and 11). This important observation opens the way to the preparation of bigger size particles, since the content of the solution in cobalt carbonyl can now be increased further.

Finally, the decomposition temperature is revealed to be a determinant factor. At 110 °C, the boiling temperature of toluene, no particles have been formed. All the collected observations with this first system, i.e. AOT/OA, are in accordance to the mechanism previously proposed by LaMer for the formation of well-defined monodisperse nanoparticles [25]. At experimental conditions, the surfactant concentration is around 0.01 M so above the cmc of the surfactants and in addition, the solubility of the  $\text{Co}_2(\text{CO})_8$  complex is not negligible in the high boiling-point solvent (mesitylene). Thus, in the starting solution, surfactant micelles are formed and cobalt carbonyl is distributed both inside the hydrophilic micellar core (high concentration) and outside the micelles in solution in mesitylene (lower

concentration). By rapid rising of the temperature, nucleation occurs by thermal decomposition of the cobalt carbonyl dissolved inside the micelles of surfactant, where its concentration is the highest. Then, the local concentration inside the micelles decreases and the growth of the particles starts by continuous diffusion of the cobalt carbonyl from the solution to the surface of the nuclei.

Aggregation of the nuclei or Ostwald ripening processes are avoided by the surfactant. The surfactant located at the surface of the nuclei controls the growth rate. When a surfactant is used, that interacts too strongly with the cobalt surface, such as oleic acid, the growth is slowed down too much and particles are not obtained. When AOT as surfactant is present, an equilibrium between surfactant monomers linked to the particle surface and free in solution exists which allows the growth of the nuclei. When AOT is used alone, particles are formed, but the hydrophobic repulsions between the short alkyl chains are not strong enough to stabilise highly interacting magnetic particles (i.e. big size Co particles). The mixture of both surfactants conjugates the high stability of the particles by the long C17-alkyl chains of OA with the fast dynamic exchange of AOT, which is necessary for the particles growth.

*Table 3-2: Use of various surfactants for the synthesis of Co nanoparticles.*

	<b>Co<sub>2</sub>(CO)<sub>8</sub></b>	<b>Surfactant 1</b>	<b>Surfactant 2</b>	<b>Solvent</b>	<b>T (°C)</b>	<b>Particle size</b>
1	86 mg	TOPO, 13 mg	OA, 26 $\mu$ L	Mesitylene	170	3.5 nm
2	125 mg	Decanol, 2.56 $\mu$ L	OA, 2 $\mu$ L	Mesitylene	170	15 nm Polydisperse
3	125 mg	TDS, 11.93 mg	-	Mesitylene	170	9.3 nm
4	160 mg	TOPO, 90 mg	-	Mesitylene	170	7.5 nm

Expectedly, a variation in the ratio of both surfactants only affects the kinetics of the growth but not the particles size, since all the particles are expected to be coated by both types of surfactant. Changes in the surfactant to cobalt ratio, while keeping constant the surfactant ratio, mainly affects the particle size, the number of starting nuclei being similar. The temperature has to be high enough to allow the nucleation and the control of the growth by surfactant exchange. The effect of dilution is less obvious, dilution will affect both the number of micelles and the cobalt carbonyl concentration. Since the amount of cobalt com-



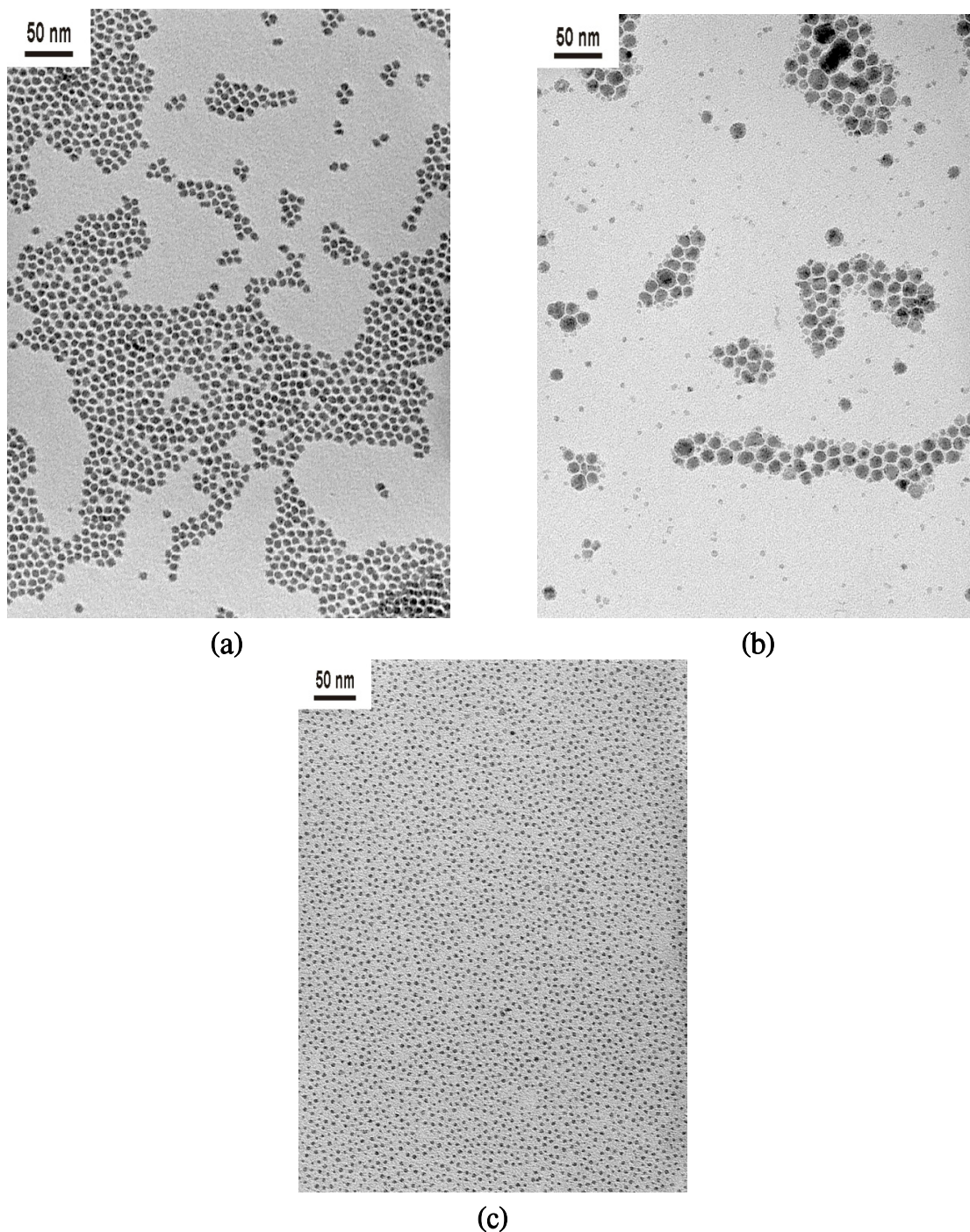


Figure 3-3: TEM images of Co particles prepared in various surfactant solutions:

a) TDS; b) Decanol; c) TOPO using  $\text{Co}_2(\text{CO})_8$  as precursor.

pound is rather high, the saturation in the micellar core should be achieved even in the diluted system. The surfactant in diluted media still forms micelles, but with a smaller number of  $\text{Co}_2(\text{CO})_8$  molecules per micelle, which then mainly affects the kinetics of the growth but not the particles size as observed in our experiment.

With this growth mechanism in mind, other kinds of surfactants have been tested to prepare cobalt nanoparticles (see Table 3-2 and Figure 3-3). First of all, the ionic head of the AOT surfactant has been kept, but the length of the alkyl chains has been increased. When tridecyl-sulfosuccinate (TDS) is used as surfactant, oleic acid is no more required to get a stable suspension of the particles. This surfactant combines strongly interacting sulfosuccinic groups and a long alkyl chain for a stable particle suspension. Where AOT fails to stabilise the particles, this surfactant is able to regulate both the growth and the stabilisation of the particles suspension even for particles of 10 nm in size (Figure 3-3a and Table 3-2 entry 1).

In parallel to the modification of the alkyl chain, it was also considered to vary the surfactant head. Decanol has then been substituted for AOT. Interestingly enough, this substitution led to the formation of bigger size particles (Figure 3-3b and Table 3-2, entry 2), but dramatic increase of the size distribution. This could be due to a less strong binding of the decanol to the cobalt as compared to AOT, which is then less efficient to prevent aggregation of the nuclei and Ostwald ripening occurs. However, the interest to use decanol as surfactant is, that it is well-known, that alcohols can act as reducing agent for easily reducible metals like gold [26]. When Au@Co core-shell particles would be the goal, the presence of a reducing agent (the alcohol functions) at the surface of the cobalt particles would be of great importance.

For comparison with results reported earlier, a commonly used surfactant to control the particle size, trioctyl-phosphine oxide (TOPO), has been studied using our experimental conditions. Table 3-2 entry 3 and Figure 3-3c demonstrate the formation of small, but monodisperse particles yielded by using a mixture of oleic acid and TOPO. Increasing the concentration of surfactants decreases the particle size due to slower growth in 20 minutes of reaction time. The obtained size is smaller than the one reported for a more polar solvent at higher temperature. This might be due to the quicker growth of the particles, when the temperature is increased. When TOPO is used without further addition of oleic acid and with a concentration in the same range as AOT, the particles size increases to 7.5 nm, i.e. a little smaller than under similar conditions with AOT. This again could be due to the variation of the surfactant's head group. TOPO being more strongly adsorbed to the Co-surface than AOT.

### 3.4 Conclusions

We conclude, that there is a minimum size for the alkyl chain of the surfactant, so that particles of above 10 nm are efficiently stabilised. This minimum length is between C10 and C13, depending if the structure is linear or branched. When a non-polar, high boiling point solvent is used, only a little surfactant (in the range of 0.01 M) is sufficient to control nucleation and growth of the particles. The chemical nature of the head of the surfactant is an additional important parameter. It should not interact too strongly with cobalt, to allow the growth of the nuclei, but must be strong enough to ensure stability. The sulfosuccinate head-group appears to fulfil this compromise.

### 3.5 References

- [1] K.J. Klabunde (ed.), *Nanoscale Materials in Chemistry*, Wiley Interscience, John Wiley & Sons Inc., 1<sup>st</sup> ed., 2001.
- [2] S. Sun, C.B. Murray, *J. Appl. Phys.* **1999**, *85*, 4325.
- [3] C. Petit, A. Taleb, M.P. Pileni, *J. Phys. Chem. B*, **1999**, *103* 1805.
- [4] C. Petit, A. Taleb, M.P. Pileni, *Adv. Mater.* **1998**, *10*, 259.
- [5] D.P. Dinega, M.G. Bawendi, *Angew. Chem. Int. Ed. Engl.* **1999**, *38*, 1788.
- [6] V.F. Puentes, K.M. Krishnan, P. Alivisatos, *Appl. Phys. Lett.* **2001**, *78*, 2187.
- [7] N. Cordente, M. Respaud, F. Senocq, M.J. Casanove, C. Amiens, B. Chaudret, *Nanolett.* **2001**, *1*, 565.

- [8] K.S. Suslick, S-B. Choe, A.A. Cichowlas, M.W. Grinstaff, *Nature*, **1991**, *353*, 414.
- [9] Yu. Koltypin, G. Kataby, X. Cao, R. Prozorov, A. Gedanken, *J. Non-cryst. Solids*, **1996**, *201*, 159.
- [10] G. Kataby, A. Ulman, R. Prozorov, A. Gedanken, *Langmuir*, **1998**, *14*, 1512.
- [11] M.P. Pileni, *Langmuir*, **1997**, *13*, 3266.
- [12] O.A. Platonova, L.M. Bronstein, S.P. Solodovnikov, I.M. Yanovskaya, E.S. Oblonkova, P.M. Valetsky, E. Wenz, M. Antonietti, *Colloid. Polym. Sci.* **1997**, *275*, 426
- [13] J.P. Spatz, S. Mössmer, C. Hartmann, M. Möller, T. Herzog, M. Krieger, H.G. Boyen, P. Ziemann, B. Kabius, *Langmuir*, **2000**, *16*, 407.
- [14] E. Papirer, P. Horny, H. Balard, R. Anthore, C. Petipas, A. Martinet, *J. Colloid Interface Sci.* **1993**, *94*, 207.
- [15] M. Giersig, M. Hilgendorff, *J. Phys. D: Appl. Phys.*, **1999**, *32*, L111.
- [16] V.F. Puentes, D. Zanchet, C.K. Erdonmez, A.P. Alivisatos, *J. Am. Chem. Soc.* **2002**, *124*, 12874.
- [17] C.B. Murray, S. Sun, W. Gaschler, H. Doyle, T.A. Betley, C.R. Kagan, *IBM J. Res. & Dev.* **2001**, *45*, 47.
- [18] T. Hyeon, *Chem. Commun.* **2003**, 927.
- [19] V.F. Puentes, K.M. Krishnan, A.P. Alivisatos, *Science*, **2001**, *291*, 2115.
- [20] M.P. Pileni, N. Duxin, *Chem. Innov.* **2000**, (2), 25.
- [21] M. Hilgendorff, M. Giersig in: *Nanoscale Materials*, P. Kamat, L.M. Liz-Marzán (eds.), Kluwer Ac. Publ., Boston **2003**, 335.
- [22] X. Peng, J. Wickham, A.P. Alivisatos, *J. Am. Chem. Soc.* **1998**, *120*, 5343.
- [23] T. Vossmeier, L. Katsikas, M. Giersig, I.G. Popovich, K. Diesner, A. Chemseddine, A. Eychemüller, H. Weller, *J. Phys. Chem.* **1994**, *98*, 7665.

- [24] X.M. Lin, C.M. Sorensen, K.J. Klabunde, *J. Nanoparticle Res.* **2000**, *2*, 157.
- [25] V.K. LaMer, R.H. Dinegar, *J. Am. Chem. Soc.* **1997**, *119*, 10382.
- [26] H. Hirai, Y. Nakao, N. Tohima, *J. Macromol. Sci. –Chem.* **1979**, *A13*, 727.



# *Monodisperse cobalt-nanoparticles from sulfosuccinate systems*

## 4.1 Introduction

With the facts, learned in our work described in Chapter 3, we decided to focus our work on particles made in systems with sulfosuccinates, i.e. AOT and TDS-containing solutions. Therefore, an optimisation towards more control over the parameters used in our experiments seems to be a suitable path for generation of magnetically active nanoparticles. Subsequent to successful syntheses of desired particles, the characterisation and properties of the gained particles is another objective, described in this chapter.

There is a lot of evidence in literature for nanoparticle syntheses and the interesting properties of those and their arrangement and secondary structure. Also, the field of magnetic properties of the particles, mainly in liquid solution turned to be the interest of scientists for the past decades. A systematical overview over the broad work on ferrofluid liquids is given by the ferrofluids bibliographic databases [1].

Here, the systems containing the ferrous oxides maghemite ( $\text{Fe}_2\text{O}_3$ ) and magnetite ( $\text{Fe}_3\text{O}_4$ ) are still the benchmark for all magnetic nanoparticle research. Due to their oxidised state, their handling is much more easy compared to systems of pure metallic nanoparticle systems. Also their magnetic properties can be directly ascribed to the particles contained in the solutions. On the other hand, these syntheses are very valuable for the synthesis of metallic particles, because of their general meaningfulness in terms of magnetism and mag-

netic behaviour in the nanoscale regime. Here, a lot of basic work has already been done [2-4] and also ordered particles are obtained [5].

Nevertheless, metallic ferromagnets in the nanoscale offer other ranges of magnetisation, because of the ferrimagnetic character of iron oxide particles. Thus, an increased occurrence of work on metallic nanoparticles can be registered during the past years. Using surfactants as stabilising agents, nanoparticles of Ni [6] and Fe [7, 8] could be synthesised systematically. We are focussing in this work on Co-nanoparticles. The recent challenges of synthetical work include mainly highly organised systems.

Cobalt could be obtained as uniform particles' superlattice using AOT and  $\text{Co}_2(\text{CO})_8$  [9-12], non-ionic surfactants and  $\text{Co}_2(\text{CO})_8$ -derivatives using ultrasonification [13],  $\text{Co}_2(\text{CO})_8$  in TOPO an oleic acid [14] or using reductive methods in the presence of a surfactant [15, 16]. Also rod-like particles could be obtained [17], as well as selective synthesis of different morphologies [18-20]. The ordering and the crystalline origin of the yielded particles promise to show besides of the expected magnetic properties a nanoscaled enhancement of the magnetic moments ascribed to effects of single-domain-magnetism. Indications, that such effects can occur in real solutions were already observed [21].

In this work, we describe the systematical synthetic procedure using new combinations of surfactants for  $\text{Co}_2(\text{CO})_8$ -decompositions. These procedures are optimised towards a stable synthetic process. A focus is put on the oxidation process during the generation of the particles. 2D and 3D-lattices of particles will be outlined using different paths of particle preparation. The reaction kinetics are discussed by using the comparison to the well-known TOPO/OA system. Furthermore, magnetic measurements were made to characterise the magnetic behaviour of the gained particles. Magnetism will be also discussed referring to the oxidation process during manufacturing of the solutions.

## 4.2 Experimental

### *Chemicals*

Cobalt carbonyl ( $\text{Co}_2(\text{CO})_8$ ), an orange solid (Fluka, 95% stabilised with n-hexane), was stored at  $-20^\circ\text{C}$  and has been used as received. Oleic acid (OA) (Acros, 97%) was dried by toluene azeotropic distillation. AOT (Fluka) was crystallised from dry methanol [22] and



dried by overnight heating at 80°C in a vacuum. Both products were stored in a nitrogen filled glove-box, where the water and oxygen contents were kept below 1 ppm. TDS (Chem-Service >95%) and TOPO (Aldrich, 99%) were used as received. Mesitylene has been dried three days over  $\text{LiAlH}_4$  and distilled twice at 60°C under dynamic vacuum, further condensed below room temperature in a high vacuum line under dynamic conditions using an oil diffusion pump. The latter process was carried out using Trioctyl-aluminium as drying agent.

Stock solutions of  $\text{Co}_2(\text{CO})_8$  in mesitylene were prepared in order to be able to operate with equal concentrations. A freshly opened  $\text{Co}_2(\text{CO})_8$ -batch was filled under argon into a sealed flask and the desired volume of mesitylene was added inside of a glove box. Subsequently, the solution was transferred under stirring to a CO-source and the gas was flushed under stirring into the solution. After each withdrawal of stock solution, the flask was immersed again with CO in order to keep a high CO-pressure inside of the stock solution. This procedure prevents a non-desired decomposition reaction of the  $\text{Co}_2(\text{CO})_8$  by simple shifting of the reaction equilibrium. The decomposition reaction is taking place under separation of CO, leading to more metal containing complexes [23].

### *Synthetic procedure*

In order to avoid any traces of oxygen, all syntheses were performed in small glass tubes, where the solution has been degassed via three freezing-evacuation-melting cycles by means of a high vacuum line. The tube was filled with the surfactants, the cobalt carbonyl complex and the solvent inside of the glove-box and then transferred to the high vacuum line. All glassware used for the high-vacuum procedure, including this tube, was heated in an oven at 230°C for some days. The whole high-vacuum apparatus was dried with a hot gun prior to use under dynamic vacuum in order to remove water traces on the glass surfaces. The solution was frozen in liquid nitrogen and the tube was evacuated. Under static vacuum, the solutions were then allowed to reach again gently ambient temperature. This operation was repeated until no gas evolution could be observed anymore (this state was reached usually after three cycles). The tube was finally closed under vacuum, immersed in a silicone bath preheated at the desired temperature and kept at this temperature for a certain time. After cooling to room-temperature, the tube was again transferred into the glove-box for sample preparation.

### *Electron microscopy*

**Transmission electron microscopy (TEM)** images were recorded with a Philips EM 400 T microscope operating at 80 kV. Copper grids (mesh size:  $200 \times 200 \mu\text{m}^2$ ) were coated with a

Formvar film (around 20 nm thickness) and a layer of carbon (approximately 5 nm thickness) and used as substrates for TEM analysis. The samples were prepared by evaporating a droplet of the solutions on the grid, which was in contact with a soaking tissue in order to avoid multilayer formation. **High-resolution TEM (HRTEM)** images were recorded with a CM 200 FEG (CS correcture) on a holey-copper grid, where a drop of the colloidal solution was evaporated in the way described above. Sample preparation was carried out inside of the glove-box. EDAX analyser coupled with HRTEM gives the semi-quantitative composition of the samples. With this apparatus, contact of the samples with the air cannot be completely avoided during the transfer of the samples into the microscope. Negatives were scanned on an Umex Astra scanner operating at 600 dots per inch (dpi) using constant picture sizes. Adobe Photoshop 5.5 was used for evaluation particle sizes and distances.

**High resolution scanning electron microscopy (HRSEM)** samples were imaged in an Hitachi S-5200 (Nissei Sangyo, Germany) in-lens field emission scanning electron microscope at an accelerating voltage of 30 kV using the secondary electron image. Images were recorded digitally with 1280x960 Pixels.

### *Magnetic measurements*

*Sample preparation:* The heated samples were transferred into a nitrogen-filled glove-box for an inert atmosphere. 0.1 mL portions of the Co-containing solution were transferred into a thin walled Pyrex sample tube equipped with a joint and a connection valve. In order to transfer the sample to a high-vacuum line, the valve was closed to ensure effective protection towards air and moisture. The sample tube was connected to a high-vacuum line and the sample was degassed until no further gas evolution could be observed anymore. This needed at least three freeze and pump cycles under static vacuum. The sample tube was melted off the high vacuum line to produce a long-term stable sealed sample.

*SQUID-measurements* were carried out in a commercially available SQUID-magnetometer (Quantum design MPMS) with Helium-cryostat operating between 1.9 and 400 K in a field range of  $\pm 5.5$  T. The SQUID sensor is based on the radio frequency (rf) technique [24]. The sample was introduced for the measurement with a self-created plastic tube of known magnetic properties. In order to subtract the effect of the glass tube, blind measurements with an empty vacuum-sealed glass tube were carried out prior to the measurements of the colloid-containing samples. Later these measurements were subtracted from the raw data.

*Vibrating Sample Magnetic measurements (VSM)* were performed with a Lake Shore Vibrating Sample Magnetometer Model 7300. The device is connected to a Bruker B-E25V

magnet with a maximum field of 2.3 T. The normal conducting magnet for calibration (Bruker) is supplied by a bipolar generator. The measurements were carried out at room temperature with a pole distance of 7 cm, reducing the maximum field to 1.2 T. Hysteresis measurements ( $\pm 1$  kG and  $\pm 8$  kG) were driven with a ramp speed of 8 G/s and a mean time of 10 s per data point. The same samples as for SQUID were used. Specially prepared sample holders were used to prevent side effects by vibration of the glass tubes and to prevent breaking of the thin glass tubes under vacuum.

### *High-Resolution Thermogravimetry*

The measurements were performed on a Netzsch-TG 209C Iris with an effective resolution of  $1\mu\text{g}$ , with a heating rate of 10 K/min. The measurement up to 600 °C was performed using nitrogen as inert gas, oxygen was used for pyrolysis between 600 and 1000 °C. The sample of 2.26 mg was kept in an aluminium oxide beaker during the measurement.

## **4.3 Results and discussion**

### *AOT/OA-systems*

Basing on the decomposition in AOT-oleic acid mixture, further experiments were made to determine the parameters of successful synthesis in our synthetic procedure. A screening of different ratios between the  $\text{Co}_2(\text{CO})_8$  precursor, AOT and oleic acid was performed. The results can be viewed in Figure 4-1. Instability of the solutions manifests in either aggregation of the particles or in a massive broadening of the particle size distribution. The used ratio between the growth controlling AOT and the solution stabiliser oleic acid is very important for a successful experiment. With the Co:AOT-ratio being 20, we could vary the ratio of the both surfactants in the range between 0.5 and 2 OA:AOT without notable perturbation in the particle quality. The limits here are at values approaching 0 and infinity, respectively. This means for values, which denote the presence of just one of the both surfactants.

However, decreasing the Co:AOT ratio below 20 is a critical step. Here, the particles start to form aggregates due to a too high presence of surfactant. A possible reason for this is a too big role of one of the surfactants during the nucleation and growth mechanism. One

seed or one growing particle is surrounded by a too high number of one of the both surfactants, which takes then a dominating role during the rest of the process.

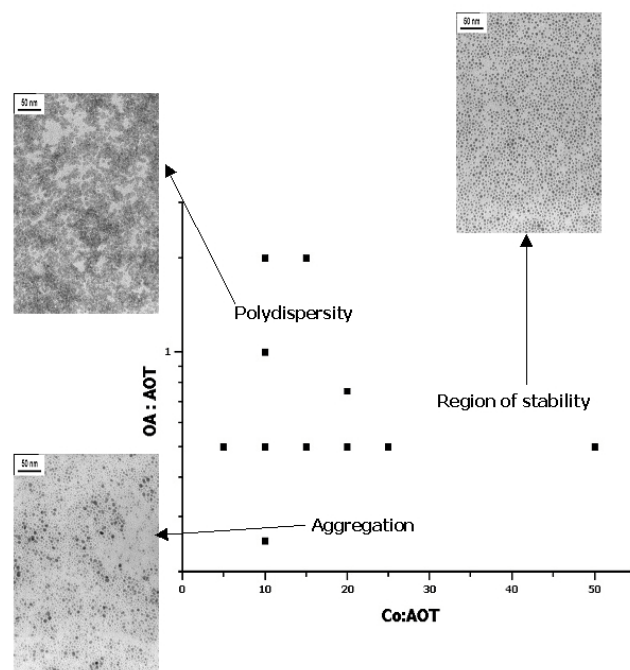


Figure 4-1: Screening of molar ratios of OA:AOT and Co:AOT. The dots show performed syntheses. The grey areas show the regions of instability. Just a small window of ratios leads to monodisperse and stable particles. The TEM-pictures show the particles yielded in the respective experiments.

In agreement with the results described in Chapter 3, a ratio of OA:AOT of 0.5 is the border between two different kinds of perturbances. A ratio of 0.5 and lower leads to aggregation of the particles. This is equal to the situation, which can be found in solutions with pure AOT as surfactant. In the case of a ratio of more than 0.5, the role of oleic acid is more pronounced. This leads to a broadening of size distribution by oleic acid adsorption [25]. In one of the experiments depicted in Figure 4-1, for the Co:AOT-ratio of 5, stable particles were obtained. However, a successful syntheses in this region of surfactant ratios is not reproducible. Going to the stable window of Co:AOT > 15, the reaction and the obtained particle sizes could be reproduced in all of the cases by a repeated synthesis with the same parameters.

In Figure 4-2, the ratio of Co:AOT is plotted against the received particle sizes. The data points show asymptotic behaviour. The suggested limit of the synthetic method is 12 nm. There was no evidence, that bigger sized particles could be produced. The biggest species

were performed in diluted solution, since the standard concentrations lead to aggregation of the particles, when the Cobalt content gets too high. This is ascribed to the dissolution limit of  $\text{Co}_2(\text{CO})_8$  in mesitylene. The lower limit is 4 nm due to the described aggregation or distribution bordering caused by the surfactants. In a dense packing of particles, the inter-particle distance was measured to be 1.15 nm.

The graph in Figure 4-2 shows, that the mathematical trend of the data points is a root function ( $x^{1/n}$ ). This is a logical consequence of the fact, that the diameter of the particles is a function of the particle volume with  $n \sim r^3$ . Thus, the particle size is almost directly linked to the Co:AOT-ratio of the solution. The latter is in consequence possible, if micelles of the surfactant take part in the reaction mechanism. Here, the particles are able to grow, until the capacity of the micellar core is reached. In the case of smaller particles, i.e. a smaller

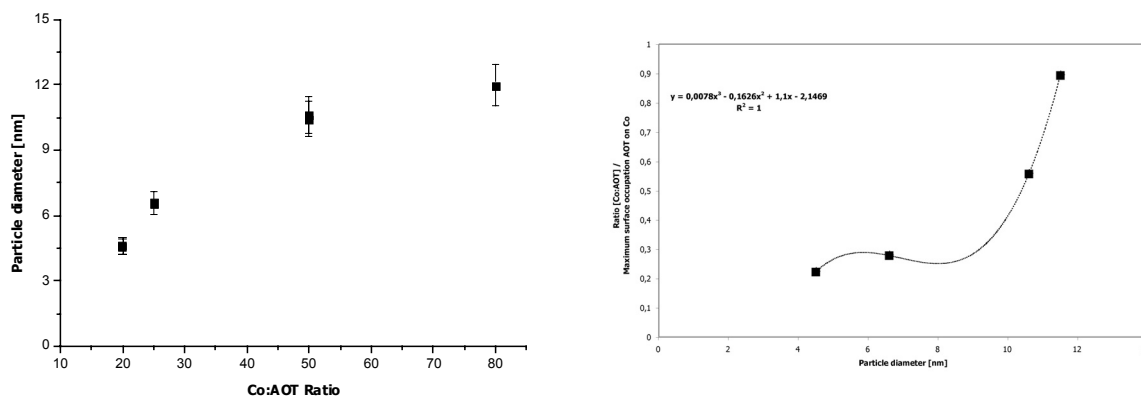


Figure 4-2: (a) Plot of the Co:AOT ratio against the obtained particle diameter. For the plot, only experiments with an OA:AOT-ratio of 0.5 were taken. Also unstable Co-solutions (see Figure 4-1) are not mentioned in the plot; (b) The used ratio is set in relation to the maximum surface occupation of AOT on Co. Of 89.4. The plot is scaling with  $r^3$ .

amount of  $\text{Co}_2(\text{CO})_8$  used, the reaction stops, because there is no more educt in the solution. The maximum surface occupation of the particle by AOT can be performed. A plot of relative surface occupation against obtained particle size is shown in Fig. 4-2b. A surface area per molecule AOT of  $66 \text{ \AA}^2$  [26] and an atomic radius of  $1,35 \text{ \AA}$  for cobalt is taken for the calculation. With these values, a maximum Co:AOT-ratio of 89,4 is calculated. In Fig. 4-2b a maximum particle size of approximately 12 nm with maximum surface coating can be concluded.

Particularly, this could lead to the possibility of “refilling” the solution with cobalt. Unfortunately, the subsequent reloading of the solution with  $\text{Co}_2(\text{CO})_8$  leads to twinning due to seed formation on the particles surface and not to a controlled, continued growth of the particles. In experiment, we could not get bigger particles by that procedure, but the particles precipitated. It seems, that the micelles are destabilised by the seed-mediated growth of the twinning particle, which can quickly overcross the micellar dimensions.

Figure 4-2 makes it possible to synthesise a desired size of particles just by correlation to the needed Co:AOT-ratio. By simply drawing an approximate connecting curve into the plot, one can read the ratio directly from the x-axis.

To refine the synthetic procedure we considered the synthesis being a multi-step process. The main goal of the synthetic enhancement is the narrowing of the particle size distribution and the prevention of oxidation during particle formation. Basically, there are 7 steps made in the synthesis, which are shown in Figure 4-3. Regarding the reaction path using an AOT-OA mixture as surfactant system, we could decrease the standard deviation of the particle size distribution from 11% to 6.5%.

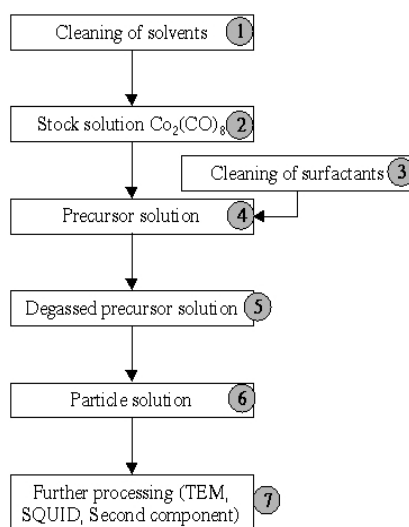


Figure 4-3: The described synthetic route is a multi-step process. The steps 1 to 7 have to be carried out carefully. Special issues about the steps are described in the text.

The steps 2, 4 and 6 are mainly responsible for the decrease in particle size distribution. In step 2 we put the  $\text{Co}_2(\text{CO})_8$  under an atmosphere of carbon monoxide. This prevents the precursor from forming multi-core clusters. The latter happens either by storage at standard atmosphere or under inert gas. Just a pressure of CO is shifting the reaction

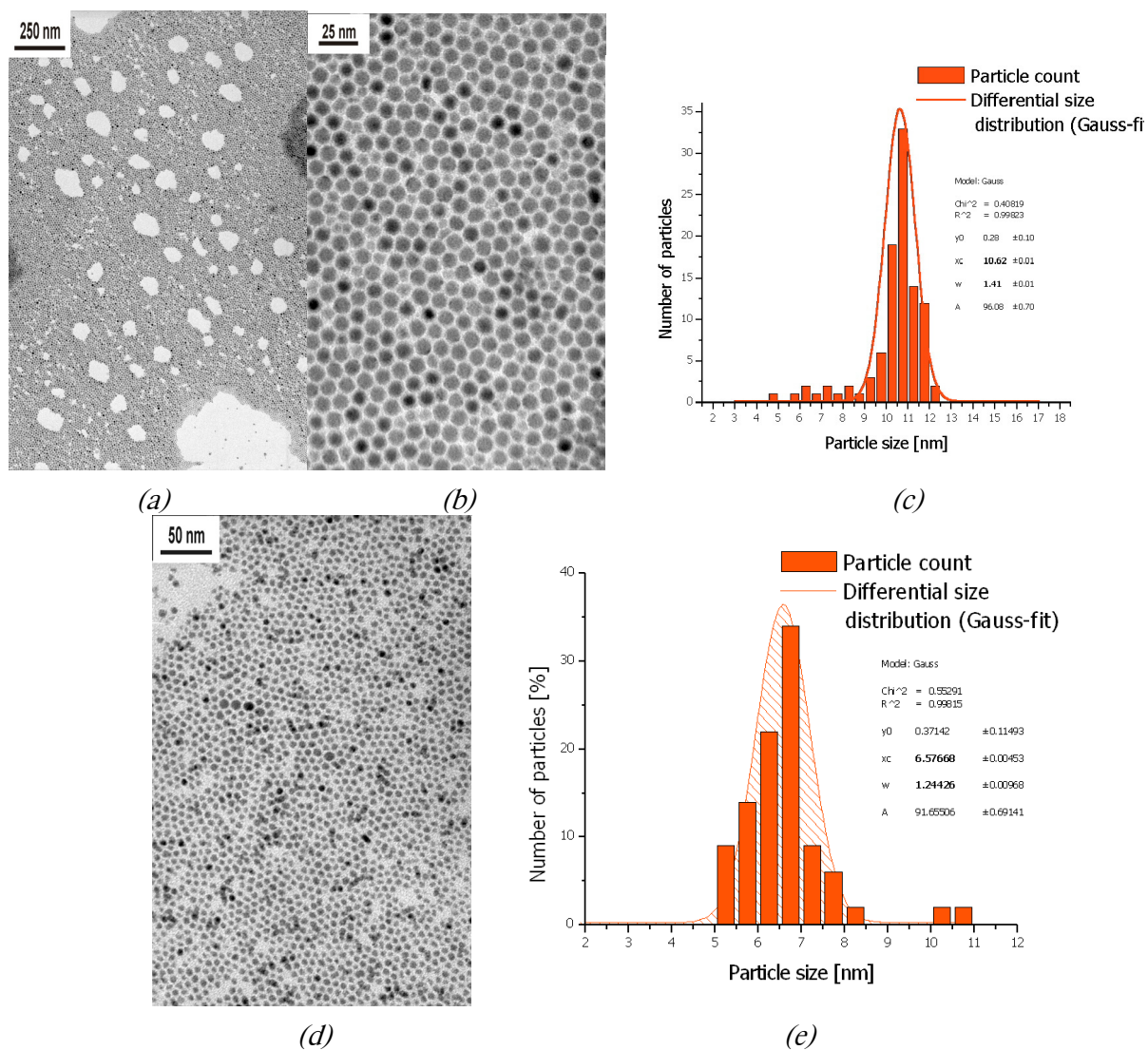
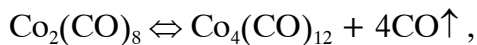


Figure 4-4:

(a),(b): Two magnifications of a TEM-micrograph of an optimised Co-particle solution. Used parameters Co:AOT=50, OA:AOT=0.5 reaction at 170 °C

(c):Size distribution for the particles in (b) giving a size of 10.6 nm with a standard deviation of 6.6%

(d):TEM micrograph of a particle solution with Co:AOT=25, OA:AOT=0.5 at 170 °C

(e): Size distribution for the particles in (d) giving a size of 6.6 nm with a standard deviation of 9.4%

which is known to be the most common decomposition reaction within  $\text{Co}_2(\text{CO})_8$ , forming a violet solid [23, 27]. This reaction is the first step of the carbonyl decomposition and takes place, when the reaction temperature is below 90 °C. Since this first step is reversible, the

reaction can be shifted by usage of CO-gas atmosphere. The second step of the reaction is described by



the irreversible second step. Due to this two-step process, it is also not suitable to perform heating as a slow process. Due to the two different reaction steps, the growth kinetics are influenced. For fast and simultaneous seed formation and a controlled growth mechanism, the basic reaction has to be quick and quantitative. This is reached by quenching of the solution at 170 °C. (reaction steps 5 to 6). The growth step has then to be carried out slowly [28]. Thus, step 2 is best performed by storage and generation of the stock solution using a CO atmosphere. Figure 4-4 shows two examples of an optimised particle syntheses.

From Figure 4-4 it is evident, that smaller particle sizes are coming along with broader size distributions. The latter can be explained by partial oxidation of the particles, which is more easy on smaller particles by a bigger surface to volume ratio. Oxidation of the particles is another big problem within the particle synthesis. In Chapter A7.1, the stoichiometric calculation on the surfactant systems is done. Proposing, that the oxidation is mainly taking place on the outer surface of the particle, building a regular shell, Eq. A7-19 (see page 185) can be taken to calculate the effect of oxygen presence in the solutions.

In a typical experiment, 2 mL of a  $\text{Co}_2(\text{CO})_8$ -containing solution are taken. In order to form just an oxide layer of 1 nm size, a gas volume of 1.2 mL of oxygen is needed to coat any Co-particle in the solution. This value is calculated for  $\text{Co}_2\text{O}_3$ . If the oxidation stops in the stage of the Co(II)-oxide  $\text{CoO}$ , only 800  $\mu\text{l}$  of oxygen is needed for a complete oxidation of any particle in the solution. With this knowledge, it is necessary to perform the reaction steps including all kinds of gas exclusion. This means for the liquid components, that degassing steps are necessary in every step of the reaction. Solvents and liquid surfactants (reaction step 1 and 3) are thus prepared on a high-vacuum line. The stock solution is also degassed to remove the last traces of oxygen (reaction step 5).

If possible, all steps should be carried out in a nitrogen-filled glove-box. A controlled atmosphere with 1 ppm of oxygen and below is sufficient for secure handling of the preparation steps. Also further processing on the Co-containing solution should be carried out in the glove-box. The best practice is to use in-situ experiments, if available. Especially TEM-analysis is a critical process due to later oxidation of the particles in the casted film on the grids. However, if the film is casted under inert gas, the solid surfactant protection is a protective medium for the particles.



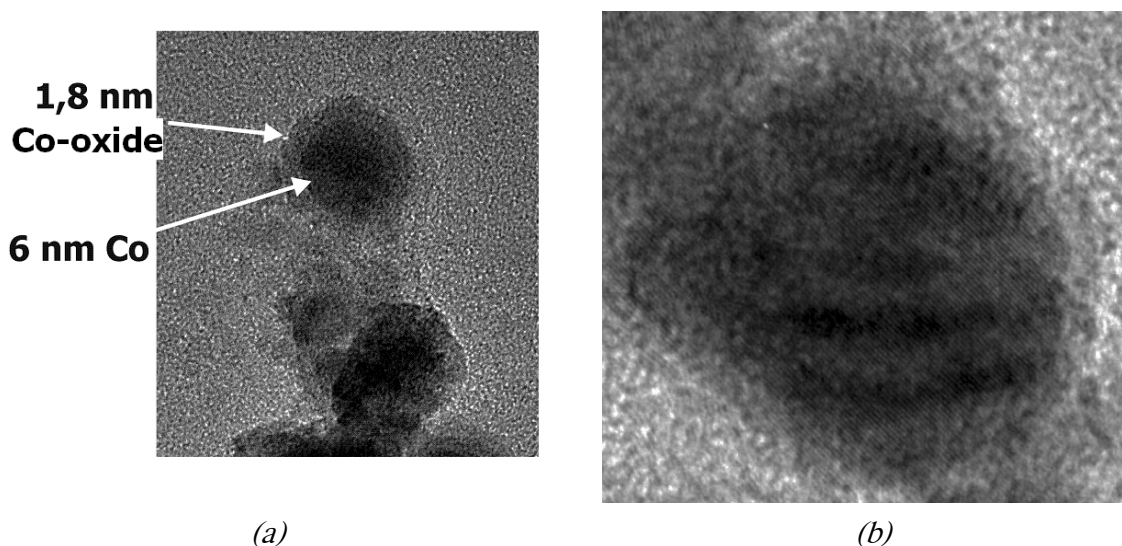


*Figure 4-5: HRTEM-micrographs of controlled oxidised Co-nanoparticles. (a) Size determination of the Co-core and the oxide shell. (b) Individual particle of the same size showing lattice fringes. The fringes were analysed and assigned to lattice spacings of the species*

We could successfully perform an experiment on controlled oxidation of the particles. One of our samples (Co:AOT=25, OA:AOT=0.5) was exposed to air during reaction step 5. While degassing the solution, we opened the sealed flask in the frozen state. Due to the low temperature of liquid nitrogen, air at ambient temperature is soaked into the flask. After 1 minute, the flask was closed again and the experiment was continued in the usual way<sup>§</sup>. In this experiment, we could show, that in fact, an oxide layer is forming as a shell around the particles. Results are depicted in Figure 4-5. The fringes of Figure 4-5(b) were measured by FFT-analysis of the particles. The results are summarised in Table 4-1.

In Figure 4-5(a), the presence of a lower contrast shell and a darker core in the particle is observed. The core measures 6 nm in diameter, while the shell of the particle has a thickness of 1.8 nm. This is a value of a cobalt-oxide layer, which resembles the native oxide layer on cobalt [29, 30]. The fringe pattern of the particle core shows, that the particles are monocrystalline, only one direction of the lattice can be seen within the particles. This seems to be the {100}-plane of hcp-cobalt. In the outer shell, the 2.43 Å plane distance indi-

<sup>§</sup> This step takes great caution towards formation of liquid oxygen, which is explosive, when it comes into contact with hot sources in the presence of ignition sources close to the reaction apparatus (contact with hot pump oil should be avoided.)

cates the presence of  $\text{Co}_3\text{O}_4$ . The other found distance of  $2.67\text{\AA}$  is a plane according to CoO.

*Table 4-1: Found lattice spacings in Figure4-5a from fast Fourier-Transform (FFT) analysis*

Lattice spacing [ $\text{\AA}$ ]	Reference value	Intensity	Corresponds to	Lattice plane
2.19	JCPDS* 5-727: 2.16	High	hcp-Cobalt	{100}
2.43	JCPDS 2-1079: 2.43	High	$\text{Co}_3\text{O}_4$	{311}
2.67	JCPDS 42-1300 2.62	High	CoO	{111}

The stability of a non-oxidised particle sample towards oxidation has also been evaluated by HR-TEM. One drop of the solution was evaporated on a copper TEM grid in the glove-box and is then transferred into the HR-TEM in order to check the crystallinity of the particles.

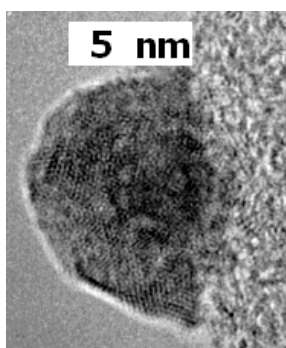


*Figure 4-6: Oxidised particle from a HR-TEM-grid. Co:AOT=25; OA:AOT=0.5, oxidation took place on the transport from laboratory to the microscope*

During the transfer of the sample to the microscope, it is not possible to avoid completely the contact with air. Figure 4-6 shows a micrograph of such a particle, showing irregular oxidation and not monocrystalline lattice fringes. On the EDAX analysis (Figure 4-7), even after a very short period of exposure time in the air, the presence of oxygen is detected on the Co particles showing the quick oxidation of these particles in ambient atmosphere. The oxidation is completed, when the sample is exposed to air. This is demonstrated in Figure 4-7b, where the oxygen peak is increased comparing to the cobalt-peak. The small surfactant shell, thus, does not protect the Co metal against oxidation when the samples are in

\* JCPDS collection codes by the Joint Committee for Powder Diffraction Studies

ambient atmosphere. These observations are in contrast to the results claimed by various authors that mentioned the air protection provided by the surfactant. We attributed this difference in results to differences in the particles size. Indeed, when the particles are bigger than 8 nm, the surface layer of oxide is able to protect the pure cobalt core from further oxidation.

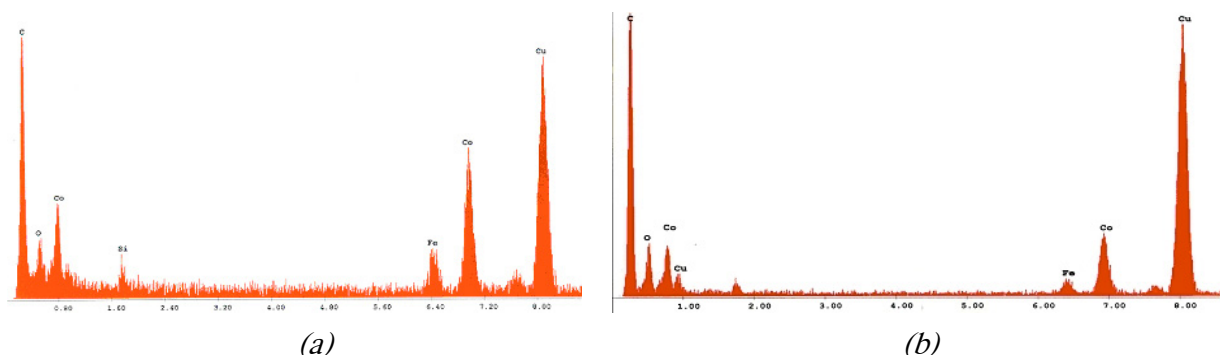
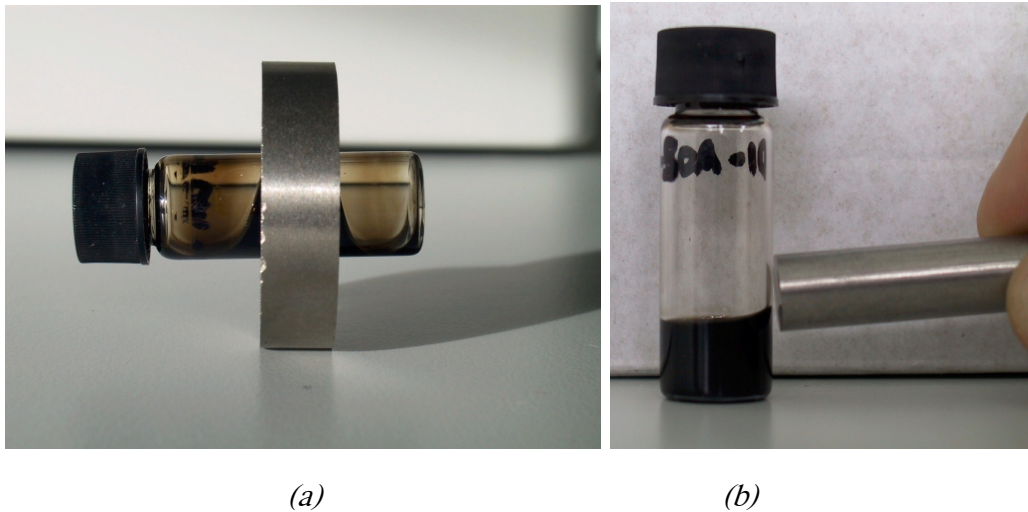


Figure 4-7: EDAX analysis of the Co particles (a) directly after synthesis, (b) after 5 days in the air

For proving the ferromagnetic character of the solutions, right after synthesis, the solution were tested by a permanent magnet ( $\text{SmCo}_5$ -ring, 40/15/10 mm from IBS-Magnet, Berlin). In Figure 4-8, pictures of ferrofluid behaviour are shown. It is seen, that the liquid shows ferrofluid behaviour, when interacting with the magnetic field of the permanent magnet. The meniscus of the solution leaves the horizontal position, when a magnet is held directly to the flask. Pushing the vessel inside of a ring-shaped magnet, the solution is almost completely torn into the ring, where the field lines of the magnet have the highest density. The magnetic “strength” of the ferrofluid is quite high. For a portion of 0.4 mL we observed a saturation magnetisation in the range of  $10^{-2}$  emu.

Magnetic measurements with the particle solutions have been performed in order to characterise and quantify the particles’ magnetic properties. To perform such a measurement, special precautions have to be taken due to the oxidation behaviour of the particles. The reaction is performed directly inside of a quartz NMR-tube, connected to the high-vacuum line. After degassing, the tube is melted off the line and the sealed tube is taken for the further experiments. Quartz-glassware is used as material of the tube, because it is known for its magnetic neutrality, being diamagnetic. Usual laboratory glassware shows paramagnetic behaviour, which influences the measured data and the necessary baseline calculation for the SQUID-measurement.



*Figure 4-8: Ferrofluid solution (Co:AOT=25, OA:AOT=0.5) in a ferromagnetic ring (a) or influenced by a rod-like ferromagnet (b). The meniscus of the solution is moving by the field-lines of the magnet. Particles in the solution have a diameter of 6.6 nm. The vessel is equipped with rubber/PTFE-inlays to prevent oxidation.*

*Table 4-2: Magnetic properties of 6.6 nm and 10.7 nm particles from SQUID-measurements*

Particle diameter	6.6 nm	10.7 nm
Size distribution ( $\sigma$ )	9.4%	6.6%
Saturation magnetisation (Bulk Co = 164 emu/g)	75 emu/g	128 emu/g
Blocking Temperature $T_B$ from SQUID	60 K	100 K

In the following, the main magnetic data of the solutions are briefly discussed. Many detailed experiments were made with different particle sizes. Those results are summarised elsewhere [31]. Magnetic properties of particles with different sizes (6.6 nm and 10.7 nm) have been measured at room temperature both by VSM and SQUID techniques. The main results of the SQUID-measurements are given in Table 4-2.

The saturation magnetisation gives a value, which is smaller than the average bulk value for Cobalt. If we consider an oxide shell of 1.8 nm also for both of measured species, we can

estimate the magnetic activity, which was eliminated by oxidation, because the values in Table 4-2 refer to the absolute values of Co in the solution. If we propose, CoO is the oxide, which is formed around the particles, the shell of 1.8 nm CoO was formed by a layer of 1.45 nm of Cobalt. This value can be calculated by multiplication with the cubic root inverse ratio of the densities of Cobalt and its oxide, since the density  $\rho \sim 1/r^3$ .

$$\frac{r_{before}}{r_{after}} = \frac{\sqrt[3]{\rho_{after}}}{\sqrt[3]{\rho_{before}}} \text{ or } r_{before} = r_{after} \cdot \frac{\sqrt[3]{\rho_{after}}}{\sqrt[3]{\rho_{before}}} \quad (\text{Eq. 4-1})$$

The percentual amount of magnetic material lost by oxidation can be determined by the ratio between the volumes of the spherical shell of 1.8 nm and the volume of the whole particle.

$$\frac{V_{Shell}}{V_{Particle}} = \frac{r_{Particle}^3 - r_{Core}^3}{r_{Particle}^3} = \frac{(r_{Core} + r_{before})^3 - r_{Core}^3}{(r_{Core} + r_{before})^3} \quad (\text{Eq. 4-2}), \text{ where}$$

$$r_{Core} = r_{Particle} - r_{after}$$

For the calculation of the saturation magnetism of the magnetically active portion,  $M_{Eff}$ , the experimentally determined magnetisation  $M_{Exp}$  has to be normalised to 100%, which can be written as:

$$M_{Eff} = M_{Exp} \cdot \frac{1}{1 - \frac{V_{Shell}}{V_{Particle}}} \quad (\text{Eq. 4-3})$$

The latter is the measured particle size decreased by the 0.3 nm of oxide growth. This gives a loss of magnetic material in the case of the 6.6 nm particles of 87% and in the case of the 10.7 nm particles of 65%. Since this would lead to  $M_{Sat}$ -values of 577 emu/g and 365 emu/g, there are two possibilities of explanation. Either there is a very strong enhancement in magnetisation in the remaining nano-magnet or there is a very low oxide content in the particles than the observed value of 1.8 nm for the completely oxidised particles described above. The first possibility is not probable, since the effect of enhancement would have to be bigger for the small particles. The smaller particles would have an oxide layer and a small magnetic core of 3 nm in diameter. For this size of particles, it is not sure, if there is a ferromagnetic effect at all or if the 3 nm core better behaves like a paramagnet. The second explanation is more clear. There is a thinner oxide layer around the particles, the magnetic cores behave approximately like bulk-Co. Taking the mathematical way back and inserting

the experimental values, the result for both particle types is rather consistent. The measured values resemble magnetisation values of Cobalt particles, which have an oxide layer of 0.7 nm thickness on their surface.

The amazing thing about the calculation is, that both particle sizes deliver the same result. Thus, we believe, that the benefit from our experimental technique is the very careful operation of oxygen enclosure, the magnetisation being not particularly different than the bulk value. Even though the calculation is just a rough point of view and surely doesn't represent the real state, the insight into our system can be approximated the best by this indirect method. It was the only experiment, which we could perform in situ, without having subsequent exposure to at least small amounts of oxygen.

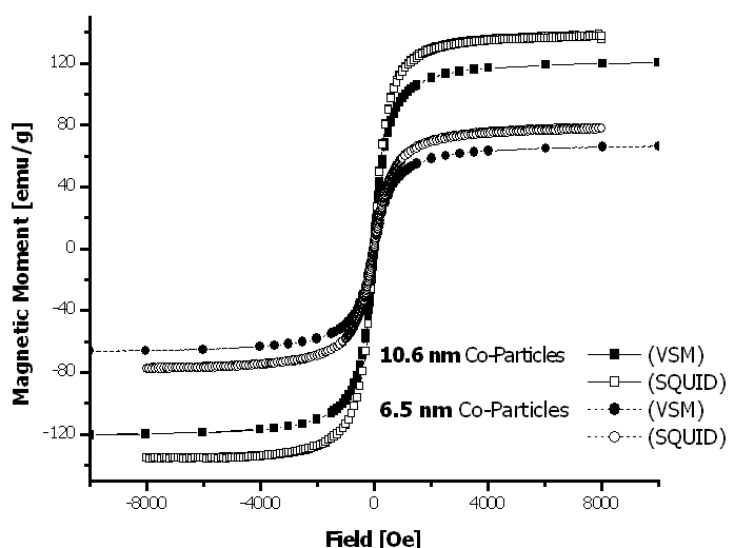


Figure 4-9: Magnetisation curves of both measured particle sizes. The dashed lines represent the measurement on a solution with 6.6 nm sized particles, the solid lines with 10.7 nm particles. The filled symbols show results from VSM, while the open symbols show results from SQUID-measurements. All experiments are made at ambient temperature. The used solutions for both measurement methods were the same

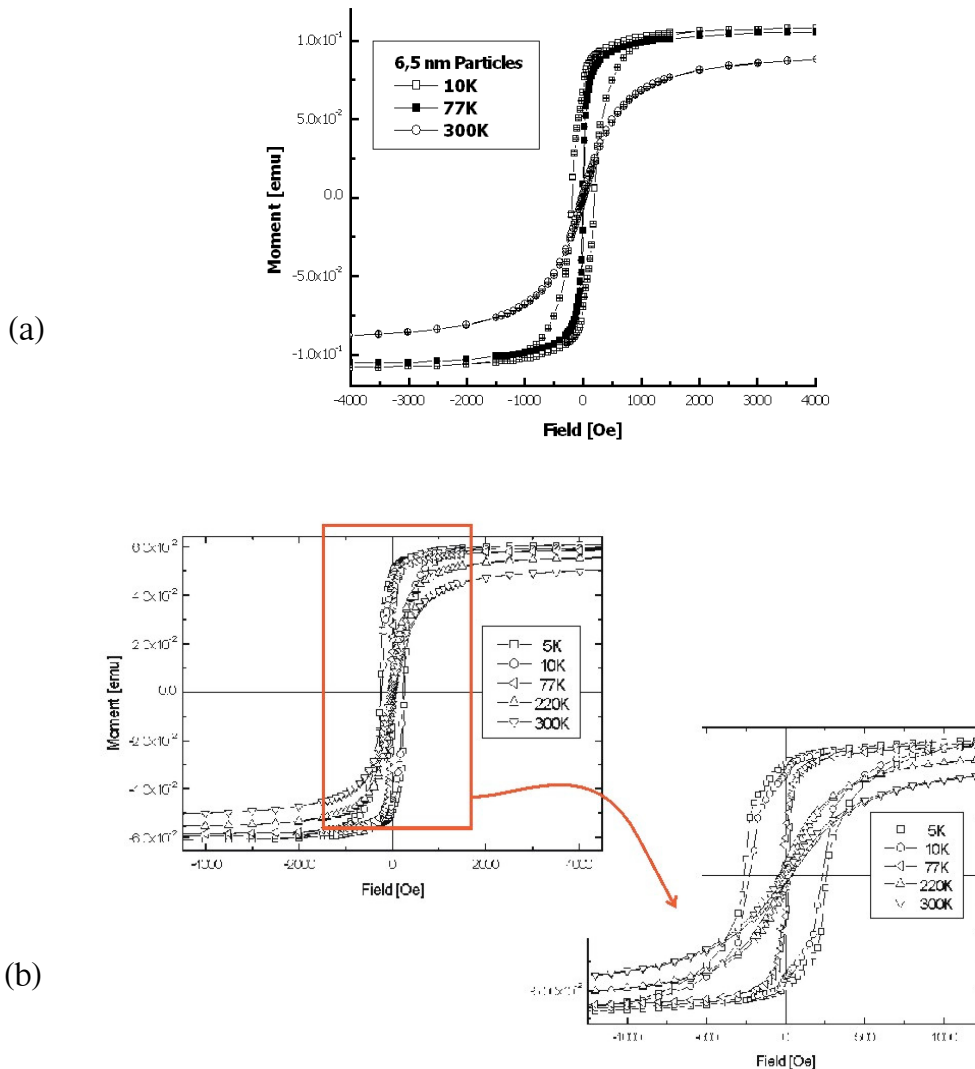


Figure 4-10: (a) SQUID-Magnetisation curves of 6.6 nm particles at three different temperatures (10, 77 and 300 K). A slight hysteresis is observed for the particles at 10 K. At 77 K, no such behaviour is observed, due to the lower blocking temperature. (b) SQUID-curves of 10.7 nm particles at 5 different temperatures (5, 10, 77, 220 and 300 K) are shown. The red frame marks the hysteresis area, which is magnified on the insert on the right hand side. At 220 K, the melting point of the solution is reached, narrow hysteresis-behaviour is already present at 77 K. All values for the magnetic moment are absolute values, not normalised to a certain portion of particles.

The magnetisation curves, shown in Figure 4-9, are comparable for both measurement methods, the observed slight differences can be accounted for different calibration. At

room temperature, no hysteresis has been observed in the liquid suspension in mesitylene [32]. The main results from SQUID are confirmed by the use of the VSM-technique.

SQUID-measurements were used to study the low-temperature behaviour of the particles. In Figure 4-10, the temperature dependence of the magnetisation curves is demonstrated.

Using the SQUID technique, measurements have been performed at low temperatures (Figure 4-10). Hysteresis could be observed for both particles sizes. Thus, the particles show blocking below a certain temperature. From Figure 4-10a), the blocking of the 6.5 nm particles occur below 77 K. The bigger particles with 10.7 nm do block already above 77 K, which can be deduced from Figure 4-10b). From the shape of the hysteresis curves at 10 K, the smaller particles show a remanent field of 64% of the saturation value, the coercivity is around 180 Oe. The bigger particles show at the same temperature a remanent field of 75% of the applied field and the coercivity is 215 Oe. As expected, the magnetisation is a function of the present temperature. At 77 K, the remanence of the bigger particles drop to 22% of the applied field, which shows, that the blocking temperature is reached not far above 77 K.

The field cooling (FC) and the zero field cooling (ZFC) method let one deduce the blocking temperature from its course. The maximum of the ZFC-curve can be taken as average blocking temperature  $T_B$  [33, 34]. In the FC-experiment, a field far above  $T_B$  is applied and the sample is cooled in a field to  $T < T_B$ . In zero field cooling (ZFC), the sample is cooled in zero field to  $T < T_B$ , and at this temperature an outer magnetic field is applied. Subsequently, the sample is heated up beyond  $T_B$ . In both cases, the magnetisation of the sample is measured, in the first case while cooling and in the latter case while heating up the sample. In Figure 4-11, the ZFC and FC measurements of mesitylene solutions of Co-particles are shown. It is worth to mention, that the heating of the sample is stopped at 230 K, which is the melting point of mesitylene, to prevent secondary effects by phase transition of the solvent from a solid matrix to a liquid environment.



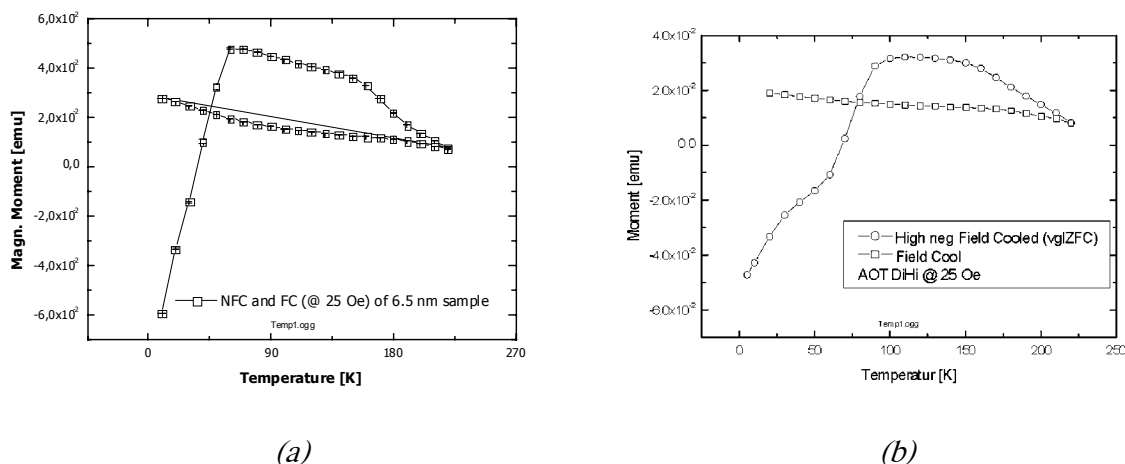


Figure 4-11: ZFC/FC-measurements of (a) 6 nm and (b) 11 nm particles in mesitylene. A negative field of 25 Oe is used during heat-up in the experiments. The blocking temperature  $T_B$  can be taken from the maxima of the ZFC-curves, being for (a)  $\sim 60$  K and for (b)  $\sim 100$  K.

The blocking temperature has been found to be 60 K and 100 K for 6.6 nm and 11 nm particles, respectively, which is in accordance to the expected theoretical values [35]. From Figure 4-11 it is evident, that the ZFC and the FC-curves do not match in the region around  $T_B$ , like it is known. However, this is an indication for ultrafine particles, which was observed before [36]. Thus, the received particles behave superparamagnetic above  $T_B$ , while they are single-domain ferromagnets below the mentioned values of  $T_B$ . From none of the above mentioned magnetic measurements, a tilting of the magnetisation-curve can be observed. The absence of this effect, originated by a Co/CoO bilayer ferromagnetic-antiferromagnetic spin-exchange coupling, suggests, that there is no stable CoO-layer formation on the surface of the particles. The result is consistent with the observations, which we described above for the oxidation of the received particles [37, 38].

### TDS-systems

As mentioned in Chapter 3, TDS seemed to be another candidate for a successful synthesis of magnetic Co-particles. Since the structure of TDS offers both, the sulfo-succinate end-group and the long  $C_{13}$ -alkyl-chain, we found out, that the same procedure as in the case of AOT can be used with this surfactant. The advantage is the fact, that there is just one component in the system, which has always the same ratio of growth controlling and dispersive character. Moreover, it is known, that TDS is used and released for cosmet-

ics manufacturing, which makes it an interesting compound for the later case of technical application.

Dicobalt-octacarbonyl was heated in the presence of both surfactants to temperatures of 170, 180, 200 and 215 °C. We made samples at different temperatures to study the influence of decomposition temperature on the resulting particles. The heating stage took 5 min in each case and the solutions were allowed to cool down to room temperature slowly before transferring them into the glove-box and the preparation of TEM samples. Some TEM-samples and some samples for HR-TEM were prepared using an applied magnetic field while the deposition process.

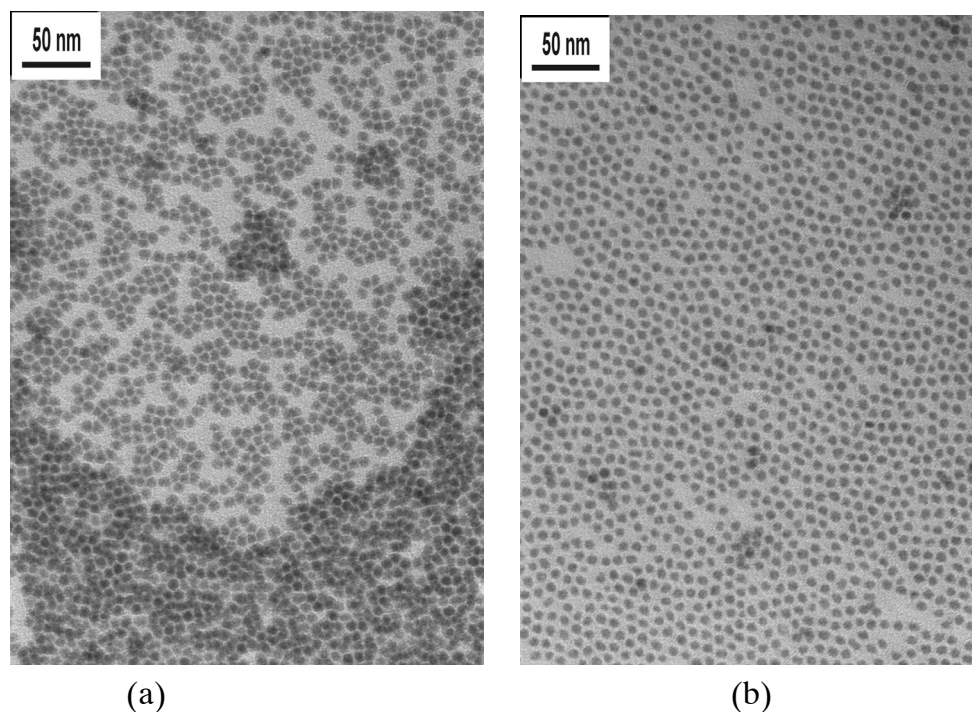
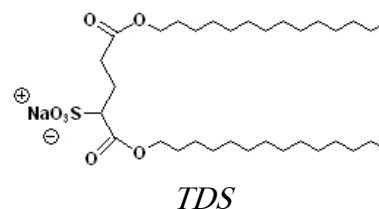


*Figure 4-12: (a): Co-Particles performed at 170°C in TDS. Here, formation of double layers can be observed frequently; (b): Same solution heated to 180°C. In both solutions, the ratio of Co:TDS is 25, all other parameters are cloned to those of the AOT/OA-experiments.*

The decomposition of  $\text{Co}_2(\text{CO})_8$  in TDS results in a brown coloured solution, if the heating is carried out at a temperature between 170 °C and 180 °C. There is no precipitate at 170 °C and just traces at 180 °C, the samples show ferrofluid behaviour. The experiments carried out at 200 °C and 215 °C, however, result in colourless solutions with a black precipitate.

While the solution at 200 °C still shows a decent brown colour, the other mentioned solutions are clear and colourless. The precipitate is ferromagnetic and can be moved using a permanent magnet. Analysis of the solutions in TEM shows, that the solutions at 170 °C and 180 °C includes dispersed nanoparticles, whereas the solutions made at 200 and 215 °C consists mainly of aggregated particles. In Figure 4-12, some examples of the particles are given.

Figure 4-12 shows, that even at 170 °C parts of the solution already start to cluster, but still the main fraction is the dispersed one forming monolayers. Clustering and aggregate formation in colloidal dispersions of magnetic particles is in general enhanced by their magnetic properties [39]. Data on the particles is summarised in Table 4-3. While it is possible to count particle sizes in the cases of the 170 °C and 180 °C-heated samples, the sizes of the high-temperature samples are deduced from magnifications of the aggregates. In fact, no particles can be found in the colourless solutions.

*Table 4-3: Data on the Co-particles from the performed experiments with TDS and  $\text{Co}_2(\text{CO})_8$*

Temperature	Particle diameter [nm]	Size distribution [nm]	Size distribution [%]
170 °C	7.8	0.8	10.0
180 °C	7.6	0.8	9.9
200 °C	7.1	0.6	8.9
215 °C	5.0	0.6	12.6

From Table 4-3 can be concluded, that between 170 °C and 200 °C, only a slight decrease of the particle sizes is visible. In the sample performed at 215 °C, the aggregate shows significantly smaller particles with a size of 5 nm. The same effect can be seen also in the pictures, which were made parallel on the HR-TEM.

It seems, that the stabilising effect of the TDS disappears with higher temperatures applied to the solution. Even though the formation mechanism is changing, if we compare the situation at 170 °C and at 215 °C, the formation of the particles is controlled. Looking at the intermediate temperatures 180 and 200 °C, the precipitation of the aggregate has a small size selection effect on the particles. The particle size of the particles in solution lowers by almost 1 nm and the standard deviation decreases by 1%.

In order to get a better insight into this process, we compared our system with the temperature dependency of TOPO-based Co-solutions. In experiments, where TOPO was used instead of TDS, a molar ratio between Co and TOPO of 4.5 to 1 was used. This ratio is a reproduction of experiments made by Alivisatos et al. [14]. Same temperatures were used for the comparison. In the experiments at 170 and 180 °C, a precipitate occurred accompanied with an intense green colour of the above solution. No colour could be observed for the samples at 200 and 215 °C, but precipitation also occurred. In the latter samples, a metallic film was deposited on the walls of the glass vessel.

*Table 4-4: Data on the Co-particles from the performed experiments with TOPO and  $\text{Co}_2(\text{CO})_8$*

Temperature	Particle diameter [nm]	Size distribution [nm]	Size distribution [%]
170°C	6.1	1.0	16.8
180°C	6.2	1.4	22.1
200°C	5.7	0.9	16.0

The origin of the green colour was examined by using UV-VIS spectroscopy. The colour of the solution, i.e. the spectrum changed twice, when the sample was opened under air. This indicates, that the initial green colour is caused by the interaction between Co(0) at the surface of the particles and the TOPO ligand in the particles' shell. This state is followed up by oxidation of the Co(0) to Co(II) and later to Co(III) indicated by the two colour changes, when the sample is exposed to air. This is an indirect proof for the initial presence of zero-valent Co in the solution, allowing the particles' surfaces to be oxidised in two steps.

In all the samples, the produced particles tend to cluster together in bigger particle arrays, resulting in a precipitate. It has ferromagnetic properties proved by interaction with a permanent magnet. At 215 °C, where all particles seem to be precipitated, not enough particles stayed in solution to be able to analyse the particles' sizes. The results of the TOPO-experiments are presented in Table 4-4.

The results suggest, that also in the case of the TOPO-solutions, the particle size is decreasing slightly with higher temperature. The reached particle size is around 6 nm, 2 nm less than with TDS under similar conditions. The size distribution of the particles is much higher as in the case of TDS. Also, the ordering of the particles is hardly to see.

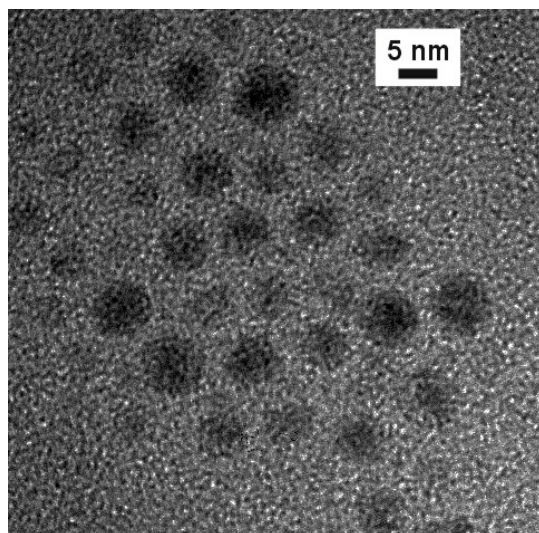


*Figure 4-13: Ordered arrays of Co-nanoparticles in TOPO-solution heated at 170 °C made visible by HR-TEM. Such patterns are present also in the samples at 180 °C and 200 °C.*

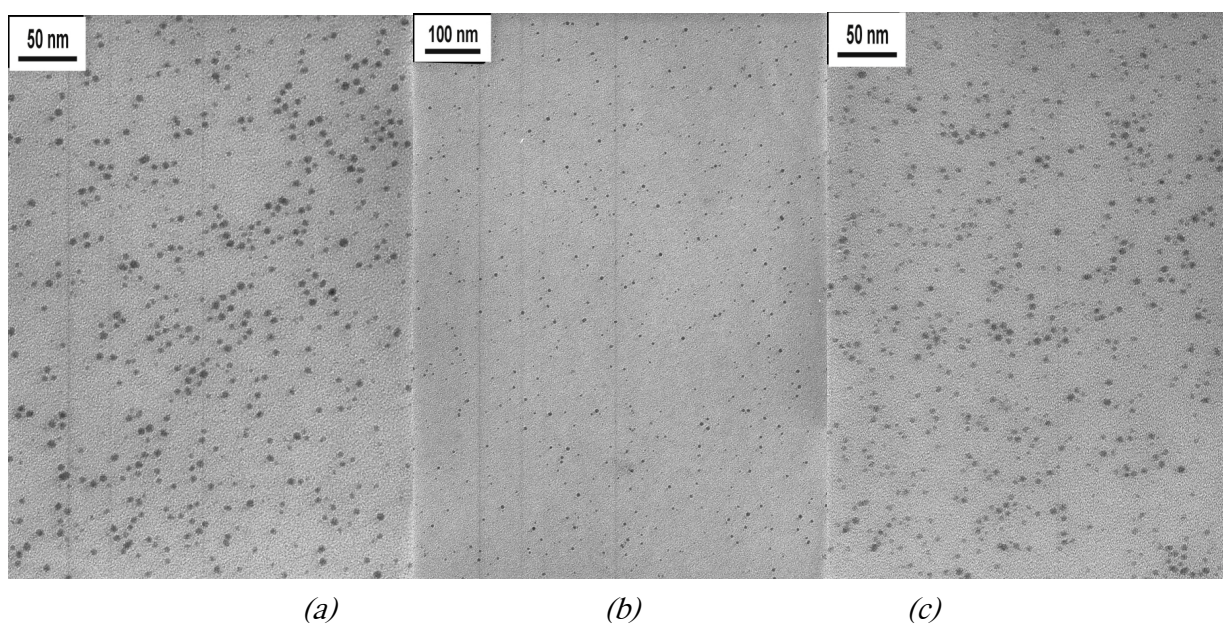


*Figure 4-14: TEM-micrographs of Co-Particles performed at (a)170 °C, (b)180 °C and (c)200 °C in TOPO using mesitylene as solvent. A ratio of Co:TOPO of 4.5 is used. Table 4-4 shows the sizes of the particles*

The formation in TOPO-solution leads to a higher content of precipitate as compared to TDS. The consequence is a lower coverage of the TEM samples by the particles. The missing ordered deposition of the particles seems to be a consequence of the low concentration of Co-particles in the solution. Still, the forma-



tion of well-ordered arrays can take place in regions, where the Co-concentration is higher, like at the edges of the TEM-grid. Figure 4-13 shows a picture from the solution at 170 °C taken with HR-TEM, where ordering could be observed. Such arrays could be recognised also at 180 °C and 200 °C reaction temperature.

Comparing the particle formation in TOPO and TDS, the main difference is the achieved particle size distribution. Using TOPO as the controlling surfactant results in particles, which vary much more in size. This can be easily seen by the presence of many small particles on the pictures taken from the TOPO-solution as shown in Figure 4-14.

As mentioned above, the TDS-containing solutions were forming aggregates. These aggregates were consisting of Co-particles as well. Having a look on the aggregates in the TEM, the aggregates are structured from monodisperse particles forming multilayers. Thus, aggregation occurs because of a collapse in the structure of the surfactant, in this case TDS. Figure 4-15 shows the particle aggregates at 200 °C and 215 °C. The aggregates are ferromagnetic as well and form needles, which are moving, while approaching with a permanent magnet.

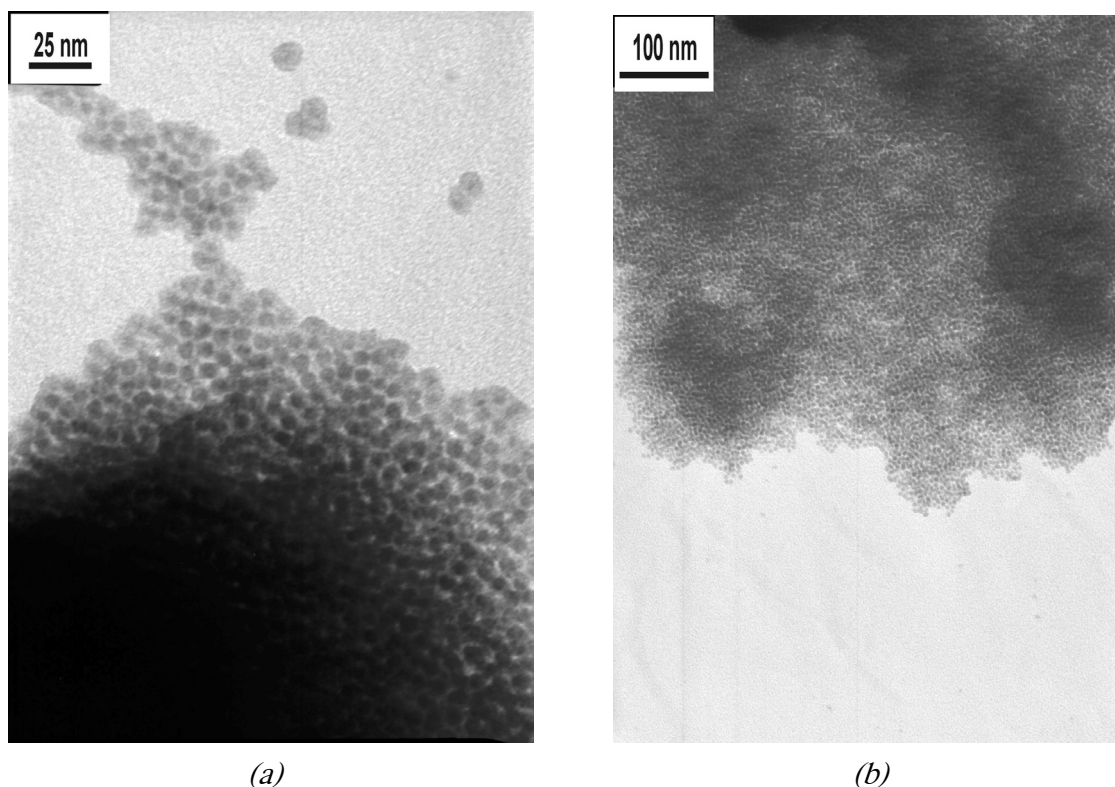


*Figure 4-15: Grain borders of aggregates formed at (a)200 °C and (b)215 °C in TDS. At the borders, monolayers of particles can be recognised. The particles are ordered and narrowly distributed..*

To increase the order in the packing of the particles, samples from the solution were deposited on the TEM-grid, while applying a magnetic field below the TEM-grid. This procedure was used formerly to induce a 2D-structuring of magnetic nanoparticles. The direction of the field lines are influencing the deposition behaviour of the solution. Thus, the direction of the magnetic field can be applied either parallel to the substrate or perpendicular to the substrate. This can be done e.g. by selective placement of a permanent magnet in the neighbourhood of the deposition area, called magnetophoretic deposition [40].

In our experiment, we first put the magnet in that way, that the field lines lie parallel to the deposition area. In consequence, the starting of 3d-arrangements of the nanoparticles could be observed. Needle-shaped grains do form on the substrate. Figure 4-16 shows these grains.

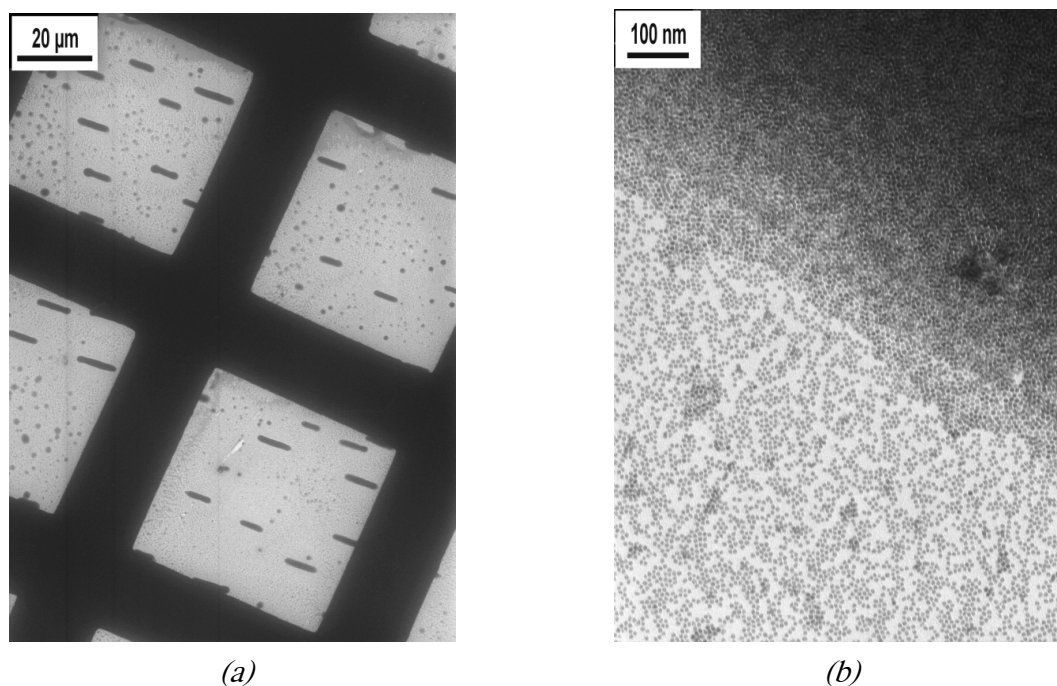


*Figure 4-16: Aggregates formed at 170 °C during deposition in a magnetic field parallel to the substrate (TEM-grid) (a) Overview; (b) Onset of one of the stripe-shaped aggregates.*

Due to its response to the magnetic field, the entire aggregates orient along the field lines of the magnetic field. This can be seen on Figure 4-16a. When zooming to one of the large needles, which is demonstrated on Figure 4-16b, still, the substrate is covered by particles. However, a closely packed layer is forming to build up the 3d-structures. These structures obviously are formed from closely packed nanoparticle layers. In Figure 4-16b a terrace-like

onset of the needles is observed, which suggests, that the needles are more extended perpendicular to the sample, when moving to the middle of the needle.

When the field lines run perpendicular to the substrate, the deposition pattern changes. Instead of needle-like, 3d-rrangements, a close packing of layers is observed. This pattern is

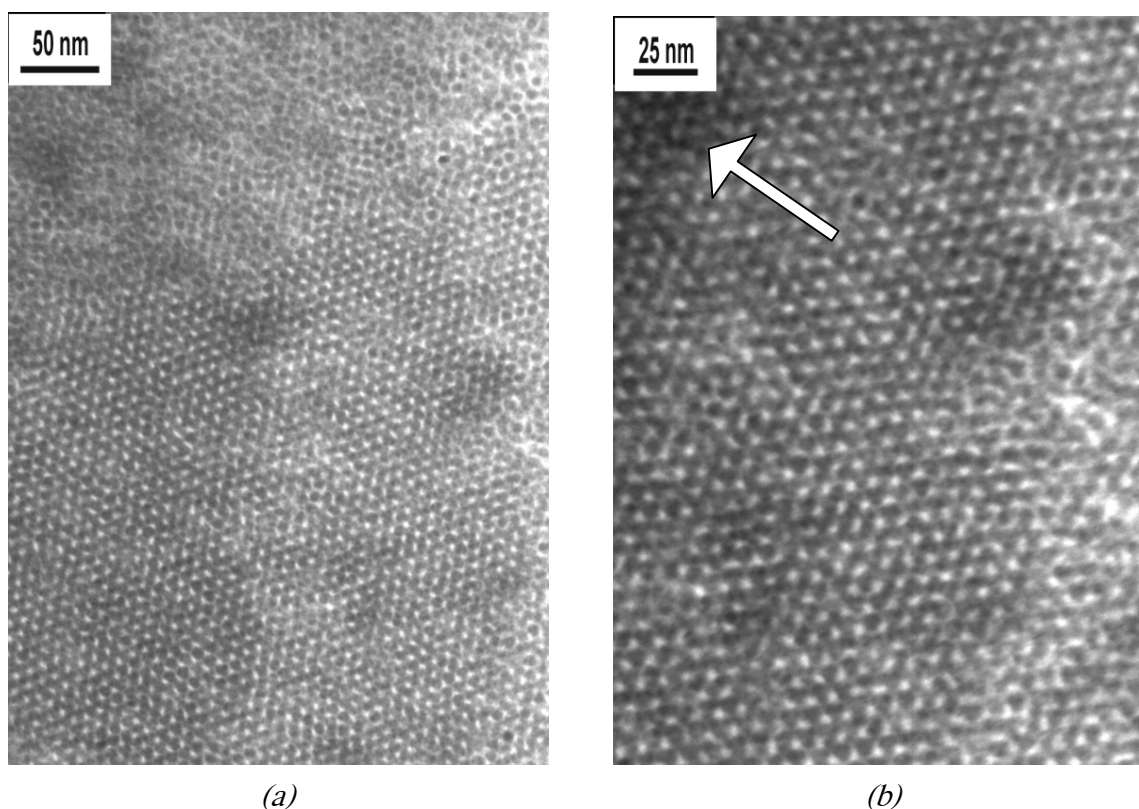


*Figure 4-17: Double layer formed on a substrate, while a droplet is deposited in a magnetic field perpendicular to the TEM-grid. (b) is a magnification of the area in (a). The sample used is a Co-solution formed with TDS at 180 °C. The arrow marks an area, where no substrate can be seen.*

shown in Figure 4-17. The pattern represents an overlay of two 2d-hexagonal patterns. This is known from the layer packing of dense packing patterns. It is worth to be noted, that even the holes form a hexagonal pattern. The fact, that no substrate can be seen in aggregates with more than two layers, suggests, that the packing of the aggregates is bcc instead of hcp [41, 42]. In the latter packing structure, the alternation of two staggered layers is present and the substrate would have to be visible, because just the half of the octahedral gaps are filled by the second layer. In the bcc-packing structures, three layers are alternating, being staggered in a way, that all of the holes are covered by a particle. An area, where this can be



seen is marked by an arrow in Figure 4-15b. The regularity of the pattern is visible by appearance of linear interparticle fringes.

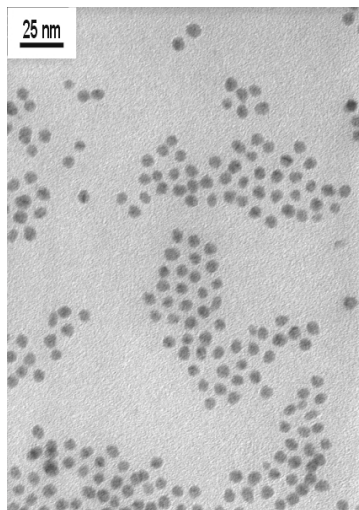


*Figure 4-18: Aggregate formed at 200 °C in oleic acid, redispersed by means of a small amount of oleic acid. The OA-containing mesitylene-solution was fed with the aggregate and heated in a heatable shaker for 30 minutes at 80 °C.*

As mentioned above, the TDS-containing solutions were forming aggregates. These aggregates were consisting of Co-particles as well. By addition of a droplet (0.5  $\mu\text{L}$ ) of oleic acid, the aggregates could be redispersed again and formed stable particle solutions. The redispersion took about 30 minutes at 80 °C. On TEM-micrographs, as shown in Figure 4-18, it can be seen, that the addition of oleic acid increases the dispersibility and the particles are present as individual, surfactant-protected particles with a tendency to form a hexagonal arrangement in a packed monolayer.

The aggregate could be isolated by simple extraction from the solution with use of a magnet. A long-term-stability of the 3d-arranged particles could be observed. When keeping the precipitate at ambient atmosphere, we found out, that the particles were still stable after one year after synthesis. The protection by the TDS-surfactant, thus, is very efficient. The stability of the particles was tested by checking the magnetical response of the powder. Indeed, there is still a very strong response to the field of a permanent magnet. This suggests, that oxidation of the particles did not occur in a significant extent.

This result is very important due to the fact, that the solution behaviour of the particles is quite different. It seems, that the solid surfactant is able to protect the very oxidation sensitive Co-particles, but that in solution, the mobility of the dissolved surfactant is a factor,

which contributes considerably to the permeability of the gas towards the particle surface. In the case of TDS-solutions, the dispersed particles were not responding to the magnet after minutes on ambient atmosphere, as it was observed before with the AOT/OA-solutions. The difference between the systems is the aggregated state. When we formed aggregates in a AOT-solution, these aggregates didn't stay magnetic, while the TDS-aggregates are magnetic.

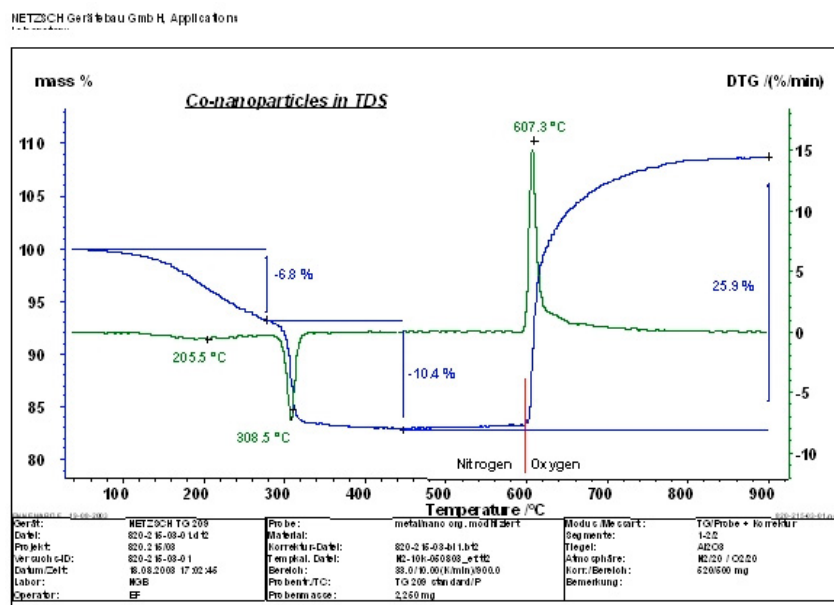
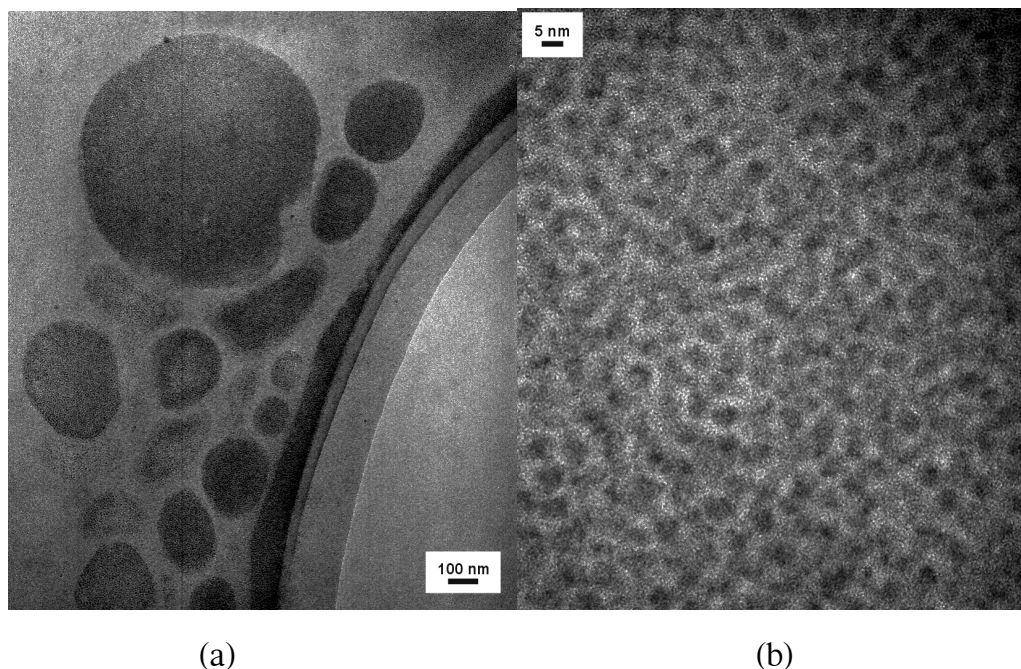


Figure 4-19: HR-TG-measurement on a small portion of TDS-precipitate of a solution made at 170 °C reaction temperature. The ferromagnetic sample was prepared for measurement after 6 months at ambient atmosphere. The temperature is drawn vs. the percentual weight of the sample (left axis) and its derivative (right axis).

High resolution thermogravimetry (HR-TG) was used to study the thermal behaviour of the magnetic aggregate. A small portion of this aggregate was heated up to 1000 °C. Figure 4-19 shows the result of this measurement. Up to 308 °C, the organic components are decomposed completely. One can see a two-step pyrolytic process, where most likely some rests of solvent are removed. This removal is slow. Then, a second component, which is most likely the organic surfactant TDS is decomposing. There is a percentage of approx. 83% remaining above 310 °C. When the gas flow has to be changed from nitrogen to oxygen at 600 °C, a very rapid increase of mass is observed. Here, the oxygen from the carrier gas starts to react with the sample. Most likely, the very rapid way, in which this reaction occurs, belongs to the high surface of the sample because of its nanostructuring. The increase in weight is very

high. 26% of mass increase means, that neither an oxidation solely from Co to CoO nor from CoO to  $\text{Co}_2\text{O}_3$  has occurred. The mass increase would be much lower in this case, around 15%. Thus, metallic cobalt is present in the sample. A complete oxidation of Cobalt to  $\text{Co}_2\text{O}_3$  would bring an increase of weight of 34%. In this experiment, a value of 26% was reached. Since parts of the Cobalt are already oxidised (deducing from the calculations on AOT/OA-systems around 0.7 nm outer layer per particle), the value of 26% is very close to the expected value for the complete oxidation of Co to  $\text{Co}_2\text{O}_3$  of the metallic Cobalt core.  $\text{Co}_2\text{O}_3$ , which is an adduct of  $\text{Co}_3\text{O}_4$  with  $\text{O}_2$  in the crystal layer, could be stable enough under oxygen atmosphere, while under ambient condition, a subsequent reaction with moisture happens.



*Figure 4-20: (a) Examples of aggregates formed in the TOPO-experiments in HR-TEM; (b) Monolayer of particles inside of the droplets showing their consistence of small Co-nanoparticles. Pictures from a solution performed at 200 °C.*

Aggregates of particles, synthesised in TOPO-containing solutions, can be seen in HR-TEM as islands with diameters between 150 nm and 1  $\mu\text{m}$ . Figure 4-20a shows an overview of those islands, Figure 4-20b is an area within the islands of Figure 4-20a.

The size of the particles inside of the aggregates is in the range of the particles outside of the aggregates. The difference is, that there are no particles having diameters of below 5 nm. This means, that the small particles fraction can be found almost exclusively outside of the aggregates. Hence, this is a hint that the particle precipitation is size-selective.

There is an interesting phenomenon, which can be observed inside of the particle aggregates of the TOPO-solutions. In some regions of the precipitate, elongated particles are formed. Those particles are not present throughout the entire film, but they appear occasionally. Elongated particles (see Figure 4-21) are present in many of the examined aggregates, but they appear only in the sample heated to 180 °C.

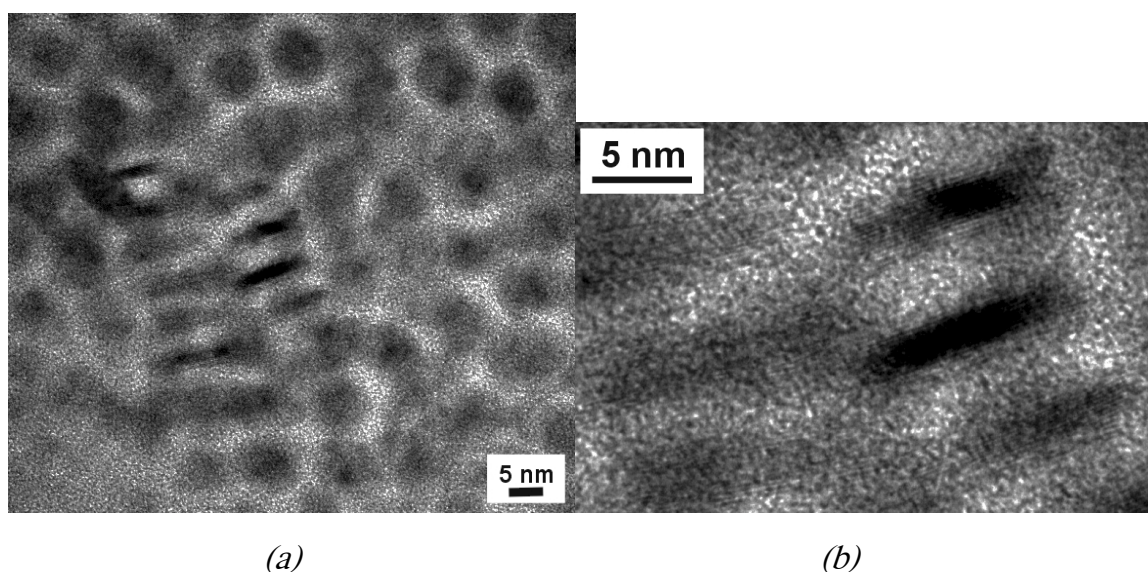


*Figure 4-21: (a) Array containing elongated particles in a TOPO-solution heated at 180 °C (b) Magnification of the elongated particles showing their monocrystalline structure.*

Further examination of the anisotropic particles shows, that they are built from former spherical particles, which are bridging together. The length of the particles is 13 or 20 nm, whereas the width of the elongated particles is 3.5 nm, which means around the half of the initial diameter of the spherical particles. This results in an aspect ratio of 3.7 to 5.7. The elongated particles are monocrystalline and show crystal fringes. The fringes are all oriented into the same direction. Hence, the crystalline growth of the particles is anisotropic and directed. A possible explanation is a magnetically induced crystallisation or the presence of locally high concentrations of the surfactant, which starts to form a non-spherical phase [43].

## 4.4 Conclusions

We conclude, that it is possible to synthesise Co-nanoparticles in a controlled way, either using a mixture of AOT and oleic acid or TDS as surfactant, when using  $\text{Co}_2(\text{CO})_8$  as precursor compound. Using the mixture of AOT and OA gives a small range of ratios, where the particles lead to stable solutions with a narrow size distribution. The size of the particles can be influenced exclusively by the ratio between Co and AOT, giving particles between 4 and 12 nm in diameter. We could show, that a thoroughly prepared solution can be generated with a very thin oxide layer on the surface. Particles solutions are superparamagnetic, showing ferromagnetic behaviour either under influence of a strong magnetic field or going to low temperatures below 100 K. The values reached for the magnetisation are in the range of bulk Cobalt.

Switching to a surfactant like TDS, which combines the properties of AOT and OA, leads to other attractive possibilities. At lower temperatures, stable dispersions with narrowly distributed particles can be made. The size of the particles corresponds approximately to the values of the for comparable AOT-OA systems. Turning to higher temperatures, a ferromagnetic powder of protected Co-nanoparticles can be synthesised. This powder is long-time stable and keeps its magnetic properties for one year and longer. The solid can be re-dispersed, which leads to a chemically attractive material. By application of magnetic fields while deposition on a substrate, the resulting film can be manipulated. 2d and 3d-structures can be induced by a magnetic field. Using TOPO as surfactant, aggregates can also be made at elevated temperatures, which are not long-time stable. The aggregates contain elongated particles, as well as spherical particles. All particles in solution show low resistance toward oxygen, in solution, no protection of the particles can be achieved.



## 4.5 References

- [1] S.W. Charles, R.E. Rosensweig, *J. Mag. Mag. Mater.* **1983**, *39*, 192; S. Kamiyama, R.E. Rosensweig, *J. Mag. Mag. Mater.* **1987**, *65*, 403; E. Blum, R. Osols, R.E. Rosensweig, *J. Mag. Mag. Mater.* **1990**, *85*, 305; V. Cabuil, S. Neveu, R.E. Rosensweig, *J. Mag. Mag. Mater.* **1993**, *122*, 439; S.P. Bhatnagar, R.E. Rosensweig, *J. Mag. Mag. Mater.* **1995**, *149*, 199; L. Vekas, V. Sofonea, O. Balau, *J. Mag. Mag. Mater.* **1999**, *201*, 454; S. Odenbach, S. Thurm, K. Melzner, *J. Mag. Mag. Mater.* **2002**, *252*, 421; C. Scherer, *J. Mag. Mag. Mater.* **2005**, *289*, 487.
- [2] T. Sugimoto, E. Matijevic, *J. Colloid Interface Sci.* **1980**, *74*, 227.
- [3] M. Ronay, *IBM Tech. Discl. Bull.* **1976**, *19* (7), 2753.
- [4] N. Buske, H. Sonntag, T. Götze, *Colloids and Surfaces*, **1984**, *12*, 195.
- [5] T. Fried, G. Shemer, G. Markovich, *Adv. Mater.* **2001**, *13*, 1158.
- [6] N. Cordente, M. Respaud, F. Senocq, M-J. Casanove, C. Amiens, B. Chaudret, *Nano Lett.* **2001**, *1*, 565.
- [7] L. Guo, Q. Huang, X. Li, S. Yang, *Phys. Chem. Chem. Phys.* **2001**, *3*, 1661.
- [8] T. Hyeong, *Chem. Commun.* **2003**, 927.
- [9] C. Petit, A. Taleb, M.P. Pileni, *J. Phys. Chem. B*, **1999**, *103*, 1805.
- [10] C. Petit, A. Taleb, M.P. Pileni, *Adv. Mater.* **1998**, *10*, 259.
- [11] M.P. Pileni, *Adv. Funct. Mater.* **2001**, *11*, 323.
- [12] M. Giersig, M. Hilgendorff in: *Cluster and Nanostructured Interfaces*, Puru Jena (ed.), World Scientific, Singapore, **2000**, 203.

- 
- [13] Kurikka VPM Shafi, A. Gedanken, *Adv. Mater.* **1998**, *10*, 590.
- [14] V.F. Puentes, K.M. Krishnan, A.P. Alivisatos, *Science*, **2001**, *291*, 2115.
- [15] S. Sun, C.B. Murray, H. Doyle, *Mat. Res. Soc. Symp. Proc.* **1999**, *577*, 386.
- [16] S. Sun, C.B. Murray, *J. Appl. Phys.* **1999**, *85*, 4325.
- [17] F. Dumestre, B. Chaudret, C. Amiens, M.C. Fromen, M.J. Casanove, P. Renaud, P. Zurcher, *Angew. Chem.* **2002**, *114*, 22.
- [18] C.P. Gibson, K.J. Putzer, *Science*, **1995**, *267*, 1338.
- [19] D.P. Dinega, M.G. Bawendi, *Angew. Chem.* **1999**, *111*, 1906.
- [20] V.F. Puentes, D. Zanchet, C.K. Erdonmez, A.P. Alivisatos, *J. Am. Chem. Soc.* **2002**, *124*, 12874.
- [21] J.P. Chen, C.M. Sorensen, K.J. Klabunde, G.C. Hadjipanayis, *Phys. Rev. B*, **1995**, *51*, 11527.
- [22] J.B. Peri, *J. Colloid Interface Sci.* **1969**, *29*, 6.
- [23] R. Tannenbaum, *Inorg. Chim. Acta*, **1994**, *227*, 233.
- [24] J. Clarke in: *Superconducting Electronics*, H. Weinstock, M. Nissenoff, Springer Series F: Computer and systems sciences, **1989**, 59.
- [25] K.J. Davies, S. Wells, S.W. Charles, *J. Mag. Mag. Mater.* **1993**, *122*, 24.
- [26] K. Fontell, *J. Colloid Interface Sci.* **1973**, *44*, 318.
- [27] E. Papirer, P. Horny, H. Balard, R. Anthoe, C. Petipas, A. Martinet, *J. Colloid Interface Sci.* **1983**, *94*, 207.
- [28] X. Peng, J. Wickham, A.P. Alivisatos, *J. Am. Chem. Soc.* **1998**, *120*, 5343.
- [29] K. Nielsch, F.J. Castano, C.A. Ross, R. Krishnan, *J. Appl. Phys.* **2005**, *98*, in press.
- [30] C.A. Ross et al., *Phys. Rev. B*, **2000**, *62*, 14252.

- [31] K. Zürn, *PhD Thesis*, Universität Ulm, in progress.
- [32] M.P. Pileni, N. Duxin, *Chem. Innovation*, **2000**, 25.
- [33] D.H. Tarling, in: *Principles and Applications of Palaeomagnetism*, Santype Ltd., Great Britain 1971, p. 71.
- [34] I. Zhitomirsky, M. Niewczas, A. Petric, *Mater. Lett.* **2003**, 57, 1045.
- [35] *Nanoscale Materials in Chemistry*, K.J. Klabunde (ed.), Wiley Interscience, John Wiley & Sons Inc., 1<sup>st</sup> Edition, 2001.
- [36] B.H. Sohn, R.E. Cohen, G.C. Papaefthymiou, *J. Mag. Mag. Mater.* **1998**, 182, 216.
- [37] M. Rubinstein, *J. Appl. Phys.* **1999**, 85, 5880.
- [38] J.P. Chen, C.M. Sorensen, K.J. Klabunde, G.C. Hadjipanayis, *Phys. Rev. B*, **1995**, 51, 11527.
- [39] D.Y.C. Chan, D. Henderson, J. Barojas, A.M. Homola, *IBM J. Res. & Dev.* **1985**, 29, 11.
- [40] M. Giersig, M. Hilgendorff, *J. Phys. D: Appl. Phys.* **1999**, 32, L111.
- [41] C.B. Murray, S. Sun, W. Gaschler, H. Doyle, T.A. Betley, C.R. Kagan, *IBM J. Res. & Dev.* **2001**, 45, 47.
- [42] M. Hilgendorff, B. Tesche, M. Giersig, *Aust. J. Chem.* **2001**, 54, 497.
- [43] K. Esumi, K. Matsuhisa, K. Torigoe, *Langmuir*, **1995**, 11, 3285.



# ***Complexation of cobalt-precursors in PS-*b*-P2VP block copolymer micelles***

## **5.1 Introduction**

In this and the following chapter, we will discuss experiments, which were done, in order to perform Co-nanoparticles in block copolymer solution. Due to the fact, that our experiments showed, that the reduction step is quite difficult, we will deal with the reduction in Chapter 6. In the following Chapter, the primary step is examined in detail. It is the solubilisation of a precursor compound into the micellar core of a micellar solution of an amphiphilic block copolymer. This step was done mainly with different PS-*b*-P2VP block copolymers, which differ in the polymerisation degrees of the respective block.

Using diblock copolymers in solution leads to micellar solutions, when the both blocks of the polymers are incompatible and the solvent is chosen to be selective just for one of the both blocks [1]. Using unpolar solvents like benzene, toluene or mesitylene, the PS-*b*-P2VP molecules will form inverse micelles with the polystyrene block forming the corona and the poly(2-vinylpyridine)-block forming the core of the micelles. Dependent on the ratio of polymerisation degree, star-shaped, crew-cut or symmetrical micelles will form [2]. The cmc of micelle formation is very low and is far below a concentration of 1 mg/mL.

The concept, we followed to form single nanocrystalline Co-particles inside each micelle, is based on the knowledge, we have for a similar process, which was successfully applied to the formation of gold nanoparticles [3]. For cobalt, it is shown in Figure 5-1.

Following the approach in Figure 5-1, it is the goal in this chapter to show successful trapping of a Co-precursor compound selectively in the micellar core of the polymer micelle. Only with the condition of selectiveness, the particles are later formed only inside of the micellar core. It is known, that polymers are an excellent matrix for Co-nanoparticle crystallisation even without the condition of micelle formation [4]. Thus, the particles will form outside of the micellar cores, if still some precursor compound will remain in solution or adsorbed on the PS-corona of the micelle.

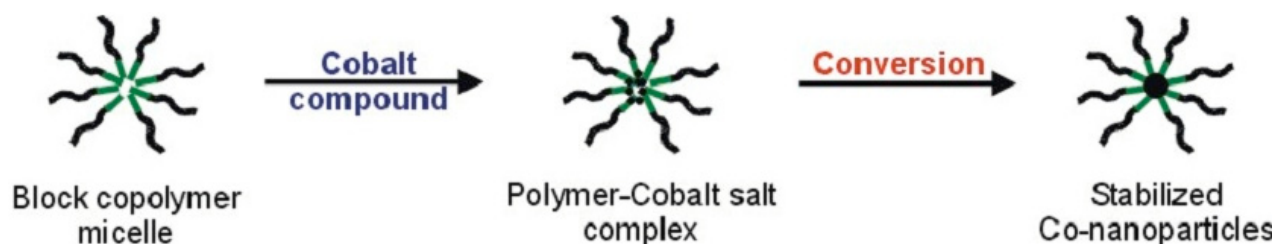


*Figure 5-1: Main strategy for Co-particle-formation in block copolymer micelles. The first step is the uptake of the cobalt precursor inside of the micellar core (this chapter). After selective confinement in the micellar core, a conversion step transfers the precursor into the metallic particles (Chapter 6)*

The uptake into the micellar core is studied by TEM of casted films of the solutions. The Cobalt-salts show higher electron density than the organic components of the system. Thus, the localisation of the precursor can be seen by the higher contrast in TEM-micrographs. Film formation of the micellar systems will lead to 2d-patterns, because of the incompatibility of the both blocks [5,6].

## 5.2 Experimental

### *Chemicals*

Cobalt carbonyl ( $\text{Co}_2(\text{CO})_8$ ), an orange solid (Fluka, 95% stabilised with n-hexane), was stored at  $-20^\circ\text{C}$  and has been used as received.  $\text{CoCl}_2$  and  $\text{CoCO}_3$  (both 98% from Fluka) were dried 3 days at  $80^\circ\text{C}$  in a vacuum oven to remove crystalline water. Other Co-salts were dried in the same way to remove crystalline water. p.A.-grades (>98%) from Fluka or Merck were used in all the cases. Toluene and mesitylene were dried three days over  $\text{LiAlH}_4$  and distilled twice at  $60^\circ\text{C}$  under dynamic vacuum, further condensed below

room temperature in a high vacuum line under dynamic conditions using an oil diffusion pump. The latter process was carried out using trioctyl-aluminium as drying agent.

Anhydrous hydrazine was synthesised by thermolysis of hydrazine cyanurate. The synthetic procedure is described elsewhere [6, 7], dimethyl-glyoxime (Merck, p.A.) was used as received.

PS-*b*-P2VP block copolymers were synthesised using living anionic polymerisation. The procedure is described in detail in the Appendix of this chapter. A summary on the used polymers, differing in block lengths is given in Table 5-1.

The synthetic procedure for the used glyoximato-complexes is described in the Appendix to this chapter as well.

*Table 5-1: Molecular weights of applied PS-*b*-P2VP polymers*

<i>Polymer label</i>	<i>DP (PS)</i>	<i>DP (P2VP)</i>	<i>Total molecular weight [g/mol]</i>	<i>Block length ratio R</i>
<i>1700-450</i>	<i>1700</i>	<i>450</i>	<i>224,368</i>	<i>3.78</i>
<i>1350-400</i>	<i>1350</i>	<i>400</i>	<i>182,300</i>	<i>3.38</i>
<i>710-210</i>	<i>710</i>	<i>210</i>	<i>96,200</i>	<i>3.38</i>
<i>750-50</i>	<i>750</i>	<i>50</i>	<i>83,445</i>	<i>15.00</i>
<i>190-190</i>	<i>190</i>	<i>190</i>	<i>40,900</i>	<i>1.00</i>
<i>800-860</i>	<i>800</i>	<i>860</i>	<i>173,820</i>	<i>0.93</i>
<i>600-800</i>	<i>600</i>	<i>800</i>	<i>146,662</i>	<i>0.75</i>
<i>550-1400</i>	<i>550</i>	<i>1400</i>	<i>204,479</i>	<i>0.39</i>

### *Sample preparation*

Typically, a volume of 1-2 mL of the solutions was made for a single experiment. The polymer was dissolved in the solvent with a concentration of 2.5 mg/mL. The solution was stirred in a nitrogen-filled glove-box for at least 2 days to ensure complete dissolution of polymer. Sealed glass-vessels were used in order to avoid contact with moisture and solvent evaporation due to nitrogen flow. The ending point of dissolution was considered, when the solution was clear. Filtration with a 0.45 $\mu$ L syringe filter was done to remove undissolved polymer and macroscopic impurities. The amount of salt or complex was calculated and

added to the polymer solution. The typical amounts of inorganic compound was in the range of 0.1 to 10 mg. For this purpose, a Sartorius MC5 quartz micro balance was used. The maximum dissolution of the balance was  $1\mu\text{g}$ , which was necessary in order to avoid large errors in loading of the right amount of inorganic salt. The salt was weighed into specially designed PTFE-vessels to avoid two things: First, the use of glass or paper leads to wrong weighing in glove box environment due to the air flow and formation of static charging of the salt. Second, the very small amount of salt will end up in a big error, if the weighed amount is not transferred completely into the polymeric solution. Thus, the weighed amount has to be put into the solution including the PTFE-vessel to ensure complete salt transfer.

The solution was allowed to stir as long as the solution became clear. This took in the most cases at least 3 days. Vigorous stirring had to be applied to the solution using identical stirring bars for each solution. The use of mechanical shaking is not recommended due to its lower efficiency. If the solution did not become clear after 4 weeks, filtration with a syringe filter was performed to remove the undissolved component.

### *Electron microscopy*

**Transmission electron microscopy (TEM)** images were recorded with a Philips EM 400 T microscope operating at 80 kV. Copper grids (mesh size:  $200 \times 200 \mu\text{m}^2$ ) were coated with a Formvar film (around 20 nm thickness) and a layer of carbon (approximately 5 nm thickness) and used as substrates for TEM analysis. The samples were prepared by evaporating a droplet of the solutions on the grid, which was in contact with a soaking tissue in order to avoid multilayer formation. **High-resolution TEM (HRTEM)** images were recorded with a CM 200 FEG (CS correcture) on a holey-copper grid, where a drop of the colloidal solution was evaporated in the way described above. Sample preparation was carried out inside of the glove-box. EDAX analyser coupled with HRTEM gives the semi-quantitative composition of the samples. With this apparatus, contact of the samples with the air cannot be completely avoided during the transfer of the samples into the microscope. Negatives were scanned on an Umex Astra scanner operating at 600 dots per inch (dpi) using constant picture sizes. Adobe Photoshop 5.5 was used for evaluation particle sizes and distances.

### *UV-VIS spectroscopy*

UV-VIS absorption spectroscopy was performed on a Lambda 16 UV-VIS spectrometer from Perkin-Elmer. Samples for spectroscopy were always treated by a centrifuge working on 5000 rpm, in order to remove dispersed solids. The latter influence the measurement by

broadening or hiding the spectrum of the solution. The spectrum was recorded, using pure solvent as reference, which was subtracted from the spectrum. The polymer is not disturbing the spectrum in the visible range, because its absorption is completely in the UV-region of the spectrum. For the exceptional cases, where information was needed on the UV-part of the spectrum, a solution of the respective polymer in same concentration was used as a reference.

*X-ray photoelectron spectroscopy (XPS)* was performed in a FISON ESCALAB-210 electron spectrometer which allowed to prepare a sample and analyse its chemical state by means of monochromatised Al-K $\alpha$  radiation (1486.6 eV) without breaking the ultrahigh vacuum conditions.

*Scanning force microscopy (SFM)* investigations were performed with a Nanoscope III (Digital Instruments, Santa Barbara, California, USA) operating in Tapping Mode<sup>TM</sup> and contact mode. The oscillation frequency for Tapping Mode<sup>TM</sup> was set in the range of 320-360 kHz depending on the Si cantilever ( $k \sim 50$  N/m, Nanosensors). Si<sub>3</sub>N<sub>4</sub> cantilevers ( $k \sim 0.06$  N/m, Nanosensors) were used for contact mode imaging. Films were prepared by dipping a substrate into a micellar solution by use of a dipping machine with vibration-free electric motor. The machine was self-made.

### 5.3 Results and discussion

The uptake of inorganic salts is the first step towards Co-nanoparticle synthesis within polymeric nanoreactors. The concept was used successfully to produce gold, palladium and semiconductor nanoparticles in a matrix, which is able to self-assemble [6, 8-10]. The self-assembly is induced, when a film from the solution is cast on a substrate. Here, the nature of the substrate plays an important role for the formation of a 2d-hexagonal pattern [11]. By variation of the used polymer, the polymeric matrix is also able to conduct the shape of the obtained particles [12]. Only a few examples were published so far, dealing with the transfer of the principle towards cobalt [6, 13]. Much effort was spent in this work, to closely examine the conditions and possibilities, which is offered by switching from metals like gold to cobalt. Here, the most important differences are, that cobalt is a non-noble metal and undergoes completely different reactions comparing to gold. The first is responsible for the lability against oxygen, the second is influencing the process of the basic reactions within the

nanoreactors.

In a first step, we tried to entrap a Co(II)-salt or compound within the micellar core. In order to perform this step, it is necessary to consider, that the uptake is based on a complexation reaction of Co(II) with the pyridine units within the core-building block of the polymer. This is different comparing to e.g. gold, where the initial step is based on the protonation of the pyridine unit and the formation of a binary salt with the gold-containing anion. This fact will be proved in the following text. First, we want to consider the whole Co-(II) uptake and show, that the formation of Co(II)-uptake into the micelles is a multi-step process, where each of the steps can influence the resulting solution. Figure 5-1 shows the steps of the Co(II)-uptake into the micelles as a general consideration for the process.

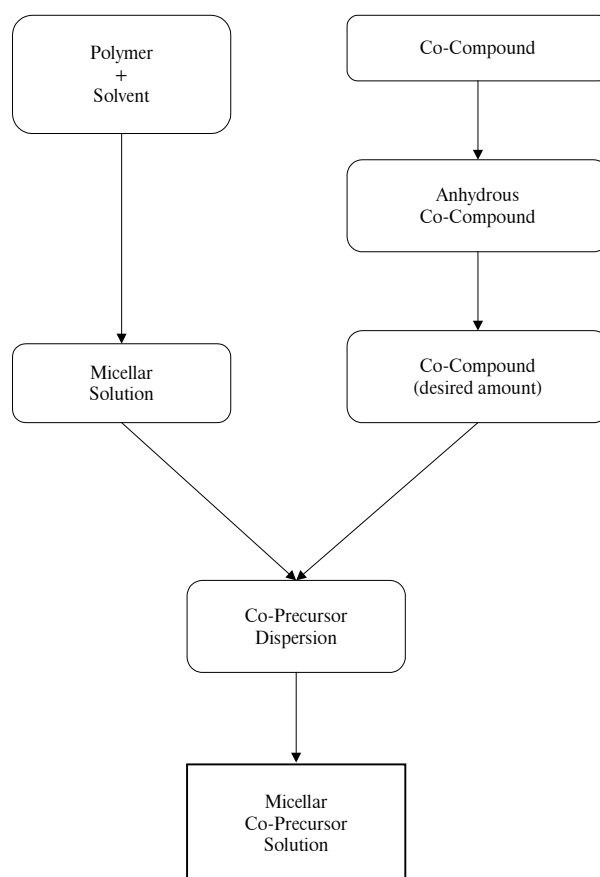


*Figure 5-1: Procedure for preparation of precursor solutions of Co-(II)-salts or  $\text{Co}_2(\text{CO})_8$  in polymeric micelle solutions. Every step has to be studied properly in order to achieve reproducible results.*

*Step 1: Polymer and solvent to form micellar solution*

The solvent has to be dried carefully in order to remove traces of water. In unpolar solution, the PS-*b*-P2VP polymer forms inverse micelles. Traces of water are dissolved in the polar regions within the micellar solutions. This ends up in the filling of the polar micellar cores with all water, remained in the system. Water presence, however, leads to three undesirable side-effects: First, the subsequent conversion of the Co-compound will take place under influence of water. Second, the micelles are destabilised by means of aggregation to bigger species. Finally, if Co-(II) is present in the system, solvation of Co-(II) will takes place, which is a common reaction of Co-(II). All mentioned side-effects were present, when we made solutions containing water in the solvent, by using non-dried toluene for micelle formation. The size distribution of the micelles increased and the reaction of water with Co(II) could be observed by a colour change from azure to an almost colourless, pinkish solution.

*Step 2: Choice of the desired Co-compound*

The used Co-compounds have to be free from crystalline water, i.e. anhydrous. Anhydrous Co-salts consist of a solvatised  $\text{Co}^{2+}$ -ion and the counterion. For these stable salts, thus, the uptake into the micellar cores is a ligand exchange reaction, which will run slowly. We observed for compounds like  $\text{CoCl}_2 \cdot 6\text{H}_2\text{O}$ , that the compounds were still present as small grains on the ground of the vessel even after 4 weeks of stirring in the micellar solution.

We had, however, many successful incorporations of those salts, which were free from crystalline water. For almost all hydro-complexes of Co-(II), the removal of crystalline water is possible by heating to 80 °C at vacuum for 48 hours. In exceptional cases like  $\text{Co}_3(\text{PO}_4)_2 \cdot 8\text{H}_2\text{O}$ , water removal is done by addition of hygroscopic acids. In the further work, only anhydrous compounds were used for investigation of Co-salt uptake.

*Step 3: Anhydrous Co-compound*

Great importance is attributed to the solubility of the respective salts in anhydrous toluene. On the one hand, the Co-compound doesn't have to have a good solubility. In these cases, distribution between micellar core and the solution around will take place. Depending on the solution enthalpies in the solvent and the pyridine units of the micellar core, the system will be described by a distribution constant  $K_{\text{Dist}}$ , which will be the best for our purposes, if it

is shifting the uptake towards the pyridine groups. On the other hand, if the interaction between solvent and Co-(II) compound will be repulsive, the salt will show no mobility and will stay within the crystalline composite. For the choice of the right compound, we made first an examination of the solution behaviour of several Co-(II) compounds. The results are shown in Table 5-2.

It can be seen from Table 5-2, that the Cobalt-complexes with organic ligands do well dissolve in the solvent, but there is no selective uptake into the micelles. Anhydrous Cobalt(II)-carbonate is a good example for a salt, which is completely insoluble and is neither found in solution nor inside of the micellar core. The ideal case seem to be the loading of micelles with  $\text{CoCl}_2$  or  $\text{Co}(\text{SCN})_2$ , which are also insoluble in toluene. Those compounds however have a good affinity to the 2VP-core and can be localised selectively. Speaking with the words of complex chemistry, the latter substances undergo complexation with the polymeric pyridine units.  $\text{Co}(\text{CO}_3)$  does not form stable complexes and is thus not localised in the micellar cores. In the case of the acetylacetonate, there is a ligand exchange. However, the equilibrium exchange between acetylacetonate and pyridine ligands is disturbing the selective localisation in the micellar core.

*Table 5-2: Dissolution behaviour of Co-(II) compounds in degassed, anhydrous toluene. The solutions were stirred overnight, centrifuged and examined with UV-VIS spectrometry. Different concentrations were measured in order to obtain precise values for the solubility.*

<i>Compound</i>	<i>Solubility</i>	<i>Chosen bands in UV-VIS [nm]</i>	<i>Selective uptake in micelles</i>
Cobalt-(II)acetylacetonate $\text{Co}(\text{acac})_2$	>10.19 mmol/L (quantitative)	280-350 (broad); 450-550 (triplet)	weak
Cobalt-(II)acetate $\text{Co}(\text{OAc})_2$	>3.5 mmol/L (partial dissolution)	420-550 (broad)	weak
Cobalt-(II)carbonate	<1.6 mmol/L	None	Almost none
Cobalt-(II)oxalate	<1.04 mmol/L	None	Almost none
Cobalt-(II)nitrate	<1.48 mmol/L	None	weak
Cobalt-(II)thiocyanate	<1.14 mmol/L	None	good
Cobalt-(II)chloride	<1 mmol/L	None	very good



*Step 4: Weighing of anhydrous Co-salts*

The used anhydrous salts have to be weighed under inert gas. As an example, the hydration enthalpy of the  $\text{Co}^{2+}$ -ion is  $-2 \text{ MJ/mol}$  [14]. This is the double amount compared to the hydration of protons ( $\text{H}^+$ ). Using a balance in ambient atmosphere makes the blue powder getting violet within 10 seconds, which indicates the formation of  $\text{Co}(\text{H}_2\text{O})_6\text{Cl}_2$ . This, however, is an undesired product by means of selective uptake into the micelles, since it is saturated by water ligands. Thus, the weighing has to be carried out necessarily in an inert gas atmosphere. Further details on processing Cobalt(II) under these conditions is given in Chapter 5.2 of this thesis.

*Step 5: Entry of the Cobalt salt into the micellar solution*

This step has to be carried out precisely. First, the polymer has to be dissolved completely in the chosen solvent. By our experience, the time needed for complete dissolution is depending on the block length ratio. While polymers with a ratio of  $>1.5$  PS:P2VP are dissolved within 1-3 days, the dissolution of symmetrical and crew-cut polymers takes usually much longer. Here, it is sometimes necessary to wait more than 2 weeks, until the solution gets clear. Heating of the samples below the boiling point accelerates this procedure by the factor of 2-3. The dissolution has to be complete in order to obtain regularly arranged patterns of micelles and is thus indispensable. The transfer of small amounts of Co-salts into the micellar solution has to be carried out without loss. We used special weighing caps for this purpose, which are made from PTFE. This material is neutral to the solution. In order to maintain the best results, the caps are placed in the inner side of the top of the vessel. This decreases the contact to the solution and increases the efficiency in stirring.

*Step 6: Micellar solutions*

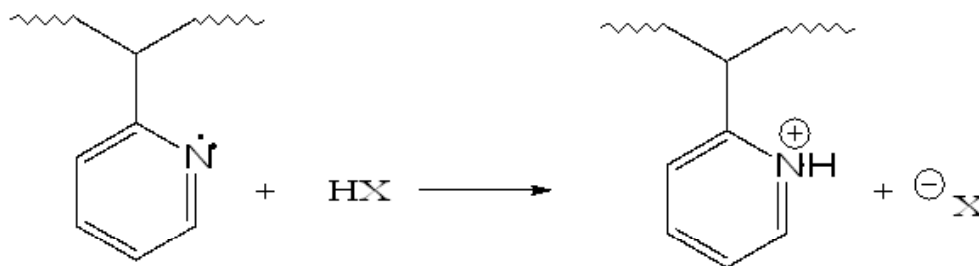
The stirring of the solutions is best performed inside of a glove-box, due to possible entries of moisture into the system when stirring at ambient conditions. The micellar solution is finished, when the solution gets clear. In cases of high loading, the solution is filtered or centrifuged, in order to undissolved Co-salt. The solutions have to be kept tightly closed, in order to avoid evaporation of the solvent, which makes the micellar solution collapse, when the concentration of micelles gets too high. With this step, the procedure is finished and the samples can be either examined or be used for other applications.

With this procedure, the solutions with Cobalt(II)-salts can be reproduced in a very good way. Many observations on the experimental technique helped us to understand the chemical and physical processes within the generation of micellar Co(II)-solutions.

For the purpose of Co-nanoparticle formation, the loading of the micelles is an important factor. The loading  $L$  of the micelles is defined as:

$$L = \frac{n_{\text{totalCo}(x)}}{n_{\text{totalVP}}} \quad (\text{Eq. 5-1}),$$

where  $n_{\text{totalCo}(x)}$  is the moles of Co in oxidation state  $x$  within the used Co-compound and  $n_{\text{totalVP}}$  is the total moles of vinylpyridine-units in the solution. The loading  $L$  gives us an idea, in which ratio the Co is incorporated into the 2VP-containing micellar core. The analogous consideration was made for gold and led to the final conclusion, that the pyridine units of the micellar core are protonated by tetrachloroauric acid [12]. In this case, the state, from which the gold compound is reduced to elemental gold is reached by



For cobalt, the basic reaction cannot be described in this way, since the used compounds do not contain protons. When  $\text{CoCl}_2$  is incorporated into the micelles, an azure solution is formed. This colour can be measured by UV-VIS spectrometry and gives spectra as shown in Figure 5-2. In Figure 5-2a, a complete spectrum is shown. Here, the characteristic absorption of the solutions is a triplet in the region between 580 and 640 nm. This spectrum leads to the consideration, that the complex within the micellar cores is a tetrahedral species, for which the blue colour is typical [15- 17].

In Figure 5-2b, a superposition of spectra from solutions with different  $\text{CoCl}_2$ -loadings is shown. Interestingly, the loadings seem to reach a saturation level in a very early stage of loading. Plotting the maximum intensities, this observation is confirmed. This plot is shown in Figure 5-3.

The results in Figure 5-3 are consistent with considerations and observations made for the

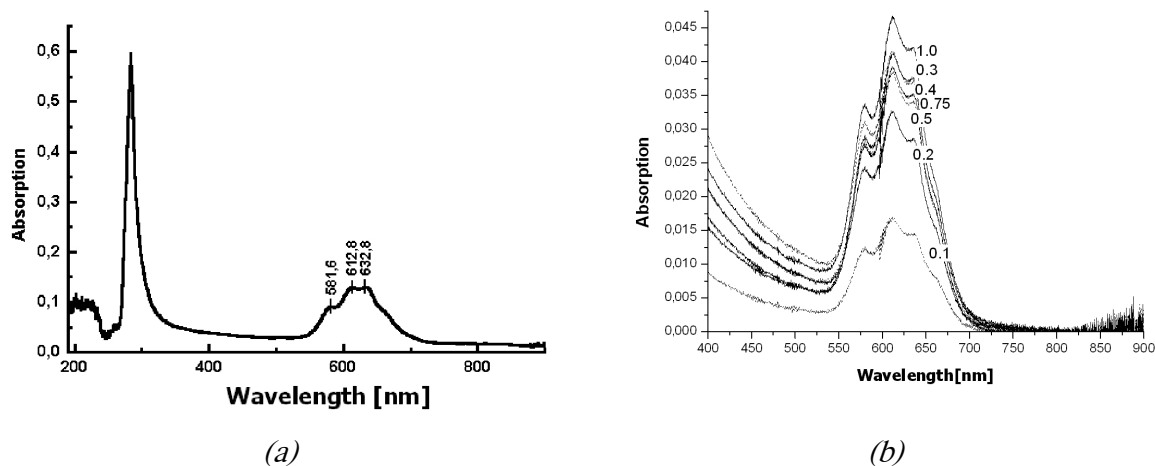


Figure 5-2: UV-VIS spectra of micellar solutions of  $P(S_{1700}\text{-b-}2VP_{450})$  containing  $\text{CoCl}_2$ .

(a) Sample containing  $\text{CoCl}_2$  with a loading of  $L=0.2$ . The main maxima of the characteristic bands of the solutions are labelled (581.6 nm, 612.8 nm and 632.8 nm).

(b) Superposition of spectra done with different loadings  $L$ . The respective loadings are labelled in the picture. The maximum absorption does not follow the order of loading. The graph is a cut-out from the spectra in the region between 400 and 900 nm showing only the characteristic region)

behaviour of the solutions. Starting from a loading of  $L=0.3$ , the centrifuged solutions show a residue of excess  $\text{CoCl}_2$ , which is initially finely dispersed in the solvent. Two very important conclusions can be made from this result:

First, the complex chemical nature of the species dissolved in the micelles could be cleared and can further be used for experiments and second, the maximum loading, which can be achieved by the loading with binary Co-salts is 0.25, above, a residue of undissolved  $\text{CoCl}_2$  will disturb film formation and further conversion of this compound.

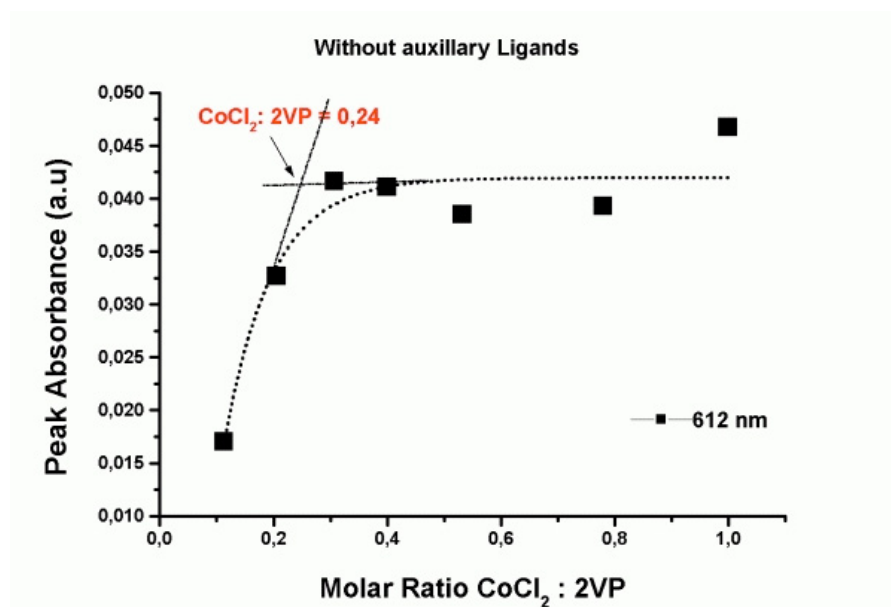
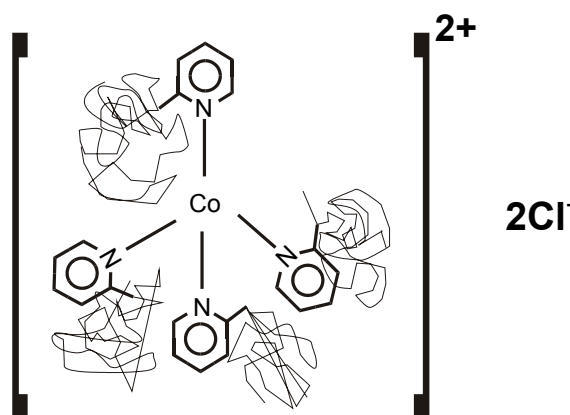


Figure 5-3: Intensities of the main band of the UV-VIS Spectrum at 612 nm from micellar  $\text{CoCl}_2$ -solutions. The intensity first increases rapidly to reach a saturation level. The two regions are fitted (solid line), the curve (dashed line) gives a tentative saturation curve. The crossing point of the fitting lines is at a loading of  $L=0.24$ . The solutions were stirred for 4 weeks and centrifuged after stirring..

The latter conclusion leads to the problem, that the size of potentially synthesised Co-nanoparticles in  $\text{CoCl}_2$ -loaded micelles will be very small. Indeed, further work on the most highly loaded micelles with  $L=0.25$  led to particles with a diameter of 2-3 nm. Such particles were generated directly on films from these solutions by reduction with a  $\text{H}_2$ -plasma [18, 19].

The concluded structure for the observed complexation behaviour is:



The shown structure, where the polymer is illustrated by a coil with anchoring 2VP-units, suggests a solvated  $\text{Co}^{2+}$ -cation by 2VP-units as macroligands. The chloride forms the counterion, rather to act as inner sphere ligand, which could also be the case. However, the uptake should be then  $L=0.5$ , which was never observed for pure micellar  $\text{CoCl}_2$  solutions. Moreover, the spectrum does not show a band at approx. 700 nm, which is characteristic for complexes of the type  $[\text{Co}(\text{py})_2\text{Cl}_2]$ , which do exist in several polar organic solvents [20]. Also the octahedral complexes can be excluded, due to their pinkish, almost colourless,

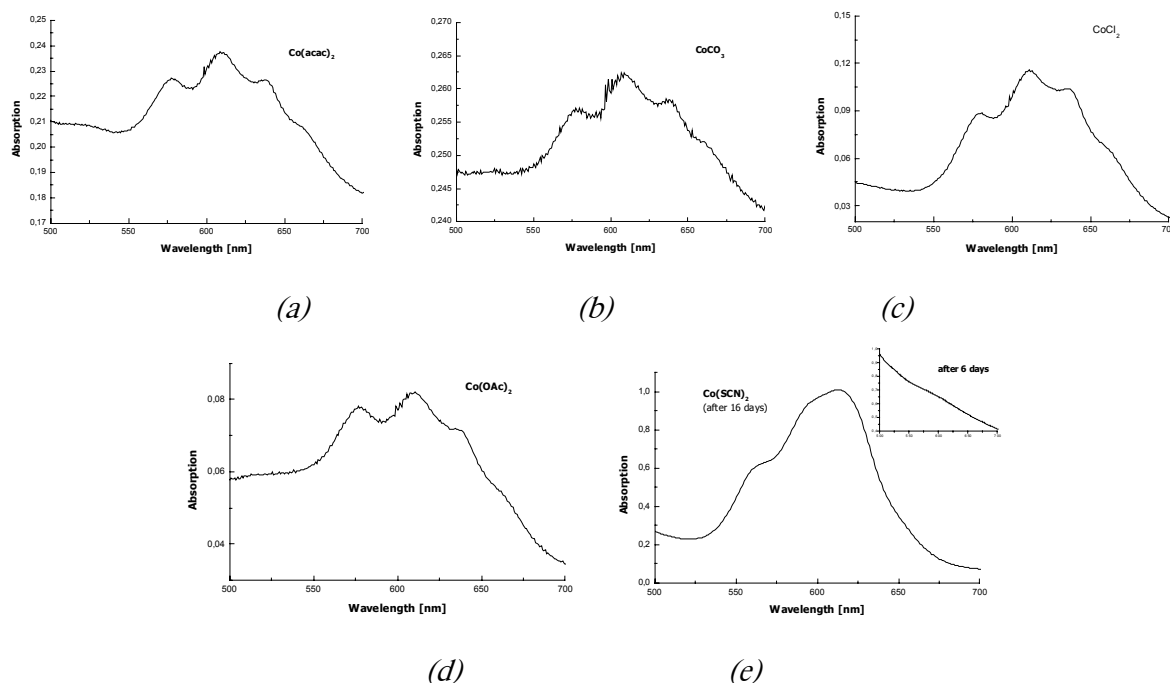


Figure 5-4: UV-VIS spectra of different  $\text{Co(II)}$ -salts in toluene solutions of  $\text{PS}_{1700}\text{-b-P2VP}_{450}$  block copolymers. The salts show very similar spectra in the absorption region between 500 and 700 nm. (a)  $\text{Co(II)}$ -acetylacetonate;  $L=0.1$ ; (b)  $\text{Co(II)}$ -carbonate;  $L=0.1$ ; (c)  $\text{Co(II)}$ -chloride;  $L=0.1$ ; (d)  $\text{Co(II)}$ -acetate;  $L=0.1$ ; (e)  $\text{Co(II)}$ -thiocyanate;  $L=0.5$ ; spectrum after 16 days of stirring – the inset shows the same solution after 6 days.

colour.

Interestingly, we observed in all of the used binary salts the same spectrum in UV-VIS spectrometry. Usually, the different micellar salt solutions tend to yield a colour similar to the colour of the pure, anhydrous salt. In the most cases, after centrifuging the solution, this colour in fact was the colour of undissolved Co-salt. The supernatant solution, however, is also coloured azure like in the case of cobalt. Yet, the species present inside of the micellar cores is always the same. This fact also favours the idea of a tetrahedral Tetrapyridino-

cobalt-(II) anion in polymeric matrix. The most interesting shift in colours is observed in the case of  $\text{Co}(\text{SCN})_2$ , which turns in micellar solution from brown via green to the deep blue colour. Figure 5-4 shows some of the yielded spectra.

Due to the complex nature of the micellar solutions, one possibility to increase the maximum loading with Co-(II)-salt is to add an auxiliary ligand, i.e. to add a low molecular compound which is able to block a certain amount of ligand sites by stronger or sterically easier coordination (see Figure 5-5). Ethanol is known to form stable complexes with  $\text{Co}^{2+}$ . For this reason, we tried to add a droplet of dry ethanol to a micellar  $\text{CoCl}_2$  solution. Indeed, the colour of the solution intensifies immediately and the solution becomes clear within one second. In order to check the feasibility of this idea, we made systematical additions of ethanol to the micellar solutions. The results are shown in Figure 5-6.

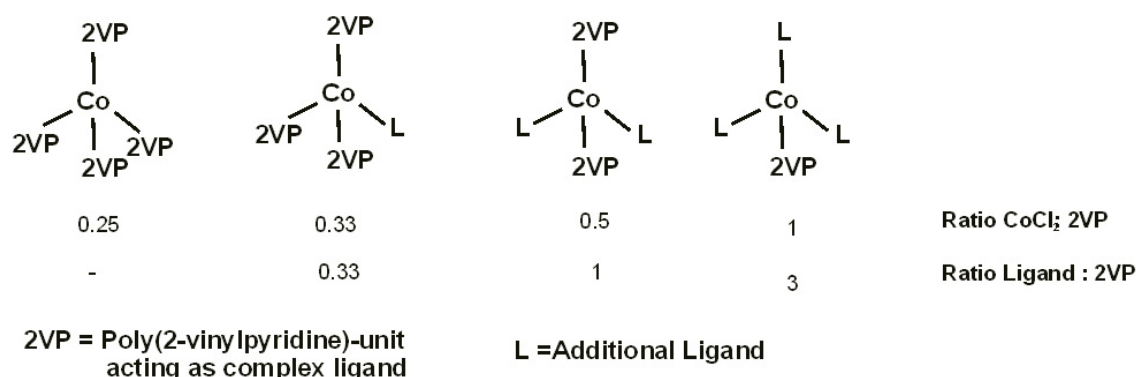


Figure 5-5: Principle of complexation, driven by the addition of an auxiliary ligand. The loading of the micellar core can be driven by blocking coordination site of the complex.

From the figure, it can clearly be seen, that the predicted effect of the auxiliary ligand is working with the micellar solutions. Figure 5-6a shows, that also the amount of ethanol added influences the maximum uptake of  $\text{CoCl}_2$ . If the ratio ethanol:2VP is 0.5, only a slight change of intensity of the band at 612 nm is observed. Also, the centrifuged solution still contains undissolved  $\text{CoCl}_2$ . With the ratio of ethanol:2VP > 1, even the highest loaded solutions become clear. The graph for ethanol:2VP = 1 shows strange behaviour with increasing loadings. Here, a change of complexation can be observed. At higher loadings, a new band at 690 nm appears. That is also present for higher ethanol-contents. A band in this region is, as mentioned above, characteristic for inner sphere ligation of the chloride anion. Most likely, higher loadings of  $\text{CoCl}_2$  are compensated by a change in coordination with blocking of more coordination sites by the also increasing content of chloride ions.

The micellar structure of the films [21] is kept in all of the experiments, also when ethanol is added to the solutions. The TEM-micrographs in Figure 5-7 show the comparison of micellar  $\text{CoCl}_2$  solutions with and without ethanol addition.

From Figure 5-7 it is evident, that the domains, marked with  $\text{CoCl}_2$  are not changing significantly. The black spots, caused by the higher electron density of  $\text{CoCl}_2$  comparing to the polymer, represent the selective uptake in all experiments using ethanol as auxiliary ligand. Thus in general, the addition of ethanol keeps the possibility of Co-particle synthesis with higher loading of the precursor compound.

To examine further the affinity of  $\text{Co(II)}$  to the polymeric pyridine units, we incorporated stable, chelate complexes into our micellar systems. We performed these experiments with

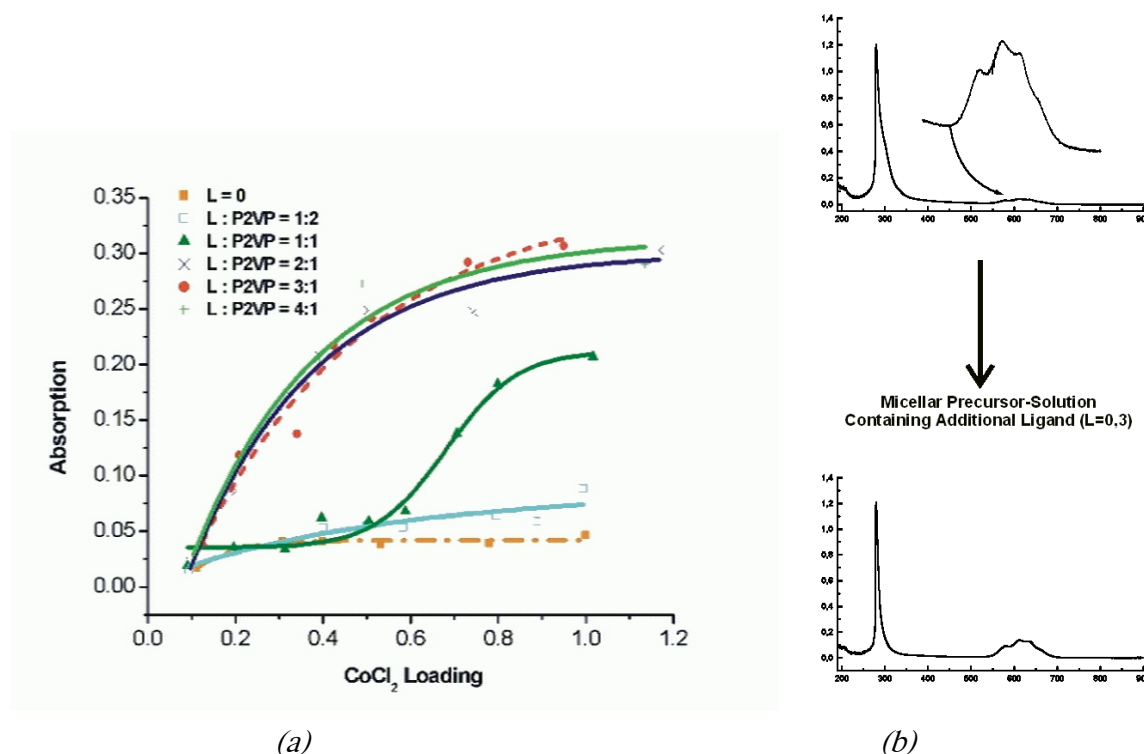


Figure 5-6: (a) Spectra of various ratios of ethanol in a micellar solution of  $\text{PS}_{1750}\text{-b-P2VP}_{450}$ . The loadings were performed over a range from 0 to 1 for all different ethanol concentrations. The ethanol addition was done in stoichiometric ratio. After ethanol addition, the solutions were loaded with  $\text{CoCl}_2$ . The intensity of the band at 612 nm was taken for the graphs (b) UV-VIS spectra of a solution of  $\text{PS}_{1750}\text{-b-P2VP}_{450}$  with  $L(\text{CoCl}_2) = 0.3$  before and after addition of a droplet of ethanol. The intensity of the characteristic triplet is increasing significantly.

Dimethyl-glyoximato-complexes of Co(II), which we synthesised for this purpose. The synthesis is described in the appendix of this chapter. From biochemistry, it is known, that the glyoximato-complex has a square plane structure, often used to simulate the porphyrine complexation in the Vitamin B<sub>12</sub>-structure [22, 23]. Two free coordination sites, situated at the top and the bottom of the complex can be occupied by other ligands [24, 25]. Performing the synthesis of the complex under ambient atmosphere is oxidising the complex to Co(III) and results in coordination of water on the two free sites. Under argon atmosphere, the complex is not oxidised and can be obtained as neutral complex compound Dimethyl-glyoximato-cobalt(II) ([Co(DMG)<sub>2</sub>]).

We synthesised the following complexes depicted in Figure 5-8:

After addition of the three complexes into a solution of PS<sub>1700</sub>-*b*-P2VP<sub>450</sub> in toluene, the

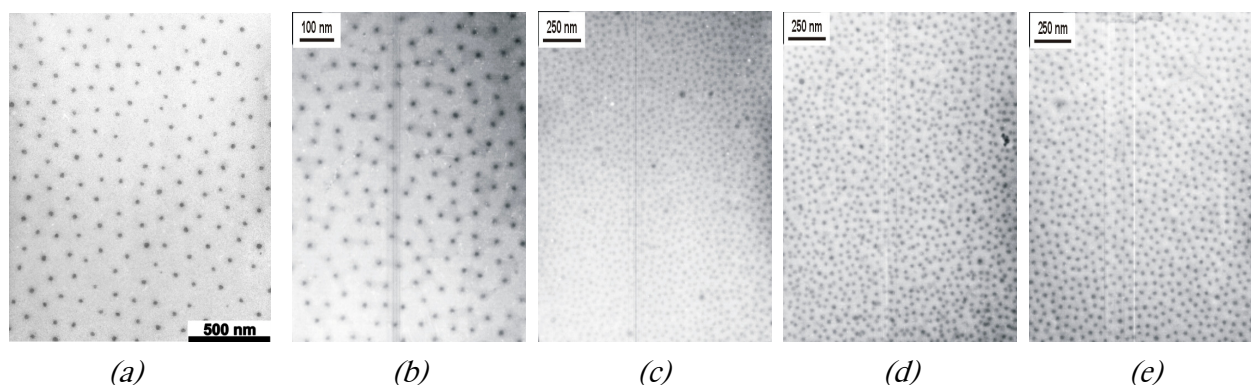


Figure 5-7: TEM-micrographs of CoCl<sub>2</sub> solutions in PS<sub>1700</sub>-*b*-P2VP<sub>450</sub> in toluene

- (a)  $L=0.3$ ; Ethanol:2VP = 0
- (b)  $L=0.3$ ; Ethanol:2VP = 0.5
- (c)  $L=0.3$ ; Ethanol:2VP = 2
- (d)  $L=0.75$ ; Ethanol:2VP = 2
- (e)  $L=0.3$ ; Ethanol:2VP = 4

uptake into the micellar core of the micelles shows to be dependent on the base B depicted in Figure 5-8. The pictures of such solutions in TEM are shown in Figure 5-9.



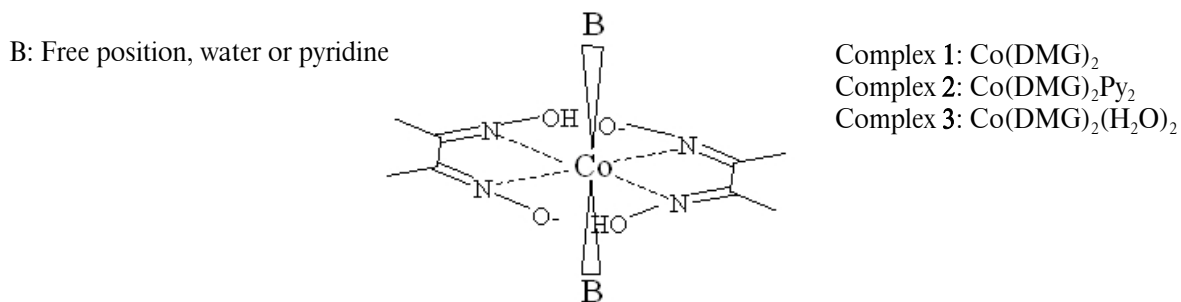


Figure 5-8: Formulae of the used glyoximate-Co(II)-complexes

The uncoordinated DMG-complex forms well-ordered films, where a selective uptake into the micellar cores can be seen. No aggregation of the micelles is observed. However, the water and the pyridine-coordinated complexes are behaving in a different way. In the case of water, aggregation takes place in a bigger scale. There is a selective uptake into the micelles, which can be ascribed to a ligand exchange, but the released water destabilises the micelles. Which finally leads to formation of bigger aggregates. The darker background also shows, that there is still complex in the solvent phase, which is confirmed by the observation, that the solution is inhomogeneous. Thus, the uptake into the micelles is not

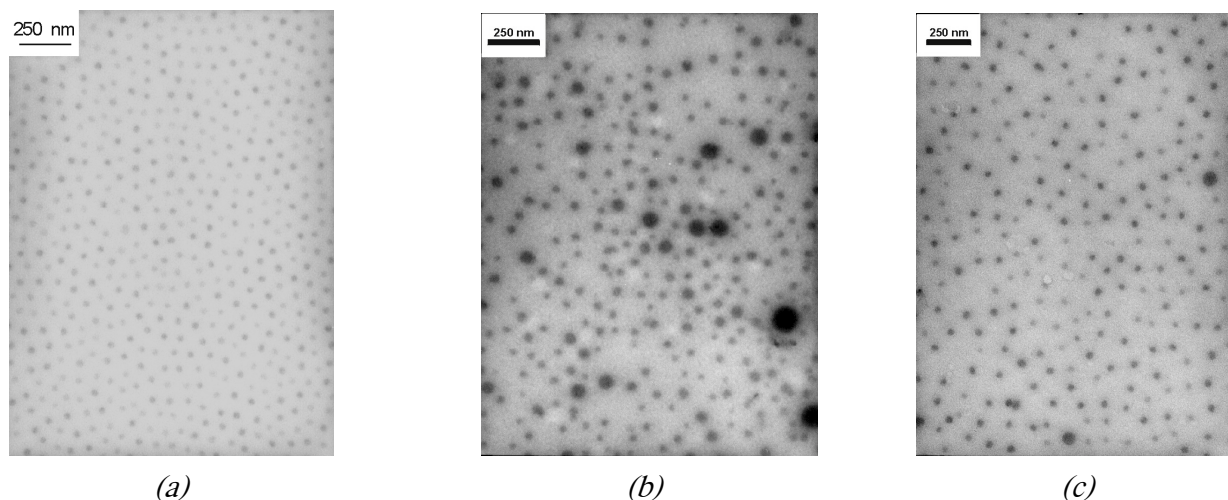
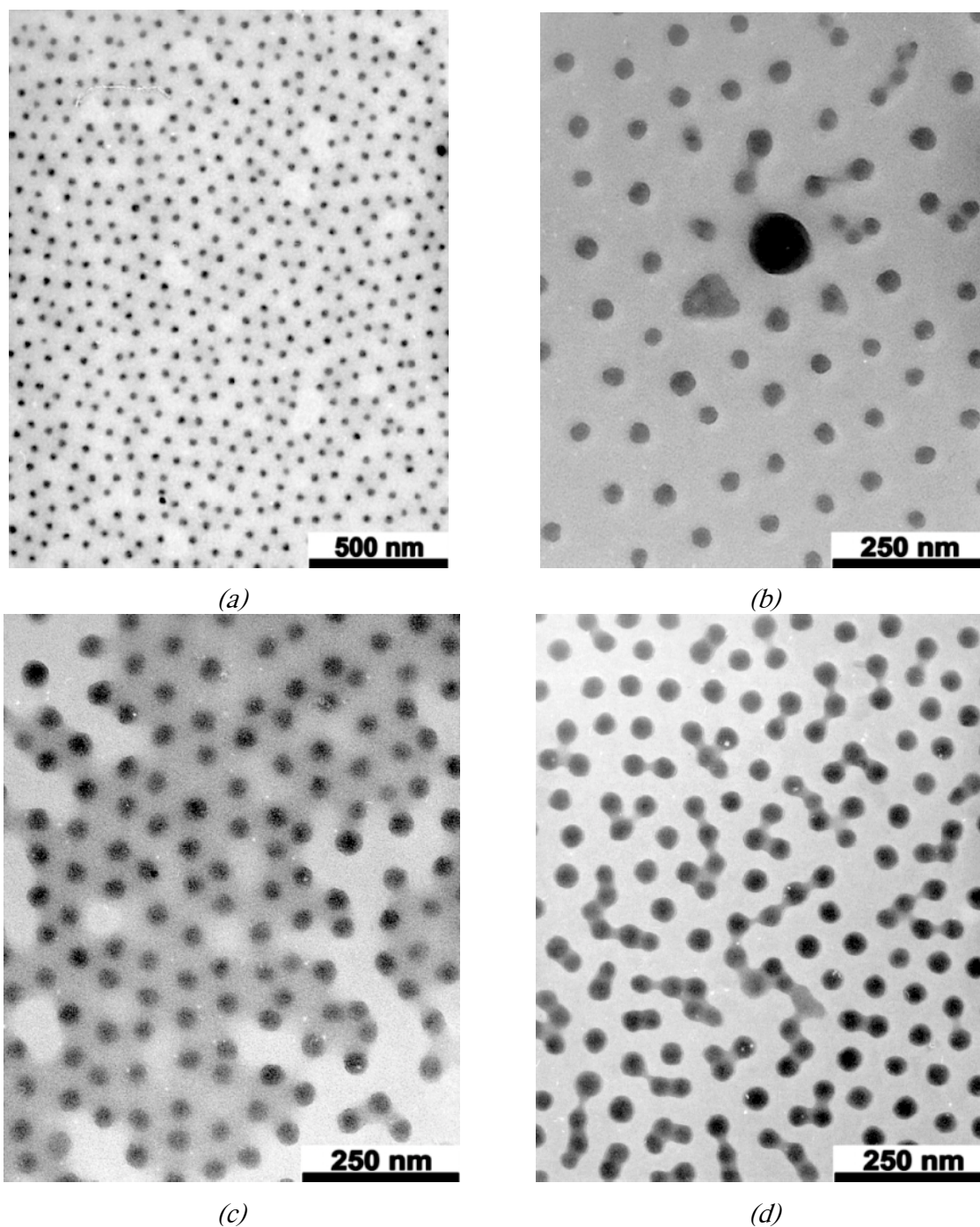


Figure 5-9: TEM-micrographs of  $\text{Co}(\text{DMG})_2$ -complexes in block-copolymer-micelles of  $\text{PS}_{1700}\text{-b-P2VP}_{450}$  in toluene.. The loading of the micelles was  $L=0.1$ . (a):  $\text{Co}[\text{DMG}]_2$ ; (b):  $\text{Co}[(\text{DMG})_2(\text{H}_2\text{O})_2]$ ; (c):  $\text{Co}[(\text{DMG})_2(\text{Py})_2]$ .

that selective. When pyridine is taken as coordinating ligand in the complex, the incorporation into the micelles is also working.



*Figure 5-11: TEM-micrographs from cast polymer solutions in toluene on carbon coated copper grids. The solutions are loaded with  $\text{CoCl}_2$  with  $L=0.5$  and centrifuged. (a)  $\text{PS}_{1700}\text{-}b\text{-P2VP}_{450}$ ; (b)  $\text{PS}_{800}\text{-}b\text{-P2VP}_{860}$ ; (c)  $\text{PS}_{600}\text{-}b\text{-P2VP}_{800}$ ; (d)  $\text{PS}_{550}\text{-}b\text{-P2VP}_{1400}$*

Unlike in the case of water, aggregation of micelles takes place, but not in the same extent. Here it seems, that pyridine is interacting strongly with the 2VP-units of the polymer. The uptake shows, that there is an exchange between polymeric and monomeric pyridine.

Thus, the process of uptake can be regarded as very sensible, but effective method to localise salts of Co(II) inside of micellar cores of a block copolymer. Especially the vinylpyridine block as core-building block has a high efficiency on localisation. Like in the case of the DMG-complexes or in the case of ethanol addition, the borders given by complex chemistry can be overcrossed by stoichiometric blocking of coordination sites. The usage of auxiliary ligands could be confirmed, when using Dimethyl-glyoxime as auxiliary ligand. If this is done, a maximum loading of  $L=0.5$  can be reached.

The amount of confined Co(II)-salt can also be influenced by the usage of polymers of different block length ratios and sizes of blocks. For a later conversion of the Co(II), the absolute amount of Co(II) per micelle is important to influence the particle size. In Figure 5-10, the size of the inner domains, marked with  $\text{CoCl}_2$  are plotted against the length and the length ratios of some used polymers. For a comparison, anhydrous  $\text{FeCl}_3$  is used for loading in the same way like  $\text{CoCl}_2$ .

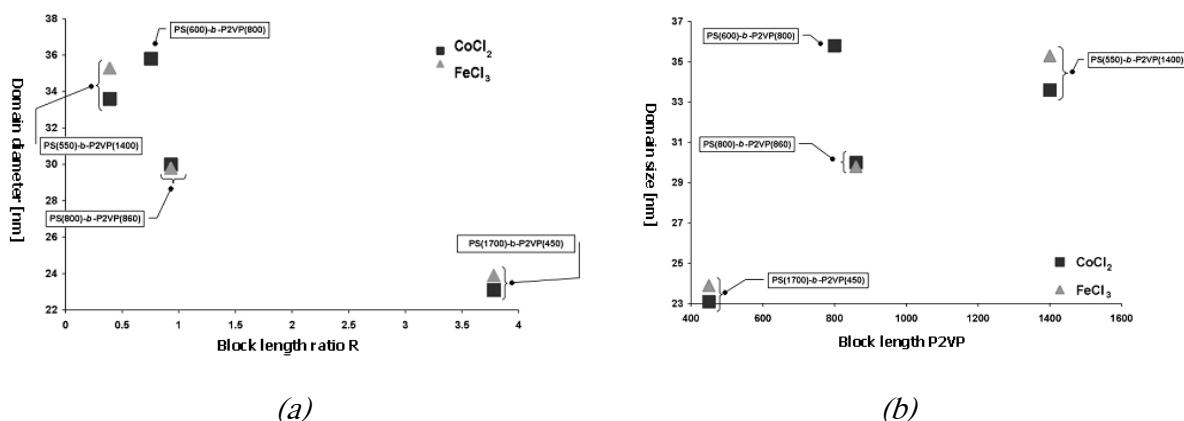


Figure 5-10: Plot of block copolymer parameters against the size of the loaded micellar cores. (a) Block length ratio; (b) Block length of P2VP. The solutions were loaded with  $L=0.5$ , the excess of salt was removed by centrifugation.

From the plot of block length ratio in Figure 5-10 it is evident, that there is a shift of domain size from hairy towards more symmetrical-type micelles. The size increases with lower ratio PS:P2VP and with a bigger size of the core-building block itself. Thus, the used

polymer is a tool to influence the accessible particle sizes by a latter conversion of the Co(II)-salt. The incorporation of FeCl<sub>3</sub> was done in the same way and by use of the same techniques of solution formation. We found out, that the knowledge about CoCl<sub>2</sub> in micellar solutions can be transferred completely to systems containing FeCl<sub>3</sub>. Later, we confirmed our observations also for solutions containing Pd(II), Pt(II), Zr(II), Ni(II). In all these cases, the precursor compound is incorporated by complexation, and shows the limits and possibilities described in this chapter. The observation, however is limited to precursors, which do not act as proton donators, but as binary salts with tendency for complex formation.

Regarding films cast on carbon coated copper grids for TEM-analysis, the deposition ends up with the formation of well-ordered films. In Figure 5-11 examples are given for film formation using Co(II)-filled PS-*b*-P2VP micelles of different block lengths.

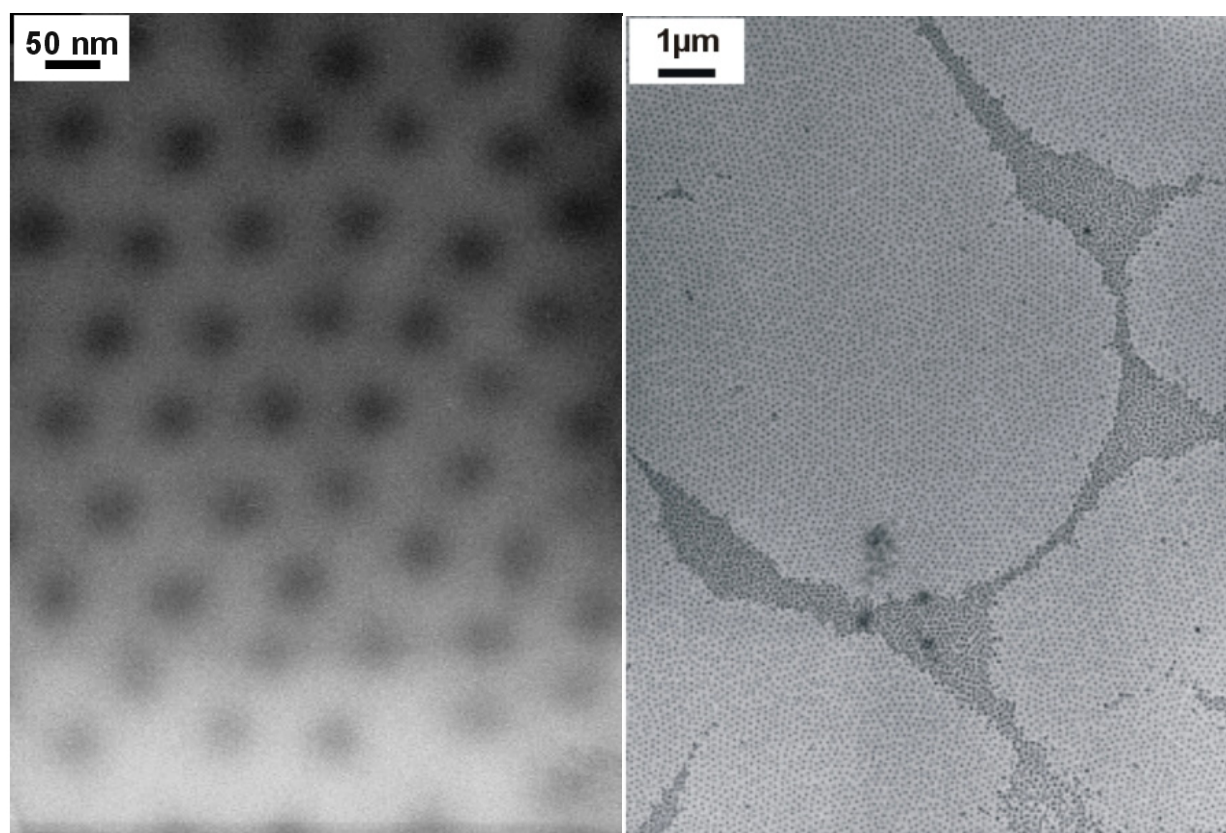
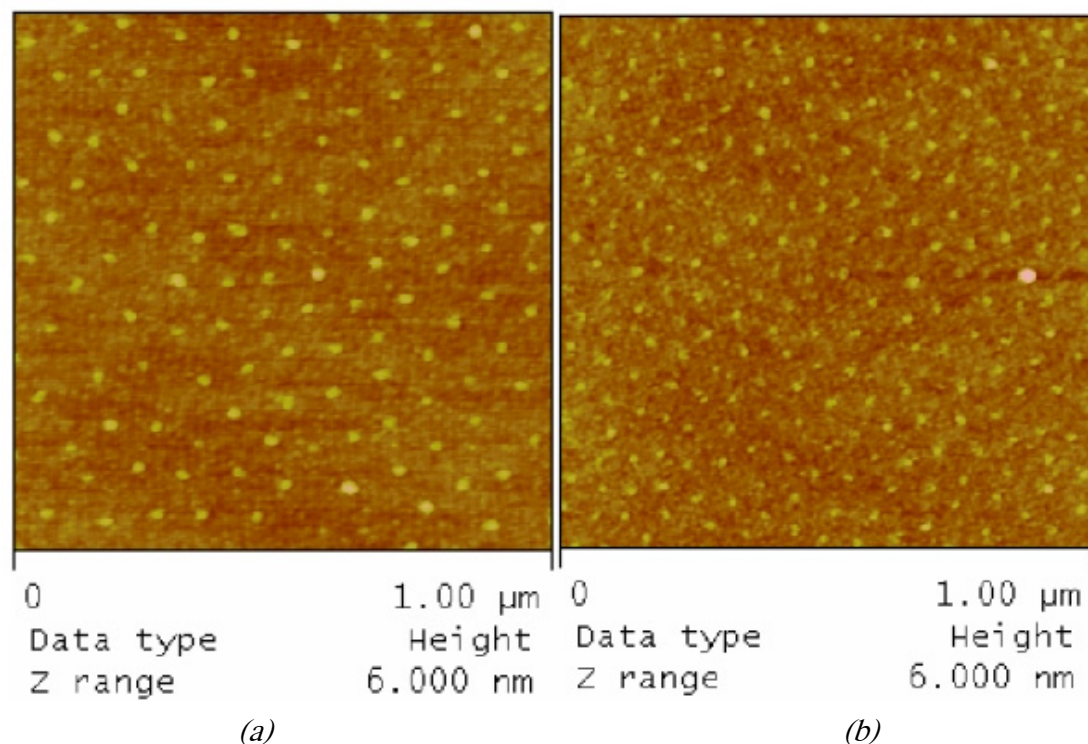


Figure 5-12: Micellar solutions of PS<sub>710</sub>-*b*-P2VP<sub>210</sub> in mesitylene loaded with CoCl<sub>2</sub> with  $L=0.2$ . (a) is a cut-out from (b). The regular hexagonal pattern is disturbed only by double layer formation.



For the casting of films from the Co(II)-solutions, we found out, that loadings of 0.2 and below form better films than overloaded micelles, which are later centrifuged. Here, still some disturbing aggregates disturb film formation. The switch from toluene to mesitylene also increases order within the films. Mesitylene has a higher boiling point than toluene, but is also a selective solvent for PS-*b*-P2VP. It seems, that in this case the bigger evaporation time of the solvent has a positive influence on film formation. Figure 5-12 shows, that a very regular hexagonal pattern is available from mesitylene solutions of PS-*b*-P2VP.

Patterns like in Figure 5-12 were accessible with very good reproducibility. We could transfer the film formation advantage from carbon coated grids also to Silicon wafers. Such samples can be taken for further treatment by a hydrogen plasma, which is removing the polymer component and reducing the Cobalt(II) to metallic Cobalt. This procedure is then a path to produce naked Co-dots, hexagonally ordered on an unpolar substrate. Two examples of such naked particle arrays recorded on AFM are given in Figure 5-13.



*Figure 5-13: AFM-height profile from a film of naked Co-particles on a freshly prepared Si-wafer. Film is made by casting a solution of  $\text{CoCl}_2$  in  $\text{PS}_{710}$ -*b*- $\text{P2VP}_{210}$  in mesitylene with  $L=0.2$  with a polymer concentration of 5 mg/mL. The film is treated 20 minutes in a hydrogen plasma and examined in AFM. Film formation is influenced by the pulling speed (a) is pulled with 7.2 mm/min, (b) is pulled with 15 mm/min giving different interparticle distances. The height of the particles is 1-2 nm.*

As shown in Figure 5-13, the ordering of the films changes with the pulling speed while film formation. This is a known effect in film formation [9]. With films like the shown ones it is possible to study in situ physical small particles properties like the transversal magnetic resist. Also the selective use of oxygen plasma can be used to study oxidation characteristics. Experiments on particle films from above preparation are very complex and are described in detail in other publications [18, 19, 26-28].

The switching of oxidation states could be pursued with in-situ XPS-measurements. This measurement is shown in Figure 5-14a, where a film of  $\text{CoCl}_2$  containing micelles cast on a  $\text{SiO}_2$ -Si substrate is treated by plasma. The  $\text{Co-}2p_{3/2}$  band of Cobalt is shifted initially towards higher binding energies. This is due to the higher oxidation state in the  $\text{Co(II)}$ -compound  $\text{CoCl}_2$ . When applying a hydrogen plasma, after 5 minutes, a partial shift towards the  $\text{Co-}2p_{3/2}$ -band of metallic cobalt is observed. This shift is completed, when the plasma is applied for another 15 minutes. A comparison of the sample with a pure Cobalt-film shows that the reduction is quantitative.

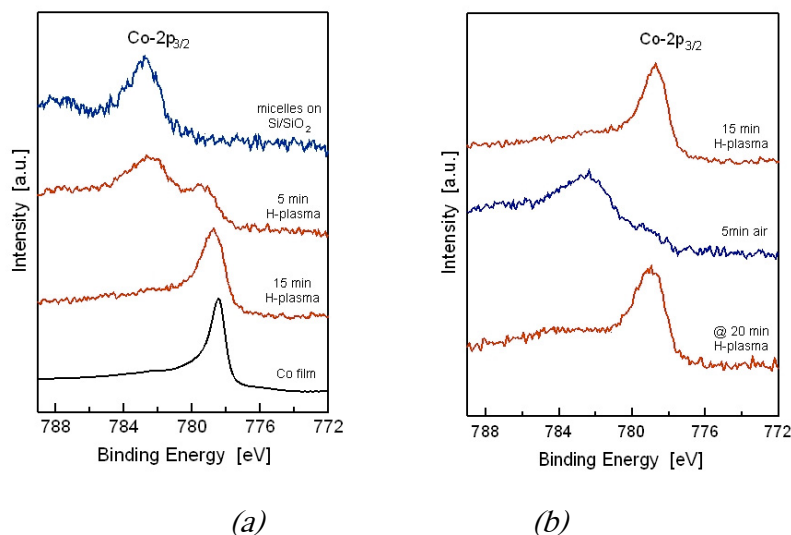


Figure 5-14: XPS-experiment with  $\text{CoCl}_2$  loaded  $\text{PS}_{1350}\text{-b-P2VP}_{400}$  block copolymer in toluene ( $L=0.5$ , filtered). (a) The initial solution shows a chemical shift of the  $\text{Co-}2p_{3/2}$  band of Cobalt (blue spectrum) followed up by treatment with hydrogen plasma (red spectra), which is reducing  $\text{Co(II)}$  to metallic Cobalt (black reference spectrum). (b) The reduced particles are kept 5 minutes on ambient atmosphere and the chemical shift shows after re-entry of the sample the shift caused by oxidation (blue spectrum). The oxidation can be reversibly alternated by repeated application of a hydrogen plasma (red spectrum on the bottom).

In this stage, the Co-particles are naked, because the protecting polymer coating is removed completely by the hydrogen plasma, which can also be studied in XPS by observation of the polymers C-1s band. In Figure 5-14b it is shown, that exposure of the particle film to oxygen leads to regaining of the initial oxidation state. For this experiment, the sample can simply be removed from the in-situ cell of the XPS-device and be kept for 5 minutes on air. A re-entry of the sample with subsequent H<sub>2</sub>-plasma treatment recovers the metallic character of the particle film. Thus, the oxidation procedure is a reversible process, which is proceeding very quickly. The in-situ XPS-measurement allows a flexible treatment of the Co-films towards further physical studies [18].

## 5.4 Conclusion

It could be demonstrated, that the uptake of Co(II)-salt inside of block copolymer micelles of PS-*b*-P2VP is possible. However, precautions have to be taken while processing in order to keep the procedure reproducible. There is a high evidence, that the basic process of binding the salt inside of the micellar cores follows a complex-chemical reaction. This reaction is very common for Co(II) and is regulating the uptake procedure.

By adding only Co(II)-salt into the micelles, the coordination sphere of the ion is responsible for the amount of Co(II), which can be maximally taken up into the cores. In the case of PS-*b*-P2VP polymers, the pyridine units are solvating the Co(II) and lead to a tetrahedral structure. This structure gives a limit to the micellar loading of around 0.25.

The limit can be shifted to higher values by two mechanisms. Either, some low-molecular helping ligands are used, to block coordination sites of the Co(II), which leads to a more loose connection of the polymeric pyridine units to the Co(II) central atom. The consequence is the increasing number of central atoms, which can be bound directly to the polymeric ligands. The other possibility is to use strong complexes of Co(II), which are sterically regulating the coordination sphere of Co(II). This is demonstrated by the planar Co(DMG)<sub>2</sub> complex, which leads to octahedral complexes, where the inner square is blocked by the chelating ligand DMG.

The block length of the core-building block is influencing the overall amount of pyridine units per micelle and thus also the amount of Co(II), which can be bound into the micellar core. With the usage of mesitylene, a higher-boiling, unpolar solvent, the film formation can

be optimised towards a higher order in the films. Substrates containing  $\text{CoCl}_2$  are a good precursor tool for further physical investigations. The possibility of generation of a naked Co-particle film by hydrogen-plasma treatment is a key for basic understanding of the interesting properties of nanoscaled Co-particles.



## 5.5 References

- [1] Z. Tuzar, P. Kratochvil, *Surface and Colloid Science*, Vol.15, Plenum Press, New York, 1993.
- [2] See Chapter 2 of the present work.
- [3] J.P. Spatz, S. Mößmer, M. Möller, *Angew. Chem.* **1996**, *108*, 1673.
- [4] P.H. Hess, P.H. Parker Jr., *J. Appl. Polym. Sci.* **1966**, *10*, 1915.
- [5] J.P. Spatz, S. Sheiko, M. Möller, *Macromolecules*, **1996**, *29*, 3220.
- [6] S. Mößmer, *PhD Thesis*, Universität Ulm, 1999.
- [7] E. Nachbaur, G. Leiseder, *Monatsh. Chem.* **1971**, *102*, 1718.
- [8] S. Riethmüller, *PhD Thesis*, Universität Ulm, 2002.
- [9] C. Hartmann, *PhD Thesis*, Universität Ulm, 2002.
- [10] G.A. Roescher, *PhD Thesis*, Universiteit Twente, Enschede, 1995.
- [11] M. Möller, J.P. Spatz, *Curr. Opin. Colloid Interface Sci.*, **1997**, *2*, 177.
- [12] J.P. Spatz, S. Mößmer, M. Möller, *Chem. Eur. J.* **1996**, *2*, 1552.
- [13] O.A. Platonova, L.M. Bronstein, S.P. Solodovnikov, I.M. Yanovskaya, E.S. Oblonkova, P.M. Valetsky, E. Wenz, M. Antonietti, *Colloid Polym. Sci.* **1997**, *275*, 426.
- [14] F.A. Cotton, G. Wilkinson, *Advanced Inorganic Chemistry*, 3<sup>rd</sup> edition, Wiley-Interscience, New York, 1972, 645.

- [15] D. Nicholls, *Cobalt* in: J.C. Balar Jr., H.J. Emeleus, R. Nyholm, A.F. Trotman-Dickenson (eds.), *Comprehensive Inorganic Chemistry Vol.3, Chapter 41*, 1<sup>st</sup>ed., Pergamon Press, Oxford, 1973, 1053.
- [16] F.A. Cotton, D.M.L. Goodgame, M. Goodgame, *J. Am. Chem. Soc.* 1961, 83, 4690.
- [17] H.C.A. King, E. Körös, S.M. Nelson, *J. Am. Chem. Soc.* 1963, 85, 5449.
- [18] H.G. Boyen, G. Kästle, K. Zürn, T. Herzog, F. Weigl, P. Ziemann, O. Mayer, C. Jerome, M. Möller, J.P. Spatz, M.G. Garnier, P. Oelhafen, *Adv. Funct. Mater.* 2003, 13, 359.
- [19] K. Zürn, *PhD Thesis*, Universität Ulm, in progress.
- [20] F. Emmenegger, M. Piccand, H. Piekarski, J. Mokrzan, *J. Chem. Soc., Dalton Trans.* 1997, 785.
- [21] E.L. Thomas, D.J. Kinning, D.B. Alward, C.S. Henkee, *Macromolecules*, 1987, 20, 2934.
- [22] G.N. Schrauzer, R.J. Windgassen, *Chem. Ber.* 1966, 99, 602.
- [23] G.N. Schrauzer, *Acc. Chem. Res.* 1968, 1, 97.
- [24] N. Yamazaki, Y. Hohokabe, *Bull. Chem. Soc. Jap.* 1971, 44, 63.
- [25] A. Bakac, M.E. Brynildson, J.H. Espenson, *Inorg. Chem.* 1986, 25, 4108.
- [26] A. Schröder, *Diploma Thesis*, Univesität Ulm, 2002.
- [27] G. Kästle, *Electron transport in Nanomodulated, Epitaxial Gold Films*, Fortschritt-Berichte VDI, Reihe 9, 368, 2003, 75.
- [28] G. Kästle, A. Schröder, H.-G. Boyen, A. Plettl, P. Ziemann, O. Mayer, J. Spatz, M. Möller, M. Büttner, and P. Oelhafen, *Eur. J. Inorg. Chem.*, 2005, 18, 3691.

## *Appendix Chapter 5*

---

### *Synthesis of polymers and complexes*

#### **A5.1 Diblock copolymers by living anionic polymerisation**

##### *Introduction*

In order to gain new polymeric materials for the nanoreactor concept, the task was to rebuild the method of living anionic polymerisation in our group. Different points had to be cleared for succeeding, including the reconstruction of glassware, choice of pure and suitable materials, the right polymerisation conditions and the recovery and analysis of the resulting products.

##### *Experimental*

The purification steps for the educts were carried out in a high-vacuum line, the final purification steps were combined with a degassing step to remove traces of oxygen. The high-vacuum-line reaches pressures of  $10^{-5}$  mbar of remaining gaseous compounds. All glassware was dried and heated under dynamic vacuum in order to remove traces of water on the glass surface. The polymerisation was carried out in a nitrogen-filled glove-box under controlled inert gas atmosphere of less than 1 ppm of water and oxygen.

Styrene (Fluka, >99.5%) and 2-vinylpyridine (Merck, >98%) both stabilised with 4-tert-butylcatechol) were twice distilled on the high vacuum line using  $\text{CaH}_2$  (Merck, 95%)

and trioctyl-aluminium (Merck, 90% Al) as drying agents. The monomers were stored at  $-25\text{ }^{\circ}\text{C}$  after purification in order to reduce radical pre-polymerisation. THF (technical grade) was twice distilled over  $\text{LiAlH}_4$  under  $\text{N}_2$ -atmosphere. It was further condensed over trioctyl-aluminium. Methanol (technical grade, used as termination agent) was dried over Mg and degassed by three freeze and pump cycles. n-heptane, used as cooling bath, was dried over  $\text{LiAlH}_4$  and degassed prior to use to avoid a contamination of the glove-box atmosphere. LiCl (Fluka p.a.) was dried in a vacuum oven at  $150\text{ }^{\circ}\text{C}$ . Sec-butyllithium (Aldrich, 1.3 M solution in cyclohexane) was used as received and stored in dark at  $-25\text{ }^{\circ}\text{C}$  in the glove-box. Iodomethane (Merck,  $>99\%$ , stabilised with silver) was used as received.

SEC-measurements of the first block (Homo-PS) were carried out in THF as eluent, except for two measurements in  $\text{CHCl}_3$ . The setup consisted of Waters  $\mu$ -Styragel columns with pore sizes of  $10^5$ ,  $10^4$ ,  $10^3$ ,  $500\text{\AA}$ , a Waters/Millipore Styragel column with a pore size of  $10^6\text{\AA}$  and a guard column for THF and of Waters  $\mu$ -Styragel columns with pore sizes of  $10^5$ ,  $10^4$  (counterflow),  $10^3\text{\AA}$  for  $\text{CHCl}_3$ . The detection was performed by a Wyatt Dawn DSP laser light scattering detector, followed up by a parallel arrangement of a Waters 410 differential refractometer detector and a Viscotek viscometer detector HSORB. Calibration was done with narrow PS-samples (PSS, Mainz). The block copolymers were eluted by DMF in Waters/Millipore Styragel columns of type HT3, HT4 and HT5 in order of appearance. Detection was performed by a Waters RI 2410 differential refractometer detector. For all samples, a concentration of 10 mg/mL of the respective polymer was used. The molecular weight was calculated by PSS Win-GPC 4.02 software for SEC.

Elemental analyses were performed on a Heraeus CHNO rapid analyser, getting back values for the C-, the H- and the N-content. Infrared-spectra (FT-IR) were recorded on a Bruker IFS 113 V spectrometer. Samples were prepared by either as KBr-polymer-pellets or as thin film, casted on a pure KBr-pellet.  $^1\text{H}$ -NMR-spectra were performed in  $\text{CDCl}_3$  on a Bruker DRX 400 NMR-spectrometer operating at 400 MHz.

#### *Description of the polymerisation procedure*

The polymerisation procedure was carried out in the glove-box. The reaction flask was fixed in a cooling bath of n-heptane at  $-70\text{ }^{\circ}\text{C}$ . During the reaction, the flask was kept close to avoid condensation of traces of moisture. First, the needed volume of solvent (ca. 10-20-fold volume compared to the volume of all monomers) was transferred into a scaled glass bottle and then added into the cool flask, which was additionally equipped with a magnetic stirring bar. LiCl (5-fold excess in relation to the living chain ends) was first dissolved in a

small portion (4 mL) of THF and subsequently added to the reaction flask. The mixture was allowed to stir additionally for 10 minutes to get a homogeneous mixture. The initiator and the monomers were left to stand until room temperature was reached, which is especially important for the initiator solution, where the organometallic compound crystallises at  $-25^{\circ}\text{C}$ . To remove last impurities in the flask, a titration of the liquid was carried out prior to the polymerisation. In order to perform this titration, one drop of styrene was added under slow stirring by a plastic syringe. Then, the initiator was added dropwise by a glass syringe until a persistent orange-yellow colour appears, which is characteristic for the living polystyryl-anion. This amount was typically 1-2 droplets, which corresponds to an initiator volume of 4-8  $\mu\text{l}$ .

After titration, the rest of the calculated amount of the initiator (sec-butyllithium) was added at once, followed up by a dropwise addition of the needed amount of styrene. While dropping the styrene into the solution, a growing intensity of the colour was observed. After 1 hour reaction time at  $-70^{\circ}\text{C}$ , an aliquot of 0.5 mL was taken out of the reaction flask and terminated with 0.5 mL methanol in order to measure the molecular weight of the first block via SEC. After this, the second monomer, 2-vinylpyridine, was added dropwise to the reaction mixture. A colour change from orange to dark clear red was observed. The mixture stirred at least additional 4 h at  $-70^{\circ}\text{C}$ . As terminating step, 1 mL of methanol was added to the stirring solution. Depending on the viscosity of the solution, a more or less rapid loss of the colour could be observed.

The colourless solution was transferred out of the glove-box and precipitated in a 20-fold excess in volume (in respect to the volume of the reaction mixture) with petrol ether.. This volume, as well as a small stirring speed and a dropwise addition of the mixture into the solvent guaranteed the best-shaped polymer. The product was filtered by a Buechner-funnel and dried for 2 days in a vacuum oven at  $45^{\circ}\text{C}$ . The dry polymer was finally weighed and analysed via SEC, elemental analysis and  $^1\text{H}$ -NMR.

On two samples, a partial quaternisation of the pyridine N-atom was performed by a polymer reaction. This reaction was carried out in a two-necked flask, equipped with an inert gas inlet and an intense reflux condenser. First of all, the required amount of block copolymer was dissolved by stirring in dry and degassed THF inside of the glove-box. Then, the solution was transferred into the reaction vessel by means of a syringe in a nitrogen counter-stream. The calculated amount of iodomethane was added into the stirring solution under nitrogen. The needed amount was referred to the grade of quaternisation, which was desired and the 25-fold excess of this amount was taken for the reaction. The reaction mix-

ture was heated to reflux of THF and was needed to be cooled intensively because of the lower boiling point of the iodomethane. While heating, a rapid switch of the colour from colourless to an intensive yellow colour was observed. This is ascribed to the colour of monomeric 2-VP reacting with iodomethane. The reaction mixture was cooled down after 1 hour of reaction. It was transferred dropwise to a 20-fold volume excess of petrol ether under slow stirring. While first the precipitation of a white solid was observed, the colour of the solution and of the precipitate turned again to an intensive yellow. The polymer was filtered in a Buechner-funnel and dried by suction. Additional drying was by heating the product for 1 day in a vacuum oven at 45 °C. Finally the product was weighed and analysed by further techniques (FT-IR, NMR, elemental analysis).

*Table A5-1: Reaction entries for the synthesised block copolymers*

<b>Polymer S<sub>x</sub>-b-2VP<sub>y</sub></b>	<b>n (Styrene) [mmol]</b>	<b>n (2-VP) [mmol]</b>	<b>n (sec-BuLi) [mmol]</b>	<b>V (THF) [mL]</b>	<b>yield [%]</b>	<b>Name</b>
500-500	43.5	43.5	0.087	60	69.2	OM1
1000-500	43.5	21.8	0.043	125	66.5	OM2
1000-250	43.5	10.9	0.043	125	89.9	OM3
1700-500	87	25.6	0.051	350	76.7	OM4
200-200	43.5	43.5	0.218	125	>100%	OM5
200-200	43.5	43.5	0.218	125	>100%	OM6

## Results

Eight anionic polymerisations were carried out in the first try. The reaction entries for these polymerisations are shown in Table A5-1. The main data on these polymers are given in Table A5-2. Also a comparison is made with the commonly used block copolymer PS<sub>1700</sub>-*b*-P2VP<sub>450</sub> synthesised in earlier works [1]. The comparison is important for a qualitative check of the yielded polymers against well-characterised polymers.

Table A5-2: Molecular weights and block lengths of synthesised PS-*b*-P2VP

Polymer S <sub>x</sub> - <i>b</i> - 2VP <sub>y</sub> <sup>1</sup>	M <sub>n</sub> (PS) [g/mol]	M <sub>w</sub> /M <sub>N</sub> (PS)	M <sub>n</sub> (block) [g/mol] <sup>2</sup>	M <sub>w</sub> /M <sub>N</sub> (block) <sup>2</sup>	DP (P2VP) <sup>1</sup> H-NMR	DP (P2VP) EA	DP <sub>PS</sub> / DP <sub>P2VP</sub>	Name
640-550	60,100	1.10	321,500	1.46	560	550	1.16	OM1
2225-0 <sup>3</sup>	231,600	1.17	354,500	1.23	0	0	---	OM2
710-210	73,780	1.09	163,400	1.19	210	180	3.38	OM3
1580-425	164,000	1.39	388,700	1.47	450	400	3.72	OM4
200-200 <sup>4</sup>	22,620	8.48 trimodal	90,270	1.39	---	---	---	OM5
200-200 <sup>4</sup>	374,100	3.18 trimodal	58,390	1.16	---	---	---	OM6
1700-450	180,200	1.09	393,400	1.33	472	466	3.60	SM18

<sup>1</sup> Resulting values, except #, calculated values

<sup>2</sup> Detected with UV-detector at 280 nm

<sup>3</sup> No initiation of second block occurred

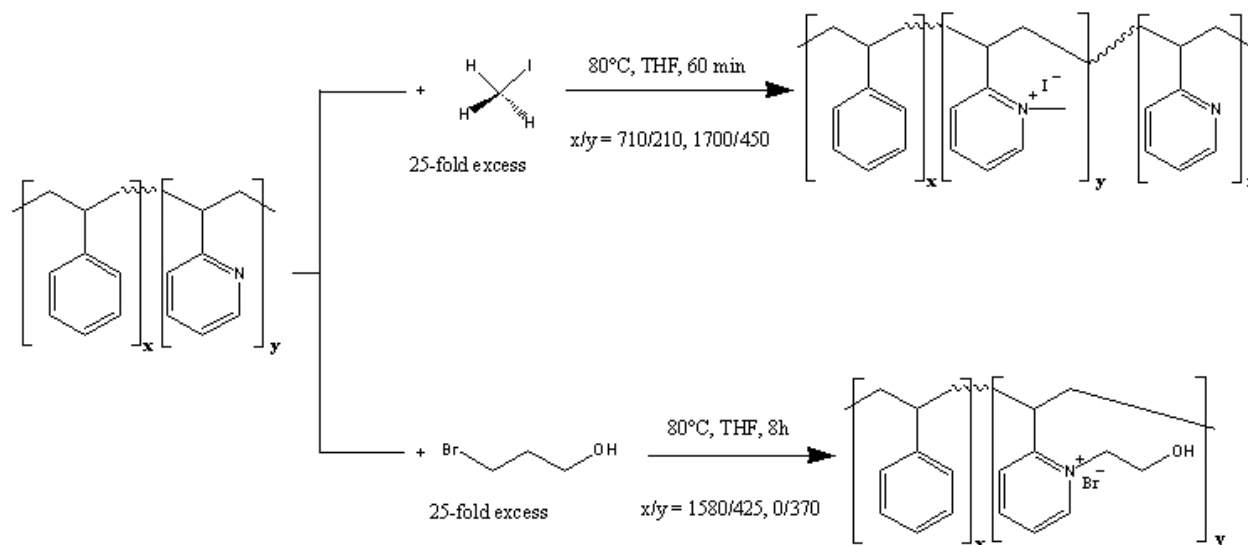
<sup>4</sup> Multimodal distribution

Polymer OM2 is a homo-PS polymer. Here, the chain was terminated while switching the monomer most likely due to impurities. The polymers OM5 and OM6 show trimodal distribution. In this case, the titration of impurities in the first stage was not done careful enough and led to living chain ends while dropwise monomer addition. The last two droplets of titration led to chain formation and represent later two additional polymeric species.

The SEC was performed in DMF as eluent. However, with this experimental setup the RI-detection could not be conducted due to heavy spiking of the resulting peaks and the very poor signal strength. This behaviour was also noticed, when a new calibration with narrow polymer standards was done. With the given polymer, also detection by a UV-detector is possible, since both blocks absorb in the UV-region. The main band occurs at 280 nm wavelength, where the signal for DMF has already decayed to an extent of 10-15%.

### Quaternisation of the 2VP-block

By quaternisation we express a direct acid-base reaction on the 2VP-units of the used PS-*b*-P2VP block copolymers. The pyridine N-atom is methylated by a strong methylation agent like Iodomethane and the polymeric units finally represent an ionic species saturated with the functional group of the methylation agent as counter ion:



As shown in the reaction scheme, not just methylation is possible, also a functionalisation can be performed by usage of a bifunctional quaternisation agent. The quaternisation was carried out with two polymers: OM3 and SM 18 shown in Table A5.2. The procedure used is based on the synthetic description by Gauthier et al. [2]. In this paper, the complete qua-



ternisation of a PS-*b*-P2VP block copolymer is described. For 2VP, extremely hard conditions were found to be able to run a complete reaction to the quaternised polymer. A typical reaction needs a 25-fold excess of the methylation agent methyl iodide and stirring overnight under reflux. We pursued only partial quaternisation of the polymer. For this purpose, the reaction conditions have to be modified by either lowering of reaction time or the methyl iodide amount. It is mentioned in [2], that a reaction time of 90 minutes with the same amount of methyl iodide leads to 20 % of ionised 2VP units. Thus, for the present experiment a reaction time of 60 minutes was chosen to obtain a quaternisation extent between 10 and 20% of ionised 2VP units.

Both reactions were carried out with 1 g of the respective polymer. These reactions yielded 1.29 g of the quaternised OM3 sample and 1.79 g of the quaternised SM18. The increase of weight happened due to the additional methyl group and the iodine anion, which is present in the product. Both products have yellow colour, the precipitate appears first to be white, but changes its colour to yellow.

The extent of quaternisation was followed with  $^1\text{H}$ -NMR, because the partial methylation cannot be followed by IR-spectroscopy due to a very poor signal. Also the band at  $1472\text{ cm}^{-1}$  does not disappear, so that a quantitative calculation is not possible and the qualitative discussion of the spectrum is complex due to the presence of both species. The  $^1\text{H}$ -NMR spectrum, however, shows in the case of the methylated sample two new peaks. One doublet with  $\delta=3.4$  and  $3.9\text{ ppm}$  due to the methyl protons next to the pyridine-N-atom and a shifted peak at  $\delta=9.3$  due to the chemical shift caused by the different chemical environment at the neighbouring methylene group inside the pyridine ring in the methylated 2VP-groups. By calculating the ratio of the integrals of these bands, for the quaternised polymer OM3 a quaternisation extent of 9.8% could be calculated. Because of the broadening of these bands and their relative low intensity a relatively big error can not be excluded. In the case of the polymer SM18 gelation occurred for the NMR-sample in  $\text{CDCl}_3$ . Due to this gelation, the spectrum is more smeared and the intensity of the bands is even smaller. A similar result as for the first sample was calculated (5-20%), but the high sensitivity towards shifting the integration limits caused a low reproducibility of more concrete values. Both samples could not be measured by SEC in pure DMF, the resulting diagrams showed a complex structure and multimodal behaviour. However, for both polymers micellisation occurred in mesitylene.

## A5.2 Synthesis of glyoximato-complexes of Co(II)

For the synthesis of the glyoximato-complexes, a known synthetic route for the Diaquo-cobaloxime(II) [3] is taken and modified for the synthesis of the dipyridino derivate and the unligated Dimethylglyoximato-cobalt(II).

For synthesis of  $\text{Co}(\text{DMG})_2$ , a 250 mL Schlenck-flask is filled with dry methanol (techn. grade, distilled over Mg) under Argon-atmosphere. Under stirring, a portion of 6.21 g (0.025 mol) of Cobalt(II)-acetate tetrahydrate (Fluka >98%) are added. During addition, the solution gets a violet colour and cools down significantly.

After complete dissolution of the Co(II)-compound, 5.79 g (0.05 mol) of Dimethyl-glyoxime (Fluka >99%) are put into the solution, while purging the flask with Argon. Immediately, the colour of the solution changes to brown and a solid precipitates out of the solution. The solution is allowed to stir for another hour. The precipitate and the solution are collected then in an inert gas filtration funnel equipped with a G3-glass filter. The phases are speared by pressure filtration, using Argon as inert gas. The subsequent washing procedure are carried out, using Argon-saturated, distilled water. The latter precaution is taken to avoid oxidation of Co(II) to Co(III). The washing is carried out by addition of three times a portion of 20 mL of the water.

The product is then dried at ambient temperature under vacuum until complete removal of water. The red-brown product is then dried another 2 days under same conditions. Then, the temperature is increased in steps of 10 °C until a colour change is observed. The colour change appears at a temperature of 40-50 °C. The temperature is held and increased to 80 °C during the next 48 hours under vacuum. The resulting product is dark violet. It is transferred into a nitrogen-filled glove-box after finishing the drying process. Elemental analysis yields C, 32.91; H, 5.05; N, 18.82 (calculated C, 33.23; H, 4.98; 19.38). The yield is 6.08 g, which corresponds to approx. 84%.

The same procedure is taken in the case of the Diaquo-complex and the Dipyridino-complex. In the first case, the synthesis is stopped in the stage before water removal and the product is not heated in vacuum. In the case of the pyridine complex, 6 mL of pyridine are added shortly after addition of the glyoxime. In the case of the aquo-complex, a yield of 7.11 g (85%) is reached, 8.91 g (81%) are yielded in the case of the pyridino-complex. The

analysis of  $\text{Co}(\text{DMG})_2(\text{H}_2\text{O})_2$  gives C, 19.63; H, 5.73; N, 17.56 (calculated C, 29.56; H, 5.54; N, 17.23) for the brown-orange solid. The black pyridine complex  $\text{Co}(\text{DMG})_2(\text{Py})_2$  gives by analysis C, 55.01; H, 5.44; N, 12.73 (calculated C, 54.17; H, 5.42; N, 12.64).

### A5.3 Synthesis of Co(II)-hydrazino complexes

Co(II)-hydrazine complexes are synthesised by a method presented by Patil et al. [4]. Another synthetic route, suggested for the chloride complex was also followed [5].

Complexes of the type  $\text{Co}(\text{N}_2\text{H}_4)_3(\text{X})_2$  were prepared, using different educts in order to vary the used counter-ion. The reaction procedure is very simple. The respective Cobalt(II) salt is dissolved in ethanol. Hydrazine hydrate is dissolved in ethanol and the alcoholic solution is added to the salt solution. The product precipitates spontaneously and is filtered, three times washed with 1 mL of ethanol and dried overnight in vacuum. In a typical example, 1.09 g (0.005 mol) Cobalt(II)-nitrate  $\text{Co}(\text{NO}_3)_2$  were dissolved in 2 mL of ethanol. 0.56 g of Hydrazine hydrate (0.02 mol) is dissolved in 1 mL of ethanol and added to the salt solution. In Table A5.1, the reaction entries and results are summarised:

*Table A5-1: Reaction entries for the synthesis of  $\text{Co}(\text{N}_2\text{H}_4)_3(\text{X})_2$  complexes*

<i>Co-salt</i>	<i>Mass [g]</i>	<i>Volume ethanol for salt [mL]</i>	<i>Hydrazine hydrate [g]</i>	<i>Vol. ethanol <math>\text{N}_2\text{H}_4</math> [mL]</i>	<i>Yield [g]/[%]</i>	<i>Product colour</i>
$\text{Co}(\text{NO}_3)_2$	1.09	2	0.56	1	0.88/88%	Light green
$\text{Co}(\text{C}_6\text{H}_5)_2$	1.58	20 mL DMSO	2.24	4	0.8/80%	Violet
$\text{Co}(\text{OAc})_2$	0.75	8	2.24	4	0.71/71%	Red-orange
$\text{CoCl}_2$	0.65	2	0.56	2	0.91/91%	Pink
$\text{Co}_3(\text{PO}_4)_2$	1.56	---	2.24	4	---	No product
$\text{CoCO}_3$	0.51	Not soluble	---	---	---	No product

Not all of the aimed complexes are accessible by the chosen synthetic route. The carbonate and the phosphate, both, are not soluble in ethanol. In the case of the carbonate, no alternative solvent could be found and the reaction was cancelled. The phosphate is soluble in ortho-Phosphoric acid. The reaction with hydrazine yields no precipitate, most likely due to a concurring reaction path due to the acidic environment. In this case, a protonation of the hydrazine is a possible alternative reaction.

For the benzoate, which was dissolved in DMSO, the analysis yields C, 42.57; H, 4.79; N, 14.2. Comparing to the calculated values C, 42.33; H, 5.58; N, 21.15, the product seems to have 1 molecule of hydrazine less in the complex. Thus, the resulting complex seems to have rather the formula  $\text{Co}(\text{N}_2\text{H}_4)_2(\text{C}_6\text{H}_5)_2$ , which could be a four-fold coordinated Co(II)-species, where the hydrazine acts as bidentate ligand. Similar considerations are made for the acetate-complex, where the analysis yields C, 19.93; H, 5.80; N, 22.96 instead of the calculated C, 17.58; H, 6.64; N, 30.77.

For the nitrate, in the FT-IR the following frequencies are found (the values from [4] are written in brackets):

3303  $\text{cm}^{-1}$  (3330  $\text{cm}^{-1}$ ,  $\text{NH}_2$  asymmetrical stretching), 3240  $\text{cm}^{-1}$  (3260  $\text{cm}^{-1}$ ,  $\text{NH}_2$  symmetrical stretching), 1627  $\text{cm}^{-1}$ , 1592  $\text{cm}^{-1}$  (1620  $\text{cm}^{-1}$ , 1590  $\text{cm}^{-1}$ ,  $\text{NH}_2$  bonding), 1178  $\text{cm}^{-1}$  (1170  $\text{cm}^{-1}$ ,  $\text{NH}_2$  twisting), 969  $\text{cm}^{-1}$  (970  $\text{cm}^{-1}$ , N-N stretching), 575  $\text{cm}^{-1}$  (540  $\text{cm}^{-1}$ ,  $\text{NH}_2$  rocking), 1351  $\text{cm}^{-1}$  (1400  $\text{cm}^{-1}$ ,  $\text{NO}_3^-$  ( $\nu_3$ )), 1044  $\text{cm}^{-1}$  (1050  $\text{cm}^{-1}$ ,  $\text{NO}_3^-$  ( $\nu_1$ )), 822  $\text{cm}^{-1}$  (820  $\text{cm}^{-1}$ ,  $\text{NO}_3^-$  ( $\nu_1$ )).

For the chloride complex, in the FT-IR, the following frequencies are found:

3288  $\text{cm}^{-1}$  (3330  $\text{cm}^{-1}$ ,  $\text{NH}_2$  asymmetrical stretching), 3228  $\text{cm}^{-1}$  (3260  $\text{cm}^{-1}$ ,  $\text{NH}_2$  symmetrical stretching), 1605  $\text{cm}^{-1}$ , 1566  $\text{cm}^{-1}$  (1620  $\text{cm}^{-1}$ , 1590  $\text{cm}^{-1}$ ,  $\text{NH}_2$  bonding), 1169  $\text{cm}^{-1}$  (1170  $\text{cm}^{-1}$ ,  $\text{NH}_2$  twisting), 974  $\text{cm}^{-1}$  (970  $\text{cm}^{-1}$ , N-N stretching), 579  $\text{cm}^{-1}$  (540  $\text{cm}^{-1}$ ,  $\text{NH}_2$  rocking).

## A5.4 References

- [1] S. Mößmer, *PhD Thesis*, Universität Ulm, 1999.

- [2] S. Gauthier, D. Duchesne, A. Eisenberg, *Macromolecules*, **1987**, *20*, 753.
- [3] G.N. Schrauzer, *Inorg. Synth.* **1968**, *11*, 61.
- [4] K.C. Patil, C. Nesamani, V.R.Pai Verneker, *Synth. React. Met.-Org. Chem.* **1982**, *12*, 383.
- [5] N.R.S. Kumar, M. Nethaji, K.C. Patil, *Polyhedron*, **1991**, *10*, 365.



# *Co-nanoparticle formation in polymeric nanoreactors*

## 6.1 Introduction

As the second step of the nanoreactor concept, the precursor compound is converted into the metal. If this step is successful, the structure of the polymer influences the arrangement of the particles. If Cobalt is chosen to be the metal of interest, the generation of Co-nanoparticles will take place within the micellar core of the micelles. Then, the structure of the polymer in bulk or casted as film on a substrate forms the pattern, in which the particles are ordered. If globular micelles are used as monolayer, the particles will arrange individually with hexagonal order. If the shape of the micelles will be wormlike, the particles will be free in one direction and could recombine to form a quantum wire. Another interesting point on Cobalt is the influence of magnetic dipolar interactions between neighbouring particles.

For Cobalt, there are two different ways of conversion, which can be taken. Either, the reduction of Co(II) to Co-metal can be performed, or a thermally labile Co-compound is decomposed to form the metal. Both ways will be described in the following chapter.

Polymers were used for this purpose already for the last 30 years [1, 2]. In these examples,  $\text{Co}_2(\text{CO})_8$  was decomposed in a matrix of PS-*co*-P2VP statistical copolymer. Particles were confined on the surface of the polymer, which was nucleation site for the particles. In recent publications, the use of block copolymers was considered to produce Co-nanoparticles [3-6]. We followed our path with PS-*b*-P2VP block copolymers and other block copolymers to

broaden the functionality range within the nanoreactors. At the end, the main goal was to obtain stable particles, one particle per micelle and the structure and separation directed by the polymer or by dipolar magnetic interactions with protection by the surrounding polymer.

## 6.2 Experimental

### *Chemicals*

Cobalt carbonyl ( $\text{Co}_2(\text{CO})_8$ ), an orange solid (Fluka, 95% stabilised with n-hexane), was stored at  $-20^\circ\text{C}$  and has been used as received. A stock solution from  $\text{Co}_2(\text{CO})_8$  was done in mesitylene and toluene, kept under CO-gas in order to reduce degradation of the carbonyl.  $\text{CoCl}_2$  (98% from Fluka) was dried 3 days at  $80^\circ\text{C}$  in a vacuum oven to remove crystalline water. Cobalt(II)-complexes with DMG and hydrazine were synthesised using the route described in Chapter A5. Toluene and mesitylene were dried three days over  $\text{LiAlH}_4$  and distilled twice at  $60^\circ\text{C}$  under dynamic vacuum, further condensed below room temperature in a high vacuum line under dynamic conditions using an oil diffusion pump. The latter process was carried out using Trioctyl-aluminium as drying agent.

Anhydrous hydrazine was synthesised by thermolysis of hydrazine cyanurate. The synthetic procedure is described elsewhere [7, 8], dimethyl-glyoxime (Merck, p.A.) was used as received.

*PS-b-P2VP*-polymers used were the same as described in Chapter 5. Also the same samples were used for further preparation steps.

*Polybutadiene-block-polymethacrylic acid (PBd-b-PMAA)*-polymers were synthesised using ATRP polymerisation. The polymers were received by a cooperating group. More details on the polymerisation can be found elsewhere [9]. In the present work, only the polymer  $\text{PBd}_{550}\text{-}b\text{-PMAA}_{100}$ , where the *subscripts* denote the degree of polymerisation of the respective block, was applied successfully for Co-nanoparticle formation.

*Polybutadiene-block-poly(ethylene oxide) (PBd-b-PEO)* was synthesised using living anionic polymerisation. All the used polymers are taken from work performed in our research group [10]. Table 6-1 summarises the used polymers of this type.



*Table 6-1: Data on the used PBd-*b*-PEO and PS-*b*-PEO polymers*

<i>Polymer label</i>	<i>DP Block 1</i>	<i>M<sub>w</sub>/M<sub>N</sub> Block 1</i>	<i>DP Block 2</i>	<i>M<sub>w</sub>/M<sub>N</sub> Block 2</i>
PBd <sub>185</sub> - <i>b</i> -PEO <sub>35</sub>	185 (Butadiene)	1.10	35 (Ethylene oxide)	1.11
PBd <sub>390</sub> - <i>b</i> -PEO <sub>500</sub>	390 (Butadiene)	1.10	500 (Ethylene oxide)	1.20

### *Sample preparation*

Typically, a volume of 1-2 mL of the solutions was made for a single experiment. When applying anhydrous hydrazine for reduction, the desired amount of hydrazine was dispersed in 1 mL of solvent (toluene or mesitylene). Then, the polymeric Co(II)-solution was added under vigorous stirring to the hydrazine dispersion.

Solutions of Co<sub>2</sub>(CO)<sub>8</sub> in PS-*b*-P2VP were prepared in volumes of typically 1-2 mL. A polymer solution (2.5 mg/mL) was made as described in the experimental part of Chapter 5. Then, the solution was united with the desired amount of Co<sub>2</sub>(CO)<sub>8</sub> stock solution. Typically, the solutions were stirred another 24 hours to guarantee quantitative uptake of the carbonyl in the micellar cores. All these operations were carried out in a nitrogen-filled glove-box, operating at defined values of oxygen and water (< 1 ppm). The solutions were then transferred to a high vacuum line, where three freeze and pump cycles were used to remove traces of remaining oxygen and CO-gas. The solutions were then thermally treated by heating the samples in vacuum at 110 °C in the case of toluene and 170 °C in the case of mesitylene. Samples of the reduced solutions were deposited on a TEM-grid inside of the glove-box.

### *Electron microscopy*

**Transmission electron microscopy (TEM)** images were recorded with a Philips EM 400 T microscope operating at 80 kV. Copper grids (mesh size: 200 x 200 μm<sup>2</sup>) were coated with a Formvar film (around 20 nm thickness) and a layer of carbon (approximately 5 nm thickness) and used as substrates for TEM analysis. The samples were prepared by evaporating a droplet of the solutions on the grid, which was in contact with a soaking tissue in order to avoid multilayer formation. **High-resolution TEM (HRTEM)** images were recorded with a CM 200 FEG (CS correcture) on a holey-copper grid, where a drop of the colloidal solution

was evaporated in the way described above. Sample preparation was carried out inside of the glove-box. EDAX analyser coupled with HRTEM gives the semi-quantitative composition of the samples. With this apparatus, contact of the samples with the air cannot be completely avoided during the transfer of the samples into the microscope. Negatives were scanned on an Umex Astra scanner operating at 600 dots per inch (dpi) using constant picture sizes. Adobe Photoshop 5.5 was used for evaluation particle sizes and distances.

### *UV-VIS spectroscopy*

UV-VIS absorption spectroscopy was performed on a Lambda 16 UV-VIS spectrometer from Perkin-Elmer. Samples for spectroscopy were always treated by a centrifuge working on 5000 rpm, in order to remove dispersed solids. The latter influence the measurement by broadening or hiding the spectrum of the solution. The spectrum was recorded, using pure solvent as reference, which was subtracted from the spectrum. The polymer is not disturbing the spectrum in the visible range, because its absorption is completely in the UV-region of the spectrum. For the exceptional cases, where information was needed on the UV-part of the spectrum, a solution of the respective polymer in same concentration was used as a reference.

### *FT-IR spectroscopy*

Infrared-spectra (FT-IR) were recorded on a Bruker IFS 113 V spectrometer. Samples were prepared by either as KBr-polymer-pellets or as thin film, casted on a pure KBr-pellet.

## **6.3 Results and discussion**

First, we tried to follow the reductive route, which is known to be successful for the reduction of Tetrachloroauric acid to metallic gold. Following this route, micellar solution of the precursor is added to a dispersion of anhydrous hydrazine and reduction of the precursor is noticed immediately by instant colour change [11]. When the procedure is transformed on a solution of  $\text{CoCl}_2$  in  $\text{PS}_{1700}$ -*b*- $\text{P2VP}_{450}$ , the azure colour of the solution disappears immediately. However, even when the colour of nanoscaled Co-particles should not be in the UV-VIS-range by means of plasmon resonance, Co-nanoparticles are known to show a brown to black colour. When the solutions were watched thoroughly, a very slight pink colour of the solutions was observed. The presence of water could be neglected due to

the very strict water exclosure. A spectrum of the UV-VIS absorption of the samples was taken in order to get an explanation for this behaviour. In Figure 6-1, the spectrum of the reduced solution is recorded.

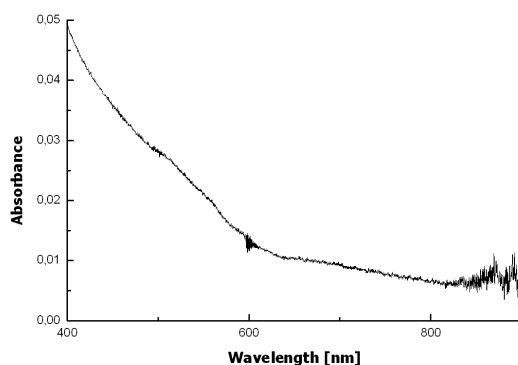


Figure 6-1: UV-VIS spectrum recorded from a solution of  $\text{CoCl}_2$  in  $\text{PS}_{1700}\text{-b-P2VP}_{450}$  with  $L=0.2$  after addition to  $0.5\ \mu\text{L}$  of anhydrous hydrazine.

Between 500 and 600 nm, the spectrum shows a shoulder, whereas the region around 600 nm is without a band. In the region, where the shoulder is recorded,  $\text{Co(II)}$  is absorbing, if it is present as octahedrally coordinated complex. This absorbance, however, is very low in intensity, because the transitions of this band are forbidden. Thus, the very slight pink colour is the colour of a complex, which is formed after addition of hydrazine. Since hydrazine can act as a base in complex chemistry [12], a simple ligand exchange reaction is suggested to take place instead of the desired reduction step.

When the hydrazine reduction step was performed with the Dimethylglyoximato complexes bound in the micellar core, a red-brown precipitate was observed in either  $\text{Co(DMG)}_2$ ,  $\text{Co(DMG)}_2(\text{H}_2\text{O})_2$  and  $\text{Co(DMG)}_2(\text{Py})_2$ . An infrared-spectrum of the initial solution containing  $\text{Co(DMG)}_2$  was recorded and compared to the FT-IR spectrum of the precipitate. The solution above the precipitate did contain empty micelles, which we concluded from the UV-VIS-spectrum, which was empty except for the characteristic absorptions of the polymer in the UV-region. Figure 6-2 shows the comparison of the mentioned FT-IR spectra.

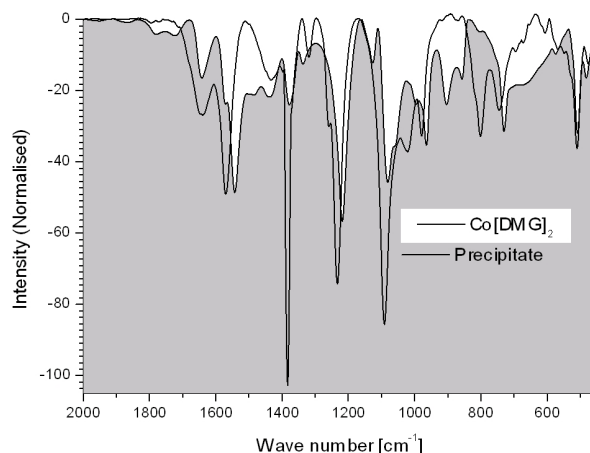


Figure 6-2: Comparison of FT-IR spectra of the  $\text{Co}[\text{DMG}]_2$ -complex (white shaded) and of the precipitate after addition of anhydrous hydrazine (black solid line).

In Figure 6-2, a shift of many peaks of the precipitate are encountered. A band at  $1383\text{ cm}^{-1}$  is the most intensive sharp band in the spectrum. This band can be assigned to the NH-vibration of complexed hydrazine [13].

This led us to the conclusion, that the direct application of the hydrazine reduction is not possible for the  $\text{Co(II)}$ -system. If the reduction step is the desired preparation method, the reducing agent has to be switched. For  $\text{Co(II)}$ , it is quite hard to find a suitable reduction agent under these circumstances. Figure 6-3 shows the possible problems, which can appear, when a reducing agent is introduced in the system.

The reducing agent has to be taken up by the micelles in order to come in contact with the precursor. The uptake also has to be selective to avoid transfer of precursor out of the micelle and bulk reduction. In our experiments, we observed the problem of selective uptake in many cases. The most organic reducing agents could not be taken due to a good solubility in toluene and mesitylene. Benzoquinone and anthraquinone were two examples, which were not successful. Also the reduction by aliphatic aldehydes and alcohols, which could work in general, could not be applied to our system.

Degradation, both, of polymers and micellar associates, can also be a limit to potential reduction agents. Degradation can be caused either by reaction between the substance and the polymer or by too extreme reaction conditions. One good example, which we followed

in our experimental work was a simple reduction of the Co(II) by H<sub>2</sub>-gas [14, 15]. We worked with a CoCl<sub>2</sub> solution and applied up to 250 °C and 200 bar to the system. These attempts always ended up with partial degradation of the polymer, which could be seen by flakes of carbon inside of the still azure solution. It should be mentioned, that also anhydrous hydrazine doesn't behave neutral to the micelles, but can react with styrene and pyridine [16, 17].

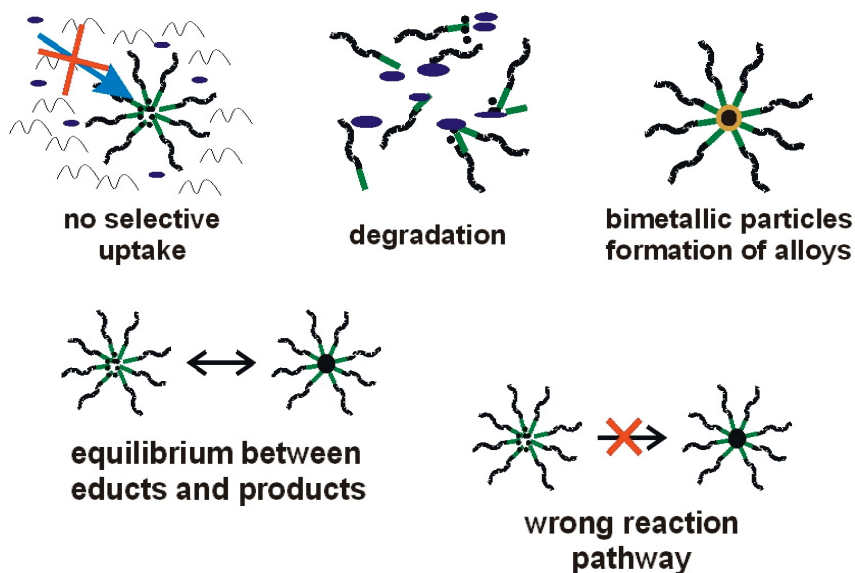
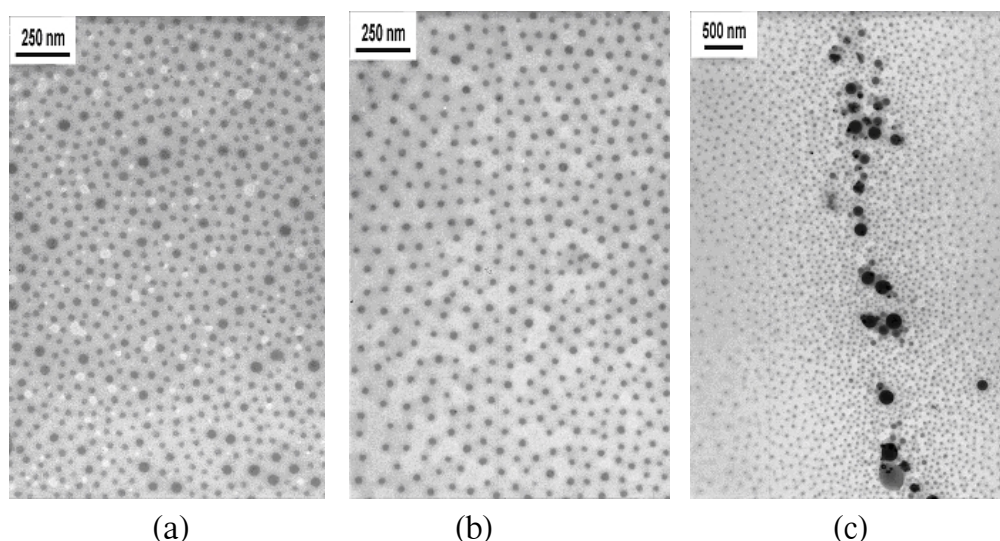


Figure 6-3: Sketches of possible problems for the reduction step in the nanoreactor concept

Bimetal and alloy formation is always a problem, when metals shall act as reducing agents. This very common method of reduction by using a metal of more negative electrochemical potential is critical, because the other metal can be incorporated while particle nucleation and growth, which can lead to undesired alloy and bimetal formation. Especially in the nanometre scale, the miscibilities of the two metals could be influenced by changing particle properties. Also the use of borohydrides can lead to a problem like this. Except for metal formation, the formation of borides is a possible side reaction. The latter is forming dependent on the medium used [18-20].

The reaction has to be quick and quantitative. Possible equilibrium products can not be removed later and stay in the system. The latter way of wrong reaction pathway is exactly the category, where the complexation reaction of hydrazine can be categorised.

Because of the many unsuccessful attempts of reduction, we chose the path of thermal decomposition instead and did not further follow the reduction step. From the thermally labile compounds of hydrazine, we first chose the hydrazino-complex itself. The synthesis of some



*Figure 6-4: Incorporation of the hydrazine complex  $\text{Co}[(\text{N}_2\text{H}_4)_3](\text{NO}_3)_2$  in micelles of the block copolymer  $\text{PS}_{1700}\text{-}b\text{-P2VP}_{450}$  dissolved in mesitylene (2.5 mg/mL): as TEM-micrographs (a) Precursor after 42 h stirring at ambient temperature; (b) and (c) After 24 h treatment at 150 °C; (b) and (c) show two co-existing regions of the film.*

of these complexes is described in Chapter A5. For our decomposition experiments we chose the complex with the nitrate counter ion. Here, the main activation is caused by nitrogen formation. It is known, that Cobalt(II)-complexes of the type  $\text{Co}[(\text{N}_2\text{H}_4)_3]^{2+}$  undergo thermal decomposition above 120 °C [21].

Figure 6-4(a) shows, that the complex is taken up by the micellar core of PS-*b*-P2VP. However, heating the solution for a long time (24 h) at 150 °C does not show the sighted effect of Co-metal formation. Instead, the order and the homogeneity of the micellar solution seem to be increased. On very small areas of the TEM-samples (Figure 6-4(c)), the strong contrast shows, that generally the reaction takes place. Here, some undissolved complex is decomposed and forms bigger particles of half a micron. It can be observed, that the surface of the micelles is a good starting point for crystallisation of the metal. It should be mentioned, that we also tried to decompose the pure  $\text{Co}[\text{DMG}]_2$  complex. The results for this experiment resemble those shown in Figure 6-3. Thus, it seems, that the pyridine units in the micellar cores show very strong interactions to all incorporated Co(II)-species. For a successful route of Co(II)-conversion, the nature of the binding site inside of the micellar cores has to be changed. This can be done either by choosing another type of block copolymer or by reaction on the pyridine unit by means of functionalisation of the pyridine ring.

We could perform successful experiments, when we switched our system towards incorporation of the  $\text{Co}_2(\text{CO})_8$ .  $\text{Co}_2(\text{CO})_8$  was already successfully incorporated in Chapter 3 and 4, when we made our experiments in low molecular surfactants.

Incorporation of  $\text{Co}_2(\text{CO})_8$  in the core of the micelles was successful. The pyridine units coordinate the  $\text{Co}_2(\text{CO})_8$ , which could be due to a disproportionation of the carbonyl compound by influence of the pyridine base [22]. Figure 6-5 shows an example of a micellar  $\text{Co}_2(\text{CO})_8$  solution with PS-*b*-P2VP block copolymer micelles.

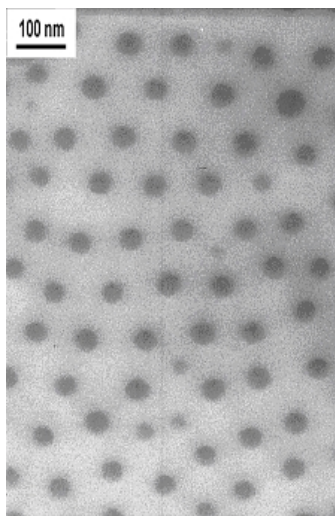


*Figure 6-5: Micellar solution of PS<sub>1700</sub>-*b*-P2VP<sub>450</sub> in mesitylene (5 mg/mL), loaded with  $\text{Co}_2(\text{CO})_8$  with  $L=0.5$  as film on a TEM-grid*

The micelles in the example of Figure 6-5 have a diameter of 45 to 50 nm, the micelles are separated by 120 nm. To change these values, the usage of other block copolymers is necessary. Mesitylene was chosen in order to increase the boiling point of the solutions. We found out, that at least a temperature of 150 °C is necessary for reproducible results, when performing the thermal decomposition. The decomposition is also advantageous, because there are no undesired side-products, just CO-gas is evolved in the reaction, which also could have good influence towards oxidation of the particles due to a scavenging effect towards  $\text{O}_2$ .

When a film on a TEM-grid is put for 24 hours into an oven operating under nitrogen at 145 °C, a change of the film can be observed. The domains of the film do not longer appear to be diffuse, but particles are build inside of the micellar cores. This means, that the principal route of the reaction is working. In solution, however, the stability of the solution and



effects of the solvent have to be taken into account, too. Figure 6-6 shows the thermal experiment on a film containing  $\text{Co}_2(\text{CO})_8$  inside of the micelles. The film is done with the same parameters of the film in Figure 6-5.

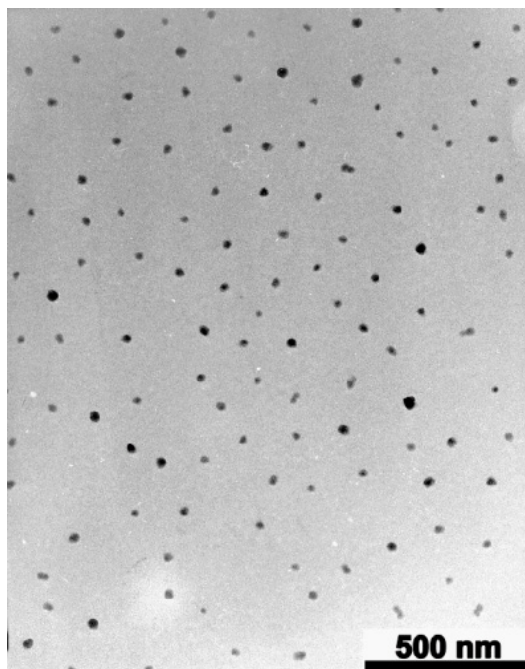


*Figure 6-6: Successful decomposition of  $\text{Co}_2(\text{CO})_8$  in a film of  $\text{PS}_{1700}$ - $\text{b-P2VP}_{450}$ . The film is from a toluene solution with  $L(\text{Co}_2(\text{CO})_8)=0.5$ , cast as a monomicellar film on a carbon coated copper-grid. The grid was kept under  $\text{N}_2$  atmosphere for 24 h at 145 °C.*

In solution, it took us heating up to 170 °C in order to get a homogeneous solution. Step-wise heating was done in order to get the particles (heating to 100 °C, followed up by increase of the temperature by 10 °C steps within 5 minutes. By this procedure, many Co-nuclei are built inside of each micellar core. Here, the loading of the micellar cores is not influencing the growth process of the nuclei, but it does control the number of nuclei, which are formed per micelle. Figure 6-7 shows a Co-metal-containing solution made from  $\text{Co}_2(\text{CO})_8$ .

In order to get one particle per micelle, i.e. a regular arrangement of single particles and an increase of particle size, we tried to join the small nuclei inside of the micelles. We added different substances in order to increase mobility inside of the micellar cores and to release the nuclei from interactions with the polymeric block. The chosen chemicals were Methanol, Tributyl-phosphine, Citric acid, Acetonitrile, Hydrochloric acid, Formic acid and anhydrous Hydrazine. None of those additive in fact could act that way, that at the end one par-



ticle per micelle could be observed. However, as it is shown in Figure 6-7, the number of nuclei could be decreased in a noticeable way. As depicted in Figure 6-7(b), the number of nuclei decreased to 2-3 per micelle, instead of up to 10 per micelle, when anhydrous hydrazine was added. The same effect could be achieved using Acetonitrile.

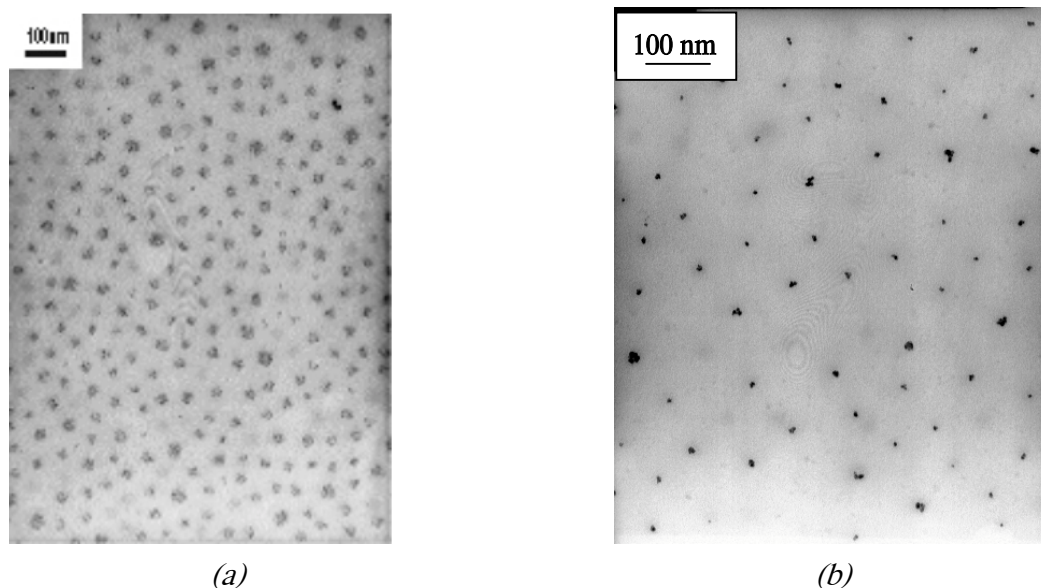


Figure 6-7: TEM-micrographs of thermally decomposed  $\text{Co}_2(\text{CO})_8$  in  $\text{PS}_{1700}\text{-b-P2VP}_{450}$  block copolymer micelles. (a) Solution heated stepwise up to 170 °C; (b) Same solution after treatment with anhydrous hydrazine

Also additional amounts of  $\text{Co}_2(\text{CO})_8$ , which were put into the solution after thermal decomposition did not lead to a fusion of nuclei.  $\text{Co}_2(\text{CO})_8$  can be added without destabilisation of the Co-solution. The following second decomposition step leads only to aggregates, which partially are removed out of the micelles. Most likely, the main fraction of the carbonyl was not bound inside of the micellar cores, but stayed in the solvent phase, where it was decomposed in bulk phase.

From these observations we concluded, that the carbonyl as well as the metallic cobalt – which are both Co in oxidation state 0- are interacting strongly with the pyridine units of the micellar core. This is an advantage for nuclei formation, because of a suitable surface for nucleation. However, the growing seeds can not release from the polymer surface and the nuclei stay individual. Thus, the further strategy consisted in lowering the interaction between the inner block of the micelles and the nuclei. This strategy is the same as we described before for a possibly more successful Co(II)-reduction.

Another valid consideration is, that for joining of two nuclei, the probability of contact between them has to be increased. Then, formation of one particle per micelle could be successful by collision between the seeds. As a comparison, we imagine to throw two marbles in a container. If the container is in the one case a beer glass, the probability for a collision is rather high. If the container is a swimming pool, then the probability is rather low. Transferring this idea to a block copolymer, the chance to get single particles per micelle increases, when the volume of the nano reactor is small. Therefore, the micellar diameters have to be decreased, means the P2VP-block has to have a lower degree of polymerisation.

In summary, the next steps of our work concentrated on the following concrete steps:

- Usage of polymers with a similar block length ratio as  $\text{PS}_{1700}\text{-}b\text{-P2VP}_{450}$  (type of micelles), but a shorter P2VP-block
- Usage of partially quaternised  $\text{PS-}b\text{-P2VP}$  block copolymers to decrease the amount of free pyridine units (blocking)
- Usage of  $\text{PBd-}b\text{-PEO}$  block copolymers to change the nature of the binding sites
- Modification of  $\text{PS-}b\text{-P2VP}$  with 2-Bromoethanol to introduce new functionality, which is maybe also suitable for the reduction step (see page 134)
- $\text{PBd-}b\text{-PMAA}$  block copolymers as an alternative for the change of binding sites

The usage of pure polymer with smaller P2VP-block didn't yield the desired single particles, but led to the same situation as in the case of the bigger polymer. Therefore, we turned to the quaternised polymers. We decided to quaternise just a relatively small amount of 10 – 15% of the pyridine units. This is necessary in order to have enough attracting groups for the incorporation of the precursor. By the quaternisation, also the character of a part of the units changes from a base to an acid. With a mixture of attractive and repulsive forces within the micellar core, the dynamics while the nucleation and growth process should be increased.

As described in Chapter A5.1, two polymers,  $\text{PS}_{1700}\text{-}b\text{-P2VP}_{450}$  and  $\text{PS}_{710}\text{-}b\text{-P2VP}_{210}$  were both quaternised to an extent of approx. 10%. The amount of quaternisation can be controlled via the reaction conditions [23, 24]. With the modified polymers, the formation of micellar associates is much more rapid than in the case of the  $\text{PS-}b\text{-P2VP}$  block copolymers. After 2-3 hours of stirring, the solution becomes clear and micelles can be watched on a film. This is possible due to the higher electron density in the micellar cores, caused by the

iodide counter ion. The micelles can be loaded with  $\text{Co}_2(\text{CO})_8$ . Both preliminary steps are depicted in Figure 6-8.

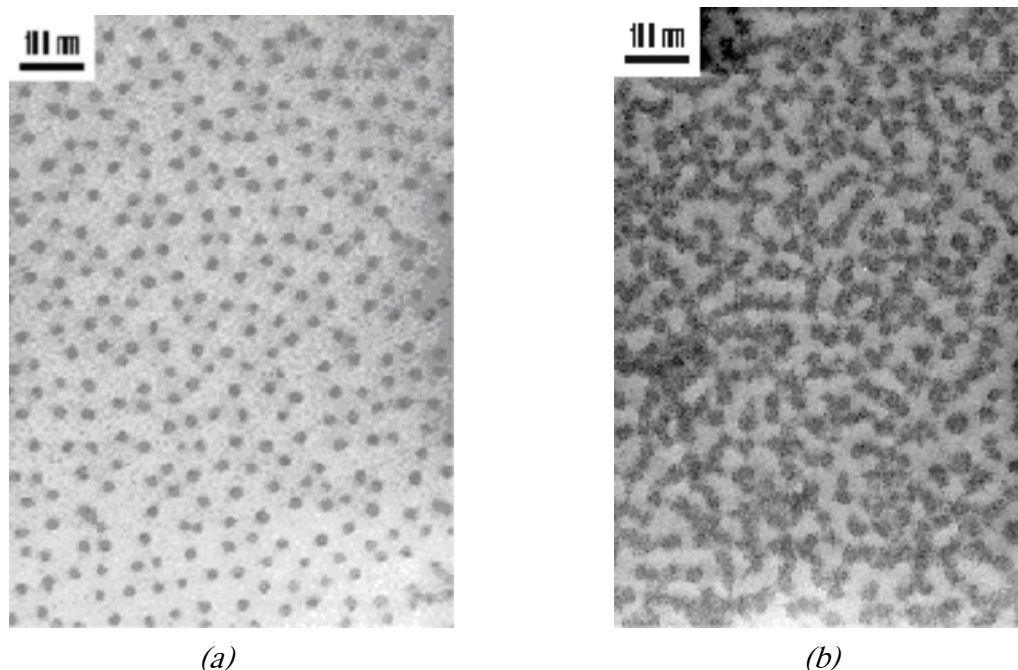


*Figure 6-8: Micelles of  $\text{PS}_{710}\text{-}b\text{-P2VP}_{210}$  dissolved in mesitylene with a concentration of 2.5 mg/mL. The quaternisation degree  $Q$  is 10%. (a) Pure micellar solution, the contrast is made by the iodide ions within the micellar core.; (b) Micellar solution loaded with  $\text{Co}_2(\text{CO})_8$  in excess after 5 days of stirring*

In Figure 6-8(a), the micellar pattern is similar to that, which can be seen in  $\text{Co}(\text{II})$ -loaded micelles. After addition of the Co-compound, the structure of the film changes significantly (Figure 6-8(b)). The micelles seem like connected to each other, forming small aggregates of 4-6 micelles. Those ‘ribbons’ are strong in contrast due to the loading with the carbonyl. Such a structure may be formed because of strong inter- and intramicellar interactions between charges within the micellar core. This behaviour is typical for ionic block copolymers [25].

When temperature is applied to these solutions, the results get widespread. We couldn’t get particles from the quaternised  $\text{PS}_{1700}\text{-}b\text{-P2VP}_{450}$ . Experiments with this polymer yielded particles like those, shown in Figure 6-7a. If the quaternised smaller polymer  $\text{PS}_{710}\text{-}b\text{-P2VP}_{210}$  is taken, particles are forming in a different way. Very small particles are yielded, when working with fast heating to 170 °C and small amounts of  $\text{Co}_2(\text{CO})_8$ . When the reaction is

driven with stepwise heating and with an 5 to 10-fold excess of  $\text{Co}_2(\text{CO})_8$ , the particles combine and form big particles in each micelle. The two different cases are depicted in Figure 6-9.

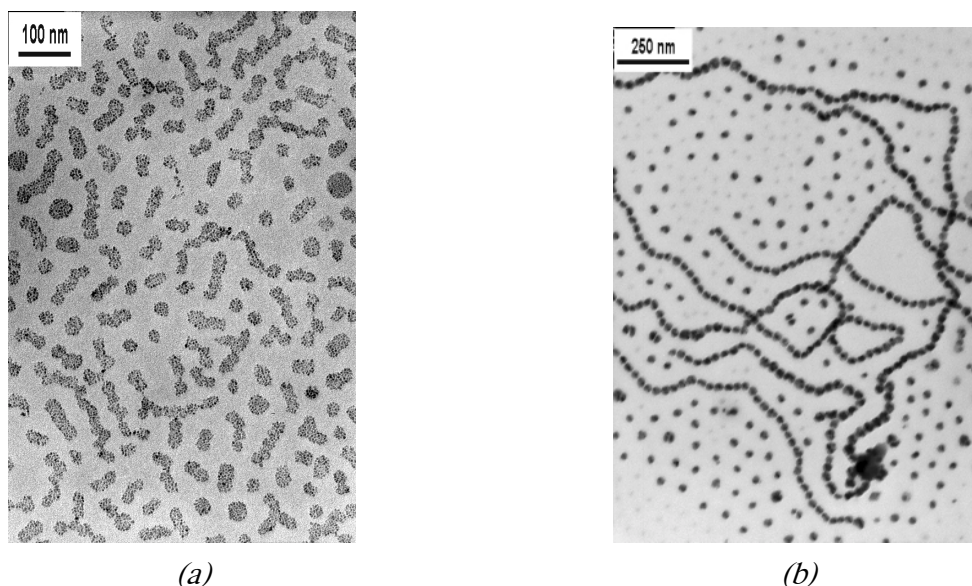
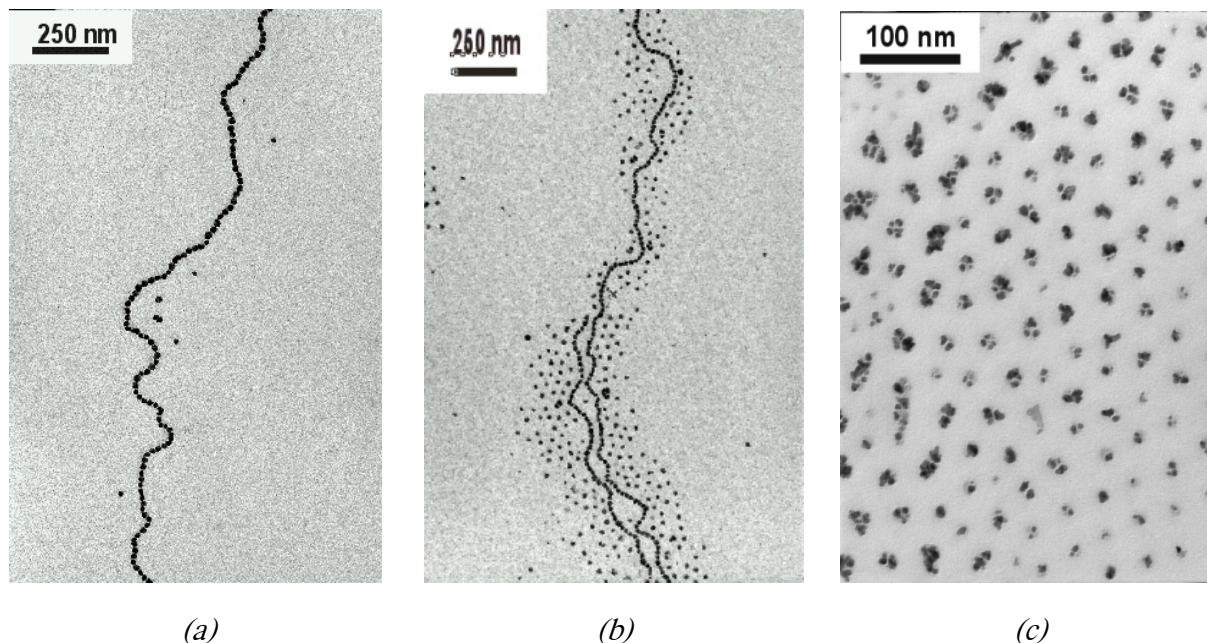


Figure 6-9: (a) Decomposition of  $\text{Co}_2(\text{CO})_8$  in quaternised  $\text{PS}_{710}\text{-b-P2VP}_{210}$  using a loading of  $L=1$  and fast heating to  $170\text{ }^\circ\text{C}$ . (b) Same type of solution heated stepwise from  $100\text{ }^\circ\text{C}$  to  $170\text{ }^\circ\text{C}$  with  $10\text{ }^\circ\text{C}$  per 5 minutes using an excess of  $\text{Co}_2(\text{CO})_8$  ( $L=10$ )

In Figure 6-9a, one can see, that many very small nuclei are formed, which do not further combine to bigger particles. The measure of the nuclei is around 1 to 2 nm. Formation of the nuclei is selectively inside of the cores of the micelles, which still show the structure of the initial micellar solution. Turning to the picture shown in Figure 6-9b, the situation changes dramatically. One particle of metallic Cobalt is within a micelle. The micelles have globular shape. In the regions, where the micelles are well divided, the particles show hexagonal arrangement. The size of the particles is 10 to 15 nm in diameter. Two things are worth to notice: First, within the arrays of hexagonally packed micelles, some of the micelles are empty. This is a hint toward intermicellar exchange of material, which took place while formation of the particles. Second, in between the ordered micelles, strings of particles are formed. These strings are known to appear, when metallic nanoscaled cobalt is formed. It is a matter of magnetic dipolar interaction between the spontaneously magnetised Co-nanoparticles. This pearl-necklace effect was observed already earlier [26, 27]. The particles behave as described in the Stoner-Wohlfarth-theory, which is described in Chapter 2. Because of the positive result in this experiment, we took a closer look on samples made in



that way. Some details can be seen, when films from the solution are inspected thoroughly. In Figure 6-10 we show some special issues from these samples.



*Figure 6-10: Pictures from a solution of  $PS_{710}$ -b- $P2VP_{210}$  with 10% of quaternised pyridine units in mesitylene (2.5 mg/mL), loaded with  $Co_2(CO)_8$   $L=10$ . (a) Chain of spheres in a region, where no film of micelles is in the background. (b) Chain of spheres in a region, which is surrounded by empty micelles or micelles with small nuclei inside. (c) Perfectly hexagonal packing with multiple nuclei within the micelles. One can see that the final 15-20 nm sized particles are set together by aggregation between micelles or within non-spherical micelles.*

In Figure 6-10a, a chain of spheres is deposited from solution, where no polymer is found in the background. This means, that the chains can move freely within the solution, once they are built. Taking a closer look on the chain shows, that the chain consists out of many particles, which stay individual and do not aggregate to a line-shaped object. There is a spacing of 1-2 nm between the particles. Our explanation is, that the polymer micelle collapses due to strong ferromagnetic dipolar interactions, but stays interacting with the surface of the particles. Thus, the polymer builds up a protective adsorption layer, which prevents the particles from coagulation. This is confirmed by the picture, shown in Figure 6-10b, where the two chains are still neighboured by an intact film of micelles, mainly hexagonally ordered. From the picture it seems, that the particles are attracted by the chain inclusive the surrounding polymer micelles. Also a size selection can be seen. The chain itself is sur-

rounded by bigger particles, while empty micelles and micelles containing smaller nuclei are more far away. A key for the initial formation of the spheres is given in Figure 6-10c. Here, only aggregating particles can be found within the micelles. All the micelles are still filled with one or more particles. Different stages of growth by ripening can be seen. On the left of the picture, also a non-spherical micellar associate can be seen. But there is evidence from this picture, that the big particles only can be formed because of the big excess of  $\text{Co}_2(\text{CO})_8$  and because of growth by intermicellar exchange.

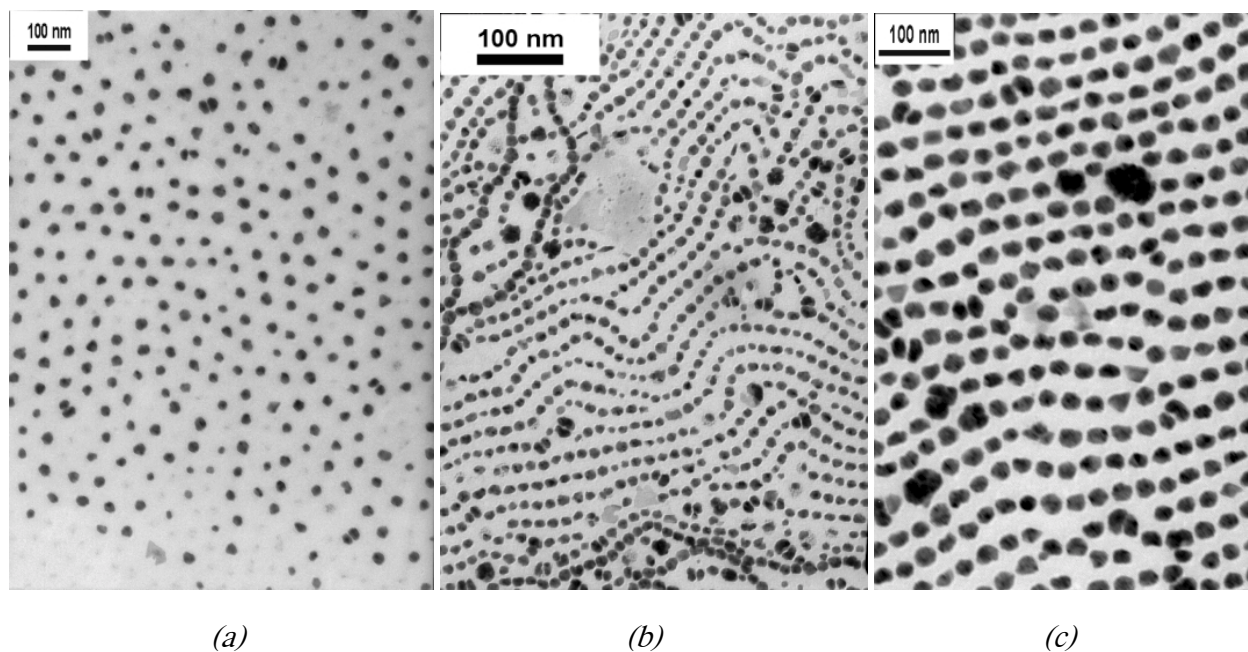


Figure 6-11: (a) Single particles in the same solution as shown in Figure 6-10 without string formation; (b) and (c): Two magnification of a TEM-grid, casted under influence of a permanent magnet.

In Figure 6-11a, a region from the solution is shown, where no string formation occurs. Again, empty micelles can be seen due to the contrast caused by the iodide in the micellar cores. Expectedly, the influence of a permanent magnet also influences the structure on a film of this solution. When we applied the magnetic field of a horseshoe magnet. In Figure 6-11b and 6-11c, this experiment is shown. The lines are arranged under the influence of the magnetic field. Bigger particles cause defects in the arrangement, but also regions of parallel arrangement of the chains do occur as main patterns. Unfortunately, we were not able to reproduce the latter results in each attempt of Co-formation within the quaternised polymer. It seems, that a closer look on experimental conditions is necessary to get control over this reaction.

We switched our work also on PB-*b*-PEO block copolymers. In the case of a micellar core built by PEO, complexation is expected, but the interaction of Co should be less pronounced than in the case of pyridine. Binding of Co in the micellar core should be similar to the coordination by crown ethers, however less strong due to sterical reasons. This is due to the fact, that the PEO block has to coordinate the precursor with the main chain and not with the side chain, as it is in the case of PS-*b*-P2VP. Thus, the conformational changes while complexing the precursor within the micellar core should avoid too strong interactions.

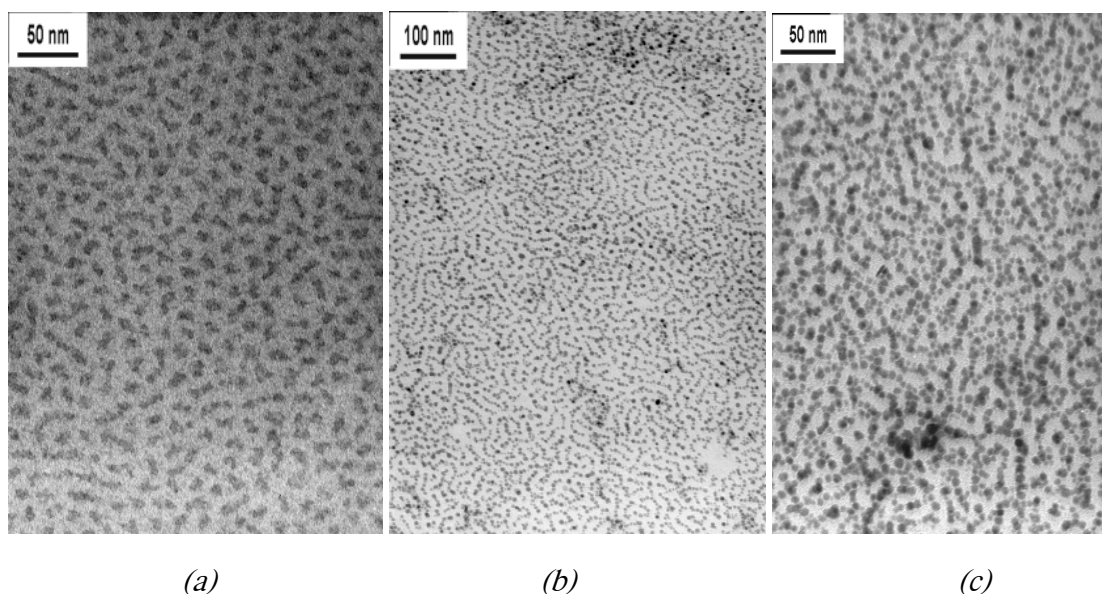


Figure 6-12:  $\text{Co}_2(\text{CO})_8$  in mesitylene solutions of  $\text{PBd}_{185}\text{-}b\text{-PEO}_{35}$ . The carbonyl is added with a loading of  $L=1$  respective to the PEO-block. (a) Precursor solution; (b) and (c) After thermal treatment at  $170^\circ\text{C}$ .

The thermal decomposition was performed in a  $\text{PBd}_{185}\text{-}b\text{-PEO}_{35}$  block copolymer. The loading of the micelles, depicted in Figure 6-12a, shows, that the incorporation inside of the micellar core was selective also in this case. Differing from the PS-*b*-P2VP block copolymers, the micelles are not spherical, but a ribbon-like structure is formed. When the carbonyl is decomposed by quenching to  $170^\circ\text{C}$ , particles are generated within the micelles (see Figure 6-12b and c). Particle formation occurs selectively inside of the ribbons. The particles formed are not monodisperse with sizes ranging between 4 and 9 nm. The polydispersity can be explained by the structure of the micelles, where the particles are nucleated. Within the dimension along the ribbons, the nuclei can be formed randomly. Only the other both dimensions can act limiting on nucleation and growth. Neighbouring nuclei can also combine to bigger particles, as one can see in Figure 6-12c.



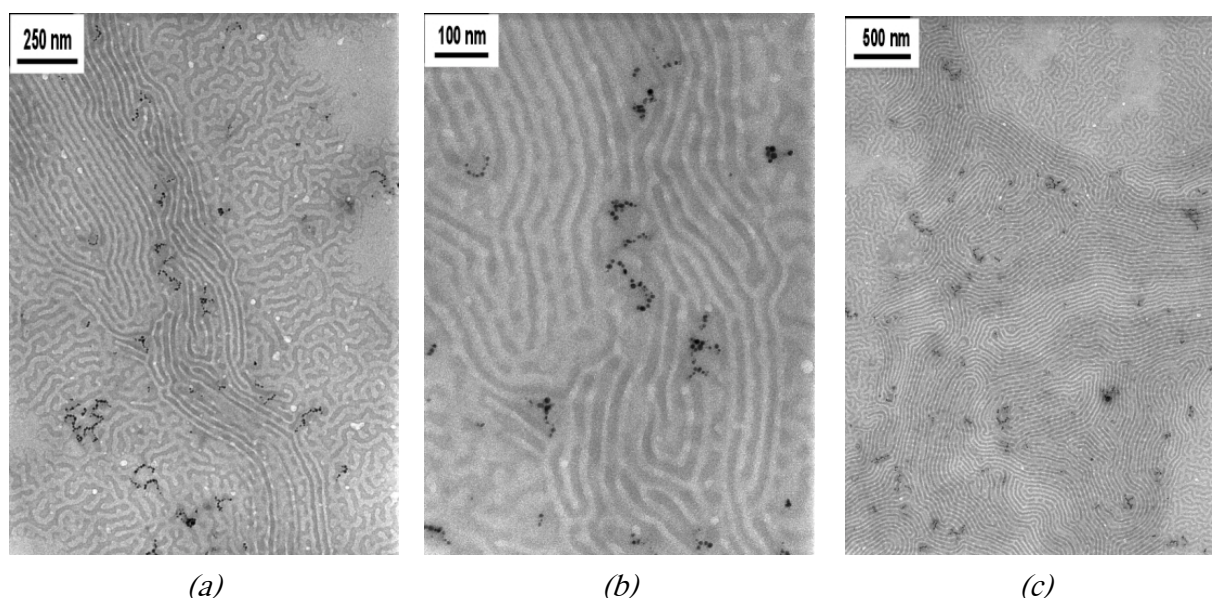


Figure 6-13:  $PBd_{390}$ - $b$ - $PEO_{550}$  block copolymer dissolved in mesitylene (2.5 mg/mL). The polymer was loaded with  $Co_2(CO)_8$  with  $L=1$  and thermally decomposed by quenching at 185 °C. (a), (b) and (c) show three different magnifications of the same sample.

The effect of structure templates in this type of polymer gets pronounced, when the polymer chosen for the experiments is changed towards higher block lengths. We took the polymer  $PBd_{390}$ - $b$ - $PEO_{550}$ . In this polymer, the size of the core-building block is bigger than the size of the soluble block. When we incorporated  $Co_2(CO)_8$  and decomposed it, this led us to an interesting structure, shown in Figure 6-13.

We yielded a lamellar structure, where the dark areas represent the PEO-block, where the  $Co_2(CO)_8$  is localised. The structure is present in a wide area of the film casted onto a carbon coated copper grid. Also particles are formed within the lamellae. However, the formation is random [28], but always within the darker lamellae. We concluded, that the most plausible explanation for the random particle formation is a conversion of non-solubilised  $Co_2(CO)_8$  outside of the polymer structure. Then, the polymeric block has the function of a nucleation site due to increased adsorption on its surface.

When we applied a magnetic field while deposition of the film, we could influence the structure of the polymer film. These experiments are shown in Figure 6-14 for a magnetic field applied parallel to the substrate and in Figure 6-15 for a magnetic field perpendicular to the substrate. In both cases, a strong permanent  $SmCo_5$ -magnet was taken to generate the magnetic field.



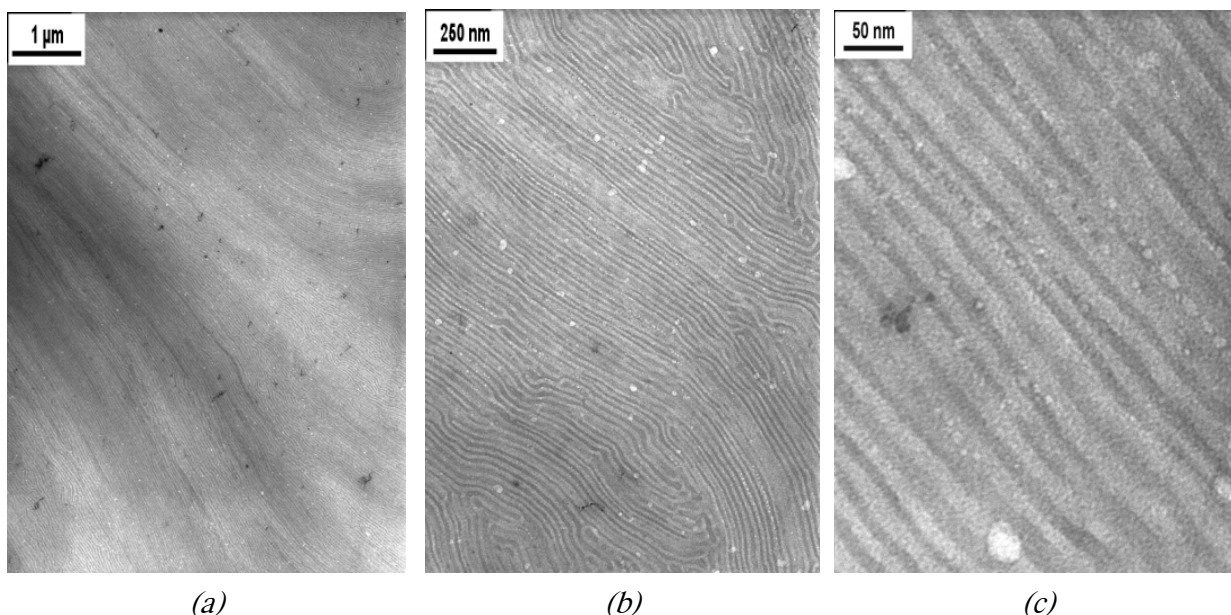


Figure 6-14:  $PBd_{390}$ - $b$ - $PEO_{550}$  block copolymer dissolved in mesitylene (2.5 mg/mL). The polymer was loaded with  $Co_2(CO)_8$  with  $L=1$  and thermally decomposed by quenching at 185 °C. The pictures are recorded from a sample casted under influence of a permanent magnet placed with its field lines parallel to the substrate (a), (b) and (c) show three different magnifications of the same sample

In Figure 6-14 it seems, that the lamellae are slightly influenced by the applied magnetic field. In the overview in Figure 6-14a the long-range ordering of the lamellar film can be seen. Almost no particles can be seen within the sample. It is not evident, that the lamellae are filled with magnetic cobalt, because there is no proof for the metallic character. Anyway, the sample responds to the magnetic influence and the polymer phase is more ordered than in the case without magnetic field shown in Figure 6-13, where the structure is often disturbed by lamellae going out of plane.

For a comparison, if it is the magnetic field, which influences deposition, the experiment was repeated with a magnetic field, applied perpendicular to the substrate. As known from Chapter 4, the orientation of the magnetic field is an important parameter for the deposited film. The pictures in Figure 6-15 show a completely different structure. First, individual particles are present in the film. Second, there is a terrace-like stacking of the polymer, which leads to a structure in the micrometer range. On the magnification in Figure 6-15b, it can be seen, that the terraces are built up by a lamellar phase of the polymer. It seems that high-temperature and magnetic interaction is able to influence the wetting behaviour of the polymer solutions and leads to different morphologies [29].

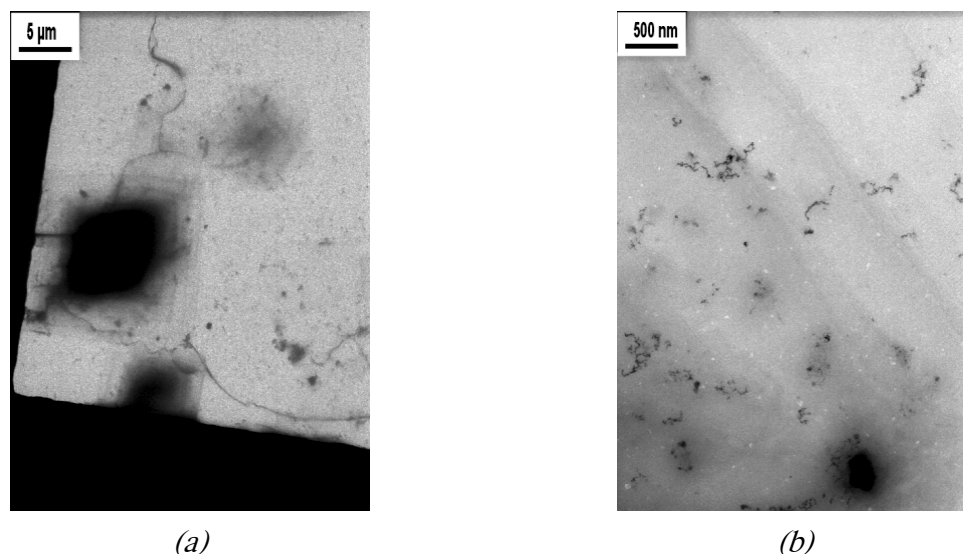
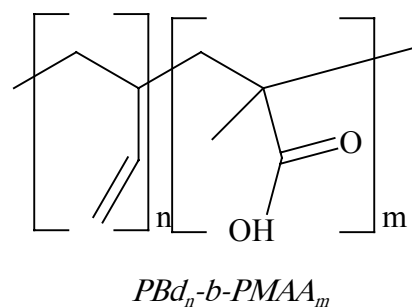
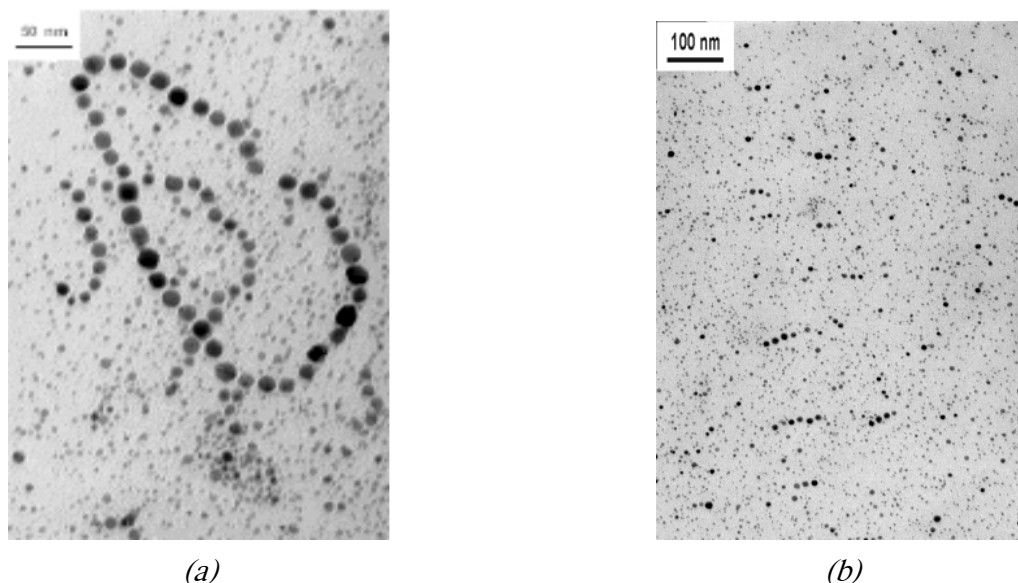


Figure 6-15: Two magnifications of a film made in the same way like the films in Figure 6-14, but with the field lines perpendicular to the substrate.

Experiments were also performed with Polybutadiene-*block*-poly(methacrylic acid) block copolymers. When we incorporated  $\text{Co}_2(\text{CO})_8$  into solution of mesitylene and used the same conditions as in the experiments before, this led us to formation of two different kinds of particles in the solutions. There were very small particles confined in areas, which are most likely the micellar cores. Additionally, bigger particles were formed without an order by patterning. However, these particles were forming rings and strings of particles. This was the reason, why we considered them to be ferromagnetic, because formation of these structure is typical for directed dipolar interactions of single-domain particles surrounded by an environment, which provides non-directed van-der-Waals forces [30]. When we applied a magnetic field while deposition of the solution on a Cu-grid, the film didn't show any ring formation, but only small lines of particles. While the particles are responding to the external magnetic field, ring formation is no more favourable, because of magnetic moments antiparallel to the field direction. Thus, the rings are 'opened by the magnetic field. TEM-pictures of these experiments are shown in Figure 6-16.





*Figure 6-16: Solution of  $PBd_{550}$ - $b$ - $PMAA_{100}$  in mesitylene (2.5 mg/mL).  $Co_2(CO)_8$  with  $L=1$  is decomposed by quenching to 180 °C. (a) Ring formation and particles in background without magnetic field; (b) Application of an external magnetic field while droplet deposition leads to opening of the rings. The permanent magnet was oriented parallel to the deposition plane.*

The appearance of two different species, however, indicates, that no selective uptake into the micellar cores takes place. Also, the particles present in the background, are different in size. Thus, this polymeric system does not allow a good control over the particle synthesis, which was the objective of the experiments.

We finally also performed the functionalisation of the pyridine ring by means of 2-Bromoethanol. This compound had to be cleaned via rotating band fractionation in order to remove traces of 1,2-Dibromoethane, which would cross-link the polymer under the chosen conditions. We were not able to dissolve the modified polymer by a single solvent. By using mixtures of mesitylene with 10-20% of polar solvents like THF, Methanol, Chloroform or Dichloromethane the polymer could be dissolved. Without loading, the bromine is responsible for the dark areas seen in a TEM-micrograph. In Figure 6-17, pictures of such polymer solutions are given.

The addition of polar solvent accelerated the reaction significantly. The problem, which can be seen from Figure 6-17 is, that the micelles undergo swelling and aggregation due to the polar additive. This additive has to be removed by elevated temperatures. For this reason, high-boiling point solvents were not taken for this purpose. We did numerous experiments

in order to generate particles in these system. However, none of the experiments yielded the desired controlled way of co-particle formation. Nevertheless, a possibility, which still

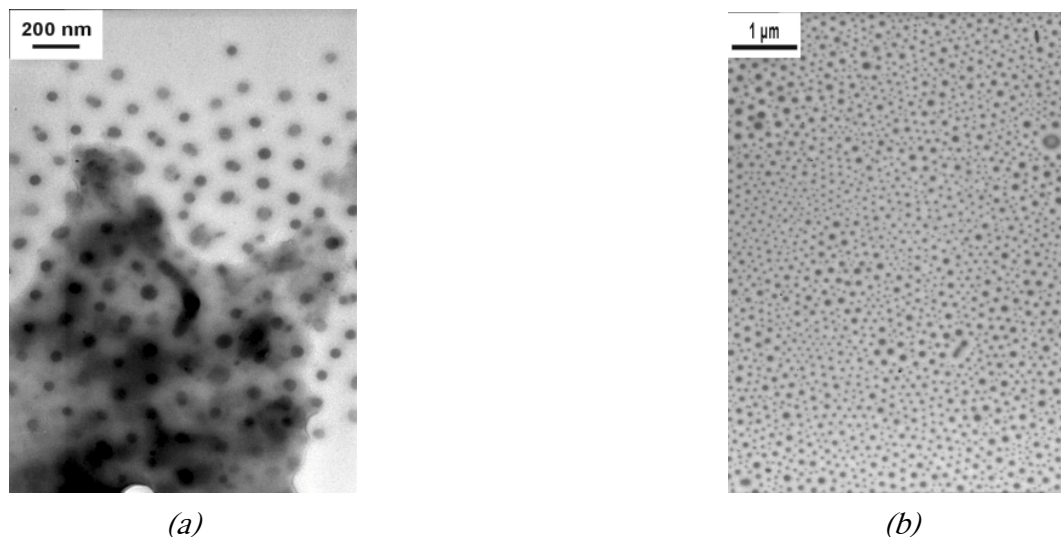


*Figure 6-17: The polymer  $PS_{1580}$ -b- $P2VP_{425}$  was functionalised with 2-Bromoethanol. (a) The resulting polymer was stirred in Mesitylene (2.5 mg/mL) for 6 weeks. (b) Picture from a solution with 80% of Mesitylene and 20% of Ethanol (2.5 mg polymer/mL). The sample was prepared after 1 hour of stirring.*

stayed open is the conversion of Co(II)-compounds within this system.

## 6.4 Conclusion

Many efforts were taken in order to perform Co-nanoparticles in a controlled way in polymeric systems. The initial path of Co(II)-reduction was discarded due to a too strong interaction of pyridine to Co(II). Anhydrous hydrazine, which was successfully taken to reduce Gold(III) did not bring the expected reaction, but was complexed by Co(II).

Thermal decomposition of hydrazino-complexes led to undefined particle formation and to partial degradation of the system. The most successful way to generate Co-metal within polymeric micelles is again the thermal decomposition of  $Co_2(CO)_8$  within the micelles.

Conversion of  $\text{Co}_2(\text{CO})_8$  leads to very small nuclei, which can partially be joined together by anhydrous hydrazine or acetonitrile. The thermal decomposition can be enhanced by usage of partially quaternised PS-*b*-P2VP block copolymers. Rapid heating and small amounts of  $\text{Co}_2(\text{CO})_8$  lead to similar results as in the case of the non-quaternised polymer.

Stepwise heating and  $\text{Co}_2(\text{CO})_8$  in excess lead to aggregation of the nuclei and to formation of Co-nanoparticles within the micelles. Parts of the particles tend to formation of chains of spheres. Here, the particles stay separated from each other. Also empty micelles can be observed in the system. By application of external magnetic fields, the particles can be arranged along the field gradient. Anyway, these experiments have a lack of reproducibility.

In PBd-*b*-PEO block copolymers, Co-particles can be formed within ribbon-like and lamellar structures. When symmetrical polymers of this type are taken, the lamellar structure is filled with  $\text{Co}_2(\text{CO})_8$  and Co. By application of an external magnetic field, the wetting of the micellar solutions is influenced and yields striped or terrace-shaped structures depending on the direction of the magnetic field.

In PBd-*b*-PMAA micelles, no selective  $\text{Co}_2(\text{CO})_8$  uptake into the polar block is observed, but a mixture of confined and unconfined particles appear. The free particles adsorb on the polymer surface and build up rings and strings, which can be arranged by a magnetic field. The smaller particles are irregular and do not show effects caused by the magnetic field.

## 6.5 References

- [1] J.R. Thomas, *J. Appl. Phys.* **1966**, *37*, 2914.
- [2] P.H. Hess, P.H. Parker Jr. *J. Appl. Polym. Sci.* **1966**, *10*, 1915
- [3] J.P. Stevenson, M. Rutnakornpituk, M. Vadala, A.R. Esker, S.W. Charles, S. Wells, J.P. Dailey, J.S. Rifle, *J. Mag. Mag. Mater.* **2001**, *225*, 47.
- [4] R. Ulrich, A. Du Chesne, M. Templin, U. Wiesner, *Adv. Mater.* **1999**, *11*, 141.

- [5] M. Rutnakornpituk, M.S. Thompson, L.A. Harris, K.E. Farmer, A.R. Esker, J.S. Riffle, J. Connolly, T.G. St. Pierre, *Polymer*, **2002**, *43*, 2337.
- [6] O.A. Platonova, L.M. Bronstein, S.P. Solodovnikov, I.M. Yanovskaya, E.S. Oblonkova, P.M. Valetsky, E. Wenz, M. Antonietti, *Colloid Polym. Sci.* **1997**, *275*, 426.
- [7] E. Nachbaur, G. Leiseder, *Monatsh. Chem.* **1971**, *102*, 1718.
- [8] S. Mößmer, *PhD Thesis*, Universität Ulm, **1999**
- [9] S. Pispas and N. Hadjichristidis, *Macromolecules*, **2003**, *36*, 8732.
- [10] B. Gorzolnik, *PhD Thesis*, RWTH Aachen, in progress.
- [11] J.P. Spatz, S. Mößmer, M. Möller, *Chem. Eur. J.* **1996**, *2*, 1552.
- [12] J.R. Dilworth, *Coord. Chem. Rev.* **1976**, *21*, 29.
- [13] D. Nicholls, M. Rowley, R. Swindells, *J. Chem. Soc. A*, **1965**, 950 and references herein.
- [14] I. Arvanitidis, A. Kapilashrami, D. Sichen, S. Seetharaman, *J. Mater. Res.* **2000**, *15*, 338.
- [15] M. Voß, G. Fröhlich, D. Borgmann, G. Wedler, *J. Catal.* **1999**, *187*, 348.
- [16] T. Kauffmann, W. Schoeneck, *Angew. Chem.* **1959**, *71*, 285.
- [17] T. Kauffmann, C. Kosel, D. Wolf, *Chem. Ber.* **1962**, *95*, 1540.
- [18] G.N. Glavee, K.J. Klabunde, C.M. Sorensen, G.C. Hadjipanayis, *Inorg. Chem.* **1993**, *32*, 474.
- [19] J. Lu, D.B. Dreisinger, W.C. Cooper, *Hydrometallurgy*, **1997**, *45*, 305.
- [20] G.N. Glavee, K.J. Klabunde, C.M. Sorensen, G.C. Hadjapanayis, *Langmuir*, **1992**, *8*, 771.
- [21] Y.D. Li, L.Q. Li, H.W. Liao, H.R. Wang, *J. Mater. Chem.* **1999**, *9*, 2675.

- [22] O.A. Platonova, L.M. Bronstein, S.P. Solodovnikov, I.M. Yanovskaya, E.S. Oblonkova, P.M. Valetsky, E. Wenz, M. Antonietti, *Colloid Polym. Sci.* **1997**, *275*, 426.
- [23] S. Gauthier, A. Eisenberg, *Macromolecules*, **1987**, *20*, 760.
- [24] S. Gauthier, D. Duchesne, A. Eisenberg, *Macromolecules*, **1987**, *20*, 753.
- [25] F. Essler, F. Candau, *Colloid, Polym. Sci.* **2001**, *279*, 405.
- [26] P.H. Hess, P.H. Parker Jr., *J. Appl. Polym. Sci.* **1966**, *10*, 1945
- [27] C.H. Griffiths, M.P. O'Horo, T.W. Smith, *J. Appl. Phys.* **1979**, *50*, 7108.
- [28] R. Pastor-Satorras, J.M. Rubí, *J. Mag. Mag. Mater.* **2000**, *221*, 124.
- [29] P.M.-Buschbaum, *J. Phys.: Condens. Matter*, **2003**, *15*, R1549.
- [30] S.L. Tripp, S.V. Pusztay, A.E. Ribbe, A. Wei, *J. Am. Chem. Soc.* **2002**, *124*, 7914.





# ***Surface modification of Co-nanoparticles***

## **7.1 Introduction**

Modification of particle surfaces is an important step, if the particles should fulfil functions or if the new surface shall combine the particles surface with the properties of a surface layer.

Among the possibilities of surface modification is the functionalisation of the particle surface. This can benefit either changing surface properties like solubility, colour or affinity towards other substances like in the case of biofunctionalisation [1, 2]. The other possibility is the attachment of functional groups, which can later interact with other surfaces or be an intermediate layer prior to further modification [3-7, 10]. Also layer-by-layer construction of particles is possible [8]. In the way vice versa, silica bead surfaces could be metallised [9].

Another way of surface modification is the coating of the particles with a second metal in order to generate bimetallic particles. In the best case scenario, this second metal is forming a closed layer around the inner particle and the resulting particles have a core-shell structure. The goal of such a metal coating is either the protection of a metallic nanoparticle against oxidation or the combination of two different properties [10, 11]. In the case of Co-nanoparticles, both possibilities can be united. If a noble metal like gold is forming a closed layer around the particle, the oxidation-sensitive Co-particles are protected by a stable gold-layer. The magnetic properties are thus conserved by the layer of gold. If the particle size of the core-shell particles is small enough, the nanoscaled gold-shell will display a colour due

to plasmon resonance. By magnetic alignment, the colour could then be switched, if the dimensions of the interacting gold surfaces are able to interact in only one direction.

There is evidence, that certain combinations of metals do form core-shell-type particles [12, 13]. Other combinations of two metals can lead to alloy formation [14]. This is sometimes also a desired product of bimetallic particle synthesis, since alloys offer many properties, which are not accessible by the pure metals. A good example is CoCr(10)Ta(6), which is used for years as functional layer on magnetic recording media. The reason is an enhanced magnetism by alloy formation in combination with a hysteresis curve matching the needs of storage media [15].

In this chapter, we will give a brief overview over experiments, we made to influence the surface of Co-nanoparticles. This was mainly done by functionalisation with silane  $\text{SiH}_4$  and by extraction of surfactant covered Co-particles into polymeric micelles. Also the combination Co-particles with a noble metal is discussed. Here, surface coating and alloy formation was the objective.

## 7.2 Experimental

### *Chemicals*

Generation of particle solutions in AOT/OA-mixtures and in TDS were done as described in Chapter 4. The used systems had a Co-to-surfactant ratio of 25:1 and an OA:AOT ratio of 0.5. The solutions were heated in mesitylene for 20 minutes at 180 °C.

*PS-b-P2VP*-block copolymers are listed in Chapter 5. For extraction, solutions of 2.5 mg/mL

*Table 7-1: Molecular weights of additional PS-b-P2VP polymers*

<i>Polymer label</i>	<i>DP (PS)</i>	<i>DP (P2VP)</i>	<i>Total molecular weight [g/mol]</i>	<i>Block length ratio R</i>
<i>960-11</i>	<i>960</i>	<i>11</i>	<i>101,238</i>	<i>87</i>
<i>375-25</i>	<i>375</i>	<i>25</i>	<i>41,725</i>	<i>15</i>
<i>390-15</i>	<i>390</i>	<i>15</i>	<i>42,236</i>	<i>26</i>

in mesitylene were made. Additionally to the known polymers, we took some polymers with short 2VP chain, which are listed in Table 7-1.

Bis[1,2 : 5,6- $\eta$ -(1,5-cyclooctadiene)]dimethylplatinum(0) (written as Pt[(COD)<sub>2</sub>Me<sub>2</sub>]) from Strem Chemicals was used as received. It was stored under inert gas at -20 °C in the dark prior to use.

Tetrachloroauric(III) acid (HAuCl<sub>4</sub>·2H<sub>2</sub>O) from Fluka was used as received. Silicon hydride SiH<sub>4</sub> (Silane) from Merck was used without further purification.

### *Sample preparation*

The samples for silane modification are prepared as described in Chapter 4 in AOT-OA mixtures. After heating of the solution, it is cooled down to ambient temperature, a sample is taken for TEM and the ampulla is fixed again to the high vacuum line. The line is now equipped with a tube for the silane supply. The entire system is evacuated and subsequently filled with dry nitrogen. An outlet is made, going directly to a NaOH solution in order to deactivate excess of SiH<sub>4</sub>. The nitrogen pressure should be high enough to keep constant bubbling through the solution. Under this nitrogen flow, a Teflon capillary leading to the SiH<sub>4</sub> is introduced until it dips into the Co solution. Then the silane is allowed to bubble gently for 5 minutes through the solution. Then the SiH<sub>4</sub>-capillary is removed and the silane supply is interrupted. The solution is then again heated up to 170 °C. After heating precipitation in the solution is observed. The line is flushed carefully with nitrogen to remove the remained silane and then the closed ampulla can be removed from the line and put in the glove box for further analysis.

Redispersal experiments are performed either by separating solid precipitate under inert gas from the solution by removing the solution by a syringe. To the solid, a freshly prepared polymer or surfactant solution is added. The mixture is then transferred to a shaker and shaken until the solution gets clear. The uptake is usually accelerated by applying a temperature of up to 80 °C. For this purpose, the shaker is equipped with a aluminium heating mantle.

For direct extraction of surfactant protected particles into polymer solutions, a droplet of the surfactant solution is simply inserted into a freshly prepared polymer solution.

Experiments, using mixtures of cobalt and platinum precursor were performed as described in Chapter 4. The platinum compound was then added simply into the solution before the start of the reaction.

Pure platinum nanoparticle solutions were performed by addition of the precursor to the surfactant solution inside of a closed vessel. The thermal decomposition was not performed under inert gas, since the oxidation was considered to be negligible in the case of Pt.

Experiments on direct coating of micellar Co-solutions were performed directly on a carbon coated copper grid for TEM. For this, the grid was put into a solution of the second metal precursor and the reduction agent was added instantly. The solution was allowed 15 minutes to stand, before the grid was removed from the solution.

### *Electron microscopy*

**Transmission electron microscopy (TEM)** images were recorded with a Philips EM 400 T microscope operating at 80 kV. Copper grids (mesh size:  $200 \times 200 \mu\text{m}^2$ ) were coated with a Formvar film (around 20 nm thickness) and a layer of carbon (approximately 5 nm thickness) and used as substrates for TEM analysis. The samples were prepared by evaporating a droplet of the solutions on the grid, which was in contact with a soaking tissue in order to avoid multilayer formation.

**High-resolution TEM (HRTEM)** images were recorded with a CM 200 FEG (CS corrector) on a holey-copper grid, where a drop of the colloidal solution was evaporated in the way described above. Sample preparation was carried out inside of the glove-box. EDAX analyser coupled with HRTEM gives the semi-quantitative composition of the samples. With this apparatus, contact of the samples with the air cannot be completely avoided during the transfer of the samples into the microscope. Negatives were scanned on an Umex Astra scanner operating at 600 dots per inch (dpi) using constant picture sizes. Adobe Photoshop 5.5 was used for evaluation particle sizes and distances.

## 7.3 Results and discussion

In order to coat the Co-nanoparticles with a shell of Ag or Au, direct deposition of the silver was tried. This step can be done using the known reduction conditions for gold and silver. For gold, the reduction of  $\text{HAuCl}_4$  with anhydrous hydrazine is a suitable method, for silver, the lactate can be reduced using hydroquinone. As we observed in first experiments, the direct addition of these systems to surfactant stabilised Co-particles is not working. We think, that the interaction of the surfactant with the particle surface is so high, that the par-

ticle surface is not reached by the second metal. Figure 7-1 sketches the direct approach.

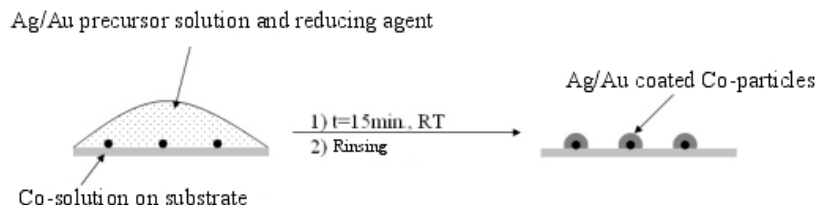


Figure 7-1: Strategy for direct coating of Co-particles with Ag or Au.

As a substrate we tried TEM-grids (carbon) and Si-wafers. The direct approach didn't yield a coating on the particle surface as suggested by Figure 7-1. By this method, we yielded pure

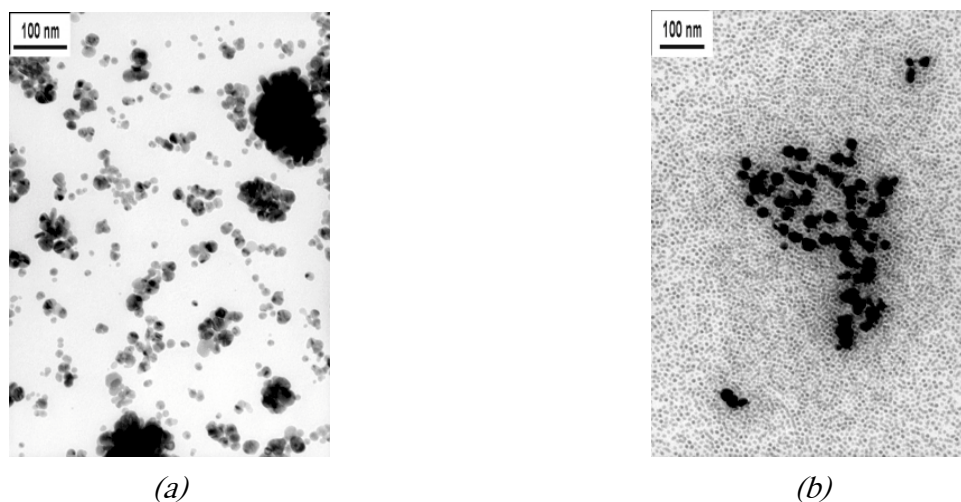


Figure 7-2 (a) A Co-sample on a TEM-grid, where the strategy from Figure 7-1 was performed using silver lactate and hydroquinone. (b) Direct reduction of  $\text{HAuCl}_4$  by anhydrous hydrazine within a solution of AOT-OA protected Co-nanoparticles.

gold particles, while the cobalt oxidised and went into solution. The direct approach by addition of the second precursor and the reducing agent to the solution led to two different particle sorts. Pictures from these attempts are given in Figure 7-2. From Figure 7-2a it is evident, that the reduction on the substrate didn't yield coated particles. With an analysis of the material by means of HR-TEM, the only metal, which can be found on the substrate is Ag. Therefore, the Co was oxidised by the Gold(III) and dissolved in the solution, which was removed. In the case of direct reduction, both metals coexist with each other. It can be seen from Figure 7-2b, that the Co is still protected by the surfactant and the gold forms particles, but is not interacting with the Co-surface.

As alternative, the surfactant stabilised particles can be transferred into a polymeric micellar system. As we found out, the transfer of the Cobalt into the micelles works and the so extracted solutions can be treated further by the precursor of the noble metal. Inside of the micellar core, there is still pyridine units available for the second precursor to bind the noble metal precursor. In the following step, the reduction of the precursor can be performed near the particle surface, which increases the coating probability.

For our experiments, we took the precipitate, which was formed in the thermal decomposition of  $\text{Co}_2(\text{CO})_8$  in AOT micelles. The same results were later obtained, when we took the precipitate from the decomposition experiments in TDS. By removing the supernatant liquid and drying the precipitate in a nitrogen filled glove box, the precipitate can be isolated. The desired polymer solution was then added to the solid and the solution was either stirred or shaken. For acceleration of the uptake, the solutions are heated at 80 °C for some days. This results in black to brown coloured solutions, which are clear after the treatment. For extraction, we used  $\text{PS}_{1700}\text{-}b\text{-P2VP}_{450}$ ,  $\text{PS}_{710}\text{-}b\text{-P2VP}_{210}$  and  $\text{PS}_{750}\text{-}b\text{-P2VP}_{50}$  block copolymers in order to take two polymers with different micellar diameters. Figure 7-3 shows results.

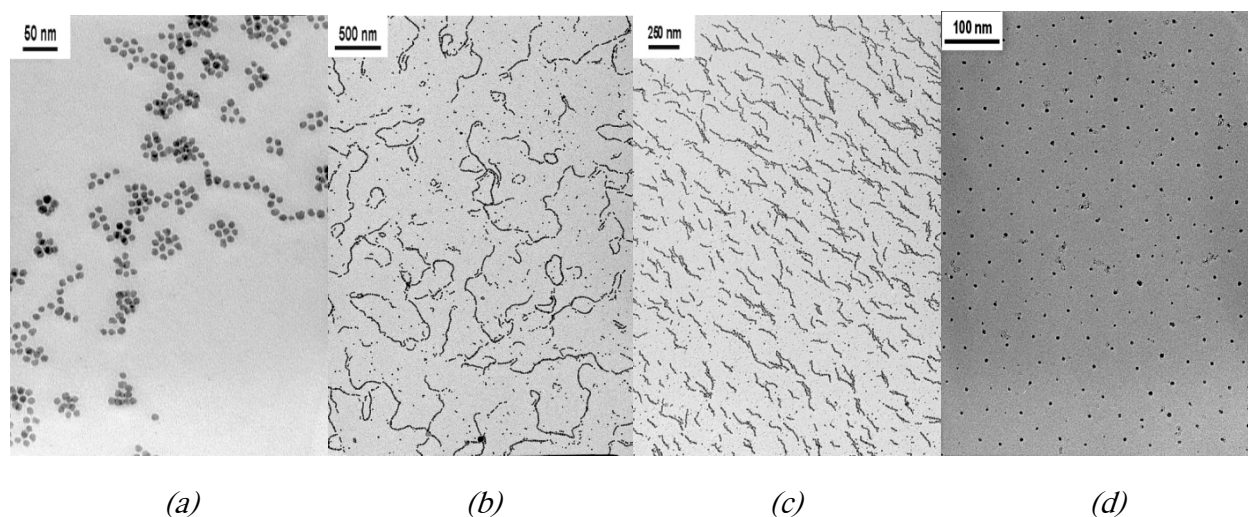


Figure 7-3: TEM images of Co particles formed in presence of AOT/OA

(a) after addition of  $\text{PS}_{1700}\text{-}b\text{-P2VP}_{450}$  block-copolymer; (b) after addition of  $\text{PS}_{750}\text{-}b\text{-P2VP}_{50}$  block-copolymer film casted onto Cu grid; (c) after addition of  $\text{PS}_{750}\text{-}b\text{-P2VP}_{50}$  block-copolymer film casted onto Ni-grid; (d) after addition of  $\text{PS}_{710}\text{-}b\text{-P2VP}_{210}$  block copolymer.

In  $\text{PS}_{1700}\text{-}b\text{-P2VP}_{450}$  micelles, the surfactant structure is still intact, but starting formation of strings show, that a slight separation took place. Simple separation of particles is not automatically a sign for polymer uptake, but can also be caused by high dilution of a surfactant

stabilised species. Also the particles in Figure 7-3b and c are not well taken up by the polymer. The formation of rings is a sign for loose interactions with the polymer, but for high interparticle interactions. As shown in Figure 7-3c, the particles align themselves, when a ferromagnetic Ni-grid is used. In picture 7-3d a good uptake into the polymeric micelles is demonstrated by usage of a  $PS_{710}\text{-}b\text{-}P2VP_{210}$  block copolymer. This solution was allowed to stir for 4 weeks. The picture is only an indication for the generally working uptake, because there are regions in the same sample, which are not that well extracted, but resemble the picture in Figure 7-3a.

In general, a shorter chain seems to increase the tendency of extraction. Also, when the core-block is decreased in degree of polymerisation, the micellar core should be that small, that only one particle is incorporated per micelle. Thus, polymers with very small 2VP block were taken for micellar uptake, too. The results of these experiments are shown in Figure 7-4.

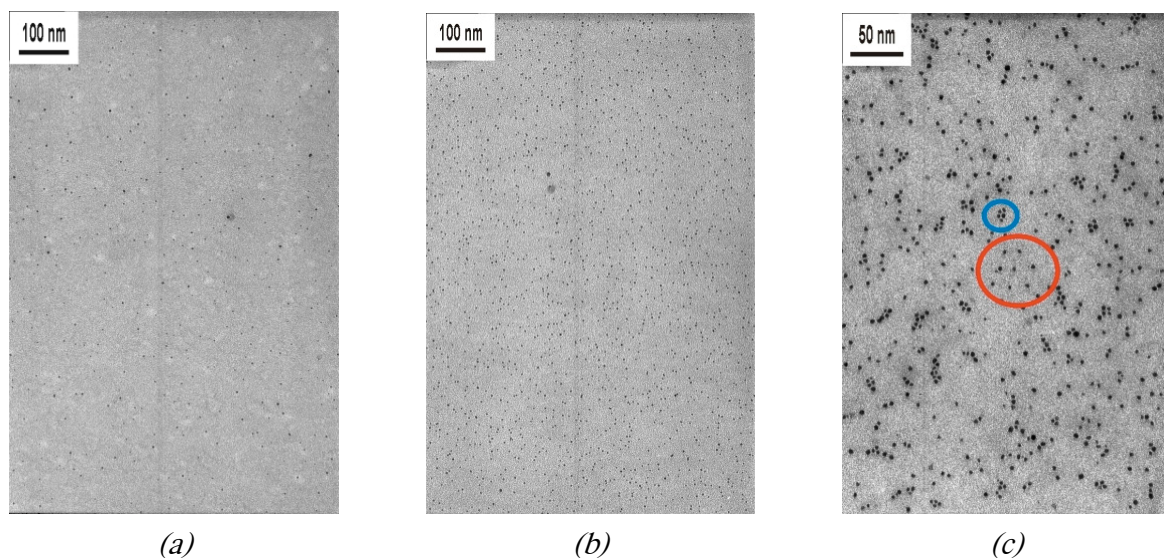


*Figure 7-4: Extraction of Co-solutions stabilised by AOT/OA into PS-*b*-P2VP block copolymer micelles with short 2VP-chain: (a)  $PS_{375}\text{-}b\text{-}P2VP_{25}$  (b)  $PS_{390}\text{-}b\text{-}P2VP_{15}$  (c)  $PS_{960}\text{-}b\text{-}P2VP_{11}$ . Here the blue circle shows an array, where the surfactant structure is displayed and the red circle shows a hexagon typical for block copolymer micelles in solution.*

From the pictures in Figure 7-4 it can be seen, that the smallest 2VP-block still carries some particles, which are surrounded by the surfactant. This is marked with a blue circle around. But separation of the particles already took place (red circle). Still a mixture of both species is present. For the polymers with the bigger 2VP-block, the separation is already so ad-



vanced, that no densely packed particles are seen in the whole sample. We found out in our experiment, that the application of temperature does not effect much the extraction process in the case of the short 2VP-chain polymers. However an increase of polymer concentration led to separation of the particles. This is evident from the fact, that we worked with highly concentrated solutions of Co-particles and the amount of particles has to be reduced by dilution, so that each particle is surrounded by one micelle.

Another possibility of change in the particle surface was performed by silane-modification of the particle surfaces. While performing the modification, we observed precipitation of the particles. One hour after finishing the reaction, the complete Cobalt was precipitated from the solution and the above liquid of the sample was clear. TEM samples could be made during the experiment, because the precipitation took 1 hour. The comparison before and after  $\text{SiH}_4$  treatment is given in Figure 7-5.

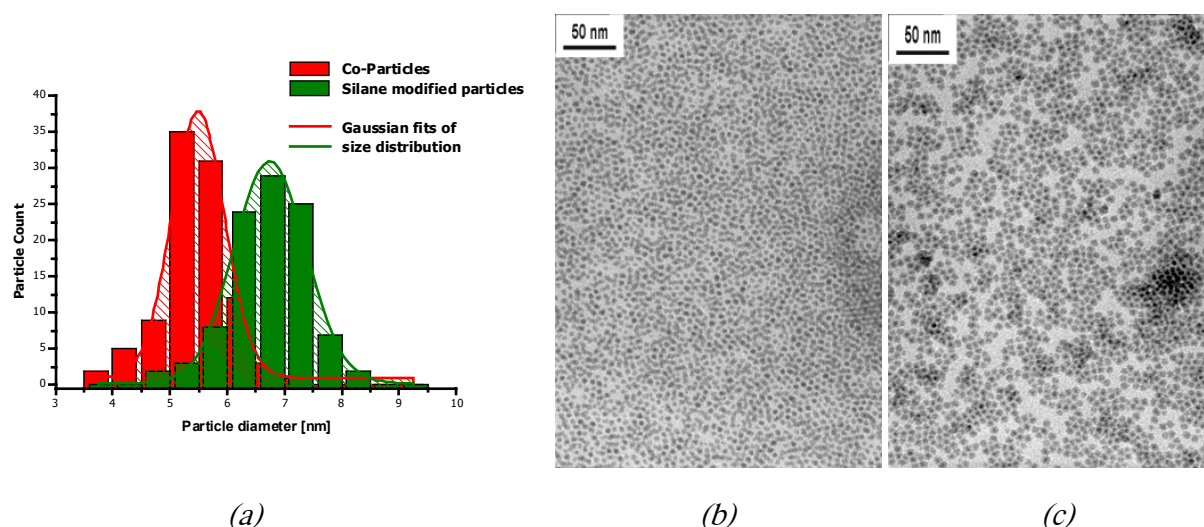


Figure 7-5: Treatment of Co-particles protected with AOT/OA with  $\text{SiH}_4$ . (a) Comparison of particle diameter distributions; (b) TEM-image of the particle solution before treatment; (c) TEM-image of the silanised sample after 30 minutes.

The comparison of particle size distributions in Figure 7-5 shows, that the particle diameter increases from 5.5 nm to 6.8 nm with a slight increase in standard deviation. This means, that the surface of the particles is covered with a layer of approx. 0.65 nm of silane-modification. The silane seems to bind very strongly to the surface of the particles. As a consequence, the dispersion of particles is destabilised and a 3-dimensional network of individual particles starts to form. The starting point of aggregation can be seen on Figure 7-5c, where the dark area represents a multilayer of Co-particles. The silane-modified particle aggregates could not be redispersed again in solvent or by addition of oleic acid. Thus, the



particles are preserved in the aggregates, but can not be used for further metal deposition. XPS measurements on the particles showed the presence of  $\text{SiO}_2$  in the solutions.

Because of the disappointing results for all experiments, we carried out with gold, we considered to find a different metal for bimetallic particle preparation. The system Cobalt-gold is very hard to control, because the both metals are immiscible. In most publication, the formation of a closed gold layer is not found, but island formation occurs, which is typical for binary systems with miscibility gaps [16-18]. Recently, some advances in coating of iron with gold were found [19]. Cobalt could be performed using perchlorate reduction with partial conversion of  $\text{Co}(0)$  to  $\text{Co}(\text{II})$  [20].

We turned our focus to the system Cobalt-Platinum. It is known, that the both metals are compatible with each other. There are two stable intermetallic phases  $\text{CoPt}$  and  $\text{CoPt}_3$ . The latter phase is known to be strongly ferromagnetic. Platinum was used recently for successful alloying or combination in the nanoscale with Fe [21, 22], iron oxide [23] and  $\text{Co}$  [24, 25] and  $\text{Fe/Co}$  [26].

In a first experiment, we tried the coating of Cobalt nanoparticles, which are only adsorbed on the surface. For this purpose, we took the particles, generated in  $\text{PBd}_{550}\text{-b-PMAA}_{100}$ . Here we stated, that there is one sort of particles, which was just slightly bond to the surface of the polymer. Those particles were building rings and coexisted together with smaller particles (see Chapter 6). We were searching for a thermally unstable compound comparable with  $\text{Co}_2(\text{CO})_8$ . We found out  $\text{Pt}[(\text{COD})_2\text{Me}_2]$  to be a suitable precursor compound for our experiments. In preliminary experiments we observed, that  $\text{Pt}[(\text{COD})_2\text{Me}_2]$  decomposes at temperatures above  $130^\circ\text{C}$ . Thus, this precursor compound was added to a solution of  $\text{PBd}_{550}\text{-b-PMAA}_{100}$  containing nanoparticles and it was heated to  $170^\circ\text{C}$ . The results are shown in Figure 7-6.

The experiment showed remarkable results. In Figure 7-6, the presence of fringes on the particles show the presence of crystalline platinum. The fringes can clearly be seen and are not distorted over the complete particle. A look on the string in Figure 7-6b shows, that the formerly separate particles are now covered by a shade of high contrast, which can be ascribed to platinum deposition. In Figure 7-6c, the presence of many square faceted particles is visible. This is very typical for Pt-metal faceted in the  $\{100\}$ -plane. Thus, if the platinum is decomposed in the presence of weakly interacting Co-particles, the coverage of the particles with a continuous film is possible and can be reproduced.

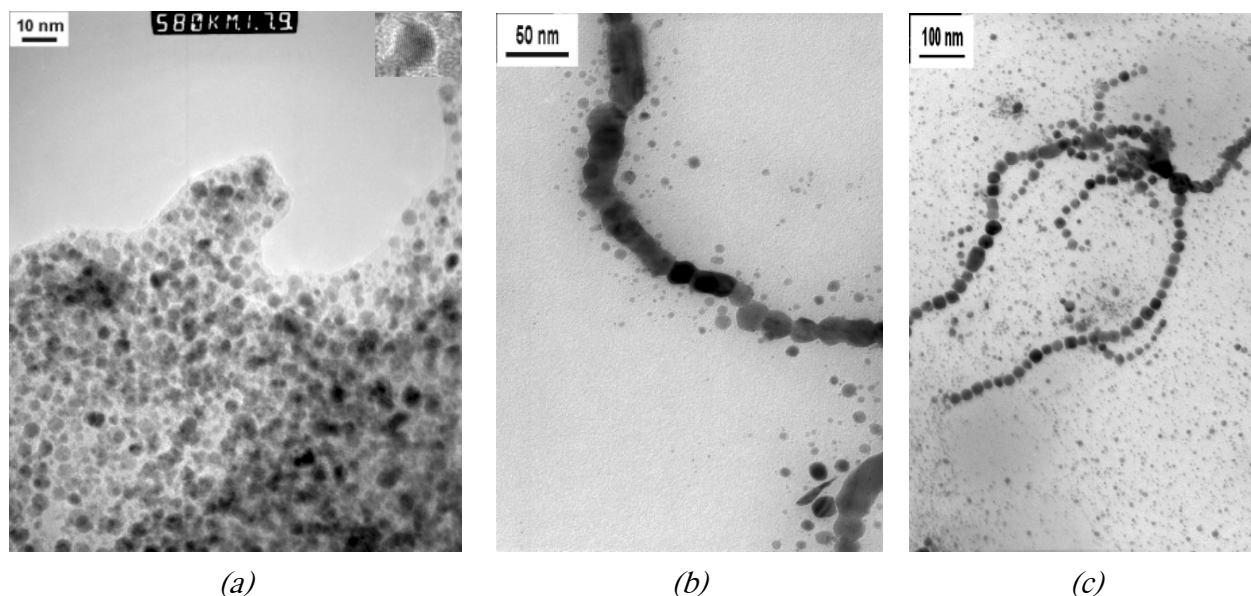
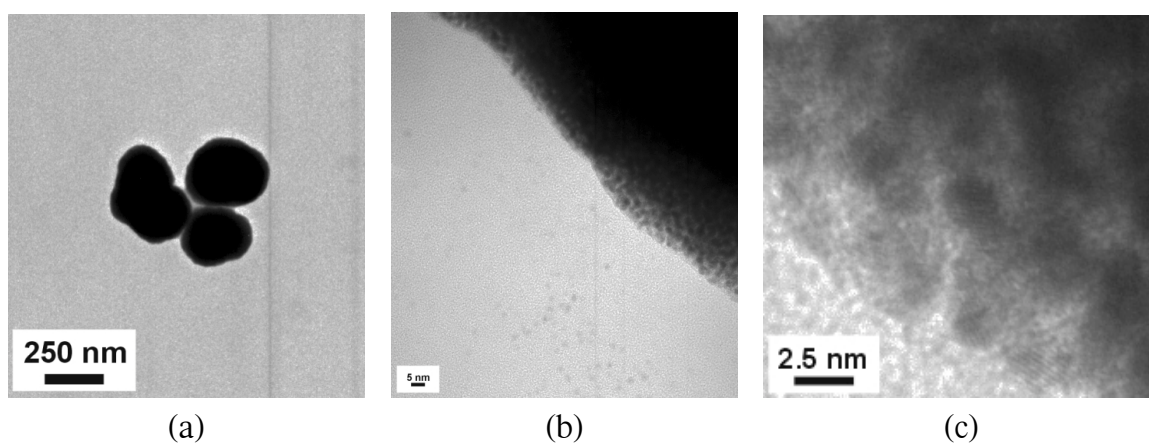


Figure 7-6: Deposition of Platinum on Co-nanoparticle rings in  $PBd_{550}$ - $b$ - $PMAA_{100}$ . The platinum was decomposed from  $Pt[(COD)_2Me_2]$  at 170 °C. (a) HRTEM image of an array of particles, the inset on the right side shows the fringe pattern of the particles. (b) and (c) Coating on ring and string shaped Co-particle arrays. The darker contrast shows the presence of Pt on the particle surface.

With this knowledge in mind, we tried the decomposition of  $Pt[(COD)_2Me_2]$  in the presence of TDS and TOPO to check the decomposition as method for generation of Pt-nanoparticles. The thermal decompositions were carried out under the same conditions like in the case of the cobalt compound, but the samples were not degassed and heated in small screw-cap vessels with rubber sealing. The analogous experiments for  $Co_2(CO)_8$  are described in Chapter 4.

The Pt-compound in Mesitylene/TDS solution is slightly pinkish. The colour of the solution is caused by the Platinum-compound. During the heating process, which was carried out within 5 minutes, a change of the colour of the solution was registered right after starting the heating process. The solution turned black within seconds and a precipitate occurred. Like in the case of the Co-samples, precipitation takes place in all of the samples. At 215 °C, the thermal treatment leads to a metallisation of the glass surface of the vessel. Investigation of the black liquid in the TEM showed substrates with bigger particles without any order. Further investigation of the samples in HR-TEM showed, that these “particles” were arrays consisting of small, ordered particles.

These arrays could not be resolved by means of standard TEM. Regarding the samples in HR-TEM, the edges of the bigger arrays could be resolved. The size of the nanoparticles was approx. 2.2-2.5 nm. The packed particles consist of multilayers of such particles. However, on the edges of the arrays, single Pt-nanoparticles were recognised. A statistical analysis of these particles seemed not to be useful regarding the low amount of particles, which can be distinguished from each other. Particles beyond the arrays are present in a minimal amount, almost all of the platinum is concentrated in these arrays. Figure 7-7a shows a cluster of these arrays, Figure 7-7b gives a detailed view on a sample performed at 170 °C.



*Figure 7-7: (a) Arrays of Pt-Nanoparticles from  $\text{Pt}[(\text{COD})_2\text{Me}_2]$  produced at 170 °C in presence of TDS; (b) Focus on the edge of one of the arrays from (a) showing a small amount of not arranged particles around; (c) Particles from the array in (b) at high magnification. The particle shows single-crystalline fringes, the particle size is 2.2-2.5 nm.*

The experiments at 180 °C and at 200 °C showed identical results. The particles within these arrays are of remarkably same size, no influence on temperature is visible. Pictures like in Figure 7-7 can be taken from all the mentioned solutions. The solution obtained at 215 °C did not show the presence of any particles on the grid, neither on the sample for TEM nor on the sample for HR-TEM. This suggests, that at this temperature all Pt has precipitated or built a bulk film on the glass vessel as mentioned above.

The equivalent experiments to the ones described above were carried out, using TOPO instead of TDS. The results in these experiments are very similar to those presented for the TDS-solutions. Again, the particles do form arrays consisting of small particles. The packing of these particles seemed to be more loose. Occurrence of small regions with monolayers of the particles are visible. The particle size was slightly higher than in the experiments in TDS with roughly 3 nm. Additionally, the particles in these experiments seem to be a bit broader

distributed in size. Again, the size of the particles and their arrangement are not affected by the decomposition temperature. An exception was again the experiment carried out at 215 °C. The structure of the particles again broke down, the solution was colourless and a bulk Pt-film on the glass vessel occurred. Figure 7-8 shows representative pictures of the solutions.

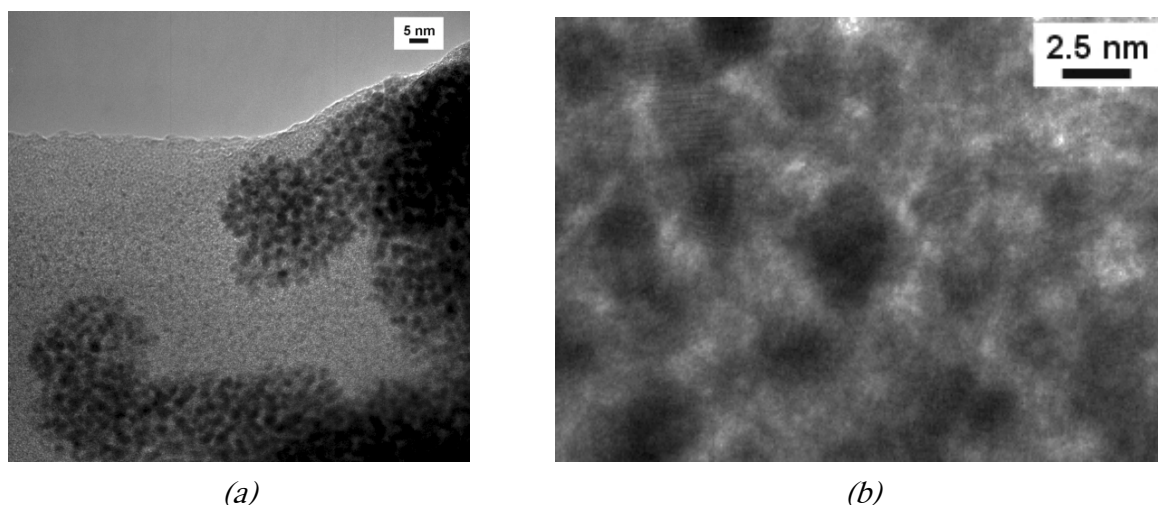


*Figure 7-8: Arrays of Pt-Nanoparticles from  $\text{Pt}[(\text{COD})_2\text{Me}_2]$  produced at 180 °C in presence of TOPO; (a) is an overview, (b) shows some individual particles, which have non-interrupted fringes, indicating monocrystallinity; the particle size is 3 nm.*

Decomposition experiments of  $\text{Pt}[(\text{COD})_2\text{Me}_2]$  in TDS and TOPO were a suitable method for reproducible synthesis of Pt-nanoparticles. The method is easy and quick to perform and has not to be carried out under inert gas. At different temperatures between 170 °C and 200 °C, a change in particle size and distribution was not observed. Experiments made at 215 °C led to lose of control over particle formation and a metallic film was generated instead. Particles made in TOPO are bigger, but broader distributed in size than the particles in TDS. The precipitate produced in the experiments contains well-ordered and narrowly distributed particles. The precipitates could be redispersed by addition of a bigger amounts of surfactant and heating to 80 °C.

Unfortunately, the experiments with a mixture of both metal precursors in order to form alloys and experiments, with an additional coating of Pt by adding  $\text{Pt}[(\text{COD})_2\text{Me}_2]$  to a Co-particle solution did not lead to the expected bimetallic particles. Instead, the presence of pure Co and the presence of pure Pt-nanoparticles coexisting with each other were observed in the following experiments. In the case of alloy formation, a ratio of  $\text{Pt}:\text{Co} = 3:1$

was chosen already in the stage of the precursor. HRTEM results show again the formation of very small aggregates with monocrystalline Pt-particles and bigger particles of Co. Interestingly, when we made the Pt-particle formation in the presence of Co-particles, the Pt-particles were often arranged in the shape of hollow rods consisting again of many monocrystalline particles. We didn't understand that ordering of particles, but we will show two pictures as a final snapshot in this thesis in Figure 7-9.

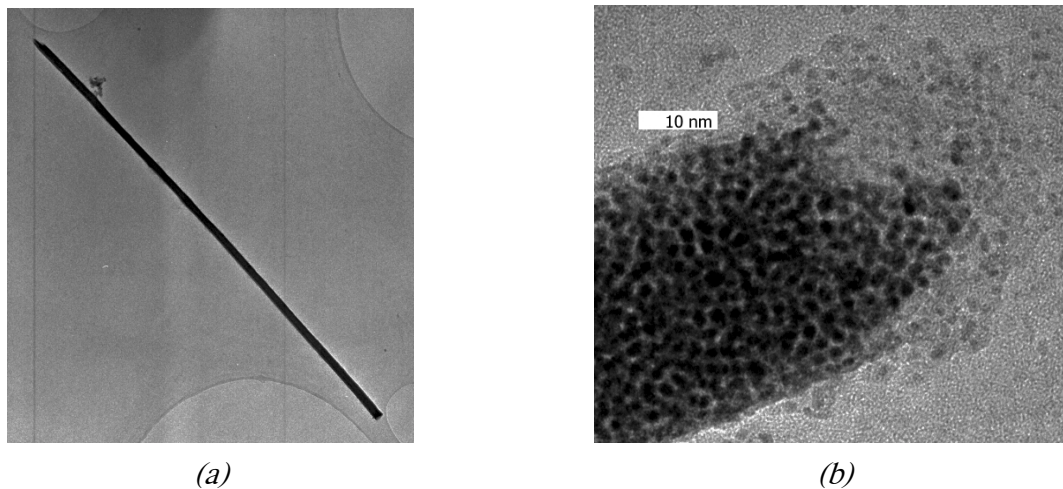


Figure 7-9: Hollow rods consisting of small, monocrystalline Pt-particles from experiments, where  $\text{Pt}[(\text{COD})_2\text{Me}_2]$  was decomposed in the presence of  $\text{Co}_2(\text{CO})_8$  in a solution containing AOT/OA. (a) shows the dimension of the rod (around  $1\text{-}2\mu\text{m}$ ), (b) shows the onset of the rod, which consists out of Pt-particles

## 7.4 Conclusion

In this chapter, we described the attempt of manipulation of the particle surface and some tries to gain bimetallic particles by our synthetic methods. The main problem we encountered was a very strong interaction of the particle surface to the stabilising agent. Redispersion and extraction of surfactant stabilised Co-particles do work. The redispersion by means of addition of a low molecular surfactant can be performed as universal method for particle redispersion. The extraction into PS-*b*-P2VP block copolymer micelles is a long and hard to control process. But an exchange between surfactant and polymeric environment is

possible to perform.

Modification by  $\text{SiH}_4$  on surfactant stabilised Co-particles is working, but leads to an increase of aggregation of the particles. The silane interacts with the  $\text{CoO}$  and  $\text{Co}_3\text{O}_4$  surface layer and forms a sticking surface layer.

Experiments leading to bimetallic particles were very poor in result. Direct coating of the Co leads either to oxidation of the Co-metal or to formation of coexisting particles of both sorts. This is true for Ag, Au and Pt. In the case of Pt, we developed a novel, easy synthetic method for surfactant-protected Pt-nanocrystals. The small size of the particles could lead to easy to handle nanoscaled catalyst-solutions.

We could finally show, that in general, the deposition of Pt onto Co-nanoparticles does work, if the particles are not too strongly interacting with the protective agent. In the case of Co-particles from a  $\text{PBd-}b\text{-PMAA}$  solution, the loose bound cobalt structures were covered with Pt. This was evident from the still present magnetic dipolar interactions between the cobalt particles and the cubic high-contrast Pt-cover layer.

## 7.5 References

- [1] C. Abdelghani-Jacquín, M. Dichtl, L. Jakobsmeier, W. Hiller, E. Sackmann, *Langmuir*, **2001**, *17*, 2129.
- [2] D.I. Gittins, F. Caruso, *Angew. Chem.* **2001**, *113*, 3089.
- [3] M. Schierhorn, L.M. Liz-Marzán, *Nano Lett.* **2002**, *2*, 13.
- [4] C. Damle, K. Biswas, M. Sastry, *Langmuir*, **2001**, *17*, 7156.
- [5] M. Giersig, T. Ung, L.M. Marzán, P. Mulvaney, *Adv. Mater.* **1997**, *9*, 570.
- [6] S. Ramesh, R. Prozorov, A. Gedanken, *Chem. Mater.* **1997**, *9*, 2996.
- [7] F. Caruso, A.S. Susa, M. Giersig, H. Möhwald, *Adv. Mater.* **1999**, *11*, 950.



- 
- [8] F. Caruso, M. Spasova, A. Susa, M. Giersig, R.A. Caruso, *Chem. Mater.* **2001**, *13*, 109.
- [9] A. Warshawsky, D.A. Upson, *J. Polymer Sci. A – Polymer Chem.* **1989**, *27*, 2963.
- [10] F.G. Aliev, M.A. Correa-Duarte, A. Mamedov, J.W. Ostrander, M. Giersig, L.M. Liz-Marzán, N.A. Kotov, *Adv. Mater.* **1999**, *11*, 1006.
- [11] R.D. Shull, L.H. Bennett, *Nanostruct. Mater.* **1992**, *1*, 83.
- [12] N. Toshima, *J. Macromol. Sci.-Chem.* **1990**, *A27*, 1225.
- [13] P.M. Paulus, H. Bönnemann, A.M. van der Kraan, F. Luis, J. Sinzig, L.J. de Jongh, *Eur. Phys. J. D*, **1999**, *9*, 501.
- [14] T. Shibata, B.A. Bunker, Z. Zhang, D. Meisel, C.F. Vardeman II, J.D. Gezelter, *J. Am. Chem. Soc.* **2002**, *124*, 11989.
- [15] B. Cord, M. Geisler, E. Koparal, O. Keitel, J. Scherer, *Datatech Magazine Vol.2*, 97; available online at <http://www.semiconductorsfabtech.com>.
- [16] K. Temst, M.J. van Bael, V.V. Moshchalkov, Y. Bruynseraede, *J. Appl. Phys.* **2000**, *87*, 4216.
- [17] R. Sellmann, H. Fritzsche, H. Maletta, *Surf. Sci.* **2001**, *495*, 185.
- [18] D. Kahn, *AMP J. Technol.* **1991**, *1*, 43.
- [19] W.L. Zhou, E.E. Carpenter, J. Lin, A. Kumbhar, J. Sims, C.J. O'Connor, *Eur. Phys. J. D*, **2001**, *16*, 289.
- [20] N.S. Sobal, M. Hilgendorff, H. Möhwald, M. Giersig, M. Spasova, T. Radetic, M. Farle, *Nano Lett.* **2002**, *2*, 621.
- [21] S. Sun, C.B. Murray, D. Weller, L. Folks, A. Moser, *Science*, **2000**, *287*, 1989.
- [22] B. Stahl, N.S. Gajbhiye, G. Wilde, D. Kramer, J. Ellrich, M. Ghafari, H. Hahn, H. Gleiter, J. Weißmüller, R. Würschum, P. Schlossmacher, *Adv. Mater.* **2002**, *14*, 25.
- [23] X. Teng, D. Black, N.J. Watkins, Y. Gao, H. Yang, *Nano Lett.* **2003**, *3*, 261.

- [24] A.C.C. Yu, M. Mizuno, Y. Sasaki, H. Kondo, K. Hiraga, *Appl. Phys. Lett.* **2002**, *51*, 3768.
- [25] E.V. Shevchenko, D.V. Talapin, A.L. Rogach, A. Kornowski, M. Haase, H. Weller, *J. Am. Chem. Soc.* **2002**, *124*, 11480.
- [26] M. Chen, D.E. Nikles, *Nano Lett.* **2002**, *2*, 211.



## *Appendix Chapter 7*

---

### *Stoichiometric calculations on core-shell-type particles*

#### **A7.1    Oxide shell around particles**

In order to be able to determine the amount of oxygen, which is able to oxidise nanoparticles, a calculation has to be made. In this work, the goal to produce oxidation sensitive cobalt nanoparticles, makes it necessary to have a knowledge about the order of magnitude of the perturbation, which is caused by the presence of oxygen during the overall preparation.

To start the calculation, we have to define the present compounds:

$M$	is the metal, we want to synthesise
$M_xO_y$	is the formula of the oxide, which the metal is forming in the presence of oxygen
$M_iR$	is the compound, which is used as precursor for the metal formation,

For better understanding, Figure A7-1 sketches the described situations and shows some of the used values and indices.

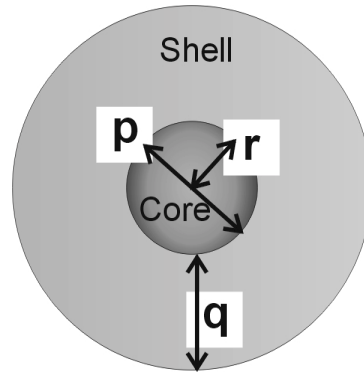


Figure A7-1: Sketch of a core-shell-type particle with some variables and indices used in the calculation

We start the calculation by asking for the unknown size. In this case, the oxidation as side-effect of the main reaction makes it most convenient to have knowledge about the volume of oxygen  $V_{oxy}$ , which is needed to make a shell of metal oxide around the particle of diameter  $p$ . This we like to know for a given aliquot of nanoparticles solution. For the complete reaction mixture, the needed volume of oxygen is the product of the needed amount of oxygen per particle and the number of particles inside of the reaction mixture.

$$V_{Oxy} = N_{Particles} \cdot V_{OxPart} \quad (\text{Eq. A7-1}),$$

with the number of particles being the quotient between total mass of the metal  $m_{total}$  and the mass of a single particle  $m_{Part}$ .

$$V_{Oxy} = V_{OxPart} \cdot \frac{m_{total}}{m_{Part}} = V_{OxPart} \cdot \frac{m_{total}}{m_{MetCore} + m_{MetShell}} =$$

$$V_{Oxy} = V_{OxPart} \cdot \frac{m_{total}}{m_{MetCore} + n_{MetShell} \cdot M_{Met}} \quad (\text{Eq. A7-2}),$$

where the mass of the particle is split into the part of the metal core and the metal in the oxide shell layer. The latter can be written as product of its molecular weight and the moles. Considering, that the metal  $M$  forms an oxide  $M_xO_y$ , the moles of the metal correspond to the  $x^{th}$  part of the moles of the metal oxide:

$$V_{Oxy} = V_{OxPart} \cdot \frac{m_{total}}{m_{MetCore} + x \cdot n_{Oxide} \cdot M_{Met}} \quad (\text{Eq. A7-3}).$$

Substituting the moles of the oxide by the mass and considering, that the mass is the product of the density and the volume of the oxide, one gets from Eq. A7-3:

$$\begin{aligned}
 V_{Oxy} &= \frac{V_{OxPart} \cdot m_{total}}{m_{MetCore} + x \cdot M_{Met} \cdot \frac{m_{Oxide}}{M_{Oxide}}} = \frac{V_{OxPart} \cdot m_{total}}{m_{MetCore} + \frac{m_{Oxide} \cdot M_{Met} \cdot x}{M_{Oxide}}} = \\
 &= \frac{V_{OxPart} \cdot m_{total}}{m_{MetCore} + \frac{x \cdot M_{Met} \cdot \rho_{Oxide} \cdot V_{Oxide}}{M_{Oxide}}} \quad (\text{Eq. A7-4}).
 \end{aligned}$$

The volume of the oxide shell depends on the desired particles. For giving a general value, we can set the particle diameter to a value  $p$  and the thickness of the oxide layer to a value  $q$  (see Figure A7-1). Taking  $r=p/2$  as the radius of the particle, the volume of the oxide shell can be written as:

$$V_{Oxide} = \frac{4}{3} \cdot \pi \cdot [(r+q)^3 - r^3] \quad (\text{Eq. A7-5})$$

Inserting Eq. A7-5 in Eq. A7-4 gives

$$V_{Oxy} = \frac{V_{OxPart} \cdot m_{total}}{m_{MetCore} + \frac{4 \cdot \pi \cdot x \cdot \rho_{Oxide} \cdot M_{Met}}{3 \cdot M_{Oxide}} \cdot [(r+q)^3 - r^3]} \quad (\text{Eq. A7-6}).$$

Substituting for the mass of the metal core

$$m_{MetCore} = \rho_{Met} \cdot V_{Core} = \frac{4}{3} \cdot \pi \cdot \rho_{Met} \cdot r^3 \quad (\text{Eq. A7-7})$$

the product of density and volume leads to:

$$\begin{aligned}
 V_{Oxy} &= \frac{V_{OxPart} \cdot m_{total}}{\frac{4}{3} \cdot \pi \cdot \rho_{Met} \cdot r^3 + \frac{4 \cdot \pi \cdot x \cdot \rho_{Oxide} \cdot M_{Met}}{3 \cdot M_{Oxide}} \cdot [(r+q)^3 - r^3]} = \\
 &= \frac{V_{OxPart} \cdot m_{total}}{\frac{4}{3} \cdot \pi \cdot r^3 \cdot \left[ \rho_{Met} + \frac{\rho_{Oxide} \cdot x}{M_{Oxide}} \cdot \left[ \frac{(r+q)^3}{r^3} - 1 \right] \right]} \quad (\text{Eq. A7-8})
 \end{aligned}$$

The total mass of the metal  $m_{total}$  can be expressed by its moles and molecular weight:

$$m_{total} = n_{total} \cdot M_{Met} \quad (\text{Eq. A7-9})$$

The reaction to produce the metal particles is based on the conversion of a precursor component  $M_zR$  containing the metal and a rest. Thus, the total moles of the used metal can be also expressed by taking the initial weight of the precursor taken to perform the reaction:

$$m_{total} = z \cdot n_{Prec} \cdot M_{Met} = \frac{z \cdot m_{Prec} \cdot M_{Met}}{M_{Prec}} \quad (\text{Eq. A7-10}).$$

This gives for  $V_{Oxy}$ :

$$V_{Oxy} = \frac{V_{OxPart} \cdot \frac{z \cdot m_{Prec} \cdot M_{Met}}{M_{Prec}}}{\frac{4}{3} \cdot \pi \cdot r^3 \cdot \left[ \rho_{Met} + \frac{\rho_{Oxide} \cdot x}{M_{Oxide}} \cdot \left[ \frac{(r+q)^3}{r^3} - 1 \right] \right]} \quad (\text{Eq. A7-11}).$$

For gases, the volume can be calculated by the product of the moles with the molar volume.

Thus, the volume of oxygen per particle,  $V_{OxPart}$  can be calculated by:

$$V_{OxPart} = n_{O_2} \cdot V_M = \frac{1}{2} \cdot n_O \cdot V_M \quad (\text{Eq. A7-12})$$

In a metal oxide containing  $y$  oxygen atoms, the  $y$ -fold amount of moles of the oxide is present:

$$V_{OxPart} = \frac{y}{2} \cdot n_{Oxide} \cdot V_M = \frac{y \cdot m_{Oxide} \cdot V_M}{2 \cdot M_{Oxide}} \quad (\text{Eq. A7-13}).$$

Inserting this in Eq. A7-11 yields:

$$V_{Oxy} = \frac{\frac{y \cdot m_{Oxide} \cdot V_M}{2 \cdot M_{Oxide}} \cdot \frac{z \cdot m_{Prec} \cdot M_{Met}}{M_{Prec}}}{\frac{4}{3} \cdot \pi \cdot r^3 \cdot \left[ \rho_{Met} + \frac{\rho_{Oxide} \cdot x}{M_{Oxide}} \cdot \left[ \frac{(r+q)^3}{r^3} - 1 \right] \right]} \quad (\text{Eq. A7-14})$$

or

$$V_{Oxy} = \frac{3 \cdot y \cdot z \cdot m_{Oxide} \cdot V_M \cdot m_{Prec} \cdot M_{Met}}{8 \cdot \pi \cdot r^3 \cdot M_{Prec} \cdot \left[ \rho_{Met} \cdot M_{Oxide} + \rho_{Oxide} \cdot x \cdot \left[ \frac{(r+q)^3}{r^3} - 1 \right] \right]} \quad (\text{Eq. A7-15})$$

The mass of the oxide per particle can be written as the product of volume and density and following Eq. A7-5 yields:

$$V_{Oxy} = \frac{3 \cdot y \cdot z \cdot V_M \cdot m_{Prec} \cdot M_{Met} \cdot \rho_{Oxide} \cdot \frac{4}{3} \cdot \pi \cdot [(r+q)^3 - r^3]}{8 \cdot \pi \cdot r^3 \cdot M_{Prec} \cdot \left[ \rho_{Met} \cdot M_{Oxide} + \rho_{Oxide} \cdot x \cdot \left[ \frac{(r+q)^3}{r^3} - 1 \right] \right]} \quad (\text{Eq. A7-16})$$

$$V_{Oxy} = \frac{y \cdot z \cdot V_M \cdot m_{Prec} \cdot M_{Met} \cdot \rho_{Oxide} \cdot [(r+q)^3 - r^3]}{2 \cdot r^3 \cdot M_{Prec} \cdot \left[ \rho_{Met} \cdot M_{Oxide} + \rho_{Oxide} \cdot x \cdot \left[ \frac{(r+q)^3}{r^3} - 1 \right] \right]} \quad (\text{Eq. A7-17})$$

$$V_{Oxy} = \frac{y \cdot z \cdot V_M \cdot m_{Prec} \cdot M_{Met} \cdot \rho_{Oxide} \cdot \left[ \frac{(r+q)^3}{r^3} - 1 \right]}{2 \cdot M_{Prec} \cdot \left[ \rho_{Met} \cdot M_{Oxide} + \rho_{Oxide} \cdot x \cdot \left[ \frac{(r+q)^3}{r^3} - 1 \right] \right]} \quad (\text{Eq. A7-18})$$

From

$$K_1 = \frac{y \cdot z \cdot V_M \cdot m_{Prec} \cdot M_{Met} \cdot \rho_{Oxide}}{2 \cdot M_{Prec} \cdot \rho_{Met} \cdot M_{Oxide}} \text{ and } K_2 = \frac{\rho_{Oxide} \cdot x}{\rho_{Met} \cdot M_{Oxide}} \text{ results:}$$

$$V_{Oxy} = \frac{K_1 \cdot \left[ \frac{(r+q)^3}{r^3} - 1 \right]}{1 + K_2 \cdot \left[ \frac{(r+q)^3}{r^3} - 1 \right]} \quad (\text{Eq. A7-19}).$$

Eq. A7-18 and A7-19 can be called in this context the core-shell oxidation equation (CSO-equation). While from Eq. A7-18, the direct calculation of the oxidation sensitivity can be calculated, the form in Eq. A7-19 shows the dependence of the needed volume of oxygen for a certain particle size. Generally, with constant oxide layer, it takes less oxygen to coat the complete surface of the particles with an oxygen layer. This is reasonable, since the surface-to-volume-ratio decreases with increasing particle size. Another benefit from this equation is the general validity for layers made with gaseous reaction partners<sup>5</sup>. Limits are set by the considerations of using spherical particles. The densities of the compound could

<sup>5</sup> The factor 2 in Eq. A7-18 is only necessary for diatomic gases. It change to 1 for gases like e.g. noble gases.

differ slightly in the nano-regime due to a more pronounced influence of the lattice structure of the metal, if the bulk values are chosen for calculation.

## A7.2 Calculation for the amount of the shell compound

To be able to run an experiment for coating of an existing particle, it is necessary to know, how much of precursor component of the shell-building metal is needed to form a defined, closed layer around the particle. Like in the last section, the consideration is the same like depicted in Figure A7-1. Again, the Volume of the shell plays an important role. The mass of metal to form a shell of thickness  $q$  is:

$$m_{Shell} = \rho_{Shell} \cdot V_{Shell} = \rho_{Shell} \cdot \frac{4}{3} \cdot \pi \cdot [(r + q)^3 - r^3] \quad (\text{Eq. A7-20})$$

or

$$n_{Shell} = \frac{4 \cdot \pi \cdot \rho_{Shell}}{3 \cdot M_{Shell}} \cdot [(r + q)^3 - r^3] \quad (\text{Eq. A7-21}).$$

Starting from a precursor  $M_xR$ , with  $n_{Shell} = 2n_{Prec}$ , the mass of used precursor has to be:

$$m_{Prec} = \frac{4 \cdot \pi \cdot x \cdot \rho_{Shell} \cdot M_{Prec}}{3 \cdot M_{Shell}} \cdot [(r + q)^3 - r^3] \quad (\text{Eq. A7-22}).$$

Substitution of the constant by

$$K = \frac{4 \cdot \pi \cdot x \cdot \rho_{Shell} \cdot M_{Prec}}{3 \cdot M_{Shell}} \quad (\text{Eq A7-23})$$

yields

$$\frac{m_{Prec}}{K} = [(r + q)^3 - r^3] \quad (\text{Eq. A7-24})$$

or

$$\frac{m_{Prec}}{K} + r^3 = (r + q)^3 \quad (\text{Eq. A7-25})$$

Taking the cubic root gives:

$$r + q = \sqrt[3]{\frac{m_{Prec}}{K} + r^3}$$

$$q = \sqrt[3]{\frac{m_{Prec}}{K} + r^3} - r \quad (\text{Eq A7-26})$$

Resubstitution of K leads to

$$q = \sqrt[3]{\frac{3 \cdot M_{Shell} \cdot m_{Prec}}{4 \cdot \pi \cdot x \cdot \rho_{Shell}} + r^3} - r \quad (\text{Eq. A7-27})$$

Eq. A7-26 and A7-27 are expressions for the growth of a single particle by addition of a certain mass of precursor to one core particle of  $2r$  diameter. The calculation has now to be extended to an array of particles inside of a reaction solution. The amount of core particles in the solution is:

$$N_{core} = \frac{m_{total}}{m_{core}} = \frac{m_{total}}{\rho_{core} \cdot V_{Core}} = \frac{n_{total} \cdot M_{core}}{\rho_{core} \cdot V_{Core}} \quad (\text{Eq. A7-28}).$$

Using a precursor  $M_zR$  for the core-particles and replacing by the volume of the core particles, this leads to

$$N_{core} = \frac{M_{core} \cdot z \cdot m_{coreprec}}{\rho_{core} \cdot M_{coreprec} \cdot \frac{4}{3} \cdot \pi \cdot r^3} = \frac{3 \cdot M_{core} \cdot z \cdot m_{coreprec}}{4 \cdot \rho_{core} \cdot M_{coreprec} \cdot \pi \cdot r^3} \quad (\text{Eq. A7-29})$$

The total mass of precursor needed is the mass of precursor by particle (Eq. A7-22) multiplied by the number of particles in the solution (Eq. A7-29):

$$m_{total} = N_{core} \cdot m_{Prec} = \frac{3 \cdot M_{core} \cdot z \cdot m_{coreprec}}{4 \cdot \rho_{core} \cdot M_{coreprec} \cdot \pi \cdot r^3} \cdot \frac{4 \cdot \pi \cdot x \cdot \rho_{Shell} \cdot M_{Prec}}{3 \cdot M_{Shell}} \cdot [(r + q)^3 - r^3]$$

and results in

$$m_{total} = \frac{x \cdot z \cdot M_{core} \cdot m_{coreprec} \cdot \rho_{Shell} \cdot M_{Prec}}{\rho_{core} \cdot M_{coreprec} \cdot M_{Shell}} \cdot \frac{1}{r^3} \cdot [(r + q)^3 - r^3] \quad (\text{Eq. A7-30}).$$

Defining  $K_{CS}$  as  $\frac{x \cdot z \cdot M_{core} \cdot m_{coreprec} \cdot \rho_{Shell} \cdot M_{Prec}}{\rho_{core} \cdot M_{coreprec} \cdot M_{Shell}}$ , it can be written as:

$$m_{total} = \frac{K_{CS}}{r^3} \cdot [(r+q)^3 - r^3] \quad (\text{Eq. A7-31}), \text{ which is}$$

$$\begin{aligned} \frac{m_{total} \cdot r^3}{K_{CS}} + r^3 &= (r+q)^3 \\ \left( \frac{m_{total}}{K_{CS}} + 1 \right) \cdot r^3 &= (r+q)^3 \\ r \cdot \sqrt[3]{\frac{m_{total}}{K_{CS}} + 1} &= r+q \end{aligned}$$

This yields an overall equation for q:

$$q = r \cdot \left( \sqrt[3]{\frac{m_{total}}{K_{CS}} + 1} - 1 \right) \quad (\text{Eq. A7-32}).$$

This equation can be called the core-shell concentration-equation (CSC-equation). For stoichiometric calculations, the form in Eq. A7-30 is better to use. Eq. A7-32, however, can help to find out, which size-increase can be maximally yielded, when a certain mass of precursor of the second metal is added. Eq. A7-32 can be again expanded by resubstitution:

$$q = r \cdot \left( \sqrt[3]{\frac{m_{total} \cdot \rho_{core} \cdot M_{coreprec} \cdot M_{Shell}}{x \cdot z \cdot M_{core} \cdot m_{coreprec} \cdot \rho_{Shell} \cdot M_{Prec}} + 1} - 1 \right) \quad (\text{Eq. A7-33})$$



## ***Chapter 8***

---

### ***Summary***

In this thesis, the aim was the defined synthesis of Cobalt-nanoparticles by help of nanoscaled, structuring stabilisers. This goal was reached using two different kinds of nanotemplate. In the first part of the present work, low-molecular surfactants were taken and special systems were optimised, until we could control size, order and dispersion of the particles. The structure of the generated particles was even kept in solid state, when a precipitate of the particles occurred.

First, we made the choice, which of the many surfactant systems could help us to reach our main goal. After several screening steps, we concentrated completely on sulfosuccinate systems like AOT/OA and TDS. Both systems turned out to be a compromise between stabilisation of particles and stabilisation of the dispersion. The synthesis in both systems could be performed systematically, that at the end, a screening of many parameters, important for the system, was performed and a desired type of particle solution could be done by realisation of the aim values. The limits of the synthesis were set to be between 4 and 12 nm. We paid a special tribute to the topic of particle oxidation. This issue is usually not mentioned too often in publications, because it is unwanted. Anyway, the reality showed us, that special precautions have to be taken, in order to reduce oxidation to a big extent. We could show, that the oxide layers on the particle surfaces is a mixture between CoO and Co<sub>3</sub>O<sub>4</sub>. If no special precaution is made, a layer of 1.8 nm of oxide is laid around the particles. For particles in the size regime of 5 nm, this is more than the half of the diameter.

With these results in mind, particle properties were understood in a better way. Magnetic properties of the particles resembled the bulk values, when care about oxidation was taken. As last consequence, we found a way of producing a long-time stable Co-powder, which was tested to be ferromagnetic at least for 1 year at ambient atmosphere. This is an aggregate, which is formed at temperatures between 170 °C and 180 °C containing TDS-protected Co-

nanoparticles, which can be redispersed from this powder even 1 year after synthesis, while the magnetic properties stay unchanged. This aggregate is present in a 3d- or 2-d structure, which can be induced by a permanent magnet while film formation. It could be shown, that HR-TGA is a method, which can benefit the quantification of the metal fraction within the Co-nanoparticle solutions.

The second part of this work was dealing with block copolymer micelles as structure and stability source. The mechanism of Co(II)-uptake into block copolymer micelles of the type PS-*b*-P2VP could be cleared. The Co(II)-salts were complexed with tetrahedral symmetry. The maximum loading of pure Co(II) salt was 0.25 due to coordinational considerations. The limit could be shifted towards higher loadings by addition of a low molecular helping ligand, which block coordination sites for the Co(II)-compound. A bigger loading is a key issue for control of particle size in the reductive use of the nanoreactor concept. As a second concept of regulation of the amount of Co(II) incorporated into the micelles was the usage of chelate complexes. In this case, the blocked coordination sites are already intrinsically defined and the amount of Co(II) in the micellar cores could be increased to a value of  $\approx 0.5$ .

Film formation of the Co(II)-loaded micelles could be enhanced by usage of a higher boiling solvent, mesitylene. Very regular patterns were produced by that method. Films, which were produced were treated by hydrogen plasma. This resulted in a very well ordered film of naked Co-nanoparticles. On these films, further physical experiments could be performed. Many efforts were taken in order to generate Co-nanoparticles in a controlled way in polymeric solutions. The initial path of Co(II)-reduction was discarded due to a too strong interaction of pyridine to Co(II). Anhydrous hydrazine, which was successfully taken to reduce Gold(III) did not bring the expected reaction, but was complexed by Co(II). Thermal decomposition of hydrazino-complexes led to undefined particle formation and to partial degradation of the system. The most successful way to generate Co-metal within polymeric micelles was the thermal decomposition of  $\text{Co}_2(\text{CO})_8$  within the micelles. Conversion of  $\text{Co}_2(\text{CO})_8$  led to very small nuclei, which could partially be joined together by anhydrous hydrazine or acetonitrile. The thermal decomposition was enhanced by usage of partially quaternised PS-*b*-P2VP block copolymers. Stepwise heating and  $\text{Co}_2(\text{CO})_8$  in excess led to aggregation of the nuclei and to formation of Co-nanoparticles within the micelles. Parts of the particles formed chains consisting of individual particles. The particles could be arranged by application of an external magnetic field. Further examination on this system is needed to overcome problems in reproducibility.

In PBd-*b*-PEO block copolymers, Co-particles were formed within ribbon-like and lamellar structures. When symmetrical polymers of this type were taken, the lamellar structure was filled with  $\text{Co}_2(\text{CO})_8$  and Co. By application of an external magnetic field, the wetting of the micellar solutions was influenced and yielded striped or terrace-shaped structures depending on the direction of the applied magnetic field.

Finally, we described the attempt of manipulation of the particle surface and some tries to gain bimetallic particles by our synthetic methods. The main problem we encountered was a very strong interaction of the particle surface to the stabilising agent. Redispersion and extraction of surfactant stabilised Co-particles worked. Modification by  $\text{SiH}_4$  on surfactant stabilised Co-particles was working, but led to an increase of aggregation of the particles. The silane interacted with the CoO and  $\text{Co}_3\text{O}_4$  surface layer and formed a sticking surface layer. Experiments leading to bimetallic particles were very poor in result. Direct coating of the Co led either to oxidation of the Co-metal or to formation of coexisting particles of both metals. This was true for Ag, Au and Pt. In the case of Pt, we developed a novel, easy synthetic method for surfactant-protected Pt-nanocrystals. We could finally show, that in general, the deposition of Pt onto Co-nanoparticles does work, if the particles are not too strongly interacting with the protective agent. In the case of Co-particles from a PBd-*b*-PMAA solution, the loose bound cobalt structures were covered with Pt. This was evident from the still present magnetic dipolar interactions between the cobalt particles and the cubic high-contrast Pt-cover layer.

The basic work is done, but the next challenge will be to build up a route of defined and controlled synthesis of bimetallic particles.

## ***Zusammenfassung***

In der vorliegenden Arbeit war das Ziel, die definierte Synthese von Cobalt-Nanopartikeln mit Hilfe von nanostrukturierten, strukturgebenden Stabilisatoren zu bewerkstelligen. Dieses Ziel wurde von uns durch zwei Arten von “Nanoschablonen” verfolgt. Im ersten Teil der Arbeit wurden niedermolekulare Surfactants verwendet und spezielle Systeme wurden so lange optimiert, bis wir die Größe, die Ordnung und die Stabilität der Dispersionen im Griff hatten. Die Struktur der Partikel konnte auch dann erhalten werden, wenn die Partikel aus der Lösung ausfielen.

Zunächst trafen wir eine Auswahl, um aus der großen Anzahl von Synthesemethoden eine auszuwählen und diese durch Feintuning zu verbessern. Nach einiger Sichtung verschiedener Systeme entschlossen wir uns, Sulfosuccinat-Systeme (AOT/OA und TDS) zu verwenden, da wir uns durch diese ein Erreichen unseres Zieles versprochen. Beide erwähnten Systeme stellen einen Kompromiß aus Partikel- und Dispersionsstabilisierung dar. Wir konnten beide Systeme so weit modifizieren, dass uns eine genaue Kontrolle der gewünschten Produkte schließlich möglich war. Die Grenzen der zu erreichenden Partikel lagen hierbei zwischen 4 und 12 nm. Besondere Aufmerksamkeit legten wir auf den Aspekt der Partikeloxidation. Dieses Thema wird in Publikation oft gemieden, da es zu den unerwünschten Effekten in Co-Partikelsystemen zählt. Die Realität zeigte uns, dass wir strenge Vorkehrungen treffen mussten, um die Oxidation der Partikeloberflächen kontrollieren zu können. Wir konnten zeigen, dass die Oxidschicht, die sich ohne solche Vorkehrungen an der Oberfläche der Partikel bildet, aus einer Mischung von CoO und Co<sub>3</sub>O<sub>4</sub> besteht. Ohne besondere Beachtung bildet sich um die Partikel ein Oxidfilm von 1,8 nm Dicke. Für 5 nm Partikel bedeutet dies mehr als die Hälfte des Partikeldurchmessers.

Mit diesem Ergebnis im Hinterkopf fingen wir an, die Teilcheneigenschaften besser zu verstehen. Die magnetischen Eigenschaften beispielsweise entsprechen denen von bulk-Cobalt, wenn die Gegenwart einer Oxidschicht berücksichtigt wird. Wir fanden so auch einen Weg, langzeitstabile Co-Partikel herzustellen. Es konnte ein Co-Partikelpulver hergestellt werden, das über einen Zeitraum von 1 Jahr hinweg an der Luft seine ferromagnetischen Eigenschaften behielt. Dieses Aggregat aus einem TDS-Ansatz, das zwischen 170 °C und 200 °C Zersetzungstemperatur gebildet wird, enthält durch TDS geschützte Co-Nanopartikel, die unter Beibehaltung der ferromagnetischen Eigenschaften auch nach 1

Jahr noch redispergiert werden können. In diesem Aggregat kann durch das Anlegen eines äußeren magnetischen Feldes eine 2- bzw. 3-dimensionale Anordnung erzwungen werden. Es konnte gezeigt werden, dass die hochauflösende TGA eine Methode darstellen kann, den Metallgehalt solcher Nano-Cobalt-Lösungen quantitativ zu bestimmen.

Der zweite Teil dieser Arbeit handelt über PS-*b*-P2VP –Mizellen als Strukturelement bei der Herstellung von Co-Nanoteilchen. Der Mechanismus der Salzaufnahme für den Fall von Co(II)-Salzen konnte aufgeklärt werden. Diese werden im Mizellkern durch die P2VP-Blöcke mit tetraedrischer Koordination komplexiert. Die maximale Beladung der Mizellen bezogen auf Co(II)-Salz beträgt 0.25 aufgrund dieser Koordination. Diese Beladung konnte durch das Einfügen von Hilfsliganden, die Koordinationsplätze blockieren, erhöht werden. Eine höhere Beladung ist für die spätere Steuerung der Partikelgröße wichtig. Ein weiterer Ansatz zur Erhöhung der Beladung ist die Verwendung von Chelatkomplexen, die diese blockierten Koordinationsplätze bereits intrinsisch enthalten. Dadurch konnte die Beladung bis zu einer Höhe von 0,5 gesteigert werden.

Die Filmbildung konnte durch den Einsatz des hochsiedenden Lösungsmittels Mesitylen verbessert werden. Filme mit stark ausgeprägter Ordnung konnten hiermit hergestellt werden. Solche Filme konnten mit einem Wasserstoffplasma behandelt werden, was zu geordneten Strukturen nackter Co-Nanopartikel führte. An diesen Filmen konnten weitergehende physikalische Messungen durchgeführt werden. Viele Wege wurden verfolgt, um Co-Partikel in Polymerlösungen zu erhalten. Es traten aber allgemein zu starke Wechselwirkungen der Co-Ausgangssubstanzen zu den Pyridineinheiten des Mizellkerns auf. Der ursprüngliche Weg der Reduktion mit wasserfreiem Hydrazin konnte nicht erfolgreich angewendet werden, da die Zugabe von wasserfreiem Hydrazin zu einer Komplexierung des Reduktionsmittels führt.

Die erfolgreichste Route ist die Verwendung der thermischen Zersetzung von  $\text{Co}_2(\text{CO})_8$  innerhalb des Mizellkerns. Die Umsetzung des  $\text{Co}_2(\text{CO})_8$  führte zu sehr kleinen Kristallisationskeimen. Diese konnten teilweise durch Einsatz einer niedermolekularen Verbindung (wasserfreies Hydrazin bzw. Acetonitril) zusammengeführt werden. Die thermische Zersetzung des Carbonyls kann durch den Einsatz eines teilweise quaternisierten PS-*b*-P2VP Blockcopolymers verbessert werden. Schrittweise Erwärmung und der Einsatz von  $\text{Co}_2(\text{CO})_8$  im Überschuss führt zum Zusammenwachsen der Kristallisationskeime und zur Bildung von Co-Nanopartikeln im Mizellkern. Einige der Partikel bildeten auch kettenförmige Assoziate. Diese konnten durch Anwenden eines äußeren Magnetfeldes ausgerichtet

werden. Weitere Arbeit ist jedoch erforderlich, da die letzteren Erkenntnisse nicht genügend reproduziert werden konnten.

In PBd-*b*-PEO Blockcopolymeren konnten wir Rippen- und Lamellenstrukturen herstellen. Wenn wir zur Herstellung symmetrische Polymere dieses Typs verwendeten, wurden die Lamellen mit  $\text{Co}_2(\text{CO})_8$  bzw. Co gefüllt. Durch Anlegen eines externen Magnetfeldes konnten wir die Benetzung des Polymers auf einem Film beeinflussen. Es bildeten sich Streifen- und Terrassenmuster.

Schließlich beschrieben wir den Versuch, die Partikeloberfläche zu ändern und Versuche, durch unsere synthetischen Mittel bimetallische Partikel zu bekommen. Das Hauptproblem all dieser Versuche war die zu starke Wechselwirkung zwischen Partikeloberfläche und dem Stabilisator. Die Redispersion und die Extraktion der Co-Lösungen gelang. Die Modifikation der Oberflächen durch Behandlung mit  $\text{SiH}_4$  funktionierte auch, allerdings stieg die Tendenz zum Zusammenbruch der Dispersion. Das Silan könnte mit den Oberflächenschichten aus CoO und  $\text{Co}_3\text{O}_4$  wechselwirken.

Experimente, die zur Herstellung von bimetallischen Partikeln unternommen wurden, stellten sich als ungeeignet heraus. Die direkte Umsetzung des zweiten Metalls auf der Partikeloberfläche führte entweder zur Oxidation von Cobalt oder zu zwei koexistierenden Teilchenspezies. Im Fall von Platin, entwickelten wir eine neue, schnelle und einfache Herstellungsmethode für Nanopartikel des Pt. Wir konnten ferner an einer Lösung des Polymers PBd-*b*-PMAA zeigen, dass locker gebundene Co-Nanopartikel grundsätzlich mit Pt überzogen werden können. Im Produkt waren sowohl die magnetische Anordnung der Partikel als auch die neuen, kontrastreichen Pt-Anteile zu sehen. Letztere zeigten eine viereckige Grundstruktur, die für Pt typisch ist.

Die grundlegenden Themen sind nun erledigt. Die nächste Herausforderung wird es sein, hieraus eine definierte Synthese von bimetallischen Nanopartikeln abzuleiten.

# *Appendix*

## ACKNOWLEDGEMENT

Die vorliegende Arbeit entstand zwischen September 1999 und Dezember 2003 in der Abteilung Organische Chemie III – Makromolekulare Chemie an der Universität Ulm.

An dieser Stelle möchte ich mich bei sehr vielen Leuten bedanken, ohne die diese Arbeit niemals zustande gekommen und abgeschlossen worden wäre.

Herrn Prof. Dr. Martin Möller für die Bereitstellung des interessanten Themas, für die Möglichkeit zu promovieren und die wissenschaftliche Diskussion und Unterstützung.

Frau Dr. Christine Jérôme für die sehr große wissenschaftliche und moralische Unterstützung und nicht zuletzt für die tolle Zeit, in der wir zusammen auf diesem Gebiet forschten.

Herrn Prof. Dr. Joachim Spatz für den Einstieg in das Thema und die Betreuung in der Anfangszeit.

Frau Prof. Dr. Katharina Landfester für die gute Integration in die neue Arbeitsgruppe und die Unterstützung in der Endphase der Arbeit.

Herrn Prof. Dr. Paul Ziemann für die Möglichkeit der Kooperation mit der Abt. Festkörperphysik sowie für hilfreiche Diskussionen zum Thema.

Herrn Prof. Dr. Hans-Gerd Boyen für die fruchtbare Kooperation auf dem Gebiet der Partikelfilme und für die Möglichkeit zu unterstützen, sowie Diskussionen rund um alle Themen.

Prof. Dr. Paul Walther, H. Fritz, H. Schmid und sein Team für viele Stunden in der Elektronenmikroskopie und die guten Gespräche während dieser Zeit.

Prof. Dr. Florian Banhart für die Unterstützung rund um das hochauflösende Elektronenmikroskop.

Dr. Masaki Ozawa für die vielen Messungen an Partikeln im hochauflösenden Mikroskop und für viele freundliche Gespräche

Dr. Gerd Kästle, Klaus Zürn, Frank Weigl und Alexander Schröder für die gute Zusammenarbeit und für einige Aktivitäten über den Rand dieser Arbeit heraus. Dem Gerd auch ein Dank für die Mitorganisation unseres Workshops ☺

Andreas Grob danke ich für die VSM-Messungen und das Engagement, einen Probehälter zu basteln.

Dr. Ulrich Ziener für die Hilfestellung bei der Anionik und die Diskussionen um die Arbeit und ums Praktikum.

Dr. Ahmed Mourran für die Diskussionen zum Thema und einige rauschende Feste.

Und aus der Organischen Chemie III waren da noch...

Dr. Silke Kupfer (vormals Riethmüller), mit der ich während meiner Arbeit viele lange Abende an den PCs saß und die halt immer da war, gell.

Dr. Michael Kraus, der Schweizer Fremdenlegionär, vormals Schwabe und zuverlässiger Partner in Labor und Cafete.

Bernd Tartsch, von dem ich noch so einiges zum Thema PC lernen konnte und der ebenfalls zu unseren „Sechststöcklern“ gehörte.

Marcell Ott, dem ewigen Streiter wider die Widerlichkeiten, die einem im Doktorandenalltag begegnen können.

Dr. Stefan Mößmer natürlich für die tollen Polymere aber auch für einiges darüber hinaus...Dieeegoooo.

Dr. Peter Eibeck für die tollen Polymere Teil2 und für aufschlussreiche Diskussionen zum Themenblock Nanotechnologie, orangene Uhrwerke und Lesotho.

Manfred Jaumann für die vielen Jahre Chemie an der Uni Ulm und die schöne Zeit außerhalb (1A auf A1)

Thomas Ameringer für Freiburg, Mannheim und was es sonst so alles im Süden zu sehen gab ☺

Dr. Christoph Hartmann für die leidige Mitstreiterschaft auf dem Gebiet der Mizelltechnologie und die Bereitschaft während des Chemiker-Faschings ans AFM zu sitzen...Respekt.



Blazej Gorzolnik für die gute Zeit an den Glove-Boxen und die tschechisch-Lektionen in Strassburg.

Krystyna Albrecht und Dr. Jürgen Groll für die Zeit im oberen Sitzzimmer, für die Parties und nicht zuletzt für die schnelle Hilfe am 11. September 2001 (My private WTC).

Dr. Vanessa Chan und Mark van der Helm für die vielen Aktivitäten rund um die Uni und Gespräche und fürs Schuhplatteln.

Prof. Dr. Sergei Sheiko für einige unvergessliche Abende.

Und auch die anderen, die während dieser Jahre n der OC3 waren und das Gesamtbild der Abteilung prägten, wie Reza Najjar, Ana Morales, Dr. Hans Götz und auch die, die ich nicht namentlich erwähnt habe.

Dr. Olga Lebedeva für die spannende Zeit während der Doktorarbeit und die tolle Versorgung, Dr. Bernd Striegel für etliche Gespräche fundamentaler Art.

Dr. Yayun Wang für einige Messungen und auch für eine nette Zeit.

Ebenfalls mein Dank an die technische Crew unserer Abteilung: Marlies Fritz, Elvira Kaltenecker (stimmt die war nicht aus unserer Abteilung), Petra, Magdalene...

Mike Wendel für die vielen GPCs und den Einheitsschritt.

Ein gaaaaanz großer Dank auch an unsere geliebte und gelobte wissenschaftliche Glasbläserei. Namentlich an Konstantin Kraft, Katharina Seibel und Jonas. Die Frühstücke, Mittagessen aber auch das ein oder andere Glas bleiben unvergessen. Und: Die Kaffeemaschine entwickeln wir noch!

Und dann gab es ja noch einige, die so gar nicht zur Uni gehörten.

Meine Freundinnen, die mir jeweils Unterstützung gaben: Ute und Nadja, vielen Dank, dass ich die Zeit mit Euch verbringen durfte.

Meine Eltern und Geschwister, die hin und wieder auch viel Geduld für mich aufbringen mussten. Vielen Dank dafür. Außerdem Dank an Eva und Jochen für die Zeit in Riefensberg, wo Kapitel 1-2 dieser Arbeit entstanden sind.

Thomas Schwarz aus Memmingen natürlich, der immer an mich geglaubt hat ☺

Meine Freunde Seyfi, Betz und Ihab sowie Christoph und Martin, Gerda und Tanja, die immer da waren, wenn sie gebraucht wurden.

Lars und Melanie, die mich auf den letzten Metern immer angefeuert haben. Hin und wieder auch mit Feuerwasser ☺.

Und schließlich mein letztes Refugium während des Endsprints, das Café d'Art, wo ich hinging, wenn nichts mehr ging.

Und nicht zuletzt meinem vernünftigen Ich, das sich letztlich gegen mein unvernünftiges durchgesetzt hat....zumindest vorerst ☺!

## Erklärung:

Hiermit erkläre ich, daß ich die vorliegende Arbeit nur unter Verwendung der angeführten Quellen und Hilfsmittel angefertigt habe.

Ulm, den 14.06.2006

.....

(Oliver Mayer)

# CURRICULUM VITAE

## PERSÖNLICHE DATEN

Name	Oliver Mayer
Staatsangehörigkeit	Deutsch, Tschechisch
Geburtsdatum	04.03.1972
Geburtsort	Prag (Tschechische Republik)

## SCHULBILDUNG

1978 - 1982	Edith-Stein-Grundschule Memmingen
1982 - 1991	Bernhard-Strigel-Gymnasium Memmingen
10.07.1991	Abitur

## STUDIUM

10/1992 - 11/1998	Chemiestudium an der Universität Ulm  03/1995 Vordiplom (gut) Studienschwerpunkte: Makromolekulare Chemie, Materialien, Umweltchemie
12/1998 – 08/1999	Diplomarbeit in der Abteilung Organische Chemie III – Makromolekulare Chemie und Materialien der Universität Ulm bei Prof. Dr. M. Möller und Prof. J.P. Spatz  Titel: „Blockcopolymermizellen als Template zur Herstellung von kolloidalen Lösungen der magnetischen Übergangsmetalle“ 31.08.1999  Diplom: Abschluß mit der Gesamtnote „sehr gut“

## PROMOTION

01.09.1999 – 31.12.2003	Promotion in der Abteilung Organische Chemie III – Makromolekulare Chemie und Materialien der Universität Ulm bei Prof. Möller
-------------------------	--

## BERUFSTÄTIGKEIT

Seit 01.01.2004	Qualitätsingenieur, Materials and Process Technology bei der EvoBus GmbH, Ulm (Daimler Chrysler Commercial Vehicles Division)
-----------------	---

